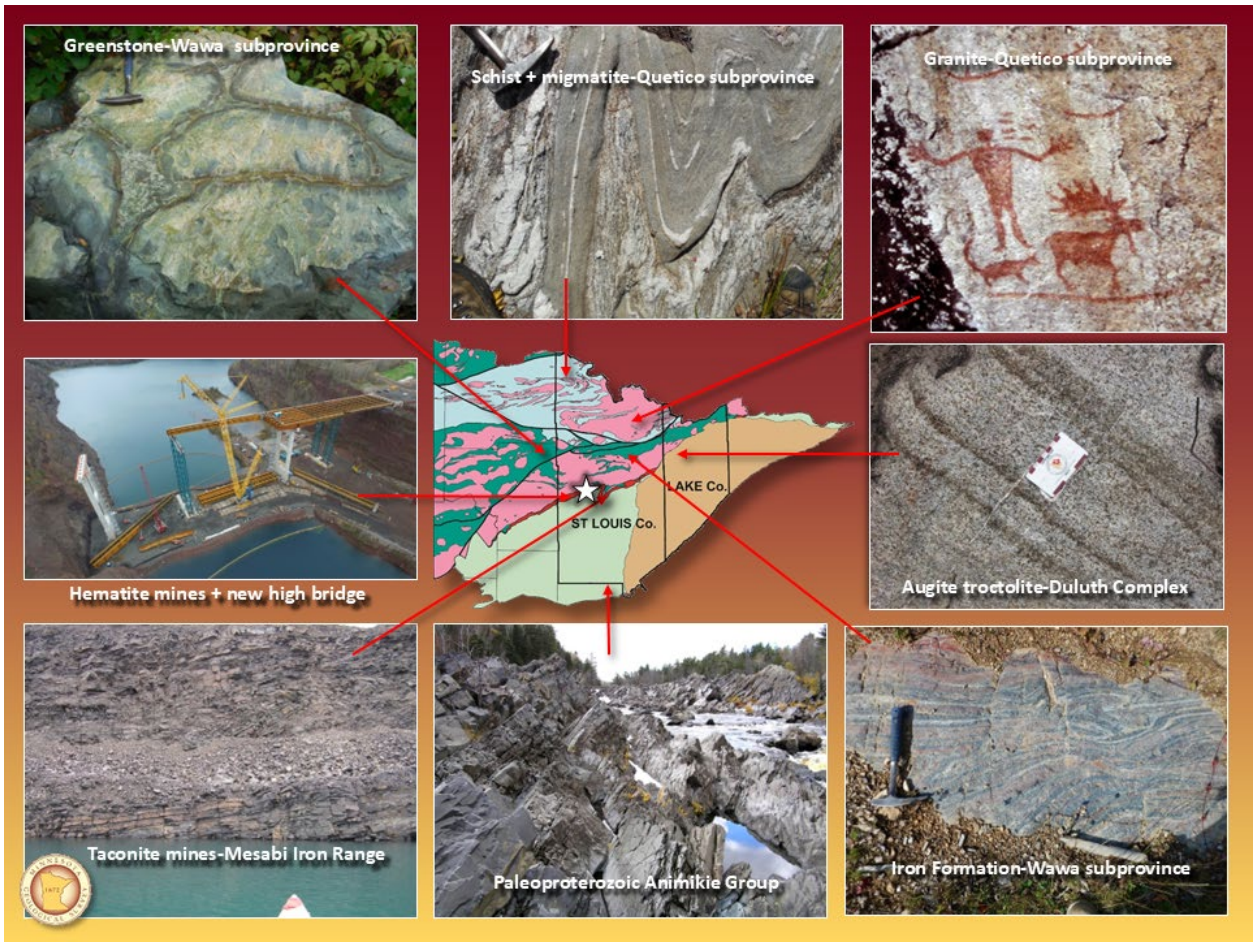
Volume 71, Part 2

INSTITUTE ON LAKE SUPERIOR GEOLOGY



71st ANNUAL MEETING

Mountain Iron, Minnesota, May 14-17, 2025

PART 2—Field Trip Guidebook

Meeting Co-Chairs

Amy Radakovich, Allison Severson, Eric Nowariak, Stacy Saari, Aaron Hirsch

Special thanks to field trip leaders:

Zsuzsanna Allerton

Terry Boerboom

Kevin Boerst

Latisha Brengman

Annia Fayon

George Hudak

Mark Jirsa

Phil Larson

Dean Peterson

Cullen Phillips

Laurie Severson

Mark Severson

Alex Steiner

71st Institute on Lake Superior Geology

Volume 71 consists of:

Field Trip 1 – Transect of the Quetico Subprovince 1

Field Trip 2 – Drill Core from three Cu-Ni Deposits of the Duluth Complex 15

Field Trip 3 – How Do You Make Iron and/or Manganese Ores in Proterozoic Iron Formation?..... 46

Field Trip 4 – New Geological Insights into the Genesis of Iron Ores at Lake Vermilion – Soudan Underground Mine State Park..... 74

Field Trip 5 – Neoarchean Alkalic Intrusions in the Wawa and Quetico Subprovinces 108

Field Trip 6 – Unique Keweenawan Inclusion (Colvin Creek) in the Duluth Complex 136

Field Trip 7 – Classic Outcrops of Northeastern Minnesota 151

Field Trip 8 – Glacial Lake Norwood and the Koochiching Lobe…. 188

FIELD TRIP 1

Transect of the Quetico Subprovince

Eric Nowariak[1] and Mark Jirsa (retired)[1]

[1] *Minnesota Geological Survey, College of Science and Engineering, University of Minnesota, 2609 Territorial Road, St. Paul, MN 55114*

Introduction

This trip will examine exposures of the metasedimentary, migmatitic, and intrusive rocks of the Neoarchean Quetico subprovince from north of Mountain Iron to near Crane Lake and along part of the Echo Trail. It will attempt to "unpack" the primary components of deposition, magmatism, deformation, and metamorphism that likely spanned 40 million years (~2700-2660 Ma). The latter is based in part on newly acquired geochronologic analyses (Jirsa and others, 2020; Salerno, 2017). The trip will also address the challenge of creating meaningful geologic maps of this and similarly complex terranes, and the apparent lithologic and temporal link between Quetico metasediments and those associated with successor basins in the region.



Figure 1-1. Complex migmatite exposed at field trip stop # 3.

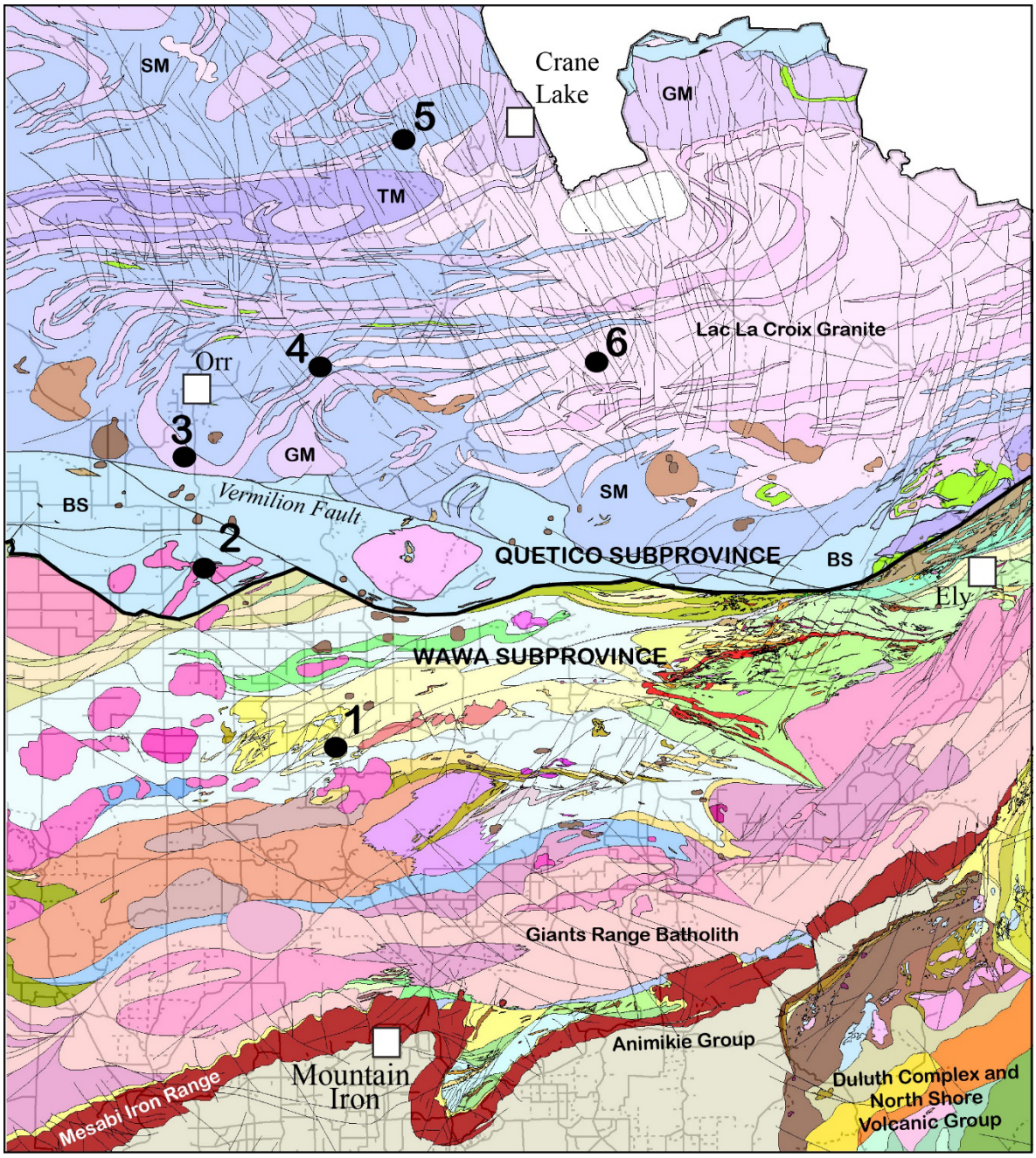


Figure 1-2. Geologic Map of Central St. Louis County. This draft version of the St Louis County Precambrian bedrock map (superceded by Jirsa, 2020) portrays parts of the Neoarchean Wawa and Quetico subprovinces of Superior Province, and the approximate location of field trip stops. Wawa subprovince colors: greens=volcanic and volcaniclastic rocks; blues=metasedimentary rocks (primarily metagraywacke); reds=iron-formation; pinks=granitoid rocks; yellows=epiclastic and volcaniclastic sedimentary rocks. Quetico subprovince is labeled: BS=biotite schist (metagraywacke); SM=schist-rich migmatite; GM=granite-rich migmatite; TM=tonalite-rich migmatite. Pale pink Lac La Croix granite is more magnetic, darker pink is less so. Bold line marks the approximate boundary between subprovinces—a fault in some places, an inferred unconformity in others.

GEOLOGIC SETTING

The Quetico is one of a number of east-trending, largely metasedimentary subprovinces in the Superior Province. It is bounded on the south by the Wawa volcanoplutonic subprovince, and on the north by the Wabigoon subprovince. It consists of schist derived from turbiditic sedimentary rocks and a complex suite of granitic intrusions and associated migmatite. In northeastern Minnesota, the subprovince displays a roughly symmetrical distribution of metasedimentary rocks on the north and south, that grade irregularly through zones of schist-rich migmatite, to a central axial zone composed largely of polyphase granitoid migmatite and younger granite. To some extent, metamorphic grade mimics this symmetry, with generally higher grade rocks in the central axis and lower grade near the bounding volcanoplutonic subprovinces. The accretionary prism model of Williams (1990) implies deposition of sediment shed from the craton to the north, and the subducting island arc to the south by submarine fans and abyssal turbidites. The Rainy Lake-Seine River Fault zone at the southern margin of the Wabigoon subprovince is thought to mimic the subduction front. The southern boundary against the Wawa subprovince is interpreted as an unconformity in some locales, and a fault in others.

DEPOSITIONAL HISTORY

Timing of deposition of the clastic sedimentary rocks of the Quetico subprovince in Minnesota has been constrained by populations of the youngest detrital zircons at 2690 +/- 12 Ma (Salerno, 2017). Similarly, geochronologic studies of the Quetico metasedimentary sequences in Canada has been constrained to 2698 Ma near Atikokan, ON (Davis and others, 1990) and <2690 according to Zaleski and others (1999) near the Manitowage Greenstone Belt of the Wawa subprovince. Zaleski and others (1999) also proved deposition of graywacke units within the Manitowage Greenstone Belt were contemporaneous, if not genetically related. A similar temporal and possible genetic link between the metasedimentary rocks of the Lake Vermilion formation and turbiditic metasediments of the Quetico in Northern Minnesota, wherein immature, volcaniclastic rocks of the Lake Vermilion formation gave way to silicic, clastic sedimentation observed in the Quetico subprovince as the basin evolved from alluvial fan deposits to a deep-water, active margin depocenter as the Quetico basin developed (Davis and others, 1990). In addition to Neoarchean zircons, small populations of older zircons including Mesoarchean zircons have also been recognized (Salerno, 2017; Davis and others, 1990). Probable sources of these older zircons have identified from multiple terranes in the southern Superior province and a proximal source for the sediments is inferred. The composition of the Quetico metasedimentary rocks suggests the source region was shedding sediment from a mixture of sialic plutonic terranes and lesser juvenile volcanic terranes. In addition to the clastic metasedimentary rocks that dominate the bulk of the Quetico subprovince, thin, discontinuous amphibolitic layers are found interbedded in many areas; likely representing volcanoclastic deposits and rare flows from active volcanism occurring near the margins of the subprovince.

VERMILION GRANITIC COMPLEX

The migmatitic and plutonic rocks in the axial zone are known collectively in Minnesota as the Vermilion Granitic Complex (Southwick and Sims, 1980). Southwick and Ojakangas (1979) subdivided migmatite for mapping purposes as schist-rich and granite-rich components, depending on the ratio of paleosome to neosome. Subsequent mapping by Jirsa (2011) and Jirsa and others (2014), applied the same terms, based instead on the extent to which the predominant fabric in the rock is controlled by neosome vs. paleosome and further distinguished units based on neosome composition. In this nomenclatural system, schist-rich migmatite is schist containing intrusions of granitoid neosome as both delaminating and cross-cutting bodies; granite-rich migmatite is neosome with inclusions of paleosome. These can be equated generally with the terms metatexite (low degree of partial melting) and diatexite (nearly complete fusion), respectively, of Sawyer, (2008). Field relationships within the complex (Southwick, 1991) indicate that earliest granitoid phases are leucogranite, tonalite, granodiorite, and trondhjemite, which make up the leucosome of a broad area of migmatite across the western portion of the Vermilion Granitic Complex. For this field trip guide, these granitoids, broadly of TTG affinity, are referred to as “neosome 1”. The

migmatite is interlayered at all scales with paleosomes of biotite schist, paragneiss, orthogneiss, and amphibolite and often carries an internal fabric similar to the paleosome. Salerno (2017) obtained a discordant U-Pb zircon age of a granodiorite phase of neosome 1 at 2684 +/- 23 Ma.

The migmatite is cut by poorly to non-foliated dikes, sills, and irregular masses of two mica leucogranite with accessory garnet, and a slightly younger biotite granite and pegmatite that contain minor magnetite. The presence of magnetite within the granitic rocks related pegmatites has proved to be an important mapping tool as these intrusive bodies create conspicuous aeromagnetic anomalies (Fig. 3b). The latter forms a large granitic mass, known as the Lac La Croix granite nearest the US/Canadian border, and apophosial intrusions that flare and pinch westward, producing aeromagnetic anomalies that highlight broad fold structures. These intrusive "fingers" generally decrease in thickness and continuity westward, suggesting that the western portion of the complex may represent the roof- or floor-zone of the batholith cored by massive granite. For simplicity within this field guide, the leucogranitic and granitic rocks of the Lac La Croix granite are referred to as "neosome 2" and represents the youngest granitic intrusive units of the Vermilion Granitic Complex. Geochronologic analyses of leucogranite and granite of the Lac La Croix granite has dated the crystallization of this unit with U-Pb zircon ages of 2658.71 +/- 0.47 Ma and 2668 +/- 10 Ma (Jirsa and others, 2014; Salerno, 2017).

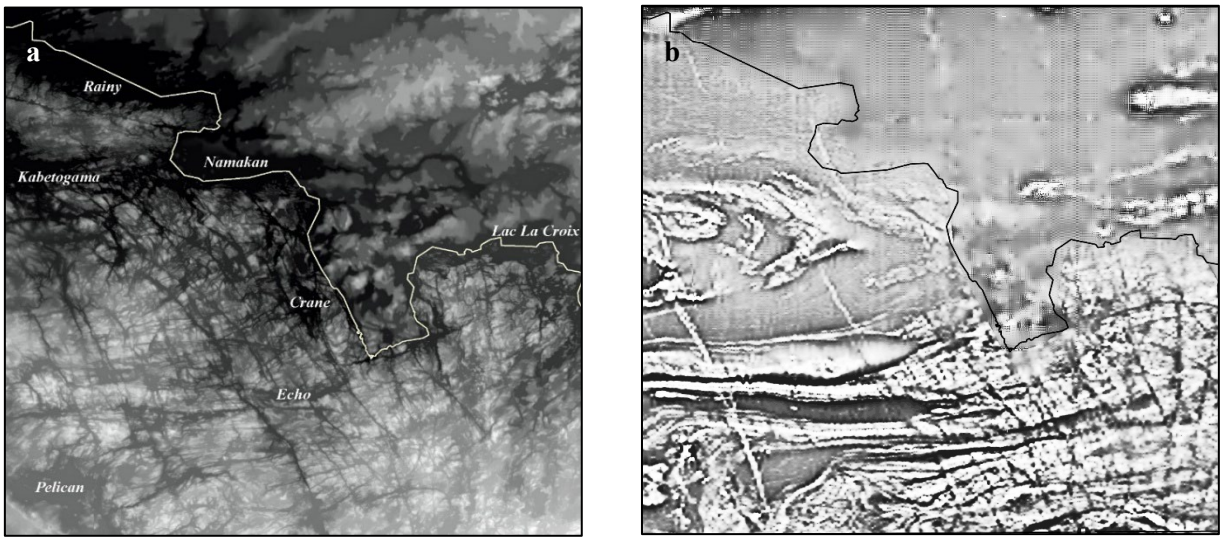


Figure 1-3. Maps of the Crane Lake and Brule Narrows 30'X60' quadrangles (US and Canada) illustrating the connections between attributes of structure, lithology, topography, and magnetite content in this area of abundant near-surface bedrock. **(a)** 30m lidar land surface topographic grid; low areas darker. Topography defines major fold structures, and massive granitic vs. foliated orthogneissic and schistose bedrock. Prominent NNW-trending linear low areas are fault and fracture systems, many of which are occupied by rivers and lakes (named). **(b)** First vertical derivative map of aeromagnetic data. Magnetic highs (lighter colored) typically are more granitic; lows, more schist-rich. Like the topographic map, the magnetic data identify folds and faults. Linear, NW-trending highs are normally polarized diabase dikes of the Paleoproterozic Kenora-Kabetogama dike swarm. Linear lows are coincident with topographic lows, implying oxidation by meteoric, or more likely hydrothermal fluids along fractures. Some field evidence indicates that rock adjacent to fractures is chemically weathered, and hence more easily eroded. The subparallelism of dikes with fractures may indicate that oxidizing hydrothermal fluids were temporally related to dike emplacement.

Neosome 1 and neosome 2 are readily distinguished in the field based on mineralogy and textural characteristics described above. Day and Weiblen (1986) used simple geochemical plots and CIPW normative mineralogy to visualize these differences (Fig. 1-4). Both plutonic suites are characterized as calc-alkaline, metaluminous to weakly peraluminous, magnesian granitoids. Neosome 1 tonalite-trondhjemite-granodiorite intrusions are inferred to have been sourced from partial melting of mafic crust.

Geochemical evidence indicates that the early neosome 2 migmatite was derived from partial melting of a metasedimentary protolith (Day and Weiblen, 1986). Southwick (1991) and Day and Weiblen (1986) suggested that the younger Lac La Croix-type granite of neosome 2 may represent further distillation of granitic liquid from partial melting of the combined older migmatite and metasedimentary rocks.

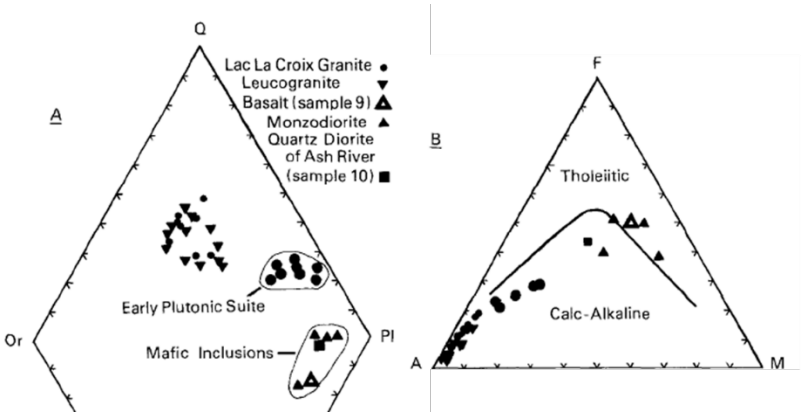


Figure 1-4. From Day and Weiblen (1986). **(A)** CIPW normative mineralogy for Vermilion Granitic Complex. Q – quartz; Pl – albite+anorthite; Or – orthoclase. "Early Plutonic Suite" is equivalent to neosome 1 of this guidebook. (B) AFM diagram of same data (Irvine and Baragar, 1971).

DEFORMATION AND METAMORPHIC HISTORY

The Quetico subprovince has undergone a complex deformation history over a relatively contracted tectonic history between deposition of sediments ca. 2690 Ma and intrusion of the Lac La Croix Granite related pegmatite dikes ca. 2658 Ma. As summarized by Bauer and others (2011), three main phases of deformation have been recognized. D_1 produced tight to isoclinal, recumbant folds plunging to the southwest and locally overturned to the southeast and produced a weak, bedding parallel axial planar foliation. Hinges of these recumbent folds are rare, and recognition of this event are often limited to overturned bedding and bedding-parallel foliation that is crenulated by subsequent deformational events. This event may locally have produced recumbent folds over a broad region (Bauer, 1985; Poulsen and others, 1980). It occurred shortly after deposition and involved burial to produce metamorphic conditions of moderate pressure and temperature (Valli and others, 2004). Fralick and others (2006) suggested D_1 deformation was contemporaneous with development of the Quetico basin as an accretionary wedge.

D_2 deformation was synchronous with peak regional metamorphism to upper greenschist facies in the Wabigoon subprovince and amphibolite facies in the adjacent Quetico subprovince, and produced the dominant structural grain observed in the Minnesota segment of the Quetico subprovince. Folding associated with D_2 deformation produced tight to isoclinal upright folds that plunge to the E-NE 10-30°. The intrusion of neosome 1 occurred slightly prior to or contemporaneous with D_2 as veins of neosome 1 are commonly folded and occupy gently to moderately plunging D_2 related fold hinges. Peak metamorphism presumed to be contemporaneous with D_2 deformation within the Vermilion Granitic Complex has been dated by U-Pb monazite geochronology by Salerno (2017) and has constrained to ca. 2675 Ma.

Continued contractional and transpressional deformation during D_3 has been noted as ductile, east-northeast trending transpressional shear zones and coaxial refolds of D_2 related structures. Folding associated with D_3 deformation is better developed near plutons of the Lac La Croix granite and related granitoids, suggesting early stages of neosome 2 intrusions were contemporaneous with deformation or used these structures as conduits (Bauer and others, 1992). D2-D3 is interpreted to be a result of the accretion of the Quetico subprovince to the Wabigoon subprovince to the north. Metamorphic indicator minerals within the Vermilion Granitic Complex including garnet, sillimanite, and locally cordierite have been well documented (Day, 1990; Tabor, 1988; Salerno, 2017). Limited thermobarometric studies have determined peak metamorphism reached amphibolite facies in the axial core of the Minnesota segment of the Quetico subprovince and upper greenschist facies along the northern margin of the subprovince, with garnet-biotite thermometry revealing metamorphic temperatures between 500-600°C and 430-475°C,

respectively (Bauer and others, 1992; Salerno, 2017). It is unknown whether the intrusion of the Lac La Croix granite and other neosome 2 intrusions produced a significant metamorphic overprint, however Tabor (1988) recognized kyanite in metamorphic assemblages of the Quetico subprovince along its northern boundary along the Rainy Lake-Seine Fault; which may represent an earlier, relatively higher pressure metamorphic regime prior to intrusion of the Lac La Croix granite.

Subsequent deformation including brittle-ductile faulting with associated planar fabrics developed locally near fault zones and minor open folds reorienting existing structures has been ascribed to continued contraction post-dating metamorphism and major plutonism has been ascribed to D4 deformation. One of the most prominent and through-going features of the Quetico subprovince in Minnesota is the Vermilion Fault—a northwest-trending structure that truncates metamorphic zones and folds that are apparent on aeromagnetic maps is likely a product of late D3 and/or D4 deformation. Based largely on geophysical maps, dextral offset along this fault is on the order of 40 km. The fault can be traced from the extreme NW corner of the state for some 250 miles southeastward to near Ely, Minnesota. There it appears to veer to the northeast, manifest as a complexly splayed, post-metamorphic thrust-system known collectively as the Burntside Lake Fault. A summary of the deformational and metamorphic features observed in the Minnesota segment of the Quetico subprovince is shown in Table 1-1 below.

Event	General Features	Associated Fabrics	Metamorphic Features	Timing	Source(s)
D_1	Recumbant folds	Bedding parallel foliation	N/A	ca. 2690 Ma	Fralick and others (2006), Bauer (1985)
D_2	Upright to inclined tight to isoclinal folds, axes plunge to the northeast and southwest	Axial planar cleavage, strong hinge-parallel lineation	Upper greenschist to amphibolite facies	ca. 2675 Ma	Bauer and others (1992) and references therein, Salerno (2017)
D_3	Upright tight to isoclinal folds – coaxial to D_2 folding, east-northeast trending shear zones	Axial planar cleavage, strong hinge-parallel lineation, shear fabrics proximal to fault zones	Amphibolite Facies	2675-2668 Ma	Bauer and others (1992) and references therein, Jirsa (2014)
D_4	Brittle-ductile faulting, broad folding	Planar fabrics proximal to shear zones	Hydrothermal alteration along fault zones	</=2668 Ma	Bauer and others (1992), Recent unpublished mapping

Table 1-1. Summary of deformational and metamorphic features observed in the Quetico subprovince within Minnesota.

CONSIDERATIONS FOR GEOLOGIC MAPPING

Complex geologic terranes recording multiple, interdependent geologic processes including sedimentation, multiple phases of deformation, and diverse polyphase intrusive histories like that of the Quetico subprovince represent a unique challenge in creating meaningful, consistent geologic maps and map units. Multiple attempts to properly portray the complicated geology of the Minnesota segment of the Quetico subprovince have used varied approaches, which have proved to require the incorporation field observation, petrography, aeromagnetic and gravity anomalies, LiDAR and aerial photography, and magnetic susceptibility measurements.

Early iterations of geologic maps in the area focused on the proportional differences between the paleosomatic and neosomatic components of the migmatitic rocks within the subprovince to distinguish geologic units (Southwick and Ojakangas, 1979), while other authors have decided to incorporate the textural, compositional, and petrophysical characteristics of paleosomes and neosomes to further distinguish coherent map units (Jirsa, 2011; Jirsa and others, 2014). In addition to traditional field observations, thousands of magnetic susceptibility measurements recorded for units across the subprovince have been used to varied effect (Chandler and Lively, 2014). While petrophysical characteristics of the host

rocks are not sufficient to determine many units, the extent and morphology of some distinct units, namely late magnetite bearing granites and pegmatites, have been found to correlate with higher magnetic susceptibilities and resultant aeromagnetic anomalies (Fig. 1-3b).

The structural complexities observed in this trip are preserved from the outcrop to map-scale. Many map-scale structures are discernable in aeromagnetic derivative maps and have been used in conjunction with the magnetic characteristics described above to outline geometric and temporal relationships between deformation and intrusive intervals where outcrop exposure is insufficient. Careful observations at individual outcrops has been found to be beneficial in comparison to regional lithologic mapping. Many geologic structures may be more readily identified by field checking and correlating the roughness and patterns of exposed outcrops using lidar and aerial photos. Recognition of post-intrusive faults visible in LiDAR derived maps and as linear magnetic lows in aeromagnetic maps have also helped reconcile locales where map patterns would be otherwise difficult to align with the known structural character of the area.

FIELD TRIP STOP DESCRIPTIONS

It should be noted that this trip derives from several years of field work to produce two geologic maps of the western-most exposed portions of the Quetico subprovince in Minnesota (Jirsa, 2011; Jirsa and others, 2014); and refinement by more recent field work to create maps of St. Louis and Koochiching Counties (Jirsa and others, 2020; Nowariak and others, in preparation). Mapping focused largely on structural and magnetic attributes that could yield a "meaningful" geologic map of this very complex terrane, and little analytical work was conducted; though ongoing work in Koochiching county has begun to tackle this. As a result, this field trip lacks details of metamorphism, petrology, and geochemisty. Instead, the focus was largely structural, in an attempt to reconcile prominent geophysical anomalies and topographic trends with field observations. The associated maps incorporate structural data, field relationships, and thousands of magnetic susceptibility measurements to ascertain the connections between lithology and magnetite content. Because glacial sediments are thin to absent in much of the area, mapping was also influenced by 10-meter (and subsequent 1-meter, for more recent mapping) LiDAR imagery (Fig. 1-3a). Mapping in the Quetico subprovince on which this field trip is based was supported by grants from the U.S. Geological Survey STATEMAP element of the National Geologic Mapping program, and by the Minnesota Environmental and Natural Resources Trust Fund.

NOTE: All locations are denoted in UTM coordinates, NAD 83, Zone 15N

STOP 1 – Feldspathic graywacke of the Lake Vermilion Formation

Location: 526342E/5288565N, (47.74991°, -92.64856°), Highway 53 Northbound, 0.4 miles north of Heino Road (County 467)



Figure 1-5. Pavement exposure of laminated feldspathic metagraywacke of the Lake Vermilion formation.

Description: This stop examines the feldspathic metasedimentary and meta-volcanogenic sediments of the Lake Vermilion formation, formally part of the Wawa Subprovince. Here, the Lake Vermilion formation is composed of feldspathic graywackes and tuffaceous slates and wackes. The stratigraphy generally tops to the north and is folded, with locally well-developed axial planar cleavage and thin shear bands. This stop serves as a reference in comparing the composition and character of the metasedimentary

rocks of the uppermost units of the Wawa subprovince and the metasedimentary rocks of the Quetico subprovince.

Directions: From the Mountain Iron Community Center, head east on highway 169 and turn north onto highway 53, continue north 20 miles and pull-off on the right side of the highway.

STOP 2 – Alkalic and Lamprophyric Intrusive Rocks, Gheen Pluton Area

Location: *515162E/5306034N (47.74992°, -92.64856°) (2a); 514380E/5306809N (-92.80754°, 47.91444°) (2c); Highway 53, ~6.5 miles northwest of Cook, MN*

Description: This series of outcrops examines exposures of alkalic granitoids and lamprophyric rocks intruded into metasediments of the Quetico Subprovince. Stop 2a (515162E/5306034N): This outcrop preserves outstanding porphyritic textures within pyroxene syenite and syenodiorite of the Gheen Pluton (Fig. 1-6). Evidence for multiple phases of intrusion and magma mingling are observed throughout. Very coarse phenocrysts exhibit compositional zoning and local magmatic-flow features. The main phase of syenite and syenodiorite contains inclusions of, and is cross-cut by medium grained, amphibole-phyric gabbro and pyroxenite. Late aplitic and pegmatitic dikes represent the youngest intrusive components of the outcrop. Chloritic slickensides are apparent on fracture faces, locally. Stop 2b (514530E/5306605N): This outcrop of the west side of the highway, **USE CAUTION WHEN CROSSING THE ROAD.** Here, pyroxene-biotite phyric lamprophyric rocks are exposed (Fig. 1-7). Beyond the dominant biotite and pyroxene, the mineralogy includes prismatic hornblende, feldspar, apatite, and trace chalcopyrite. Limited work to characterize these rocks has determined they are best described as augite bearing kersantites and spessartites (Le Bas, 2007). The mineralogy and texture vary within the



Figure 1-6. Porphyritic syenodiorite with abundant feldspar phenocrysts at stop 2a.



Figure 1-7. Representative examples of lamprophyric rocks exposed at stops 2b-2d. (a) Biotite-pyroxene bearing kersantite with inclusions of wallrock. (b) Pyroxene-hornblende phyric spessartite with plagioclase dominated groundmass. Blocky, prismatic pyroxene dominates the modal mineralogy here.

outcrop at multiple scales, where complex structural and intrusive relationships juxtapose and include multiple mineralogic and lithologic phases. Stop 2c (514380E/5306809N): This outcrop, on the east side of the highway, is composed of similar lamprophyric rocks as stop 2b, but include blocks of lamprophyric rocks of varied composition and the schist wall-rock. The schist here is commonly altered and is cross-cut by small dikes and veinlets of lamprophyric mineralogy. Schist inclusions become more abundant to the north. Stop 2d (514262/5306920): Continuing to the north from stop 2c, the dominant lithology transitions to well foliated biotite-muscovite schist cross-cut by sulfide bearing quartz veins and discontinuous dikes and veinlets of lamproid parallel to and cross-cutting foliation.

Directions: From the Stop 1, continue north along highway 53, continue north ~14 miles and pull-off on the side of the highway.

STOP 3 – Polyphase, granitoid rich migmatite

Location: *512642E/5316320N, (48.00005°, -92.83053°), Highway 53, ~2.5 miles north of Gheen Corner*



Figure 1-8. Multiphase migmatite at stop 3 showing representative intrusive relationships between the host biotite schist (dark-grey to black), tonalitic neosome 1 (grey),and granitic neosome 2 (tan-pink). Schist preserves crude structural grain.

Description: This extensive roadcut exhibits the complex features common throughout much of the migmatitic core of the Quetico subprovince. Here, we will observe and discuss the structural and intrusive relationships and geophysical properties between the metasedimentary quartz-biotite schist paleosome, early granodioritic and tonalitic neosome 1 intrusions, and granitic neosome 2 intrusions. The complexity observed here begs the question of how to create coherent geologic maps in similarly complex regions across the central Quetico Subprovince. Stop 3a (512642E/5316320N) Here, paleosomes of biotite schist have been strongly recrystallized and exhibit a granoblastic texture with faint foliation defined by biotite orientation. Multiple phases of neosome intrusions, both mafic and felsic, include lenses and irregular, blobby bodies of biotite-hornblende granodiorite ascribed to neosome 1 affinity. All units are cross-cut by pink, coarse-grained biotite granite and syenogranite with abundant pegmatitic veins and segregations. The intrusive relationships seen here generally apply to the regional evolution of magmatic rocks within the Vermilion Granitic Complex and Quetico Subprovince, at large. **Stop 3b** (512645E/5316400N) The agmatic migmatite here includes mafic and silicic paleosome blocks which are disaggregated by the intrusion of both neosome 1 and neosome 2 (Fig. 1-8). Although intrusive phases of the migmatite dominate the outcrop, the structural grain of the paleosomes is preserved as relict bedding and faint foliations. One may note that the paleosomes of differing compositions are difficult to distinguish on the outcrop. Silicic, quartz-biotite schist paleosomes are strongly recrystallized and exhibit an almost massive granular texture. Mafic paleosomes are locally present and are characterized by poorly foliated hornblende (+/- pyroxene) bearing assemblages along with coarsened biotite. Mafic paleosomes seen here may represent thin layers of primary, mafic protoliths or may be restitic components of in-situ melting of the migmatitic host rock. The exposure here is representative of many of the outcrops within the migmatitic core of the Quetico subprovince and highlights the difficulty of creating meaningful geologic maps in the region. How would you map this outcrop? **Stop 3c** (512644E/4135316N) Small, biotite-pyroxene lamproid intrusion, similar to those inspected at stop 2. Here, acicular, prismatic pyroxene is supported in potassium feldspar-rich segregations (Fig. 1-9). Chalcopyrite is present in trace amounts. **Stop 3d** (512645E/5316450N) Throughout the core of the Quetico Subprovince, migmatites are locally associated with pyroxenite and pyroxene-hornblende rich gabbroic dikes. Here, a set of pyroxenite dikes with sheared, biotite rich margins crosscut the biotite schist and neosome 1 wallrock and have mutually cross-cutting relationships with granitic neosome 2 intrusions. Stop 3e (512612E/5316833N) On the northern end of the roadcut, the complex multi-stage migmatite gives way to bedded biotite schist with graded beds and crosscutting dikes of late neosome 2 granite and pegmatite. Beds here are stratigraphically facing up, based on fining upward sequences in graded beds, and dip 45 to the south-southeast.



Figure 1-9. Acicular, prismatic pyroxene within potassium feldspar-rich matrix at stop 3c. This small intrusion is similar to alkalic rocks observed at stop 2.

Directions: From stop 2, continue north along highway 53, continue north ~6.5 miles and pull-off on the right side of the highway.

STOP 4 – Schist and schist-rich rich migmatite near Myrtle Lake

Location: *523750E/5324590N, (-92.68116°, 48.07414°), Highway 23, ~7.5 miles east of Orr*



Figure 1-10. Biotite schist with faint, relict bedding intruded by boudinaged and lit-par-lit dikelets of tonalitic neosome 1.

Description: Here, quartz-feldspar-biotite schists and schist-rich migmatite of the Quetico subprovince are exposed. This outcrop preserves moderately dipping beds (30° to the E-SE) of turbiditic metasedimentary rocks with graded beds. Though obscured by metamorphism, bedding here is interpreted to be upright with graded beds observed as decimeter scale, subtle, rhythmic changes in the amount of micaceous minerals. The base of individual beds is marked by coarse grained sandy layers, which transition to biotite rich schist marking the top of the beds. Fine grains of garnet are present locally in beds with appropriate composition. The schist is intruded by boudinaged dikes and veins up to 1 meter thick and lit-par-lit injections of tonalitic and granitic neosome 1 (Fig. 1-10). Rare dikes of coarse-grained to pegmatitic, pink, granitic neosome 2 crosscut bedding and dominant fabric of the outcrop and mark the latest intrusive event.

Directions: From stop 3, continue north on Highway 53 to the town of Orr and make a right turn on Orr-Buyck Road (Highway 23) and continue 7.5 miles east to the roadcut.

LUNCH AND STOP 5 – Vermilion Falls ***No Hammers***

Location: *531860E/5345460N, (48.26155°, -92.57072°), Picnic area off Vermilion Falls Rd (USFS 491)*

Description: This picturesque waterfall cuts through quartz-plagioclase-biotite schist and schist rich migmatite. Both upstream and downstream of the falls, the Vermilion River runs parallel to the dominant regional fabric defined by the orientation of the underlying bedded and foliated metasedimentary rocks and generally foliation parallel intrusions of neosome 1 before draining into Crane Lake. Vermilion Falls occupies a N-NW trending, post-metamorphic and post-intrusive fracture and fault zone orthogonal to the dominant internal fabric of the Precambrian bedrock (Fig. 1-3, Fig. 1-11). These fracture and fault networks are ubiquitous throughout the Vermilion Granitic Complex and the Quetico Subprovince and strongly influence the surface topography and outcrop exposure in the area. Little is known about the timing and relative offsets along these fault zones, though correlation of map units on either side of these features suggests only minor relative motion.

Near the upper portion of the falls, tonalitic neosome 1 dikes and sills delaminate the schist along bedding and sub-parallel foliation planes and occupy mesoscopic fold hinges. Downstream, tonalitic neosome 1 dikes are discordant and cross-cut the dominant fabric in the rock.

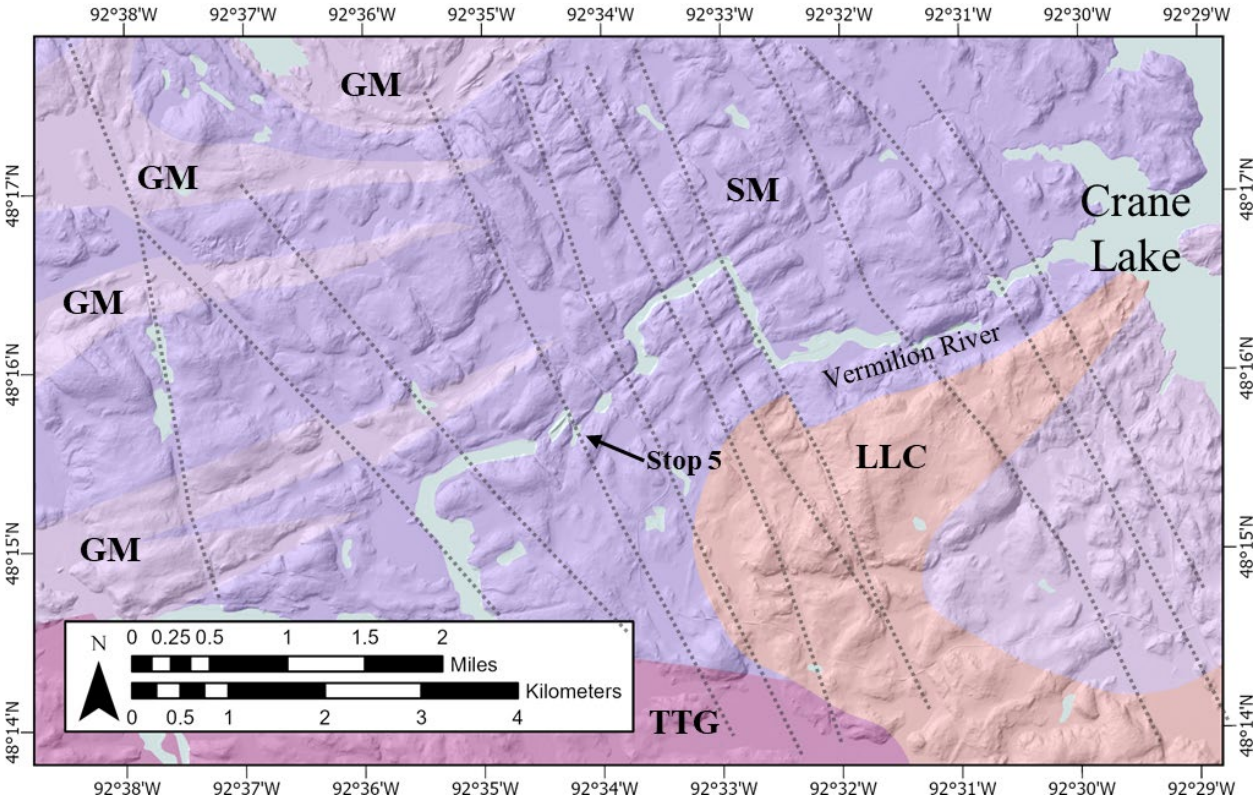


Figure 1-11. Geologic map of the Vermilion Falls area, after Jirsa and others (2011) draped over LiDAR hillshade. NW trending, post-metamorphic and post-intrusive fractures and faults have been highlighted with dashed lines. "GM" - granite rich migmatite, "SM" – schist rich migmatite, "LLC" – Lac La Croix granite, "TTG" – tonalite-trondhjemite-granodiorite gneiss.

Directions: From Stop 4, continue east on Orr-Buyck Road (Highway 23) for 8.5 miles, continue straight along Crane Lake Road (Highway 24) at the village of Buyck for 9.5 miles, turn left onto Vermilion Falls Road (USFS 491) for 5.6 miles, turn left onto single-lane access road to turnaround at the picnic area.

STOP 6 – Echo Lake Quarry

Location: *549810E/5324630N, (48.07300°, -92.33132°), Quarry off USFS 200*

Description: NOTE: This is an active quarry, permission to access this site needs to be granted from the quarry operator prior to visiting.

The photogenic exposures at this dimension stone quarry include washed, glacially scoured outcrops and fresh blast faces of taxitic, red-pink to pinkish grey granitic gneiss and granite with abundant mafic inclusions (Fig. 1-12). This unit is mapped as a gneissic phase of the Lac La Croix of the Vermilion Granitic Complex, temporally related to neosome 2 seen at other stops (Jirsa, 2011). Gneissic layering here is chaotic and boundaries between gneissic phases are diffuse. Abundant mafic inclusions and schlieren ranging from a few centimeters to multiple meters in size and are randomly oriented. Mafic inclusions are delaminated along planar features and have diffuse, fringed boundaries. Increases in the abundance of biotite and

hornblende on the margins of mafic inclusions represent restitic rinds developed during assimilation and interaction with the host granitic melt.

Directions: From Stop 5, return to Crane Lake Road (Highway 24) along Vermilion Falls Road (USFS 491) and turn right. Continue southward on Crane Lake Road (Highway 24) for 5.5 miles and turn left onto Echo Trail. Continue along Echo Trail for 8.3 miles and turn right onto USFS 200 for 5 miles. Turn Left onto unnamed forest road near Gustafson Lake.

RETURN TO MOUNTAIN IRON COMMUNITY CENTER



Figure 1-12. Gneissic granitoid with partially digested amphibolite inclusion.

Directions: From Stop 6, return to Echo Trail via USFS 200 and turn left on Crane Lake Road. Continue south on Crane Lake Road/Orr-Buyck Road to the town of Orr. Turn left onto Highway 53 and continue 44.1 miles to the Highway 169 exit ramp. Turn left onto Enterprise Drive.

REFERENCES

Bauer, R.L., 1985, Correlation of early recumbent and younger upright folding across the boundary between an Archean gneiss belt and greenstone terrane, northeastern Minnesota: Geology, v. 13, p. 657-660.

Bauer, R.L., Czeck, D.M., Hudleston, P.J., and Tickoff, B., 2011, Structural geology of the subprovince boundaries in the Archean Superior Province of northern Minnesota and adjacent Ontario: Geological Society of America Field Guide 24, p. 203-241.

Bauer, R.L., Hudleston, P.J., and Southwick, D.L., 1992, Deformation across the western Quetico subprovince and adjacent boundary regions in Minnesota: Canadian Journal of Earth Sciences, v. 29, p. 2087-2103.

Chandler, V.W., and Lively, 2014, Rock Properties Database; Minnesota Geological Survey web-accessible file data (http://www.mngs.umn.edu/).

Davis, D.W., Pezzutto, F. and Ojakangas, R.W., 1990. The age and provenance of metasedimentary rocks in the Quetico Subprovince, Ontario, from single zircon analyses: implications for Archean sedimentation and tectonics in the Superior Province. Earth and Planetary Science Letters, 99(3), pp.195-205.

Day, W.C., 1990, Bedrock geologic map of the Rainy Lake area, northern Minnesota: U.S. Geological Survey Miscellaneous Investigations Series I-1927, scale 1:50,000.

Day, W.C. and Weiblen, P.W., 1986. Origin of late Archean granite: geochemical evidence from the Vermilion Granitic Complex of northern Minnesota. Contributions to Mineralogy and Petrology, 93(3), pp.283-296.

Fralick, P., Purdon, R.H., and Davis, D.W., 2006, Neoarchean trans-subprovince sediment transport in southwestern Superior Province: sedimentalogical, geochemical, and geochronological evidence: Canadian Journal of Earth Sciences, v.43, p. 1055-1070.

Jirsa, M.A., 2011, Bedrock geology of the Crane Lake and Brule Narrows 30'X60' quadrangles, northern Minnesota: Minnesota Geological Survey, Miscellaneous Map M-192, scale 1:100,000.

Jirsa, M.S., Block, A.R., Boerboom, Chandler, V.W., and Peterson, D.M., 2020, Bedrock geology of St. Louis County, Minnesota: Minnesota Geological Survey County Geologic Atlas C-51, Part A, Plate 2—Bedrock Geology; scale 1:200,000. [contains ancillary digital files including geophysics and geochronology]

Jirsa, M.A., Boerboon, T.J., and Chandler, V.W., 2014, Bedrock geology of the International Falls-Little Fork 30'X60' quadrangles, northern Minnesota: Minnesota Geological Survey Miscellaneous Map M-197, scale 1:100,000.

Le Bas, M., 2007. Igneous rock classification revisited 4: Lamprophyres. Geology Today, 23(5), pp.167-168.

Poulsen, K.H., Borradaile, G.J., and Kehlenbeck, M.M. 1980. An inverted Archean succession at Rainy Lake, Ontario: Canadian Journal of Earth Sciences, v. 17, p. 1358-1369

Salerno, R.A., 2017. Neoarchean Deposition, Metamorphism, And Intrusion In Rapid Succession, Vermilion Granitic Complex, Superior Province Of Northern Minnesota. Master's thesis, University of Minnesota – Duluth.

Sawyer, E.W., 2008. Atlas of migmatites (Vol. 9). NRC Research press.

Southwick, D.L., 1991, On the genesis of Archean granite through two-stage melting of the Quetico accretionary prism at a transpressional plate boundary: Geological Society of America Bulletin v. 103, p. 1385-1394.

Southwick, D.L., and Ojakangas, R.W., 1979, Geologic map of Minnesota, International Falls sheet: Minnesota Geological Survey, scale 1:250,000.

Southwick, D.L., and Sims, P.K., 1980, The Vermilion Granitic Complex—A new name for old rocks in northern Minnesota: U.S. Geological Survey Professional Paper 1124A, p. A1-A11.

Tabor, J.R., 1988, Deformational and metamorphic history of Archean rocks in the Rainy Lake District, Northern Minnesota, [Ph.D. thesis]: Minneapolis, University of Minnesota, 224 p.

Valli, F., Guillot, S., and Hattori, K.H., 2004, Source and tectono-metamorphic evolution of mafic and pelitic metasedimentary rocks from the central Quetico metasedimentary belt, Archean Superior Province of Canada: Precambrian Research, v. 132, p. 155-177.

Williams, H.R., 1990, Subprovince accretion tectonics in the south-central Superior Province: Canadian Journal of Earth Sciences, v. 27, p. 571-581.

Zaleski, E., van Breemen, O. and Peterson, V.L., 1999. Geological evolution of the Manitouwadge greenstone belt and Wawa-Quetico subprovince boundary, Superior Province, Ontario, constrained by U-Pb zircon dates of supracrustal and plutonic rocks. Canadian Journal of Earth Sciences, 36(6), pp.945-966.

FIELD TRIP 2

Drill Core from three Cu-Ni Deposits of the Duluth Complex

Mark Severson[1,2] (retired), Cullen Phillips[3], and Kevin Boerst[4]

[1](1988–2012) *Natural Resources Research Institute, University of Minnesota, Duluth, 5013 Miller Trunk Hwy, Duluth, MN 55811*
[2](2013–2018) *Previously Teck American, then Teck Resources Unlimited, now NewRange (joint venture between Teck and PolyMet Mining Inc.)*
[3]*NewRange Copper Nickel, 6500 Kensington Dr., Hoyt Lakes, MN 55750*
[4]*Twin Metals Minnesota, 400 Miners Drive East, P.O. Box 329, Ely, MN 55731*

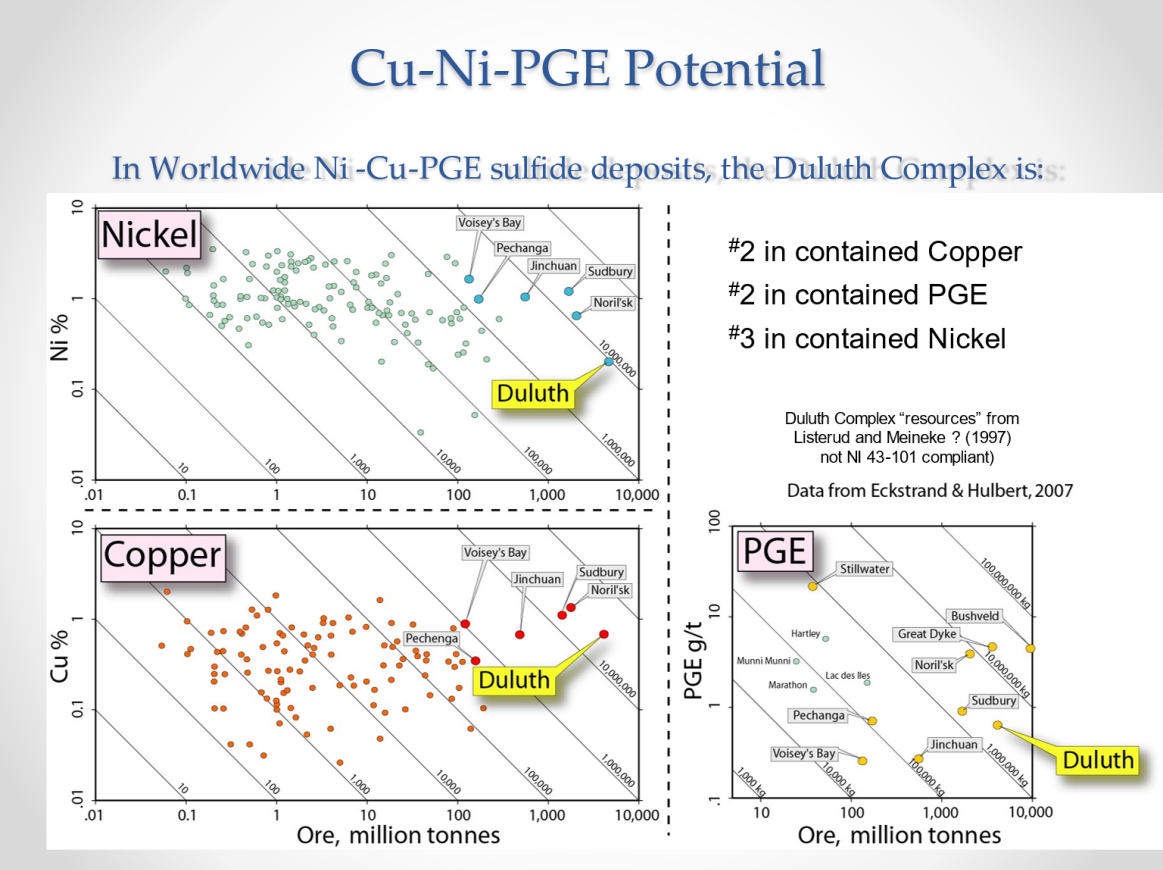


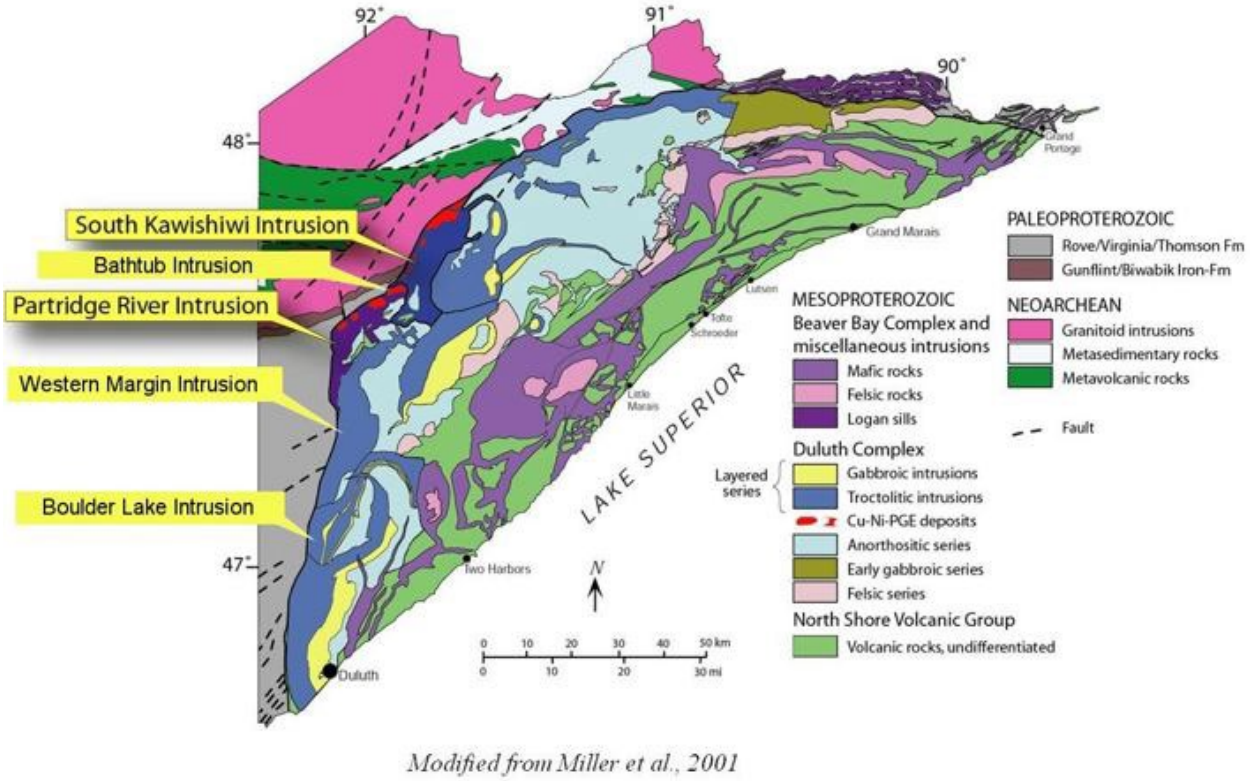
Diagram from Peterson (2010) modified from plots of Eckstrand and Hulbert (2007).

This guidebook is modified and updated from a guidebook published in 2016 for the 62nd Institute on Lake Superior Geology (pdf).

Severson, M., Ware, A., Boerst, K., and Geerts, S., 2016, Cu-Ni-PGE Deposits of the Duluth Complex. Proceedings of the Institute on Lake Superior Geology, Volume 62, Part 2-Field Trip Guidebook, Trip 3, P. 27-78

INTRODUCTION

The Duluth Complex, located in northeastern Minnesota, is a series of tholeiitic intrusions of Keweenawan age (1.1 billion years ago) that formed with coeval flood basalts along a portion of the Midcontinent Rift. The Midcontinent Rift system developed during crustal extension during the Mesoproterozoic era and is traceable in a broad arc that begins in northeastern Kansas extending northward through the axis of Lake Superior and then southeastward into Michigan. The Duluth Complex and associated Keweenawan intrusions constitute one of the largest mafic complexes in the world. These rocks cover an arcuate area over 3,000 square miles (5,000 square kilometers) extending from the city of Duluth northward 170 miles (275 km) to the Canadian border. The northwest, convex edge of the complex defines its basal contact, which dips to the southeast towards the rift. Along this contact the complex is successively underlain by Neoarchean granites (Giants Range granitic rocks) and greenstones (Vermilion District) to the north, and Paleoproterozoic sediments (Virginia Formation and Biwabik Iron Formation) to the south. Roof rocks to the Duluth Complex consist of Mesoproterozoic intrusive and volcanic rocks of the Beaver Bay Complex and North Shore Volcanic Group, respectively. Once recognized as a single large lopolithic intrusion, the complex has since been established to be collectively comprised of numerous smaller sub-intrusions (Figure 2-1) that were episodically emplaced into the base of a comagmatic volcanic edifice between 1108 and 1098 million years ago.



Modified from Miller et al., 2001

Figure 2-1. Generalized geologic map of northeastern Minnesota (modified from Miller et al., 2002).

The Duluth Complex hosts several known large low-grade disseminated Cu-Ni occurrences (Figure 2-2), all of which are located within the basal portions of the Partridge River (PRI), Bathtub (BTI) and South Kawishiwi (SKI) sub-intrusions. A cursory study by Listerud and Meineke (1977) estimated 4.4 billion tons of material averaging 0.66% Cu and 0.20% Ni, using a 0.5% Cu cutoff, in at least nine deposits. Five of these Cu-Ni deposits have recent NI 43-101 reports that estimate a combined mineral inventory well over that amount using lower cutoff values. Known resources (Measured and Indicated, and Inferred) for several of the deposits in Duluth Complex are shown in Table 2-1. Copper-to-nickel ratios generally range from 3:1 to 4:1. Primary mineralization is magmatic. Sulfur source is probably both local (from the footwall sediments) and magmatic. Sulfur isotope studies indicate that most of the sulfur was derived from the Virginia Formation. Most of the mineralization is in the basal portions of these intrusions but there are also local disseminated zones higher in the intrusions. The latter tend to be much more discontinuous except for continuous mineralized horizons, termed "Magenta" style mineralization, that are present at NorthMet and Mesaba, and to a lesser degree, at South Filson Creek. The mineralization styles at each of the Cu-Ni deposits are varied. The general geology and mineralization of the Partridge River, Bathtub, and South Kawishiwi intrusions, as well as the deposits that they host, are presented below.

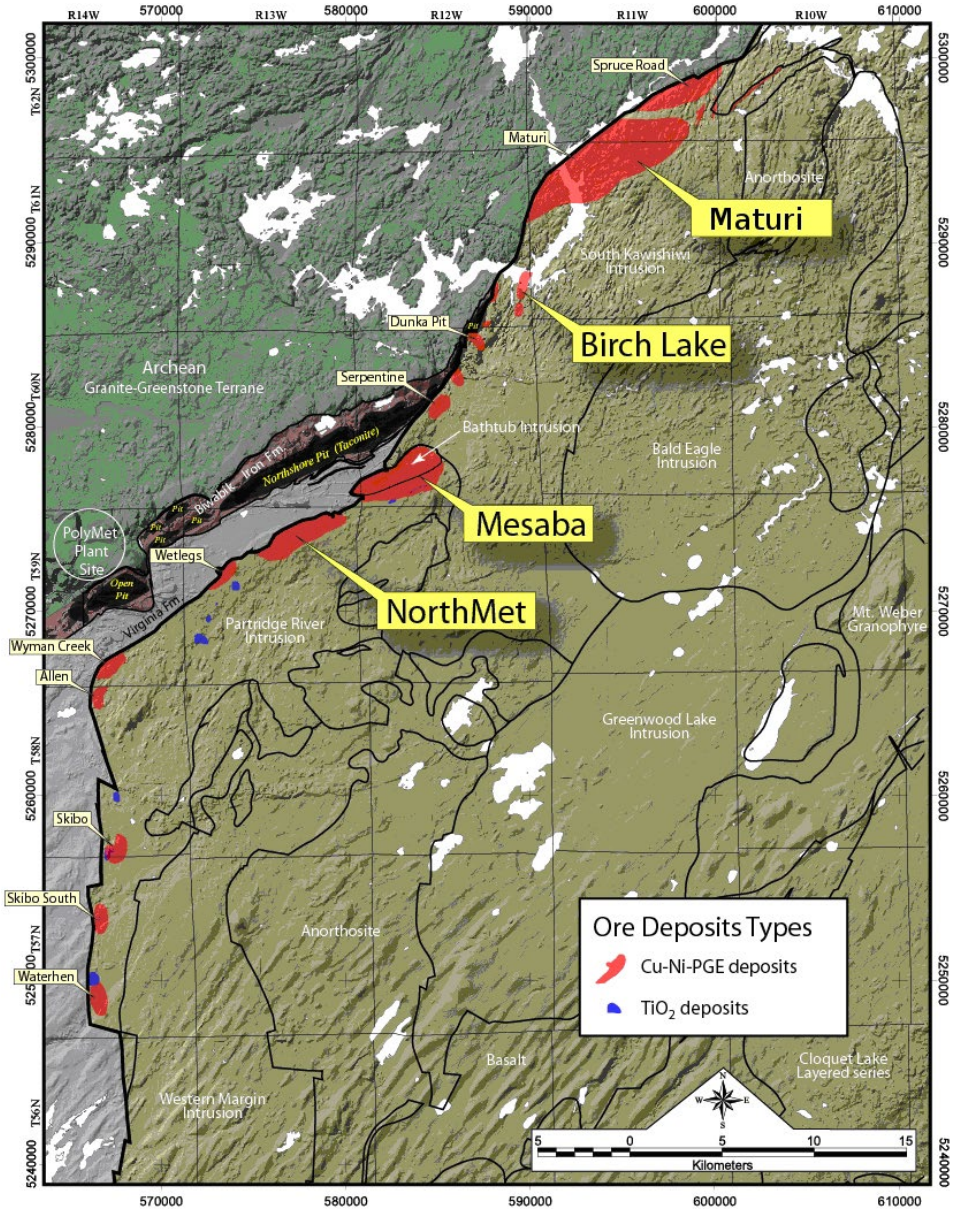


Figure 2-2. Distribution of Cu-Ni-PGE deposits (in red) and potential titanium-enriched ultramafic pipes (OUIs in blue) in the Partridge River, Bathtub, and South Kawishiwi intrusions. Note that the Mesaba deposit is mostly contained in the Bathtub intrusion.

Table 2-1. Known Resources for the Various Duluth Complex Cu-Ni-PGE Deposits at various Cut-Offs. Average values for Co and Ag are available for some of the deposits but are not shown in the table.

Deposit	Tons (st) millions	Cu %	Ni %	Pd ppb	Pt ppb	Au ppb	Cut-Off	Company	Source
Maturi – Measured and Indicated	1,233	0.58	0.19	334	147	80	0.30% Cu	Twin Metals Minnesota	43-101 AMEC Oct-14
Maturi – Inferred	563	0.49	0.16	305	134	68	0.30% Cu	Twin Metals Minnesota	43-101 AMEC Oct-14
Birch Lake – Indicated	100	0.52	0.16	515	235	115	0.30% Cu	Twin Metals Minnesota	43-101 AMEC Oct-15
Birch Lake – Inferred	239	0.46	0.15	370	180	87	0.30% Cu	Twin Metals Minnesota	43-101 AMEC Oct-14
Spruce Road – Inferred	480	0.43	0.16				0.30% Cu	Twin Metals Minnesota	43-101 AMEC Oct-14
Serpentine	425	0.41	0.14				0.20% Cu	Encampment Resources	Non 43-101 Amax 1979
NorthMet – Measured and indicated	702 Open Pit	0.25	0.07	234	67	34	0.20% Cu	New Range Cu-Ni	43-101F1 M3/HRC Dec-22
NorthMet – Inferred	441 Open Pit	0.25	0.07	243	67	34	0.20% Cu	/New Range Cu-Ni	43-101F1 M3/HRC Dec-22
Mesaba – Measured and Indicated	2,207 Open Pit	0.43	0.10	97	34	25	NSR $12/ton	New Range Cu-Ni	43-101F1 IMC/JDS Nov-22
Mesaba – Inferred	1,423 Open Pit	0.37	0.09	143	43	26	NSR $12/ton	New Range Cu-Ni	43-101F1 IMC/JDS Nov -22

Partridge River intrusion

The Partridge River intrusion (PRI) is exposed in an arc-shaped area ~10x20 miles (16x32 km) that extends from the southern edge of the Mesaba deposit on the northeast to the Water Hen deposit on the southwest as shown in Figure 2-2. Footwall rocks include the Virginia Formation and very locally the Biwabik Iron Formation. The basal stratigraphic section (Figure 2-3) was first described by Severson and Hauck (1990) and is briefly summarized below.

Unit I (PR1)

The lowest troctolitic unit of the PRI consists of intermixed troctolite and augite troctolite that locally grade to olivine gabbro. Most of the unit is sulfide-bearing with a PGE-bearing horizon at the top (Red Horizon of Geerts, 1991, 1994). Unique to PR1 are extreme variations in modal mineral percentage and average grain size. Due to this heterogeneous texture, numerous internal contacts divide PR1 into several subunits that are probably related to continuous magma replenishment. Hornfels inclusions of the Virginia Formation are most commonly present within PR1. Near the basal contact the intrusive rocks of PR1 have undergone silica contamination and norite and gabbronorite are often the dominant rock type in the bottom zone.

Unit II (PR2)

This unit is characterized by sulfide-poor, texturally-homogenous, troctolite that locally grades to augite troctolite and leucotroctolite. PR2 grades downward into a persistent ultramafic horizon(s) defined by melatroctolite, with local peridotite zones, that generally exhibits a sharp contact with PR1.

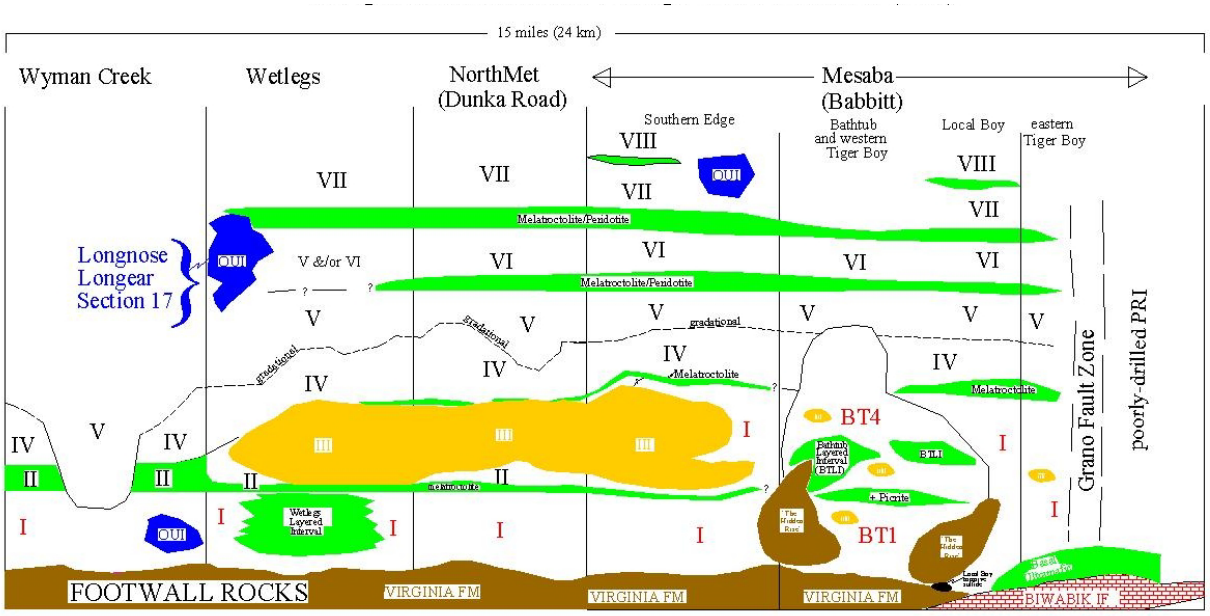


Figure 2-3. Stratigraphy of the Partridge River intrusion at the Mesaba, NorthMet, Wetlegs, and Wyman Creek deposits (note that the Bathtub intrusion is denoted by the BT-series units in the lower right corner). From Severson and Hauck (2008).

Unit III (PR3)

Unit III is the most distinctive "marker bed" of the PRI at the NorthMet, Wetlegs, and southern Mesaba deposits. This unit is fine-grained and is characterized by leucotroctolite that locally grades to troctolite and augite troctolite. In all cases, the rock presents a mottled appearance due to the presence of very coarse-grained (>2 cm) olivine oikocrysts that are irregularly distributed throughout the rock. This mottled-texture and fine-grained nature make PR3 unique relative to all the other units of the PRI. PR3 exhibits variable thicknesses at each of the Cu-Ni deposits and pinches out to the west of Wetlegs and to the southeast of Mesaba. The extreme thickness range for PR3 and its physical attributes (poikilitic) have suggested to several geologists that it may be associated with an earlier Anorthositic Series intrusive phase. In this scenario, PR3 may have been intruded earliest along the Virginia Formation-North Shore Volcanic contact and was later underplated by PR1 and PR2 in an early-formed magma chamber subject to continuous magma replenishment.

Unit IV (PR4)

Unit IV of the PRI is characterized by thick intervals of texturally-homogeneous troctolite and/or augite troctolite. In many areas, PR4 grades upward into a persistent zone of augite-rich augite troctolite and olivine gabbro, which in turn, grades upward into leucotroctolite that is characteristic of PR5. At its base, PR4 has a semi-persistent ultramafic horizon that contains one or more melatroctolite and/or peridotite layers. In some areas a thin semi-massive oxide layer containing very fine-grained chromium titanomagnetite is present immediately above the upper contact of PR3.

Unit V (PR5)

Unit V is generally an easily recognizable unit in that it is characterized by thick intervals of texturally-homogeneous, medium- to coarse-grained leucotroctolite (dominantly anorthositic troctolite). Another feature that aids in distinguishing PR5 is a highly gradational bottom contact into augite troctolite at the top of PR4. The upper contact of PR5 is sharp against one or more ultramafic horizons that mark the base of the overlying PR6.

Unit VI (PR6)

Leucotroctolite (anorthositic troctolite to troctolitic anorthosite) is the most common rock type in PR6. However, near equal amounts of troctolite and augite troctolite are more common in some drill holes at Mesaba. Overall, PR6 becomes more heterogeneous, consisting of multiple rock types, toward the southern and eastern margins of the Mesaba deposit. The base of PR6 is usually marked by a fairly persistent ultramafic horizon.

Unit VII (PR7)

This unit consists almost wholly of homogeneous leucotroctolite at the NorthMet deposit, but it is characterized by a potpourri of rock types at Mesaba with leucotroctolite being slightly more common. Overall, PR7 becomes more heterogeneous, consisting of multiple rock types, toward the southern and eastern margin of the Mesaba deposit. PR7 contains a basal ultramafic horizon(s) in most drill holes.

Unit VIII (PR8)

The uppermost PRI unit that has been drilled at Mesaba is referred to as PR8 that consists of a multitude of rock types with no consistent pattern except that leucotroctolite is slightly more dominant. PR3-like inclusions are excessively common to this unit.

Oxide-bearing Ultramafic Intrusions (OUIs)

Several plug-like, late-stage, oxide-bearing ultramafic intrusions have been delineated in the PRI, the Bathtub intrusion (BTI), and elsewhere within the Duluth Complex (Figure 2-4). The OUIs are intrusive into all units of the PRI and BTI and range in size from large bodies (>200 feet thick, >60 meters thick) to small bodies/lenses (<30 feet thick, <9 meters thick). Rock types are characterized by coarse- to very coarse-grained peridotite and dunite to pegmatitic clinopyroxenite and locally minor orthopyroxenite. These rock types contain varying amounts of ilmenite and titanomagnetite ranging from 5% to massive oxide zones (>80% oxides). The OUIs are in sharp contact with the surrounding troctolitic rocks and are clearly younger. In almost all instances the OUIs are spatially arranged along linear trends suggesting that structural control was important to their genesis.

Two of the OUIs are currently being evaluated for their titanium potential and include: 1. Longnose with a NI 43-101 inferred resource of 65.3 million tonnes of 16.4 TiO_2; and 2. Titac with a NI 43-101 inferred resource of 45.1 million tonnes of 15% TiO_2 (Farrow, 2012). A third OUI, Skibo, is being evaluated for its high-grade Cu-Ni-PGE potential where two vein stockwork zones have been identified by historic drill holes (Inco – up to 6.42% Ni in a 1 foot-thick massive sulfide and other intervals in the hole) and recent drilling by Encampment Minerals (Green Bridge Metals press release, Feb. 6, 2024 at www.greenbridgemetals. com).

NorthMet Deposit (NewRange Copper Nickel)

The NorthMet deposit is located in the PRI as shown in Figures 2-2 and 2-5. This deposit was initially drilled by United States Steel Corporation (USSC) at what they called the Dunka Road deposit. More recent drilling was conducted by PolyMet Mining Incorporated at the now renamed NorthMet deposit that is being developed by NewRange Copper Nickel (Glencore and Teck joint venture). The geology of the deposit consists of seven igneous units, originally defined by Severson and Hauck (1990) as shown in Figure 2-6.

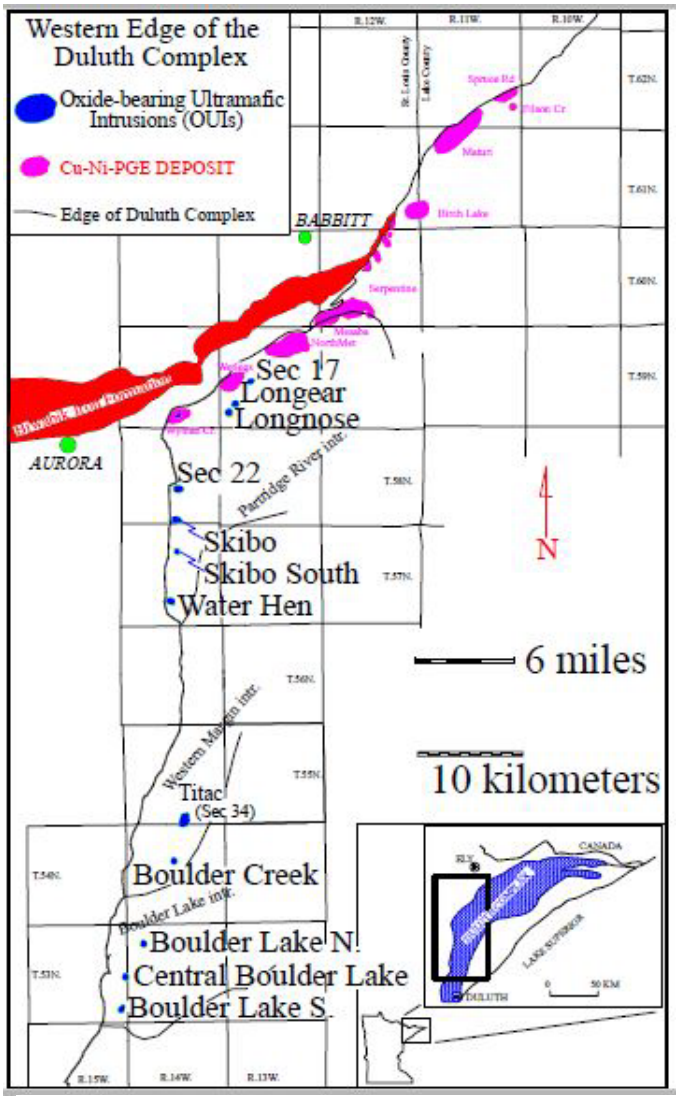


Figure 2-4. Distribution of the Oxide-bearing Ultramafic Intrusions (OUIs) within the Partridge River, Western Margin and Boulder Lake intrusions. Note the linear arrangement of OUI along various trends.

Mineralization Trends at NorthMet

Two open pits are currently planned at the NorthMet deposit - an East Pit and a West Pit (shown in Figure 2-7). The majority of economic mineralization at NorthMet occurs in three scenarios: 1. All of Unit I is mineralized at the East Pit (see cross-section in Figure 2-8); 2. mostly the upper portion of Unit I is the best mineralized in the West Pit (see cross-section in Figure 2-9) and the bottom portions of Unit I will not be mined; and 3. the cross-cutting Magenta Zone (Figs. 2-9 and 2-10) is located well above the basal contact. Grades are generally highest at the top of Unit I and decrease going down hole. However, there are exceptions, and the middle of Unit I contains the highest grades in the center of the deposit.

PGE-enriched zones at NorthMet

Geerts (1991, 1994) found that the top of Unit I often hosts a PGE-bearing zone that he referred to as the Red Horizon (also referred to as Red Zone) which was determined to be approximately 10 meters thick with an average of 0.57% Cu and 986 ppb Pt+Pd. Geerts also found two more PGE-bearing zones within Unit I referred to as Orange and Yellow horizons. All three of these horizons are positioned beneath ultramafic layers suggesting that they are the result of recharge events and magma mixing whereby a new influx of primitive, PGE-bearing magma was injected into the chamber creating the ultramafic layers (crystal settling) before mixing with the resident magma (sulfide-bearing) and forming the PGE-enriched zones beneath them. The continuity of these three PGE-bearing zones in more recent PolyMet/NewRange drilled holes is unknown and the three zones are not specifically mentioned in any NI 43-101 reports or field trip guidebooks. It is important to note that the Red Horizon/Zone has been documented to be present at the top of PR1 at Mesaba (Severson and Hauck, 2003).

Mineralized Magenta Zone at NorthMet

In addition to the Red Horizon, at the top of PR1, there is another PGE-bearing horizon that has been referred to as the Magenta Horizon (or Magenta Zone). This zone is unique in that it crosses several lithologic contacts and progressively downcuts through Units 6, 5, 4, and 3 in a northerly direction (Figure 2-10). The total resource volume of the Magenta zone relative to the rest of the deposit has not been documented in any NI 43-101 reports. Initially, Geerts (1991, 1994) found the Magenta Zone in six holes wherein it averaged about 0.72% Cu and 1,488 ppb Pd+Pt in an over 8 meters thick zone. Cu:Ni ratios in the Magenta Zone are reported to be 3.9-4.1:1. More recent drilling by PolyMet and NewRange has documented the presence of the PGE-enriched Magenta Zone in additional drill holes that are positioned in

the western half of the deposit as shown in Figure 2-8. The Magenta Zone is also present in the PRI along the southern edge of Mesaba deposit to the east where it is referred to as the PRU zone by NewRange Cu-Ni.

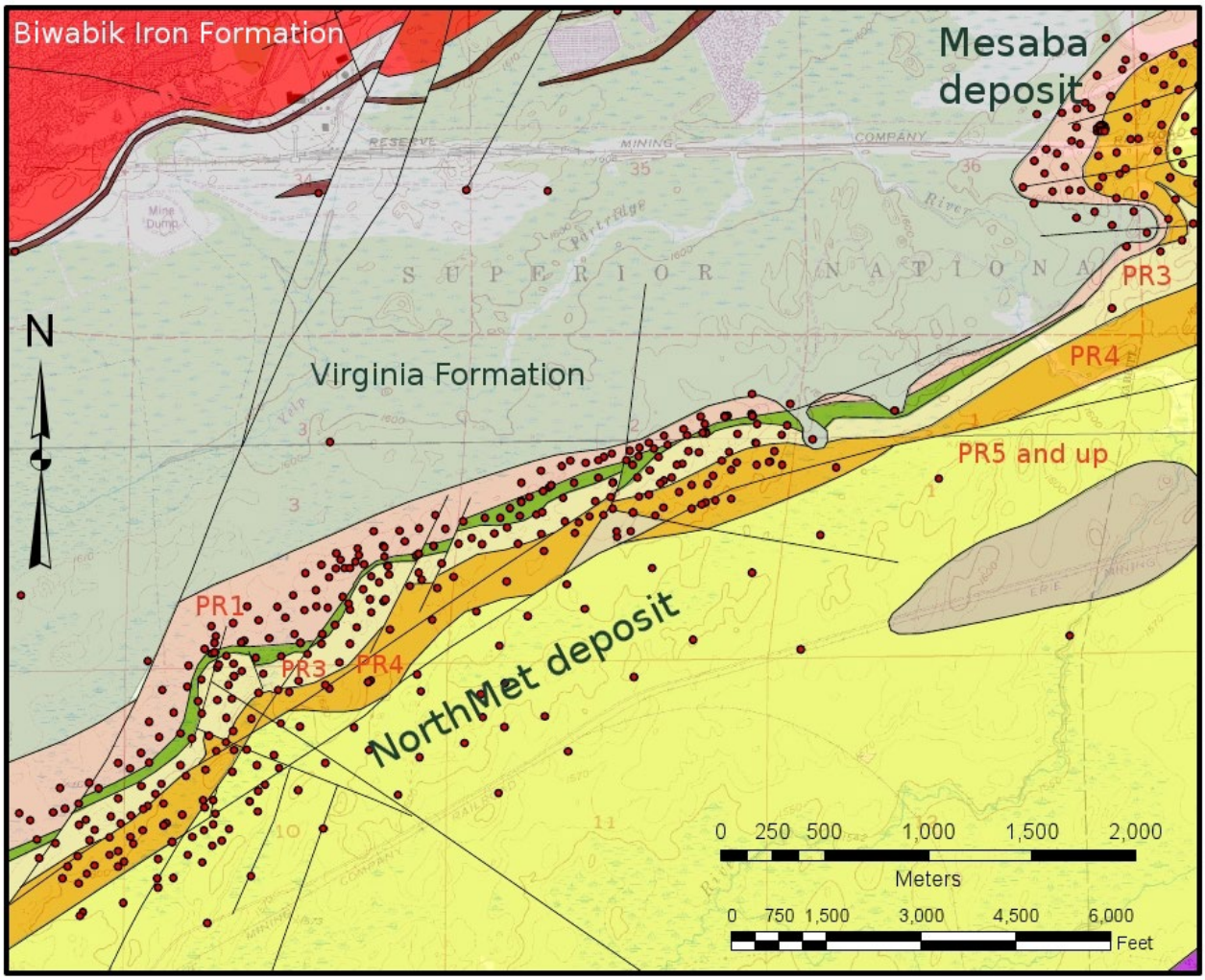


Figure 2-5. Location and geology of the NorthMet deposit relative to the nearby Mesaba deposit. Modified from combined maps of Miller and Severson (2005) and Severson and Miller (2005).

Mesaba Deposit and the Bathtub intrusion (NewRange Copper Nickel)

In 1990, the Natural Resources Research Institute (NRRI) was the first to define and describe the igneous stratigraphy of the PRI (Severson and Hauck, 1990). This same stratigraphy was documented to be present in portions of the Mesaba deposit in 1995 (then referred to as the Babbitt deposit). However, this stratigraphy applied to only the deep drill holes along the extreme southern portion of Mesaba and all

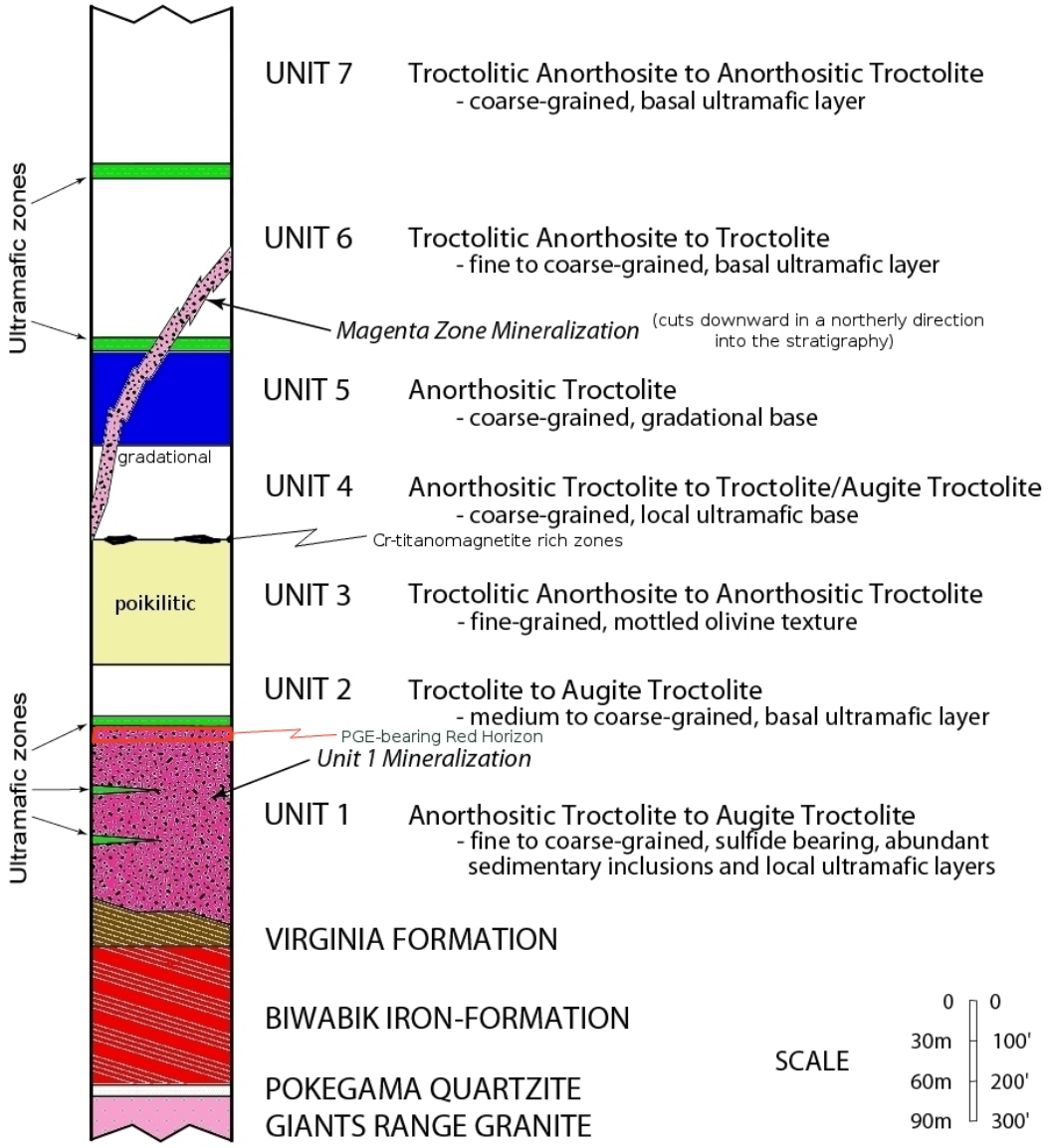


Figure 2-6. Igneous stratigraphic section recognized by NewRange Copper Nickel at their NorthMet deposit (not that these same units are also present along the southern margin of the Mesaba deposit where they are referred to as PR1, PR2, PR3 etc.)

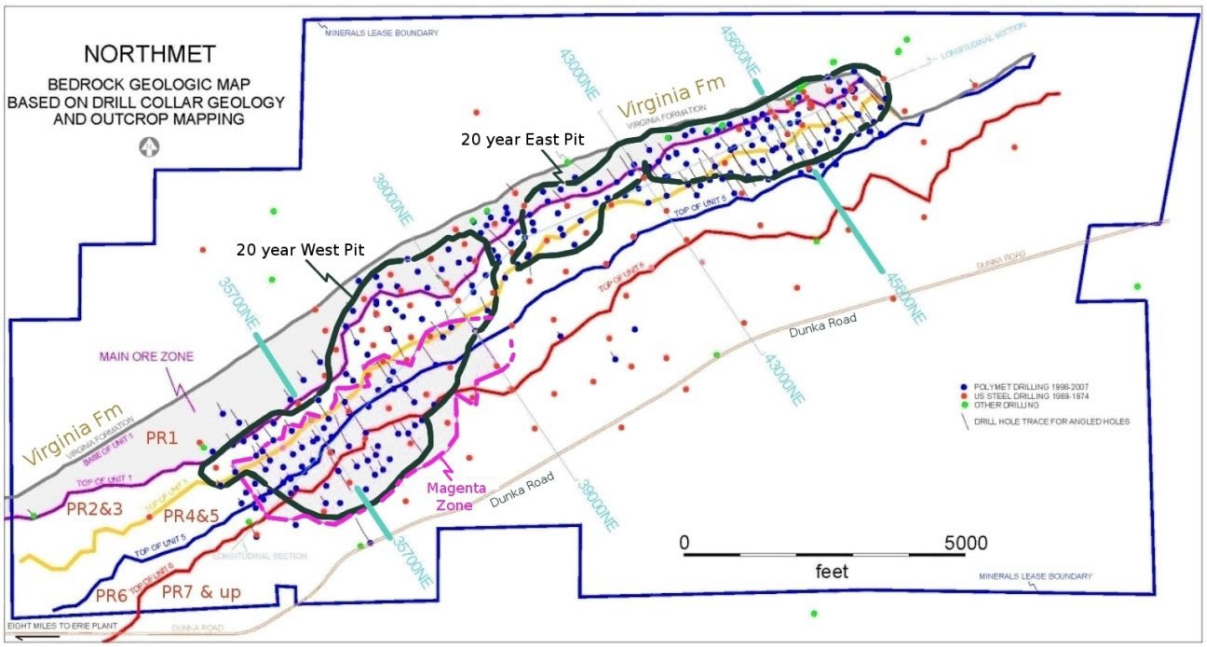


Figure 2-7. Geologic map of the NorthMet deposit showing outlines of the two planned open pits. The location of the mineralized Magenta zone is present in the southern half of the West Pit.

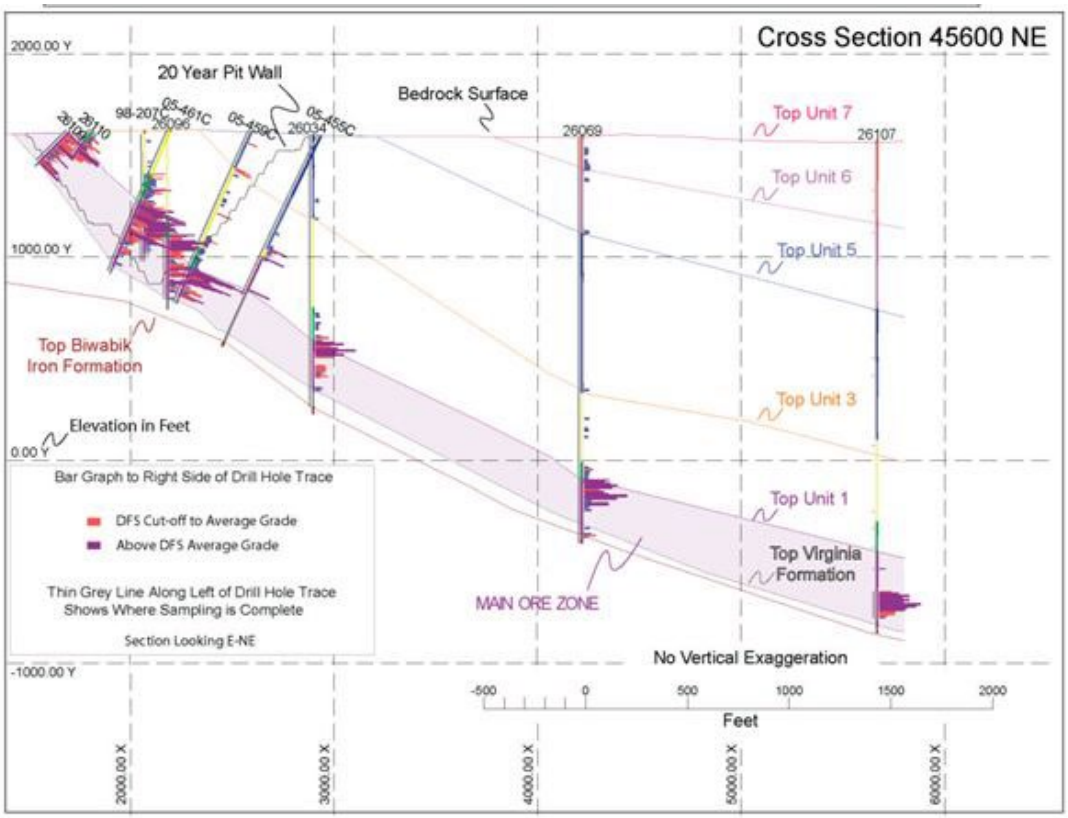


Figure 2-8. Cross-section illustrating mineralization trends in NorthMet's East Pit. Note that all of Unit I is mineralized down to the footwall Virginia Formation.

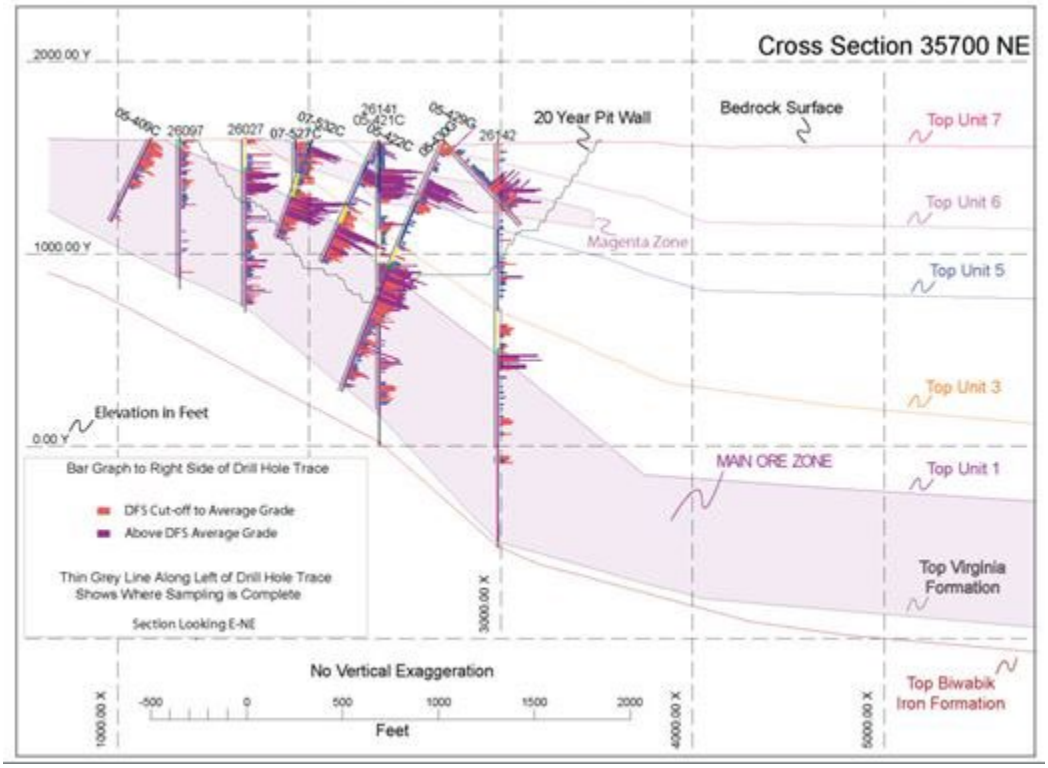


Figure 2-9. Cross-section illustrating mineralization trends in NorthMet's West Pit. Note that the top portion of Unit I will be mined as it exhibits the best mineralization. Note also that the Magenta mineralized zone is present in a downcutting relationship in Units 5, 4, and 3.

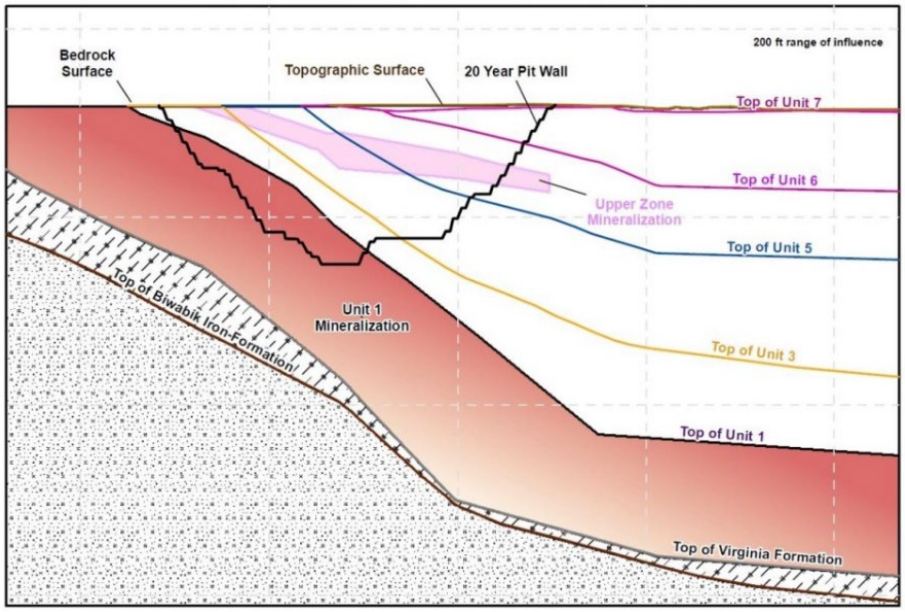


Figure 2-10. Typical cross-section at NorthMet (facing east) showing mineralized zones and modeled units. The "Upper Zone Mineralization" in this diagram is also referred to as the Magenta zone. Note how this zone progressively transects downward into the lower geologic units in a northerly direction.

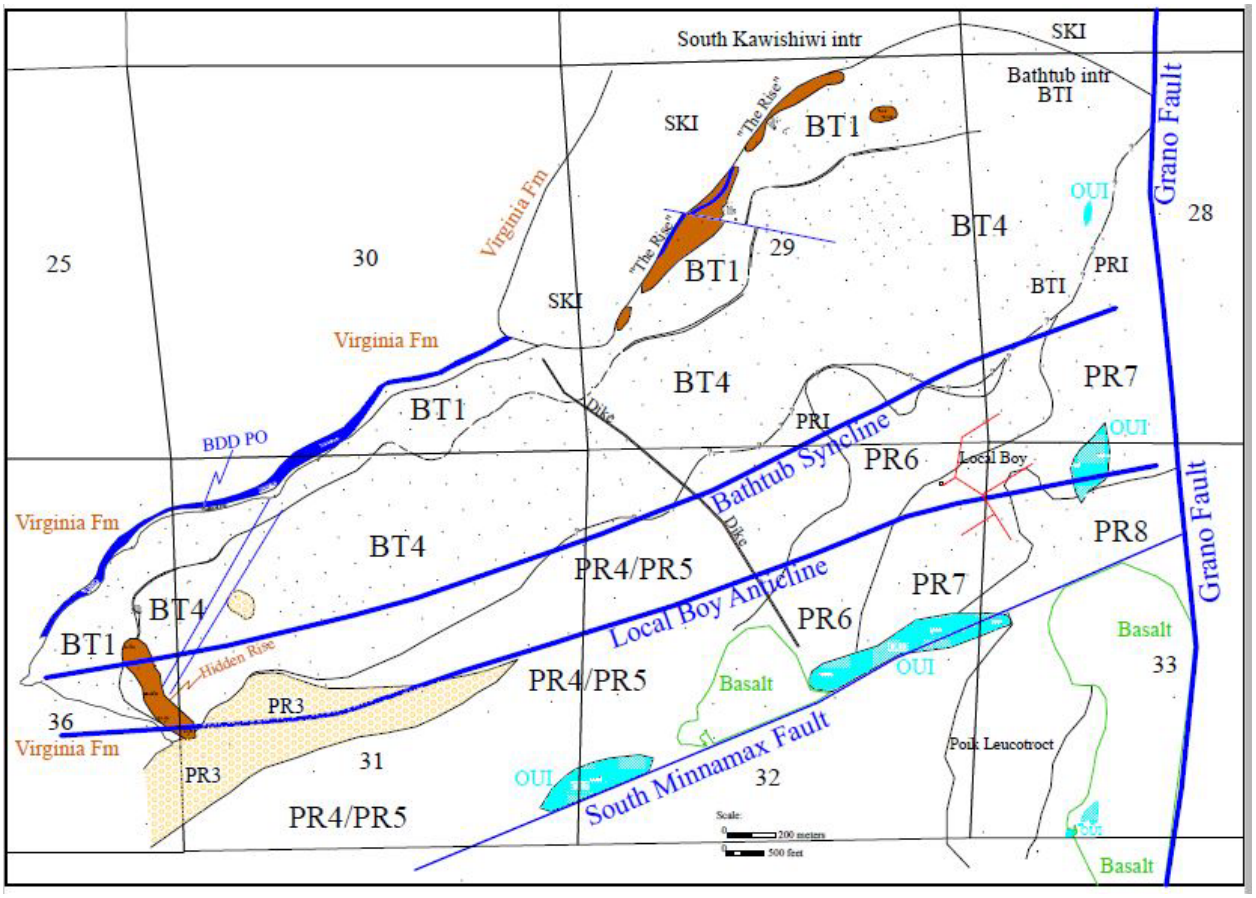


Figure 2-11. Geologic map (circa 2015) showing distribution of major igneous units in the Bathtub intrusion (BTI) and adjacent Partridge River intrusion (PRI) of the Mesaba deposit.

attempts to carry this stratigraphy to the north into the majority of Mesaba were not conclusive. Through several iterative follow-up logging campaigns by the NRRI, the Bathtub intrusion (BTI) was finally recognized as a separate intrusion (Severson and Hauck, 2008). A geologic map of the Mesaba deposit showing the geologic units (per the igneous stratigraphy) is shown in Figure 2-11. At least five criterions, listed below and discussed in Severson and Hauck (2008), were initially used to help separate the PRI from the newly named BTI:

1. Abrupt terminus of the PR3 Unit (major marker bed in the PRI) northward into the BTI at the Mesaba deposit
2. Thicker sections of heterogeneous-textured rock in the BTI relative to the adjacent PRI
3. Lack of PGE-enrichment at the top of a specific unit in the BTI (BT1 Unit) relative to PGE-enrichment at the top of a similar unit (PR1) in the adjacent PRI
4. The best mineralization at Mesaba is near the base of the BTI (base of the BT1 unit) where it is characterized by high Cu grades associated with pyrrhotite- and cubanite-rich zones. In contrast, the best mineralization at the majority of the NorthMet deposit is present at the top of the PR1 unit where it is associated with chalcopyrite-rich zones
5. Use of a hornfels-rich zone, termed the Hidden Rise, was used to help separate the BTI from the PRI.

The current igneous stratigraphy of the Bathtub intrusion, as defined by the NRRI, is summarized in Figure 2-12, and is described in the sections below.

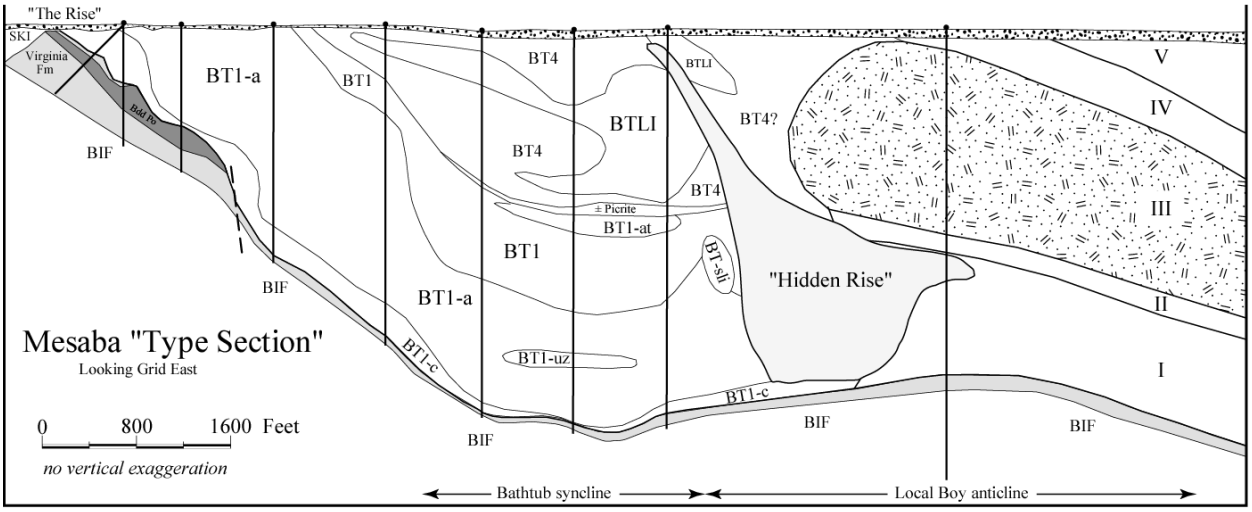


Figure 2-12. Stratigraphic section at the Mesaba deposit showing the relationships between major units (and their corresponding subunits) in the BTI and PRI. Modified from Severson and Hauk (2008).

BT1 Unit

The lowest unit of the BTI consists of intermixed troctolite and augite troctolite with localized leucotroctolite zones. Unique to BT1 are extreme variations in modal mineral percentage and average grain size; both change rapidly over zones that vary from a few feet to tens of feet thick. Due to this heterogeneous texture, numerous internal contacts subdivide the BT1 into several subunits that often cannot be correlated from drill hole to drill hole. Thus, BT1 is a mixture of various troctolitic subunits that are probably related to continuous magma replenishment. Most of this unit is sulfide bearing. Hornfels inclusions of Virginia Formation are common within the BT1 Unit, especially closer to the basal contact. The BT1 Unit has been further subdivided into several internal subunits based on the dominant presence of one rock type over other rock types. Contacts between these rock types vary from highly gradational to abrupt with locally measurable sharp contacts. The various subunits of the BT1 Unit, and hornfels-rich zones in the BT1, are presented in Figure 2-12 and some are briefly discussed below.

- BT1-c – At the base of the BT1 unit there is significant silica contamination of the magma, due to assimilation of the footwall rocks, and orthopyroxene rather than olivine crystallized to produce noritic rocks. Thus, rock types that dominate in the BT1-c subunit range from norite to gabbro norite; especially near either the basal contact or surrounding common hornfels inclusions. Overall, the BT1-c subunit spatially occurs as a rind or coating along the basal contact of the BTI where it ranges anywhere from a foot-thick to over 650 feet-thick.

- "The Rise" – along the extreme northern edge of the entire Mesaba deposit, the basal contact of the BTI rises steeply toward the surface. However, in one area, called "The Rise," the basal contact actually subcrops at the surface and then drops off again in a northerly direction beneath the South Kawishiwi intrusion (see Figure 2-11 for location); A pyrrhotite-rich and graphite-rich unit within the Virginia Formation in "the Rise" has been informally termed the Bdd Po or BDPO unit.

- The "Hidden Rise" – the "Hidden Rise" unit is a loosely-defined zone situated along the crest of the Local Boy anticline (Figures 2-11, 2-12 and 2-13) wherein scattered hornfels inclusions, and associated noritic rocks, are fairly common. Like the BT1-c unit, the Hidden Rise shows evidence

of mixing and contamination with the Virginia Formation. This unit is indicative of strong magma contamination and assimilation of what once may have been a magma chamber wall initially separating the BTI and PRI. Thus, the Hidden Rise is used to both define this hornfels-bearing zone and to artistically, and conveniently, divide the BTI from the PRI.

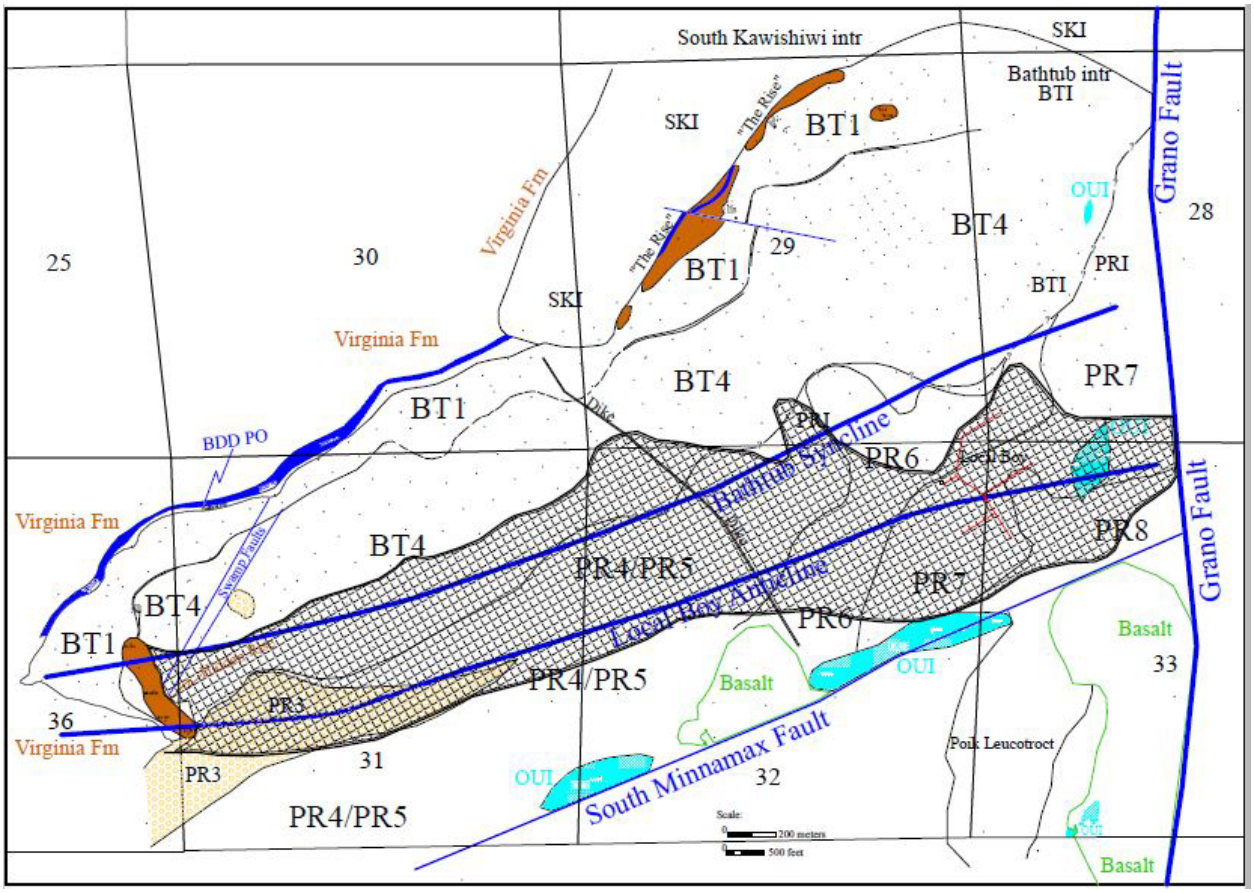


Figure 2-23. Projected distribution of the Hidden Rise at Mesaba relative to structural features. The projected location of the shaft and drifts of the Local Boy ore zone are shown in red. The southern edge of the Hidden Rise is approximated due to a paucity of drill holes.

BT4 Unit

The uppermost unit of the Bathtub intrusion is referred to as the BT4 Unit. It was originally correlated with PR4 of the PRI. However, BT4 is distinctly different from PR4 in that the BT4 Unit is heterogeneous-textured at all scales (though less heterogeneous than BT1 overall), composed of many alternating rock types, and is locally sulfide-bearing. The BT4 Unit appears to grade into thicker, more homogenous troctolitic packages toward the extreme east of the deposit. The BT4 Unit has been further subdivided into several more internal subunits based on the dominant presence of one rock type over other rock types. All these various subdivisions of the BT4 Unit are shown Figure 2-12 and are discussed below.

- "± Picrite – the base of the BT4 is defined by a semi-persistent ultramafic layer and/or package, consisting of melatroctolite to peridotite ± troctolitic beds that is referred to as the "± Picrite." The "± Picrite is present in about 60% of the drill holes in the Bathtub Intrusion and acts as a local horizon that defines the BT1-BT4 contact; however, in many instances the "± Picrite is absent and the BT1-BT4 contact is arbitrarily chosen based on its presence in nearby drill holes.

- Bathtub Layered Interval (BTLI) – this subunit designates zones (see Figures 2-12 and 2-14) where ultramafic layers are extremely common within the BT4 Unit. The ultramafic layers may represent repetitious cyclic layers and can be correlated in drill holes as an overall rock package. The inclination of internal contacts and modal bedding associated with the ultramafic layers are highly variable, ranging from 5° to 80° (even within a single drill hole). Individual ultramafic beds cannot be traced with certainty between drill holes; however, correlations of packages of the BTLI can be traced. This dichotomy for individual ultramafic beds indicates that the bedding relationships are extremely complex in the third dimension and may be related to rapid pinch-out of individual beds. In addition, the BTLI package fades out to the north with increased distance away from the Hidden Rise. If the Hidden Rise represents a magma chamber wall, the BTLI may have crystallized against it via either a static crystallization method or by current-driven crystal settling against the wall.

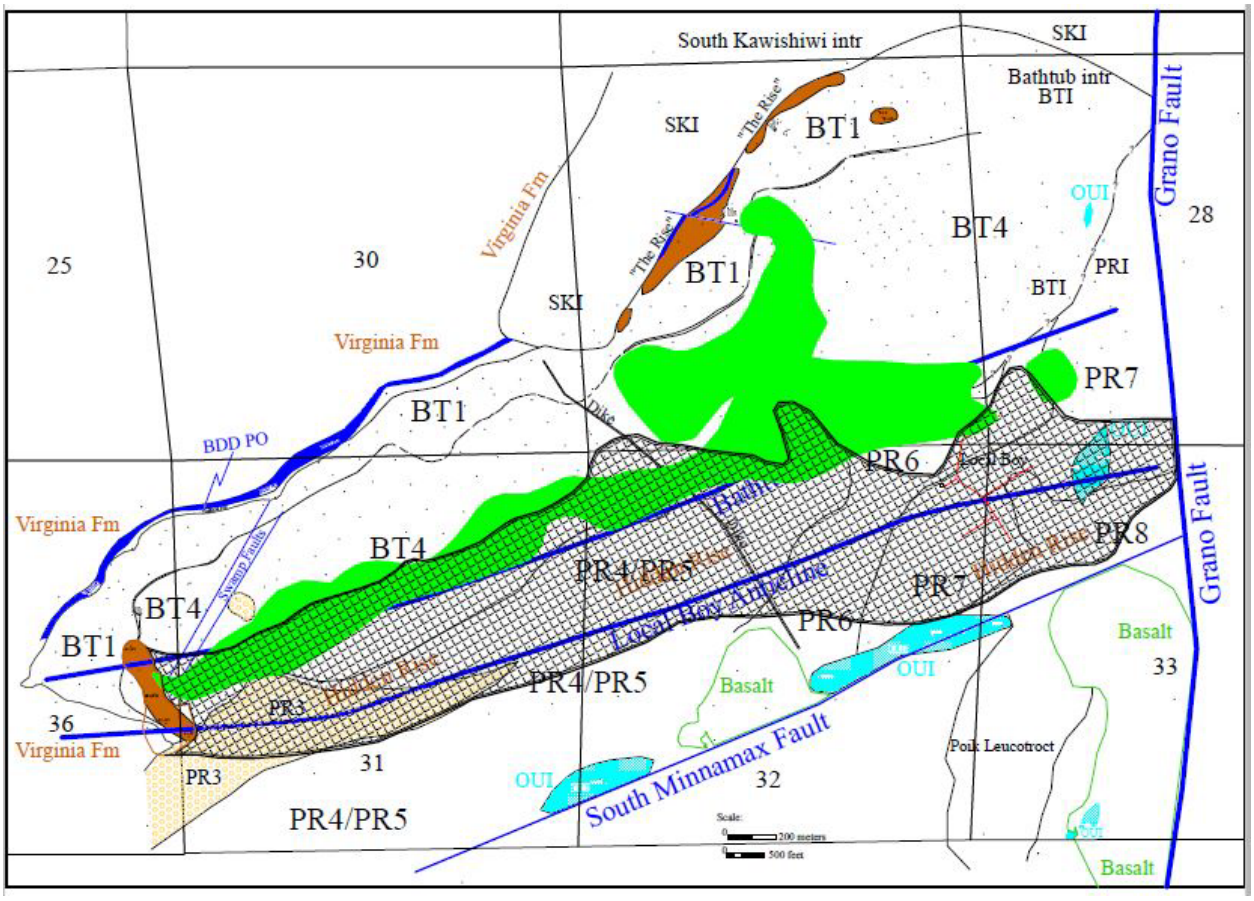


Figure 2-34. Spatial distribution of the BTLI (in solid green hatch) relative to Bathtub syncline and the Hidden Rise (cross-hatched zone). This map is circa 2015 and changes have been made by NewRange Copper Nickel based on newer information.

Footwall Rocks

The footwall rock types at both the NorthMet and Mesaba deposits consist mainly of the Virginia Formation, Biwabik Iron Formation (BIF), and very locally the Pokegama Quartzite. All are Paleoproterozoic in age (approximately 1.9-1.8 billion years ago) and collectively comprise the Animikie Group. The rock types of the Virginia Formation and BIF have undergone metamorphism and partial melting that was produced during emplacement of the Duluth Complex. The metamorphic variants of the footwall rocks are schematically portrayed in Figure 2-15 but are not discussed individually herein.

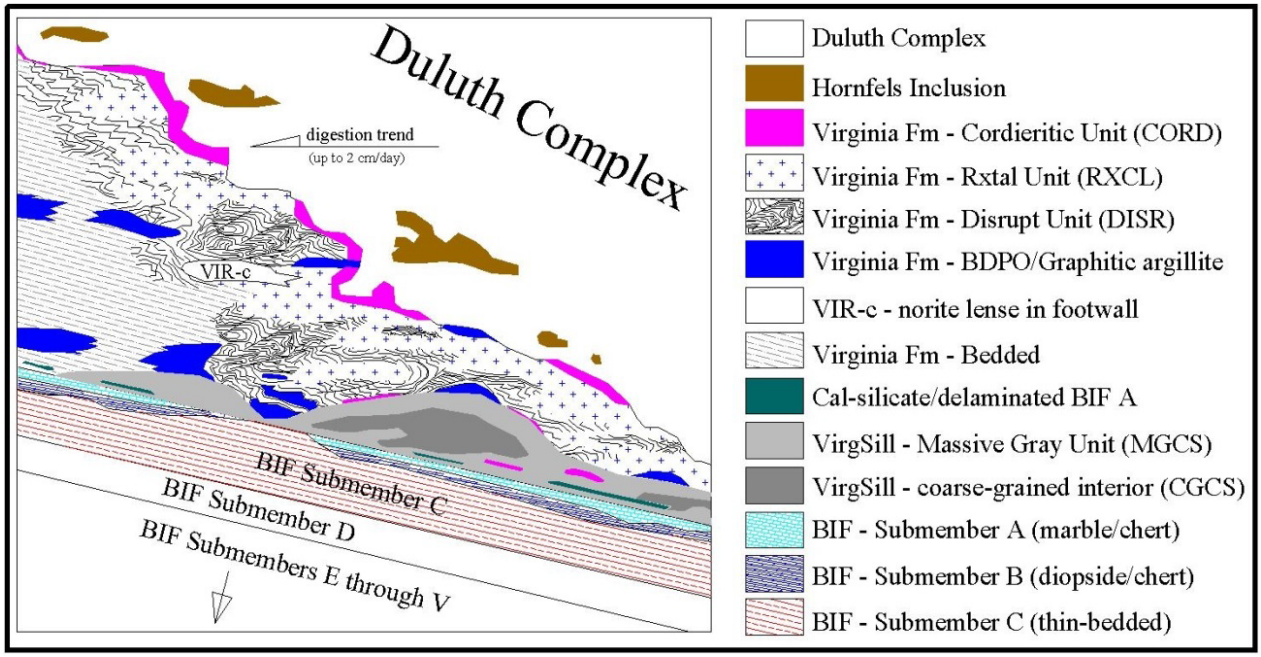


Figure 2-45. General Relationships of the Metamorphosed Footwall Rocks beneath the Duluth Complex at the Mesaba, NorthMet, Wetlegs, and Serpentine Deposits. See Severson and Hauck (2008) for more information.

Structural Features

There are several prominent structural features at Mesaba that were important to formation of the BTI and possibly to mineralization trends. These major features are shown in Figure 2-16 and discussed below (features such as the Rise and the Hidden Rise have been discussed previously).

Local Boy anticline and Bathtub syncline

The most prominent structural features at the Mesaba deposit are a pair of east-west trending parallel folds, defined by contouring the top of the footwall Biwabik Iron Formation (Figure 2-17), that are informally referred to as the Local Boy anticline and Bathtub syncline. Both of these folds probably exerted strong controls on the style of emplacement of the BTI and its basal contact mimics the form of the anticline and syncline. The trend of the Hidden Rise, the possible wall once separating the BTI and PRI, also correlates with these two fold axes. The structural history regarding the Local Boy anticline and Bathtub syncline appears to be extremely complicated and long lived.

Grano Fault

Along the far eastern edge of the Mesaba deposit is the north-trending Grano Fault (Fig. 2-16), so named for the abundant and sometimes voluminous amounts of associated late granitoid lenses and OUIs that are associated with the fault zone (Severson, 1994). Both types of late intrusive lenses are interpreted to be steeply oriented and to have been injected along subsidiary fault zones parallel to, and immediately west of the Grano Fault. These late intrusives cross-cut the troctolitic rocks and thus, demonstrate that the

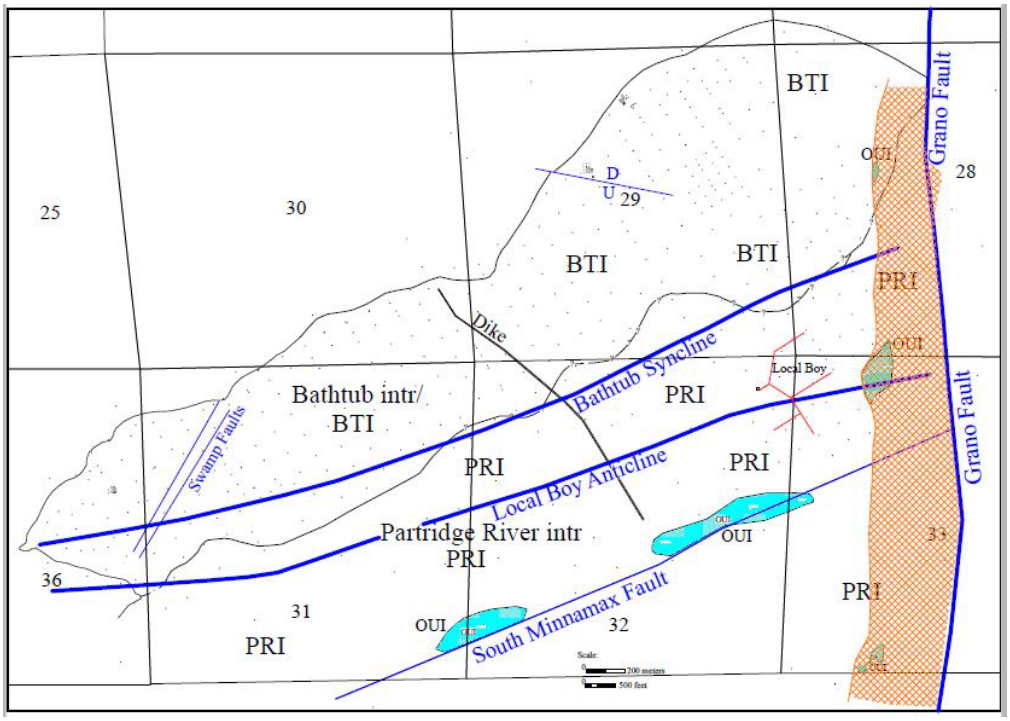


Figure 2-56. Major structural features at the Mesaba deposit. Note the orange-outlined zone to the immediate west of the Grano Fault is a zone wherein late stage subvertical lenses of granitoid and OUI (cyan outlines) commonly cross-cut the troctolitic rocks of the PRI and BTI. OUI (outlined in cyan) are also common along the inferred trace of the South Minnamax Fault.

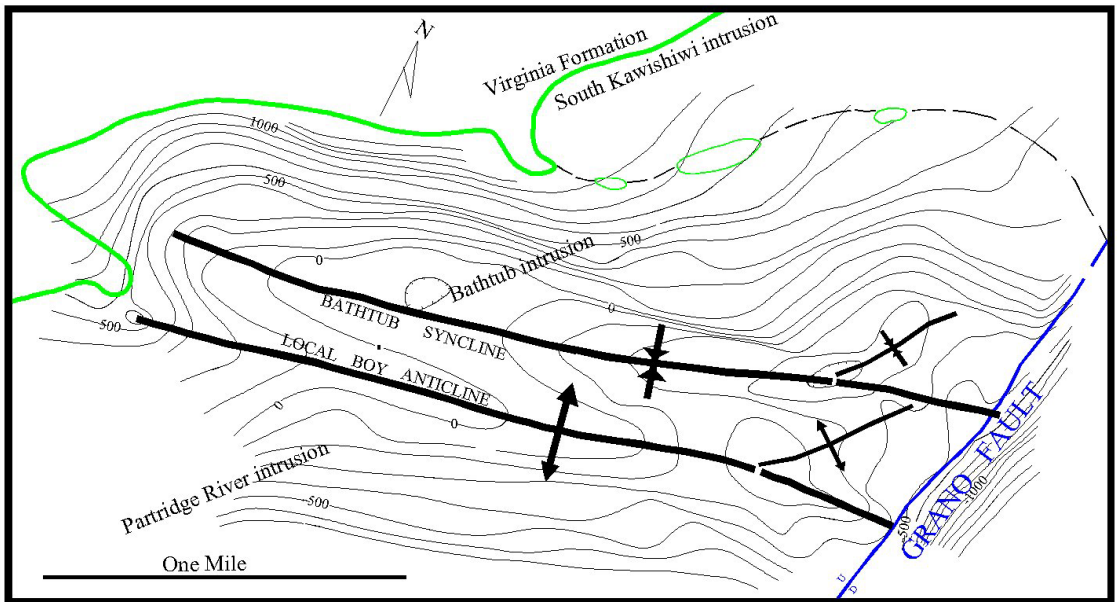


Figure 2-67. Contoured top of the footwall beneath the Mesaba deposit relative to sea level. The contour interval is 100 feet. Note that the contoured lines in this map are derived from Severson and others (1994) and do not take into account any of the more recent drill holes; however, the overall trends would remain basically the same.

fault was active during and after emplacement of the PRI, BTI and SKI. The Grano Fault is thought to be a primary feeder structure for the BTI and possibly the massive sulfides at the Local Boy ore zone (Severson and Hauck, 2008).

South Minnamax Fault

The South Minnamax Fault is an east-west trending fault along the extreme southern edge of the Mesaba deposit. Several OUIs occur at the surface along the trend of the fault (Figure 2-16). Displacement of the fault, based on correlations and projections of units between only six drill holes, is generally 100-200 feet (30-61 meters), but in one area a displacement of over 400 feet (122 meters) is indicated.

Mineralization

The Mesaba deposit is characterized by disseminated sulfide mineralization that occurs most commonly as fine- to coarse-grained, intercumulus disseminations of chalcopyrite, cubanite, pentlandite, and pyrrhotite. The most important continually mineralized zone at Mesaba is a basal zone with disseminated sulfides that is present within all or portions of the BT1 unit, and locally in the bottom of the BT4 unit (Figure 2-18). This zone commonly ranges between 200 and 600 ft (61 to 183 m) in thickness. Higher in the intrusive package, often overlapping the BT1-BT4 unit boundary, are thinner, secondary zones of erratic and discontinuous, disseminated sulfide mineralization referred to as "cloud zones."

Increased sulfide contents with depth are obvious in drill core and are manifested mainly by increasing amounts of pyrrhotite and cubanite. This dramatic increase in pyrrhotite and cubanite with depth appears to be related to contamination from the footwall rocks and has been classified as occurring mainly in the basal contaminated BT1-c unit but there are exceptions.

Talnakhite [$Cu_9(Fe,Ni)_8S_{16}$] is present in numerous holes coincident with the axis of the Bathtub syncline (and north of the Hidden Rise), as well as, in the massive sulfides at Local Boy, as shown in Figure 2-19. Talnakhite occurs as exsolution lamellae with chalcopyrite and cubanite. Talnakhite is difficult to distinguish from chalcopyrite in freshly drilled core. However, talnakhite tarnishes rapidly, sometimes within 10-15 minutes depending on the relative humidity, to a purplish brown or peacock blue similar to bornite (orange-brown color in polished sections).

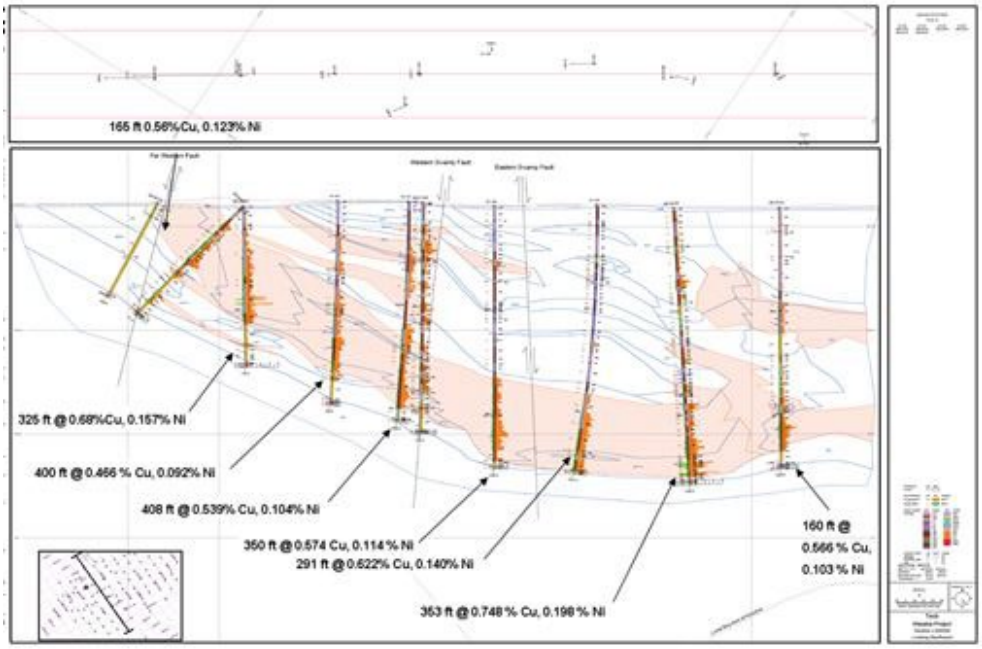


Figure 2-78. Typical cross-section at the Mesaba deposit showing mineralization throughout most of BT1 and in portions of BT4. Note the discontinuous "cloud zone" occurrences in the upper portions of the BT4 unit.

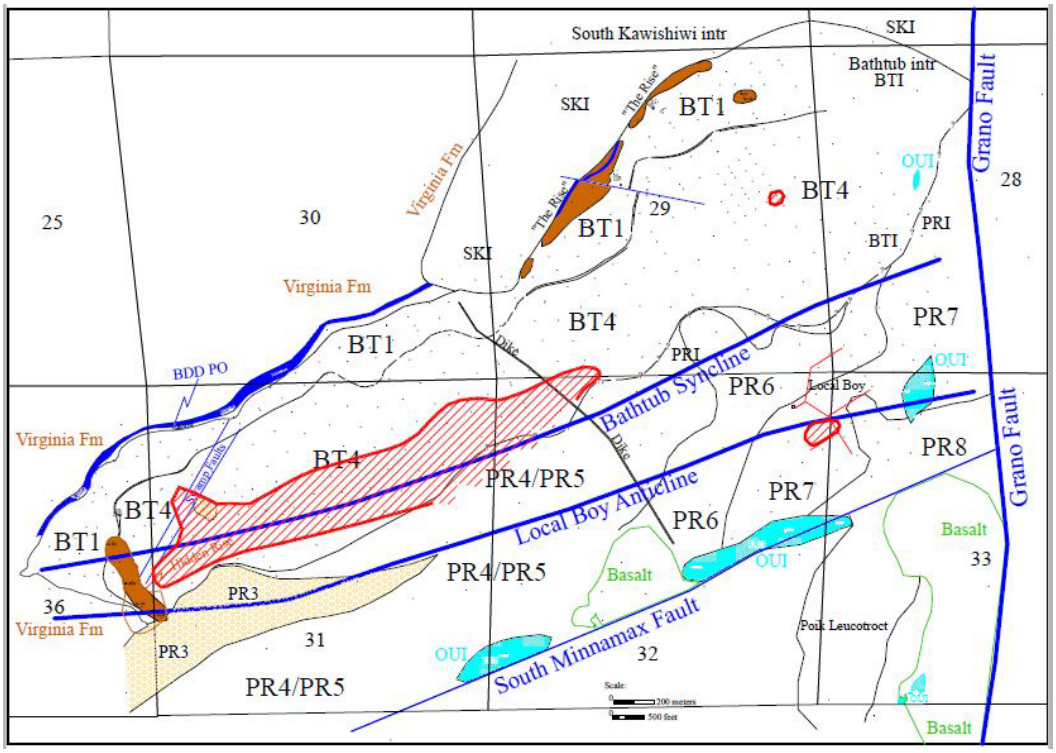


Figure 2-89. Distribution of holes that contain significant amounts of Talnakhite based on tarnished relationships observed on drill core. This map is circa 2015. Note that the Local Boy ore zone, shown in lower right red ovoid, also contains significant talnakhite.

Massive Sulfides at the Local Boy Ore Zone of the Mesaba Deposit

Cu-rich massive sulfides near the basal contact of the Complex are locally present at the Mesaba deposit in a small zone referred to as the Local Boy ore zone. In 1976, AMAX Inc. completed a 1,700-foot-deep exploratory shaft (Minnamax shaft), and in 1977, completed four drifts (A, B, C, and D; Figures 2-20 and 2-21). Underground Fan drilling (217 holes) was completed in 1978 to further define the massive sulfide distribution. Potential ore resources for Local Boy are presented in Table 2-2; high PGE values (up to 11 ppm Pd and up to 8 ppm Pt) are locally present in the ore. Sulfide minerals include pyrrhotite, pentlandite, chalcopyrite, talnakhite, cubanite, maucherite (nickel arsenide), sphalerite, bornite, late mackinawite, chalcocite, covellite, godlevskite, and native silver (Severson and Barnes, 1991).

Table 2-2. Grade/tonnage data for Cu and Ni in the Local Boy ore zone. These values are for geologic resources, not mineable ore. From Severson and Barnes, 1991.

Cu% cutoff grade	MM tons above cutoff	Avg Cu% above cutoff	Avg Ni% above cutoff
0.00	21.9	1.08	0.20
0.60	10.2	1.78	0.36
1.00	5.3	2.71	0.55
2.00	2.2	4.65	0.94
3.00	1.4	5.84	1.12
4.00	1.0	6.75	1.19
5.00	0.7	7.94	1.25
6.00	0.5	9.04	1.18
7.00	0.3	10.54	1.18

The Local Boy ore zone is also situated over the Local Boy anticline. The majority of massive sulfide ore zones, hosted mainly by the Virginia Formation (Severson and Barnes, 1991), are broadly

coincident with the axis of the anticline. The contoured top of the BIF in the Local Boy area is shown in Figure 2-20 (left). Similar anticline geometries are also present for the basal contact as shown in Figure 2-20 (right). All the data indicate that an EW-trending anticline is the major structural feature present within the footwall rocks of the Local Boy area.

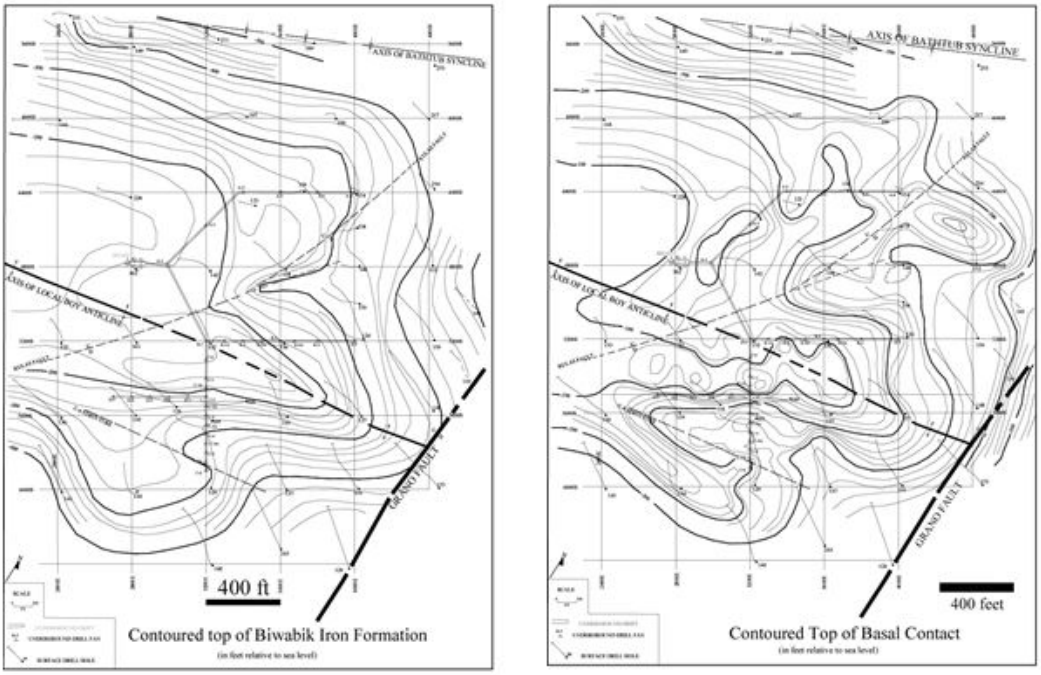


Figure 2-20. Contoured top of the Biwabik Iron Formation at Local Boy (left) and the contoured top of the basal contact between the Virginia Formation and the intrusive rocks at Local Boy (right).

Mineralization Trends in the Massive Sulfide at the Local Boy Ore Zone

The vast majority of massive sulfides at Local Boy are contained within the Paleoproterozoic Virginia Formation. Even though the massive sulfides straddle the basal contact, most of the massive sulfides are associated with either hornfelsed sedimentary inclusions above the contact or with footwall rocks below the contact while the interfingering intrusive rocks (mostly norite) are relatively barren of massive sulfides (Severson and Barnes, 1991). This suggests that the massive sulfide ores were not formed in this area by the gravitational settling of sulfides, but rather, the ores formed by injection of an immiscible sulfide melt into structurally prepared areas within the footwall rocks along the Local Boy anticline in a vein-like setting. A similar mechanism is proposed for the Norilsk-Talnakh deposits in Russia.

Even though the basal contact of the Complex with the Virginia Formation is highly undulatory, the massive sulfides exhibit a definite top and bottom. Figure 2-21 is an attempt to show, in plan view, where massive sulfide zones are present. Also shown in the figure are the different massive sulfide types (ranging from pyrrhotite-dominant to Cu-rich) relative to structural features. The relationships shown in Figure 2-21 indicate that the massive sulfides show a progressive change in an east-to-west direction from Cu-poor massive sulfides to Cu-rich massive sulfides in the vicinity of the Local Boy anticline. These relationships suggest that the injected immiscible sulfide melt underwent fractional crystallization and progressively became more Cu and PGE enriched as it moved through the footwall rocks in an east-to-west direction.

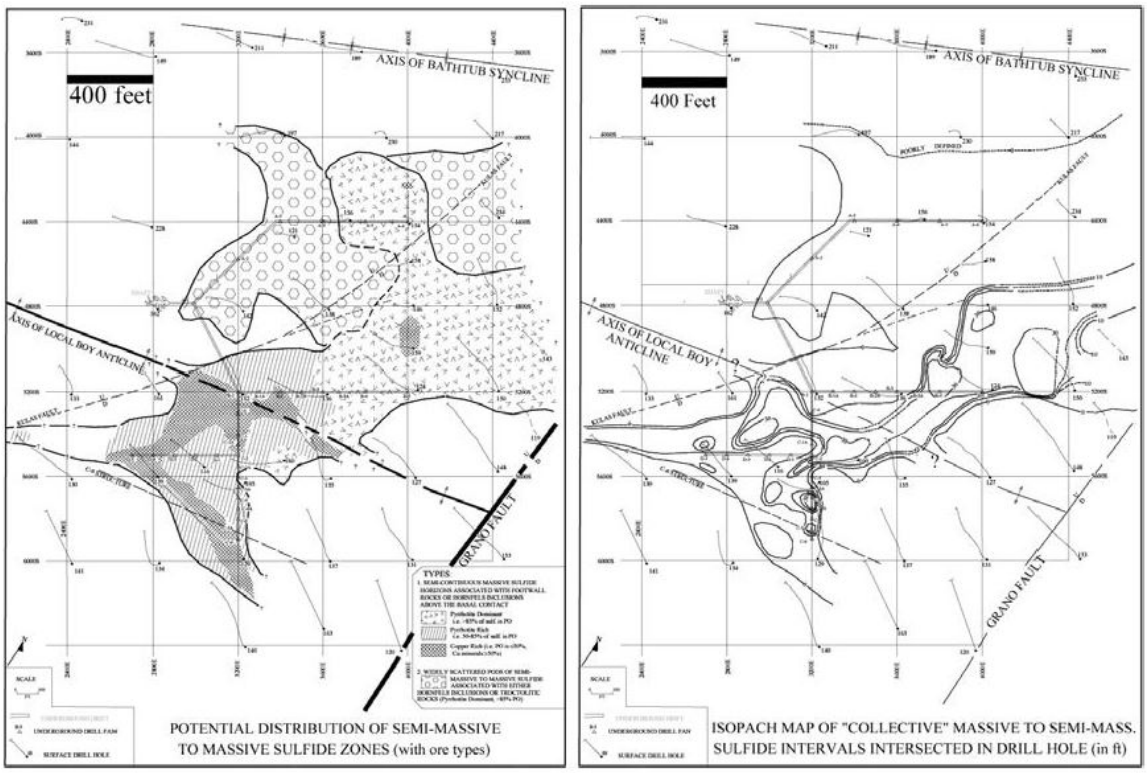


Figure 2-29. Potential distribution of semi- massive to massive sulfide types (Cu-poor versus Cu-rich) at the Local Boy ore zone (left); and an isopach map of cumulative thickness of the massive sulfides (right). Note that the massive sulfides are not present as a continuous blanket, but rather, as one or more stacked disjointed/separated multiple horizons near the basal contact.

A possible feeder vent for the sulfide injection event may have been the Grano Fault, which was repeatedly reactivated during emplacement of the Complex. Other data that indicates that the Grano Fault was a potential feeder vent include: 1) the massive sulfides are more common, and thicker (Figure 2-21 right), close to the Grano Fault (feeder) and along the axis of the Local Boy anticline (structurally-prepared site); 2) the VirgSill, at the base of the Virginia Formation, rarely contains significant amounts of disseminated sulfides – except near the Grano Fault; and 3) the Biwabik Iron Formation rarely contains sulfides – except near the Grano Fault.

In summary, the massive sulfides at the Local Boy ore zone are interpreted to be structurally controlled in that they are situated along the axis of the Local Boy anticline. The massive sulfides are Cu-rich (5-25% Cu) and are almost exclusively hosted by the Virginia Formation. Sulfide textures suggest that the massive sulfides were injected as an immiscible sulfide melt into the footwall rocks. The overall pattern of sulfide types and PGE contents suggest that the sulfides formed via a process of fractional crystallization of an immiscible sulfide melt as it migrated into the footwall rocks. The Grano Fault is inferred to represent the potential feeder zone in this scenario.

Wetlegs Deposit

The Wetlegs deposit (Figures 2-2 and 2-3) was drilled by Bear Creek (13 holes) and Exxon (12 holes). Exxon determined that there were 38 million tons of material at a 0.57% Cu equivalent (files at DNR) but details regarding their cursory calculations are unknown. Most of the igneous units that are present at NorthMet are also present at Wetlegs except: Unit II thins down to a single ultramafic horizon positioned immediately below Unit III (Figure 2-3), and Unit I contains abundant ultramafic layers that are referred to as the Wetlegs Layered interval (Miller and others, 2002). The top of Unit I (aka Red Horizon of the NorthMet deposit) contains scattered anomalous concentrations of PGEs up to 3,132 ppb Pd+Pt (Severson and Hauck, 2003). The Magenta Zone is also present at Wetlegs, but is only known in one drill hole (A4-11) with up to 6,072 ppb Pd+Pt. No work has been conducted on this property since 1998.

Wyman Creek Deposit (Encampment Minerals)

The Wyman Creek deposit (Figures 2-2 and 2-3) is located at a turning point in the basal contact of the PRI – the contact trends northeast to the east of Wyman Creek and then exhibits a drastic change to a north-south orientation to the south of the deposit. This area was initially drilled by Bear Creek, followed by more extensive drilling (21 holes) by United States Steel Corp. (USSC), and very limited drilling by Exxon. USSC determined (literally a back-of-the-envelope calculation) an open pit potential of 14 million tons of material containing 0.30% Cu and 0.18% Ni (Severson and Heine, 2007).

South Kawishiwi intrusion

The South Kawishiwi intrusion (SKI) is exposed in an arc-shaped area ~5x20 square miles (8x32 square km) that extends from the Serpentine deposit on the southwest to the Spruce Road deposit on the northeast as shown in Figure 2-2. Footwall rocks include the Virginia Formation, Biwabik Iron Formation, and granitic rocks of the Neoarchean Giants Range granitic complex; the latter is the dominant footwall rock type. The basal stratigraphic section (shown in Figure 2-22) is known in detail from studies of historic drill core (Severson, 1994; Zanko and others, 1994) and is divided into 17 different units that are present over a strike-length of 19 miles (31 kilometers).

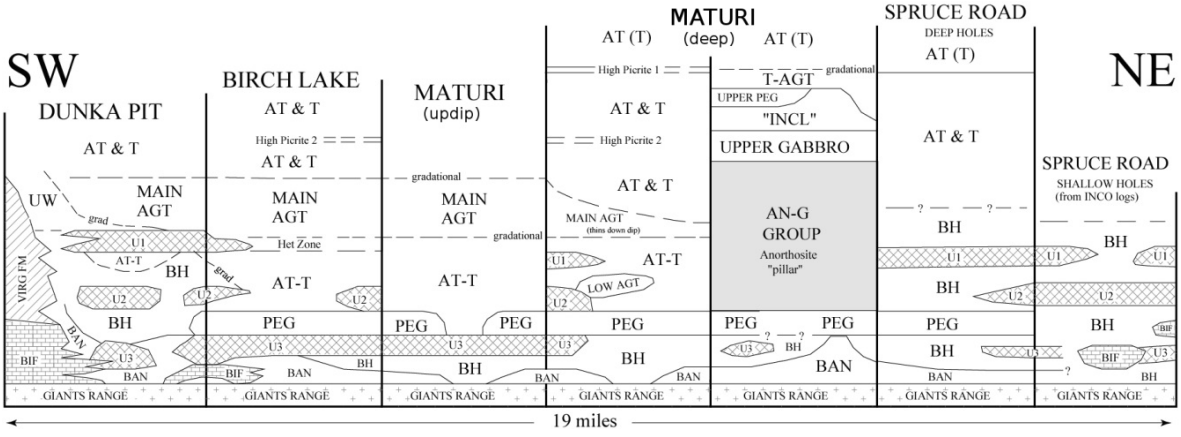


Figure 2-102. Generalized igneous stratigraphy of the basal zone of the SKI (Severson, 1994). The Lowermost units are BAN = Basal Augite Troctolite and Norite; BH = Basal Heterogeneous; U3 = Ultramafic 3; PEG = Pegmatitic unit of Foose (1984); U2 = Ultramafic 2; U1 = Ultramafic 1; AT-T = Anorthositic Troctolite to Troctolite; UW = Up dip Wedge; Main AGT = Main Augite Troctolite; AN-G Group = Anorthositic Series inclusion with internal gabbroic lenses.

The lowermost units are unevenly distributed along the strike-length of the intrusion in a compartmentalized fashion, suggesting a complicated intrusive history. The stratigraphy, as defined by Severson (1994), has been documented to be present in all the holes drilled recently by Twin Metals Minnesota (TMM) at the Birch Lake and Maturi deposits but it has since been simplified by TMM. According to Severson and Hauck (2008), a few salient features of the SKI include:

- The vast majority of sulfide mineralization is confined to the BH, BAN, and U3 units - all of these are collectively referred to as BMZ by TMM at the Maturi deposit). The PEG unit, though not particularly mineralized except locally, is also included in the BMZ by TMM
- Major marker beds include three horizons that contain abundant ultramafic layers (U1, U2 and U3) and a pegmatite-bearing unit (PEG unit – originally recognized by Foose, 1984).
- The U3 unit is unique in that it contains several massive oxide pods (titanomagnetite-rich and locally Cr-bearing) as well as recognizable inclusions of bedded Biwabik Iron Formation. The spatial correspondence between the U3 unit and footwall iron-formation suggests that most of the massive oxide pods are iron-rich "restite" produced by assimilation and a high degree of partial melting of the iron-formation. This relationship is the most prevalent at Birch Lake
- The U3 unit contains the vast majority of high PGE values; however, high PGE values are locally present in the overlying PEG unit. High PGE values are also present well above the base of the SKI at the South Filson Creek deposit
- A large inclusion of anorthosite of formidable size (3,500 feet thick) is present at Maturi and was referred to as the AN-G Group by Severson (1994). Peterson (2001) suggested that the high PGE contents within the BMZ unit (beneath the inclusion) formed as a result of confined turbulent magma flow, and thus an increased R-factor, beneath a "pillar" of anorthosite. Peterson (2001) further hypothesized that a portion of a Nickel Lake Macrodike, which served as a feeder to the nearby Bald Eagle intrusion, may have projected beneath the Maturi deposit and also served as a feeder to the SKI

Four of the Cu-Ni deposits within the SKI historically held by TMM are shown in Figure 2-23. These four deposits and others within the SKI are discussed in the following sub-sections. The information given for each of the deposits is based on various NI 43-101 reports, field trip guidebooks (Patelke and others, 2009; and Severson and others, 2016), various NRRI reports, oral presentations at professional meetings, and personal knowledge.

Maturi Deposit (Twin Metals Minerals)

The very first exploration drill hole in search of Cu-Ni deposits in the Duluth Complex was cored in the Maturi deposit by Fred S. Childers (prospector) and Roger V. Whiteside (investor) in 1951. Eventually, the International Nickel Company (Inco) picked up the property and outlined a sizeable, but low grade, Cu-Ni deposit. A shaft was sunk on the property during 1966 to 1967 to collect material for metallurgical tests. Inco took their bulk sample from pyrrhotite-rich material, which is more prevalent near the basal contact, and decided the grade was too low to support an underground mine. Three other companies (Bear Creek, Duval and Newmont) put down several scattered drill holes on the periphery of the deposit and intersected good mineralization at great depth but also determined it was too low grade to support an underground mine.

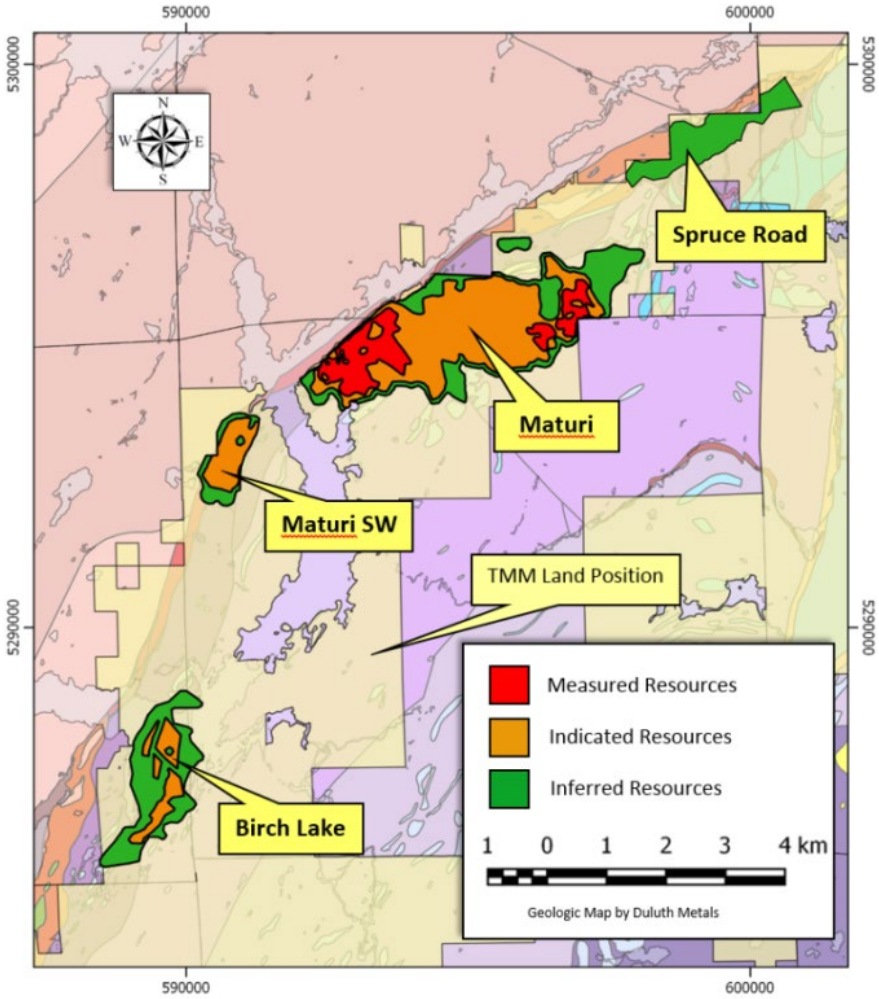


Figure 2-113. Twin Metals Minnesota (TMM) deposits and Resource Classification.

Mineralization at Maturi, and an extension referred to as Maturi SW, is present in the lower portion of the South Kawishiwi intrusion (SKI) in what TMM refers to as the Basal Mineralized Zone (BMZ). Note that the BMZ collectively consists of the PEG, U3, BH and BAN units of Severson (1994). While the Severson units are recognized by TMM at Maturi they are not consistently present throughout the deposit and for simplicity-sake TMM combined them into the BMZ unit.

In 2008, Dean Peterson from Duluth Metals (the original company from which TMM was created) theorized that the initial SKI magmas at Maturi were intruded as sulfide-bearing, crystal-laden (olivine- and plagioclase-rich), crystal slurries. Based on this new interpretation, TMM combined Severson's (1994) basal units into the BMZ unit that they believed originated by physical sorting of the crystal slurries (possibly top down) and by melting of the footwall granitic rocks (bottom up) to create the heterogeneous lithologies and textures of the BMZ as is shown in Figure 2-24.

Mineralization at the Maturi deposit consists of a tabular sheet of disseminated Cu-Ni-Fe sulfides that averages 215 feet thick (65 meters) with a range of 5 to 865 feet thick (1.5 to 260 meters) with the thickest range towards the north end of the deposit. Dips of the BMZ vary from 35 to 55 degrees with a N60E plunge along the contact. Higher grades are concentrated in the upper 100 feet (30 meters) of a zone that has been traced laterally by drilling for approximately 2.2 miles (3.5 km) and open at depth. While mineralization is mostly restricted to the BMZ, exceptions are locally present in the overlying PEG unit and in the footwall granitic rock. TMM reports that mineralization within the footwall granite occurs in appr-

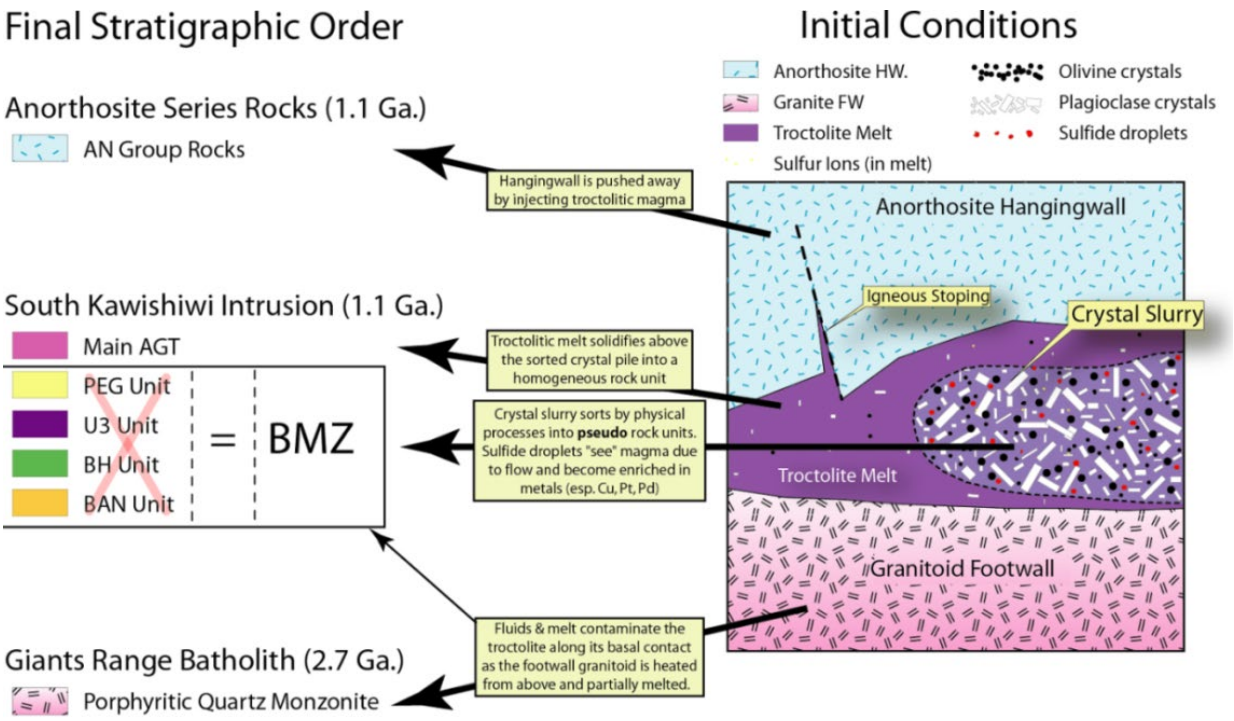


Figure 2-124. Simplified crystal-liquid slurry model for the SKI in the Maturi area.

oximately one-quarter of the holes drilled to date with about 80% of these holes showing mineralization in the overlying BMZ that continues directly downward into the footwall mineralization with little or no breaks.

Mineralization typically consists of 1-5% disseminated chalcopyrite, talnakhite, cubanite, pyrrhotite, and pentlandite. Bornite, covellite, and millerite occur in subordinate amounts. Better grades of Cu, Ni and PGE are associated with more mafic units located near the top of the BMZ. Modeling of the ore deposits by Duluth Metals, TMM, and AMEC indicated that the mineralization at Maturi can be characterized by several distinct patterns as shown in Figure 2-25.

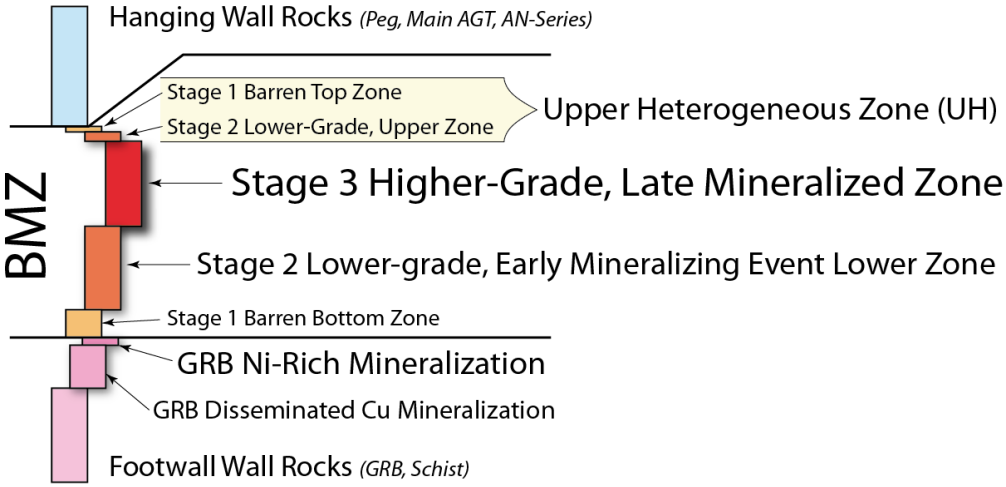


Figure 2-135. Mineralization trends of the BMZ and adjacent rocks within the Maturi area.

The three stages of mineralization within Maturi's BMZ zone include:

- **Stage 1 Mineralization** (S1, with top and bottom zones): barren to very low-grade mineralization showing low variability.
- **Stage 2 Mineralization** (S2, with top and bottom zones): moderate grade mineralized intervals showing low variability. Cu:Ni ratios are 3.0 to 3.2:1. Cu-sulfides are the dominant sulfide but pyrrhotite becomes increasingly present with depth. Cubanite and pentlandite decrease in abundance with depth. Normalized chalcopyrite/chalcopyrite+cubanite ratios are approximately 0.61 to 0.65 (Hoffmann and others, 2015).
- **Stage 3 Mineralization** (S3): higher grade mineralized intervals that are commonly bounded by low grade selvages and, interestingly, contains ultramafic units (aka U3 unit of Severson, 1994). Cu:Ni ratios are 3.0 to 3.2:1. Cu-sulfides are the dominant sulfide. Normalized chalcopyrite/chalcopyrite+cubanite ratios are approximately 0.58 to 0.67 (Hoffmann and others, 2015).

Birch Lake Deposit (Twin Metals Minerals)

The Birch Lake deposit lies to the south of Maturi (Figures 2-2 and 2-23), with mineralization also hosted at the bottom of the SKI. The area was first drilled by Duval in the 1970s but remained dormant until high PGE values were found in drill hole Du-15 by state agencies in the mid-1980s (Sabelin and Iwasaki, 1985). This discovery marked the start of serious PGE exploration in the Duluth Complex. Ernest Lehmann formed several joint ventures, the last known as Franconia Minerals LLC or Beaver Bay Joint Venture, and several holes were drilled on the property intermittently during 1988 through 2010. TMM acquired the property in 2011 and drilled 30 holes from 2011 to 2012. A total of 114 holes have been drilled at Birch Lake (excluding 154 wedge holes that were drilled mainly to obtain material for metallurgical testing).

The geology is very similar to Maturi except for the common occurrence of more (and often thicker) ultramafic layers, assimilated BIF inclusions, and discontinuous oxide-rich horizons/pods that are inferred to represent BIF "restites", all of which are present in the U3 unit. The continuity of these U3 rock types is extremely heterogeneous in 3D as revealed by wedge drilling. Mineralization is associated with what TMM also refers to as the BMZ which consists of the U3, BH, and BAN units of Severson (1994). The BMZ averages about 100 feet thick (30 meters) but is as thick as 515 feet (157 meters). The main footwall unit at Birch Lake is the Neoarchean Giants Range granitic complex, but Paleoproterozoic rocks are exposed at the surface in the Dunka Pit mine located <1 km to the southwest. The four inferred mineralization types at Birch Lake in the BMZ and GRB are shown in Figure 2-26 (non-mineralized material below the GRB_M is identified as GRB_B for barren footwall rocks).

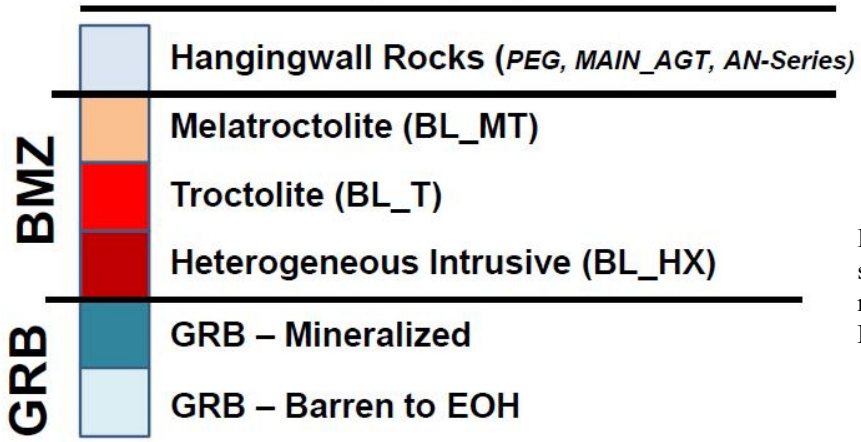


Figure 2-26. Igneous stratigraphy according to mineralization trends at Birch Lake.

Mineralization trends at Birch Lake are very similar to Maturi, with four inferred types:

1. **Melatroctolite / BL_MT Unit** (similar to S3 at Maturi and U3 unit of Severson): an upper melatroctolite to mafic troctolite unit that hosts the highest grade mineralization and is correlative across the deposit. The top and bottom of this unit are typically based on high Mg contents with values generally greater than 6% Mg. The Cu:Ni ratio is about 3.3. The base of the BL_MT unit is gradational downward into the BL_T unit. Almost all of the significant Cu-Ni and precious metal mineralization is hosted by this unit but the total volume, or percentage of the mineral resource, has not been published
2. **Troctolite / BL_T Unit** (similar to S1 at Maturi and BH and BAN units of Severson): a lower troctolitic unit with lower grades that is also correlative across the deposit. Mg contents are in the 3.5-4.5% range. Locally the top of BL_T is more mineralized and there are small, mineralized zones near the base
3. **Basal Hybrid Zone / BL_HX**: a basal hybrid rock sequence, with localized oxide-rich layers, that shows similarities to both BL_T and underlying metasomatized Giants Range granitic rocks. This hybrid sequence is marked by an abrupt increase in P and erratic Sr, Ba, Mg, and V concentrations. Iron ranges from 2% Fe to upwards of 45% Fe (largely because of assimilated BIF inclusions)
4. **Mineralized GRB / GRB_M**: consists locally of mineralized Giants Range granitic rocks as well as locally mineralized Virginia Formation and BIF. Average grade is about 0.28% Cu and 0.16% Ni with a Cu:Ni ratio of about 2.3. Local massive sulfide bodies are present and contribute significantly to the average grade

The thickness of the four units is quite variable, but the stratigraphic succession does not vary across the deposit. Any one or more of the units, however, can be missing locally from a specific drill hole. Geologic modeling indicated that there is a sinuous, channel-like body of persistent and higher Cu grades that traverse the length of the deposit and follows the thickest portion of the BL_MT unit as shown in Figure 2-27. The origin of the channel is not well understood but it may be related to a magma conduit.

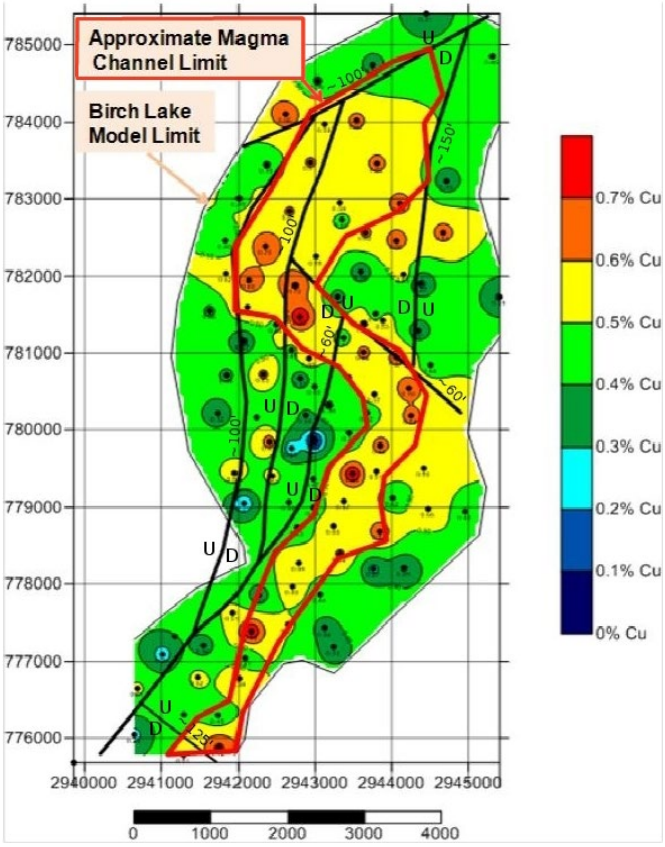


Figure 2-147. Birch Lake magma channel superimposed on average copper grade base map.

Spruce Road Deposit (Twin Metals Minerals)

The Spruce Road deposit lies to the northeast of Maturi (Figures 2-2 and 2-23). Mineralization is also present at the base of the SKI. It was at this deposit that the first good indications of Cu-Ni mineralization were uncovered while constructing a forest access road in 1948. From 1954 to 1971, Inco drilled the deposit on 200-foot centers (61 meters) for a total of 232 holes (the vast majority of which are no longer preserved after they were destroyed in a fire at Sudbury, Ontario). In 1997, Inco's subsidiary, American Copper and

Nickel Company (ACNC), joint ventured the property with Wallbridge Mineral Company Limited (from which Duluth Metals was eventually created). Wallbridge eventually drilled two holes on the property during 1999 to 2000 in search of high-grade footwall veins but failed to find significant mineralization in the footwall rocks. In 2002, Franconia Minerals Corp. entered into an agreement with Beaver Bay Joint Venture to acquire the Spruce Road and Maturi properties from ACNC but conducted no work. TMM acquired the property in 2011 and drilled 57 drill holes totaling 65,635.5 ft between September 2012 and January 2014 and a prefeasibility study technical report was issued on the TMM project in August 2014.

The geology at Spruce Road is vastly different than at either Maturi or Birch Lake. Publicly-preserved core from historic drill holes are extremely limited for this deposit in that only six Inco holes are preserved along with two Wallbridge holes. From this limited data, Severson (1994) determined that most of the igneous units that typify the SKI elsewhere are not present at Spruce Road. Rather, the mineralization appears to be present in a much thicker BH unit (also referred to as the BMZ unit by TMM) consisting of a heterogeneous mix of troctolitic rocks with common hornfelsed inclusions of basalt (North Shore Volcanic Group). Also present are extremely localized noritic rocks associated with hornfelsed sedimentary rocks (Virginia Formation and Biwabik Iron Formation) and at the basal contact with the Giants Range granitic complex. The U3 unit and massive oxide zones are also locally present. Mineralization does not appear to correlate with any specific igneous lithology and there are no known marker horizons. Historic drill logs indicate that there may be an igneous mega-breccia unit that is referred to as "Spruce Road breccia."

South Filson Creek Deposit (Encampment Minerals)

The South Filson Creek deposit, located to the east of Spruce Road, as previously presented in Figure 2-2, was initially drilled by the Hanna Mining Company (23 holes) in the late 1960s. There, the Cu-Ni mineralization is hosted by troctolitic rocks (AT&T unit of Severson, 1994), both in outcrop and in the tops of several drill holes situated well above the basal contact. In 1987, encouraging high PGE values (>1.0 ppm) were reported in these "cloud" zone sulfides by Steve Hauck of the NRRI. A subsequent study of the PGE mineralization (Kuhns and others, 1990) indicated that the PGE were concentrated by a late-stage hydrothermal event that concentrated the PGE in extremely fine, discontinuous, microscopic veinlets that were inferred to be associated with a NE-trending fault zone. Encampment Minerals drilled an additional 27 holes on the property, but results are largely unknown.

Serpentine Deposit (Encampment Minerals)

The Serpentine deposit, shown in Figure 2-26, is located to the north of the Mesaba deposit. The deposit was initially discovered by Bear Creek Mining Company in 1967 as part of a follow-up drilling campaign of an airborne electromagnetic conductor (Kulas, 1979).

The name "Serpentine" was chosen for this deposit due to the presence of a sinuous-trending massive sulfide located at the base of the SKI. When the next owner, Amax, began working on the deposit, they calculated that the deposit contained 250 million tons of resources (not NI 43-101 compliant) grading 0.41% Cu, 0.14% Ni and 1.96% S at a 0.20% copper cut-off, with a higher-grade portion of over 7 million tons, at a 0.60% copper cut-off, with a grade of 0.88% Cu, 0.30% Ni and 5.67% S (Kulas, 1979, Zanko and others, 1994).

The presence of such voluminous pyrrhotite-rich massive to semi-massive sulfide at the basal contact at Serpentine makes this an unusual deposit (Figure 2-29). There, the massive sulfide is closely related to the BDPO which provided a local sulfur source. Empirical evidence in drill core is evidenced by partially melted BDPO (present in the footwall and in inclusions) that transitions upwards and downwards into massive sulfide near the basal contact. The massive sulfide is also located close to the projected location of the Grano Fault that may have played a role in its origin. Another feature that may be related to the Grano Fault at Serpentine is a northerly-trending zone wherein subvertical olivine-rich ultramafic dikes were emp-

-laced in the troctolitic host rocks while the host rocks were still solidifying. Encampment Minerals drilled eight holes at the Serpentine deposit, but no data are known regarding their results.

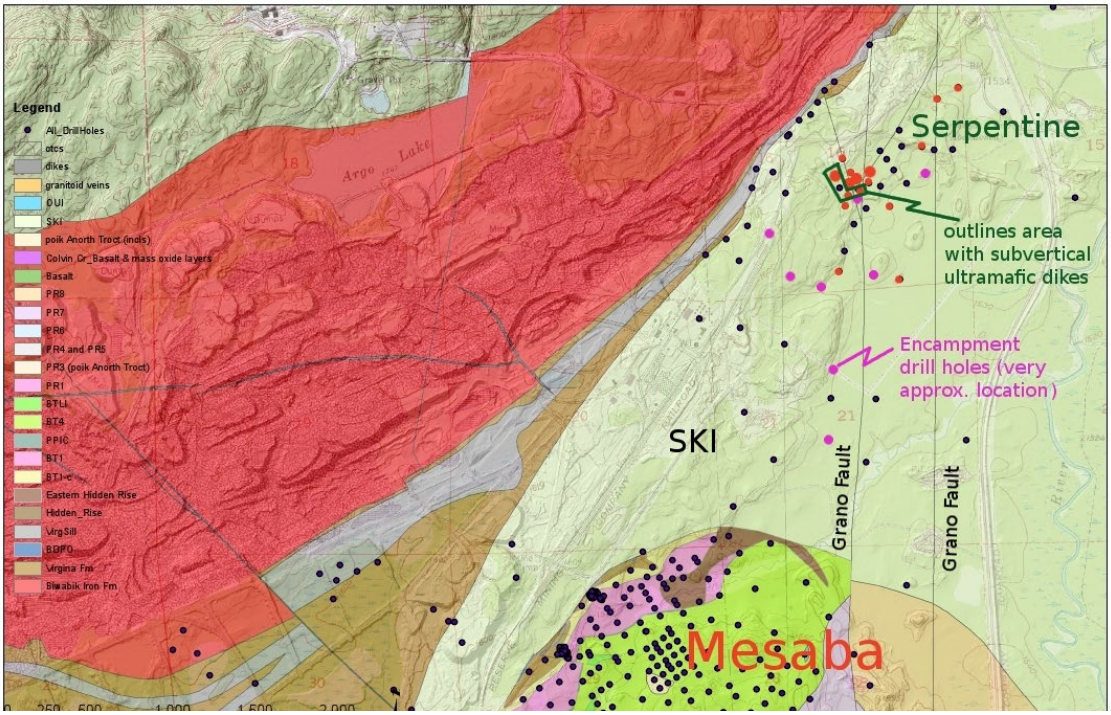


Figure 2-168. Location of the Serpentine deposit in relation to the Mesaba deposit. Note drill holes posted in red are holes that intersected massive sulfides at or slightly above the basal contact (larger red dots intersected significantly more and thicker massive sulfide zones).

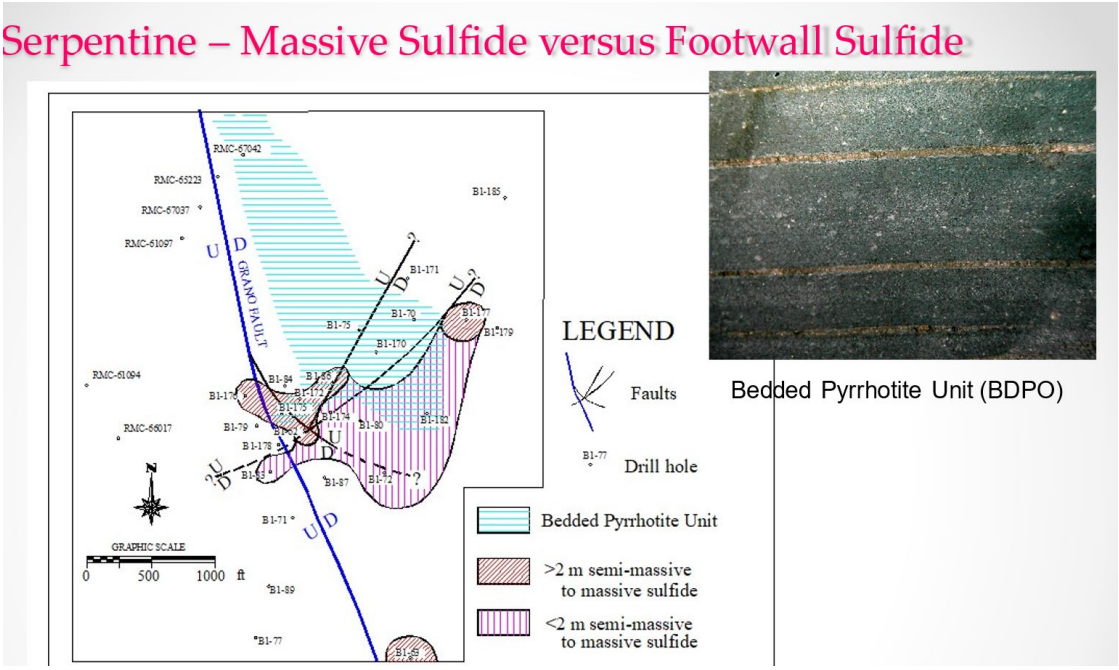


Figure 2-159. Trend of BDPO unit relative to basal massive sulfide mineralization at the Serpentine deposit (from Zanko and others, 1994).

Field Trip Stops

Drill core will be displayed at NewRange's Babbitt core facility, for both the NorthMet and Mesaba deposits, and at Twin Metals Ely office for the Maturi deposit. Cross-sections displaying the geology will be posted, as well as Cu-Ni-PGE grades, for the appropriate holes. At this point in time, the core displayed will be determined by the companies.

NewRange core facility: 578810 / 5284970, (47.71330°, -91.94930°)

Twin Metals Ely office: 585230 / 5306550, (47.90661°, -91.85949°)

References

Barber, J., Parker, H., Frost, D., Hartley, J., White, T., Martin, C., Sterrett, R., Poeck, J., Eggleston, T., Gormely, L., Allard, S., Annavarapu, S., Radue, T.,Malgensini, M and Pierce, M., 2014:, Twin Metals Minnesota Project, Ely, Minnesota, USA: NI 43-101 Technical Report on Pre-feasibility Study prepared by AMEC E&C Services, Inc. for Duluth Metals Limited, October 2014, Project 176916.

Bennett, A., Dempers, N., Neff, D., Radue, P.E., Roth, D., Schwering, R., Tahija, L., Uble, J.S. and Welhener, H.E., 2022, NorthMet Copper-Nickel Project, Feasibility Update National Instrument 43-101F1 prepared for PolyMet Minerals Corp. by M3 Engineering and Technology Corp., Project M3-PN220283, Dec. 30th, 2022, 248 p.

Eckstrand, 0.R., and Hulbert, L.J., 2007, Magmatic Nickel-Copper-Platinum Group Element Deposits; in Goodfellow,W.D., ed., Mineral Deposits of Canada: A synthesis of Major Types, District Metallogeny, The Evolution of Geological Provinces, and Exploration Methods: Geological Association of Canada, Mineral Deposits Division, Special Publication No.5, p. 205-222.

Farrow, D, and Johnson, M, 2011, January 2012 National Instrument 43-101 Technical Report on the Titac Ilmenite Exploration Project, Minnesota, USA. SRK Consulting (Canada) Inc. SRK Project Number 2CC031.004. Cardero Resources Corp.

Farrow, D, and Johnson, M, 2012, January 2012 National Instrument 43-101 Technical Report on the Longnose Ilmenite Exploration Project, Minnesota, USA. SRK Consulting (Canada) Inc. SRK Project Number 2CC031.004. Cardero Resources Corp.

Foose, M., 1984, Logs and correlation of drill holes within the South Kawishiwi intrusion, Duluth Complex, northeastern Minnesota: United States Geological Survey, Open-file Report 84-14

Geerts, S.D., 1991, Geology, stratigraphy, and mineralization of the Dunka Road Cu-Ni prospect, northeastern Minnesota: Natural Resources Research Institute, University of Minnesota Duluth, Duluth, MN, Technical Report NRRI/TR-91/14, 63 p.

Geerts, S.D., 1994, Petrography and geochemistry of a platinum group element-bearing horizon in the Dunka Road prospect, (Keweenawan) Duluth Complex, northeastern Minnesota: University of Minnesota Duluth, Unpublished M.S. thesis, 100 p.

Kuhns, M.P, Hauck, S.A, and Barnes, R.J, 1990, Origin and occurrence of platinum group elements, gold and silver, in the South Filson Creek copper-nickel deposit, Lake County, Minnesota: Natural Resources Research Institute, University of Minnesota Duluth, Duluth, MN, Technical Report NRRI/GMIN-TR-89-15, 60 p.

Kulas, J.E., 1979, Serpentine Reserve – Minnamax project: unpublished AMAX Company report on file at the Minnesota Department of Natural Resources, Lands and Minerals Division, Hibbing, MN, 5 p.

Listerud, W.H., and Meineke, D.G., 1977, Mineral resources of a portion of the Duluth Complex and adjacent rocks in St. Louis and Lake Counties, northeastern Minnesota: Minnesota Department of Natural Resources, Div. of Minerals, Hibbing, MN, Report 93, 49 p.

Miller, J.D., Jr., Green, J.C., Severson, M.J., Chandler, V.W., and Peterson, D.M., 2001, Geologic Map of the Duluth Complex and Related Rocks: Minnesota Geological Survey, Miscellaneous Map Series, Map M-119.

Miller, J.D., Jr., Green, J.C., Severson, M.J., Chandler, V.W., Hauck, S.A., Peterson, D.M., and Wahl, T.E., 2002, Geology and mineral potential of the Duluth Complex and related rocks of northern Minnesota: Minnesota Geological Survey, Report of Investigations RI-58, 207 p.

Miller, J.D., and Severson, M.J., 2005, Bedrock Geology of the Babbitt Southwest Quadrangle, St. Louis County. Minnesota: Minnesota Geological Survey, University of Minnesota, Miscellaneous Map Series, M-161.

Patelke, R, Peterson, D, Severson, M, Jefferson, T, and Lehmann, E., 2009, Cu-Ni-PGE Deposits of the Duluth Complex, Geology and Development; 55th Annual Institute on Lake Superior Geology, Ely, MN, Part 2 Field Trip Guidebook, p. 1-80.

Peterson, D.M., 2001, Development of a conceptual model of Cu-Ni-PGE mineralization in a portion of the South Kawishiwi Intrusion, Duluth Complex, Minnesota: Laurentian University – Society of Economic Geologists, Second Annual PGE Workshop, Sudbury, Ontario.

Peterson, D.M., 2010, The Nokomis Cu-Ni-PGE Deposit, Minnesota. Prospectors and Developers Association of Canada. Annual Meeting, Powerpoint presentation.

Sabelin, T., and Iwasaki, I., 1985, Metallurgical evaluation of chromium-bearing drill core samples from the Duluth Complex (Contract report of Minnesota Department of Natural Resources, Division of Minerals): Minerals Resources Research Center, University of Minnesota, Minneapolis, MN, 58 p.

Sabelin, T., and Iwasaki, I., 1986, Evaluation of platinum group metal occurrence in Duval 15 drill core from the Duluth Complex: Internal report, Minerals Resources Research Center, University of Minnesota, Minneapolis, MN, 23 p.

Severson, M.J., 1994, Igneous stratigraphy of the South Kawishiwi intrusion: Duluth Complex, northeastern Minnesota: Natural Resources Research Institute, University of Minnesota Duluth, Duluth, MN, Technical Report NRRI/TR-93/34, 210 p.

Severson, M.J. and Barnes, R.J., 1991, Geology, mineralization and geostatistics of the Minnamax/Babbitt Cu-Ni deposit (Local Boy area), Minnesota, Part II: Mineralization and geostatistics: Natural Resources Research Institute, University of Minnesota, Duluth, Technical Report, NRRI/TR-91/13b, 216 p.

Severson, M.J. and Hauck, S.A., 1990, Geology, geochemistry, and stratigraphy of a portion of the Partridge River intrusion: Natural Resources Research Institute, University of Minnesota Duluth, Duluth, MN, Technical Report NRRI/GMIN-TR-99-11, 236 p.

Severson, M.J. and Hauck, S.A., 1997, Igneous stratigraphy and mineralization in the basal portion of the Partridge River intrusion, Duluth Complex, Allen Quadrangle, Minnesota: Natural Resources Research Institute, University of Minnesota Duluth, Technical Report NRRI/TR-97/19, 102 p.

Severson, M.J. and Hauck, S.A., 2003, Platinum group elements (PGEs) and platinum group minerals (PGMs in the Duluth Complex, Natural Resources Research Institute, University of Minnesota Duluth, Technical Report NRRI/TR-2003/37. 296 p.

Severson, M.J. and Hauck, S.A., 2008, Finish Logging of Duluth Complex Drill Core (And a Reinterpretation of the Geology at the Mesaba (Babbitt) Deposit): Natural Resources Research Institute, University of Minnesota Duluth, Duluth, MN Technical Report NRRI/TR-2008/17, 68 p. + 94 plates.

Severson, M.J. and Heine, J.J., 2007, Data compilation of United States Steel Corporation (USSC) exploration records in Minnesota; Natural Resources Research Institute, University of Minnesota Duluth, Duluth, MN, Technical Report NRRI/TR-2007/25, 98 p.

Severson, M.J. and Miller, J.D., 2005, Bedrock Geology of the Babbitt Quadrangle, St. Louis County. Minnesota: Minnesota Geological Survey, University of Minnesota, Miscellaneous Map Series, M=159.

Severson, M.J., Patelke, R.L., Hauck, S.A., and Zanko, L.M., 1994, The Babbitt copper-nickel deposit, Part B: Structural datums: Natural Resources Research Institute, University of Minnesota Duluth, Duluth, MN, Technical Report NRRI/TR-94/21b, 48 p.

Severson, M, Ware, A, Boerst, K, and Peterson, D, 2016, Cu-Ni-PGE Deposits of the Duluth Complex, Geology and Development; 62nd Annual Institute on Lake Superior Geology, Duluth, MN, Part 2 Field Trip Guidebook, p, 27-78.

Welhener, H. and Crowie, S.T., 2022, NI 43-101F1 Technical Report on Mesaba Project, Mineral Resource Statement prepared for PolyMet Mining Corp. by Independent Mining Consultants, Inc. and JDS Energy and Mining, Inc., November 2022

Zanko, L.M., Severson, M.J., and Ripley, E.M., 1994, Geology and mineralization of the Serpentine copper-nickel deposit, Duluth Complex, Minnesota: Natural Resources Research Institute, University of Minnesota Duluth, Duluth, MN, Technical Report NRRI/GMIN-TR93-52, 90 p.

FIELD TRIP 3

How Do You Make Iron and/or Manganese Ores in Proterozoic Iron Formation?

Dean Peterson[1], Alex Steiner[1], and Latisha Brengman[2]

[1]*Big Rock Exploration, 2505 W. Superior St., Duluth, MN 55806*
[2]*Earth and Environmental Sciences, Swenson College of Science and Engineering, University of Minnesota, Duluth, 1114 Kirby Dr., Heller Hall 229, Duluth, MN 55812*

Introduction

Iron formations are among the most important rocks for our modern industrial world. Their extraordinary iron content facilitates the manufacture of steel, while their manganese content is of crucial importance as a steel-alloy product and a critical component of battery technologies. Fueling modern technology requires efficient production of iron resources, exploration of manganese resources, and determination of enrichment processes that lead to ore formation. This field trip will explore ore-formation processes that turn otherwise uneconomic iron formations into valuable resources of iron and manganese. The trip may include an optional stop at the Hibbing Core Library where participants will examine drill core of the Biwabik taconite ores. Participants will explore sedimentary features, diagenetic reactions, and weathering reactions that contribute to iron grade and iron distribution within ore-horizons of the Biwabik. We will then travel to the North Star Manganese/Electric Metals core logging facility in Emily, MN to look at four recent (2023 drilling) drillholes where we will discuss the formation and subsequent redistribution of manganese within the Emily Iron Formation. Participants will have the opportunity to observe high-grade manganese oxide drill core, primary iron-manganese carbonate facies iron formation, and breccia horizons possibly associated with the 1.85 Ga. Sudbury impact. The trip will then proceed to the Mary Ellen mine, a former natural ore pit, where the oxidation and weathering of the Biwabik was central to ore formation and early mining efforts on the range. Participants can observe primary features such as stromatolites and sedimentary structures as well as oxidation-weathering features. If time allows, we will wrap up the trip at the Biwabik outcrops in Virginia near the new Highway 53 bridge over the historic Rouchleau natural ore (hematite) mine before heading back to Mountain Iron.

Regional Geologic Setting

To gain a true understanding of the geology and origin of the high-grade Paleoproterozoic iron and manganese resources of the Mesabi and Cuyuna Ranges of northern Minnesota (Fig. 3-1), it is best to start with an understanding of the regional-scale geologic setting and its contained ferrous mineral resources. These Paleoproterozoic iron ranges include several categories of marine chemocline mineral systems outlined in recent USGS publications (Schulz et al., 2017 and Hofstra and Kreiner, 2020). These categories include:

1) Superior-iron deposits (Mesabi Iron Range and the Emily District of the Cuyuna Iron Range) and
2) Algoma-type iron-manganese deposits (Cuyuna North and South Iron Ranges).

Superior Type Iron Resources of the Mesabi Iron Range

Superior type iron formation resources of Minnesota are exemplified by the long-standing mining of iron resources of the Biwabik Iron Formation along the length of the Mesabi Iron Range. The Mesabi Iron Range is largely located in St. Louis and Itasca counties and has been the most important iron ore district in the United States since ~1900. The Mesabi Iron Range is 120 miles long, averages one to two miles wide, and is comprised of rocks of the Paleoproterozoic Animikie Group. The Animikie Group on

the Mesabi Iron Range consists of three major conformable formations: Pokegama Formation at the base; Biwabik Iron Formation in the middle; and the overlying Virginia Formation. On the Mesabi Iron Range, these three formations generally dip gently to the southeast at angles of 3-15 degrees.

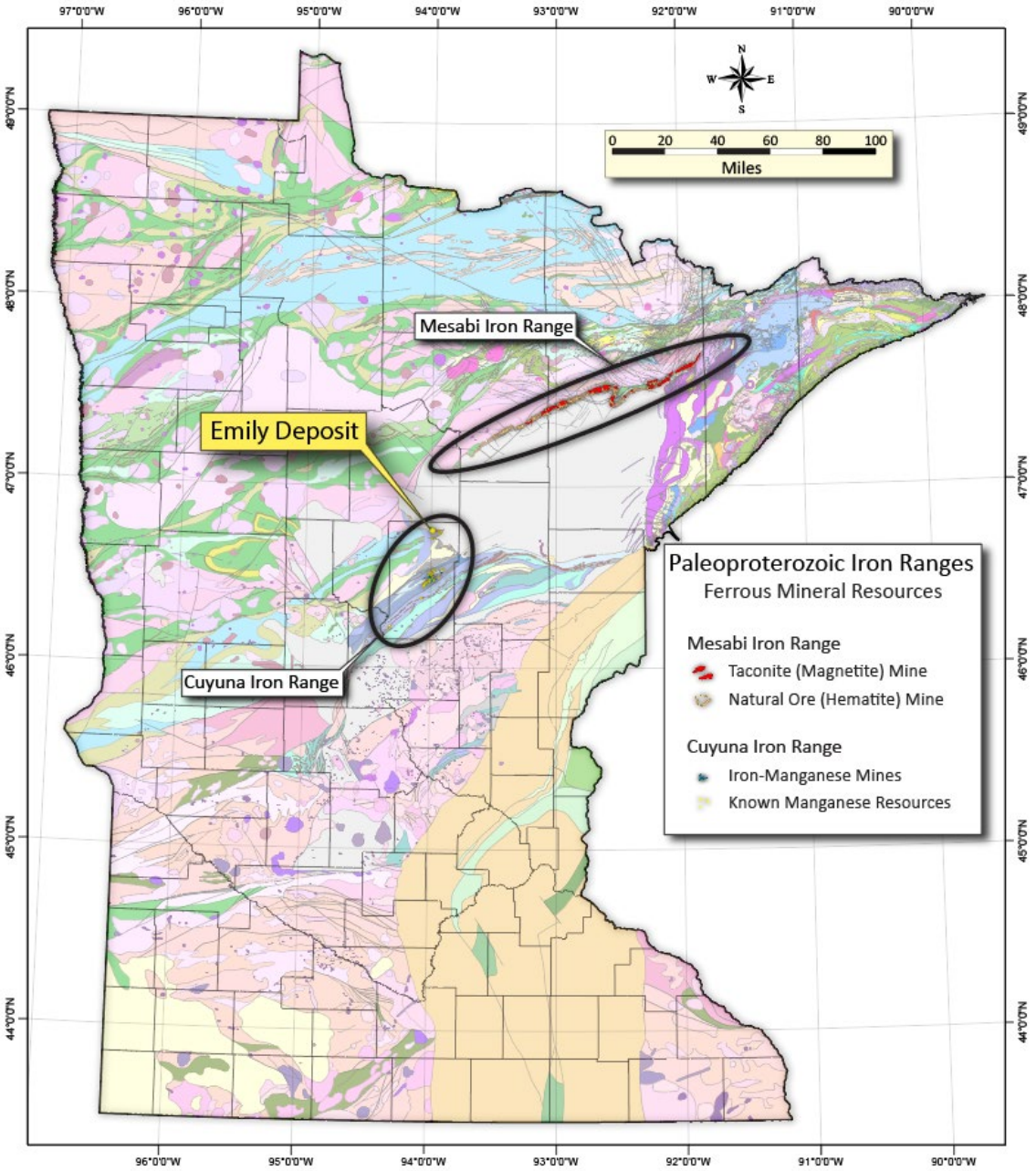


Figure 3-1. Location map of identified ferrous mineral resources in Minnesota.

Since the early 20th century, the Biwabik Iron Formation has been subdivided into four informal members referred to as (from bottom to top): Lower Cherty member, Lower Slaty member, Upper Cherty member, and Upper Slaty member (Wolff, 1917). The cherty members are typically characterized by a granular (sand-sized) texture and thick-bedding (beds ≥ several inches thick); whereas the slaty members are typically fine-grained (mud-sized) and thin-bedded (≤1 cm thick beds). The cherty members are largely composed of chert and iron oxides (with zones rich in iron silicate minerals), while the slaty members are composed of iron silicates and iron carbonates with local chert beds. Both cherty and slaty iron-formation

types are interlayered at all scales, but one rock type or the other predominates in each of the four informal members, and they are so-named for this dominance Severson et. al. (2009).

Leached and iron enriched direct ores (or natural ores) were the first materials mined, with the first shipments beginning in 1892, from strongly oxidized pockets along fault and fracture zones and the blanket oxidation of the iron formation at the surface. Taconite, which is the material that is mined today using magnetic separation methods, constitutes most of the iron formation and pertains to the hard, non-oxidized portions of the iron-formation. Production has been dominantly controlled by vertically integrated steelmakers since 1901, and therefore the mining and utilization of these ores have been dictated largely by US ironmaking capacity and demand.

Taconite typically contains 30-35% iron and 40-50% SiO_2, plus other components (Morey, 1992). The Biwabik Iron Formation is around 175-300 feet thick in the extreme eastern end of the Mesabi Iron Range at Dunka Pit, 730-780 feet thick in the central Mesabi Iron Range/Virginia Horn area near Eveleth, around 500 feet thick in the western Mesabi Iron Range near Coleraine, and eventually exhibits a "nebulous ending about 15 miles southwest of Grand Rapids" (Marsden et al., 1968) on the extreme western end of the Mesabi Iron Range. Maps of currently active taconite mining operations on the Mesabi Iron Range are presented in Figure 3-2 and compiled grade/tonnage ore reserve calculations for these operations are given in Table 3-1.

Table 3-1. Reported grade/tonnage of active taconite mines. operations.

MINE NAME	**YEAR	CATEGORY	TONNES	*FE %
Northshore	2019	Proven & Probable	829,096,800	24.3
United Taconite	2019	Proven & Probable	817,920,250	22.3
Hibbing Taconite	2019	Proven & Probable	123,856,495	19.7
Minorca	2018	Proven & Probable	101,000,000	23.5
Minntac	2019	Proven & Probable	420,644,700	?
Keetac	2019	Proven & Probable	373,906,400	?

* Reported as recoverable magnetic Fe %

** Data compiled from company annual reports

Geology of the Cuyuna Iron Range

The Cuyuna iron range is about 160 km west-southwest of Duluth in Aitkin, Cass, Crow Wing, and Morrison Counties (Fig. 3-1). It is part of an Early Proterozoic geologic terrane which occupies much of east-central Minnesota. The Cuyuna iron range is traditionally divided into three districts, the Emily district, the North range, and the South range (Fig. 3-3). The Emily district extends from the Mississippi River northward through Crow Wing County and into southern Cass County and comprises an area of about 1,165 square kilometers. Although exploration drilling has been extensive in the Emily district, mining never commenced. The North range, a much smaller area about 19 km long and 8 km wide, is near the cities of Crosby and Ironton in Crow Wing County.

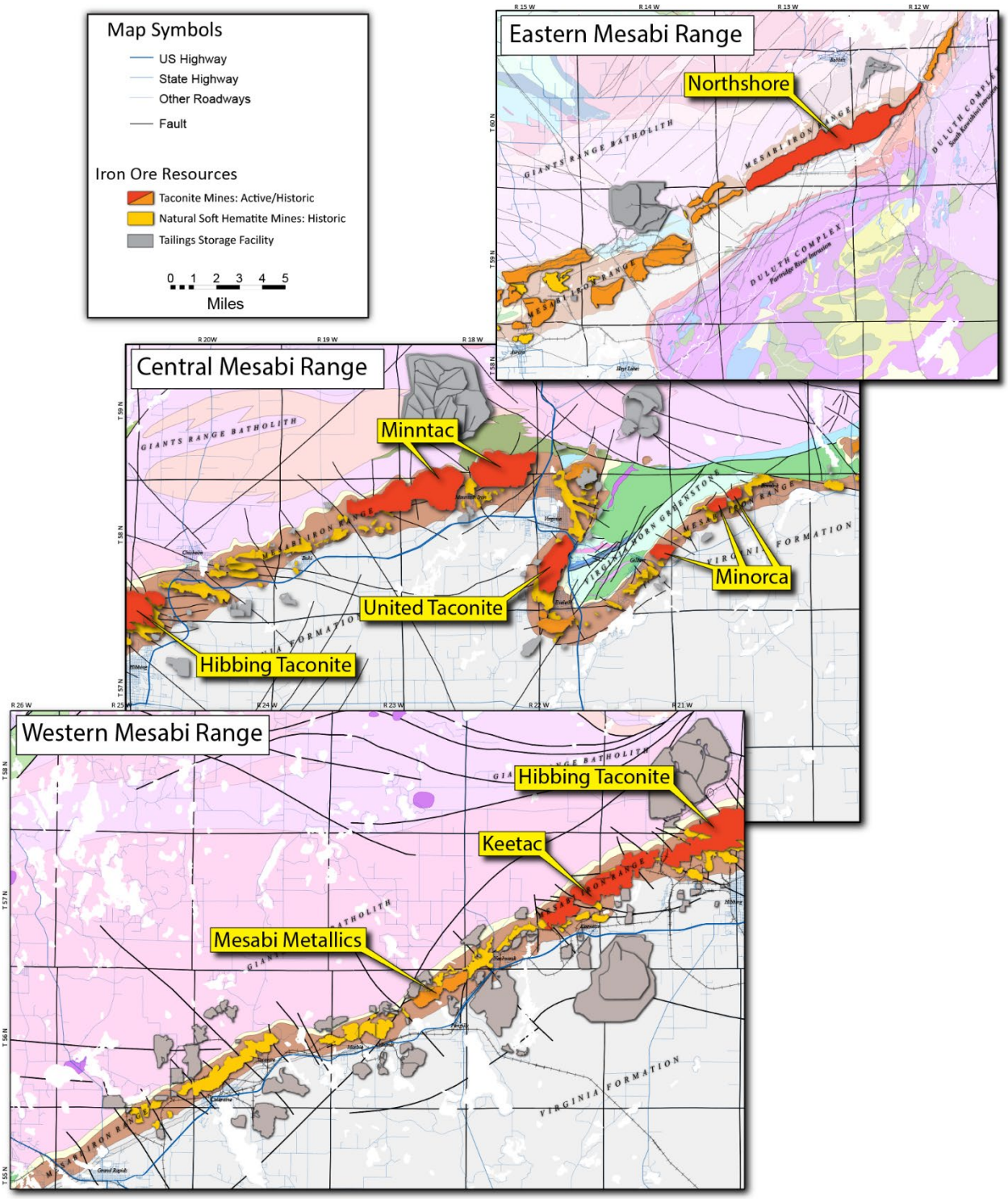


Figure 3-2. Bedrock geology and iron mining features of the Mesabi Iron Range.

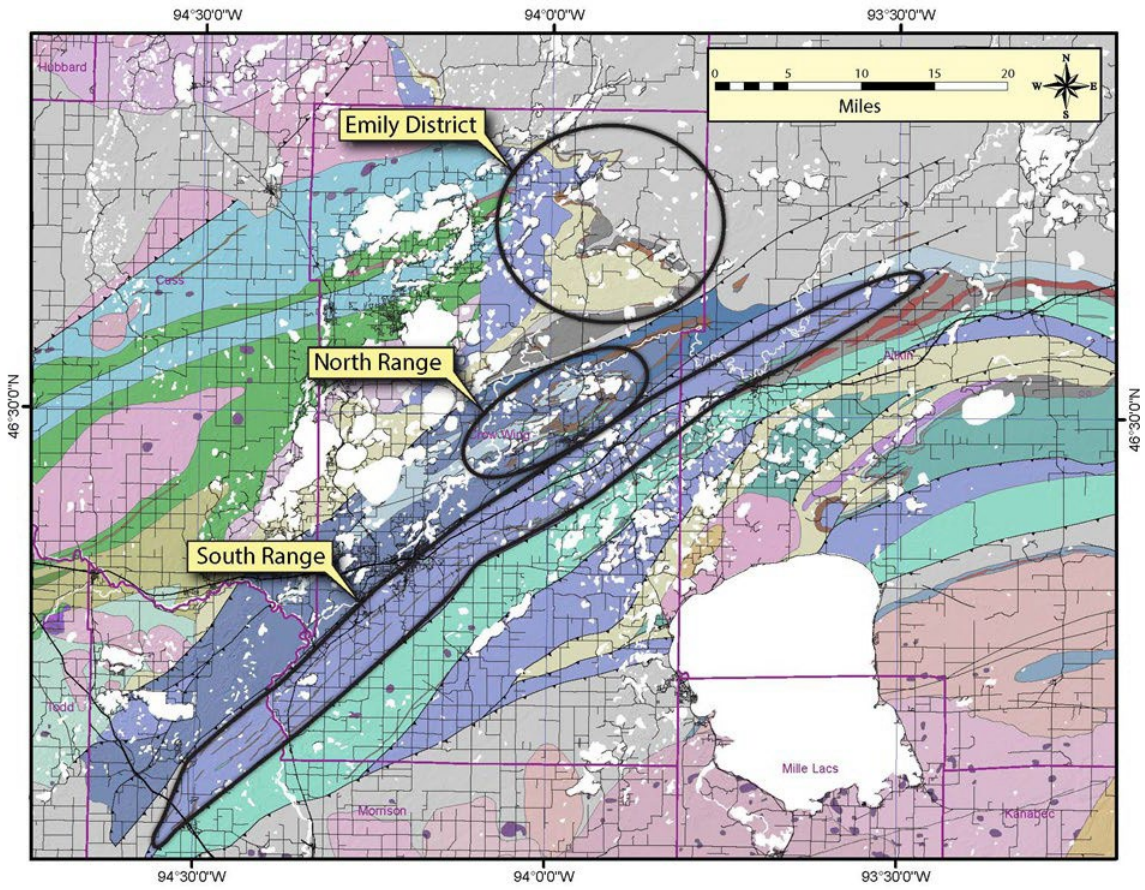


Figure 3-3. Bedrock geologic map of the Cuyuna Iron Range of Minnesota, illustrating the locations of the Emily District, North Range, and South Range.

Since their discovery in 1904, it has been recognized that the iron-formations and associated ore deposits of the Cuyuna iron range in east-central Minnesota contained appreciable quantities of manganese, and large quantities of manganese were extracted as ferromanganese ores from several mines on the North range from 1911 to 1984. The presence of this manganese resource sets the Cuyuna range apart from other iron-mining districts of the Lake Superior region.

Although relatively small, the North range was the principal site of mining activity (Fig. 3-4), which had largely ceased by 1970. The South range, where one small open pit and only a few underground mines were operated, in the 1910s and 20s, comprises an area of northeast-trending, generally parallel belts of iron-formation extending from near Randall in Morrison County northeast for about 100 km. In addition to the three named districts, numerous linear magnetic anomalies occur east of the range proper, and may indicate other, but currently poorly defined, beds of iron-formation.

Three major insights regarding the geology of the Cuyuna range have emerged from the geologic mapping (Schmidt, 1963) and associated studies which utilized geophysical and drilling data (Southwick et al., 1988). First, there is clear evidence that iron sedimentation occurred at several different times and under varying geological conditions. This observation invalidates the stratigraphic premises of Morey (1978). Major iron-formations are associated stratigraphically with volcanic rocks in the South range, with black shale, argillite and rare volcanic rocks in the North range, and with shallow-water deposits of sandstone and siltstone in the Emily district.

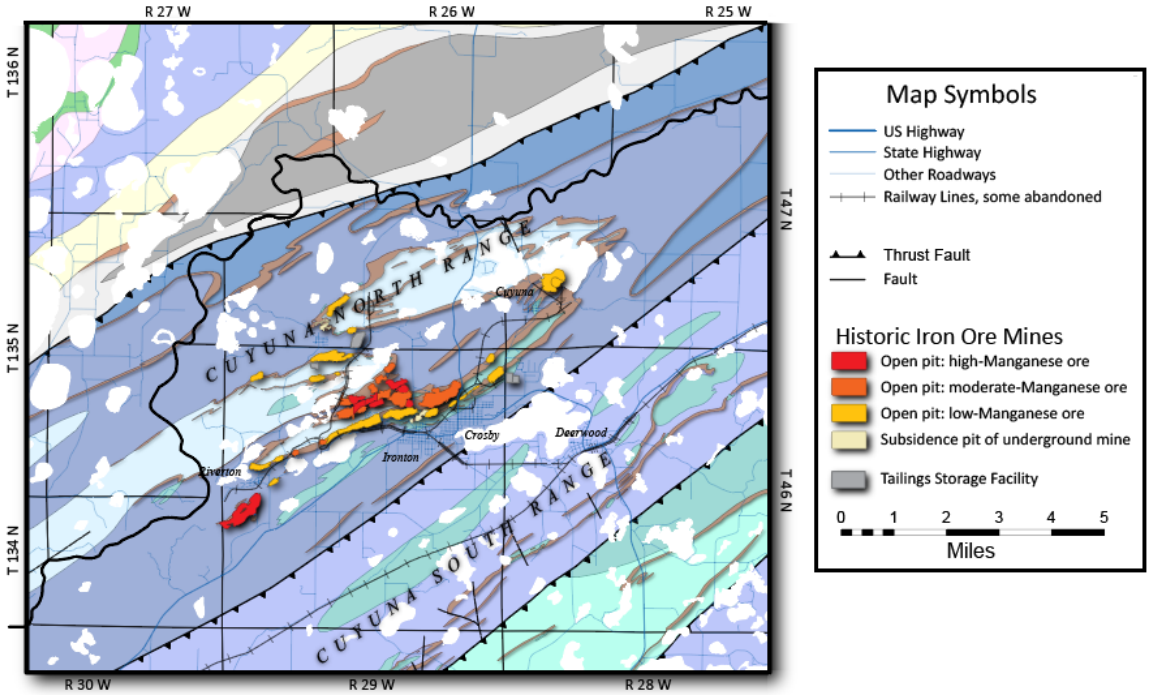


Figure 3-4. Bedrock geology and open pit Fe-Mn mine map of the North Range of the Cuyuna Iron Range.

Second, the iron-rich strata of the Emily district are correlative with the Biwabik Iron Formation of the Mesabi Range, as inferred by Marsden (1972) and Morey (1978). However, they and the other sedimentary rocks of the well-known Animikie Group occur above a major deformed unconformity that cuts across previously deformed, somewhat older sedimentary and volcanic rocks of the North range. There, a prominent iron-rich unit named the Trommald Formation, as well as several other units beneath the unconformity, forms part of a locally twice-deformed sequence. Therefore, the rocks of the North range and the Emily district cannot be correlative but are separate stratigraphic entities. Because the stratigraphic succession of folded sedimentary rocks on the North range comprises a distinct stratigraphic entity, Southwick et al., (1988) referred to it informally as the North Range group with the understanding that a formal name may be justified later. As defined by Schmidt (1963), the stratigraphic sequence in the North range consists of a quartz-rich lower sedimentary unit named the Mahnomen Formation, a middle iron- and locally manganese-rich sequence assigned to the Trommald Formation, and an upper greywacke shale interval called the Rabbit Lake Formation.

Third, Southwick et al., (1988) recognized several geophysically defined structural discontinuities in the southern part of the Cuyuna iron range, within and southeast of the South range. These discontinuities are marked by demonstrable contrasts in metamorphic grade, by differing structural styles, and by different lithic components. One of the most pronounced of these, the Serpent Lake structural discontinuity, passes along the south edge of the North range. This discontinuity is interpreted as a tectonic boundary, probably involving major thrust faults between slices of folded rocks. Thus, it seems certain that the iron-rich strata of the South range are not correlative with either the Trommald Formation of the North range or the iron-rich strata of the Emily district. The fact that iron-formation occurs within three different stratigraphic and structural contexts in the Cuyuna iron range is of considerable importance to the ultimate development of manganese resources. Since we now recognize that the Emily district, the North range, and the South range are separate entities, we can no longer develop regional syntheses that extrapolate mineralogical and structural attributes from one entity to another.

Cuyuna Iron Range Manganese Resources

Several attempts have been made over the last 70 years to estimate the size of the manganese resources of the Cuyuna iron range. For example, Lewis (1951) estimated that 455 million metric tons of manganiferous iron-formation containing from 2 to 10 percent manganese were available to open-pit mining to a depth of 45 meters. Dorr et al., (1973) used that estimate to establish that the Cuyuna range contains approximately 46 percent of known manganese resources in the United States. US Steel geologist Richard Strong (1959) estimated iron and manganese resources from several well-drilled deposits in the Emily District and Beltrame et al., (1981) estimated a minimum of 170 million metric tons of manganiferous rock with an average grade of 10.46 weight percent manganese.

All historic grade/tonnage estimates (Lewis, 1951, Strong, 1959, and Beltrame et al., 1981) should be considered with a certain amount of skepticism for at least two reasons. First, the manganese data used to make these estimates were, for the most part, by-products of data that were acquired originally by various mining companies as they explored for iron. Second, the various estimates were prepared for different reasons at different times, using different databases and different methodologies. Therefore, the results of these estimates are neither comparable, nor do they necessarily reflect the actual resource. A table listing the grade and tonnage from properties that Strong (1959) and Beltrami et al. (1981) estimated manganese resources is given in Table 3-2 and a location map of these properties is presented in Figure 3-5.

Table 3-2. Manganese grade and tonnage estimates from reports by Strong (1959) and Beltrame et al. (1981).

MAP ID	PROPERTY	AREA	TYPE	YEAR	TONNES	MN %	MN lbs	SOURCE
1	West Ruth Lake Deposit	Emily District	Measured	1959	24,012,200	15.28	8,088,891,898	DNR 136-25-00, File #1, Item #5
4	Lake Mary Deposit	Emily District	Measured	1959	8,536,562	8.30	1,561,700,137	DNR 136-25-00, File #1, Item #5
2	East Ruth Lake Deposit	Emily District	Measured	1959	4,874,300	7.65	821,956,313	DNR 136-25-00, File #1, Item #5
3	Emily-Shawnut Reserve	Emily District	Measured	1981	833,709	10.56	194,006,830	MGS Report of Investigations 24
5	Zeno Reserve	North Range	Measured	1981	1,284,211	12.81	362,676,390	MGS Report of Investigations 24
28	Pontiac Mine	North Range	Measured	1981	883,351	16.81	327,418,704	MGS Report of Investigations 24
6	Gloria Mine	North Range	Measured	1981	559,711	12.59	155,354,314	MGS Report of Investigations 24
12	Sagamore Mine	North Range	Measured	1981	641,491	8.79	124,279,088	MGS Report of Investigations 24
7	Huntington Mine	North Range	Measured	1981	866,032	3.59	68,479,191	MGS Report of Investigations 24
	Minnesota Land and Colonization Reserve	North Range	Indicated	1981	298,099	10.14	66,639,577	MGS Report of Investigations 24
	Martin Mine	North Range	Measured	1981	460,879	6.52	66,265,395	MGS Report of Investigations 24
	Milford Mine	North Range	Measured	1981	272,226	9.68	58,094,992	MGS Report of Investigations 24
	Kona Reserve	North Range	Indicated	1981	261,770	9.07	52,343,277	MGS Report of Investigations 24
	Merritt No. 1 Mine	North Range	Measured	1981	129,200	15.10	43,000,065	MGS Report of Investigations 24
	Alstead Mine	North Range	Measured	1981	119,216	13.23	34,771,874	MGS Report of Investigations 24
	Preston Reserve	North Range	Indicated	1981	232,418	4.47	22,880,709	MGS Report of Investigations 24
	Manuel Mine	North Range	Measured	1981	205,190	5.04	22,784,115	MGS Report of Investigations 24
	Carlson-Nelson Mine	North Range	Measured	1981	302,046	3.32	22,107,769	MGS Report of Investigations 24
	West Airport Mine	North Range	Measured	1981	237,077	3.50	18,311,205	MGS Report of Investigations 24
	Hillcrest Mine, North	North Range	Measured	1981	60,224	12.97	17,220,404	MGS Report of Investigations 24
	Algoma Mine	North Range	Measured	1981	57,836	12.87	16,410,074	MGS Report of Investigations 24
	Arko Mine	North Range	Measured	1981	46,738	14.38	14,820,953	MGS Report of Investigations 24
	Ferro Mine	North Range	Measured	1981	26,309	23.17	13,438,912	MGS Report of Investigations 24
	Syracuse Reserve	North Range	Measured	1981	47,005	12.68	13,140,051	MGS Report of Investigations 24
	Northland Mine	North Range	Measured	1981	64,858	8.86	12,668,669	MGS Report of Investigations 24
	Hunter Reserve	North Range	Measured	1981	71,851	7.84	12,418,886	MGS Report of Investigations 24
	Mangan No. 2	North Range	Measured	1981	135,326	3.46	10,317,782	MGS Report of Investigations 24
	Aune Reserve	North Range	Measured	1981	90,530	4.66	9,300,626	MGS Report of Investigations 24
	Rowe Mine	North Range	Measured	1981	51,121	6.06	6,830,395	MGS Report of Investigations 24
	Sisters Mine	North Range	Indicated	1981	14,631	19.70	6,354,392	MGS Report of Investigations 24
	Armor No. 2 Mine	North Range	Measured	1981	164,803	1.39	5,050,259	MGS Report of Investigations 24
	Ironton Mine	North Range	Measured	1981	45,019	4.34	4,307,441	MGS Report of Investigations 24
	Joan No. 1 and Mallen Mines	North Range	Measured	1981	5,806	21.03	2,691,845	MGS Report of Investigations 24
	Hennen Reserve	North Range	Measured	1981	22,866	3.99	2,011,393	MGS Report of Investigations 24
	Mallen Mine	North Range	Measured	1981	64,204	1.41	1,995,790	MGS Report of Investigations 24
	South Yawkey Mine	North Range	Measured	1981	3,963	3.59	313,655	MGS Report of Investigations 24
	Wearne Mine	North Range	Measured	1981	1,348	1.67	49,630	MGS Report of Investigations 24
70	Omaha Mine	South Range	Measured	1981	1,507,189	3.14	104,335,269	MGS Report of Investigations 24
	Clearwater Lake Reserve, X-43	South Range	Measured	1981	581,549	3.61	46,234,409	MGS Report of Investigations 24
	Willcuts Reserve	South Range	Measured	1981	232,767	1.45	7,440,861	MGS Report of Investigations 24

Despite their problematic nature, the estimates of Lewis (1951) and Beltrame et al., (1981) do show that the Cuyuna range contains a large, but low- to moderate-grade manganese resources remaining. This large size, combined with the fact that the manganese deposits are in an established mining district, makes the Cuyuna range an ideal place to study geological and technological factors needed to evaluate this and other sedimentary manganese deposits in the United States. Especially important are studies of the geologic habit of the manganese and the controls on its distribution and subsequent concentration into deposits of minable size.

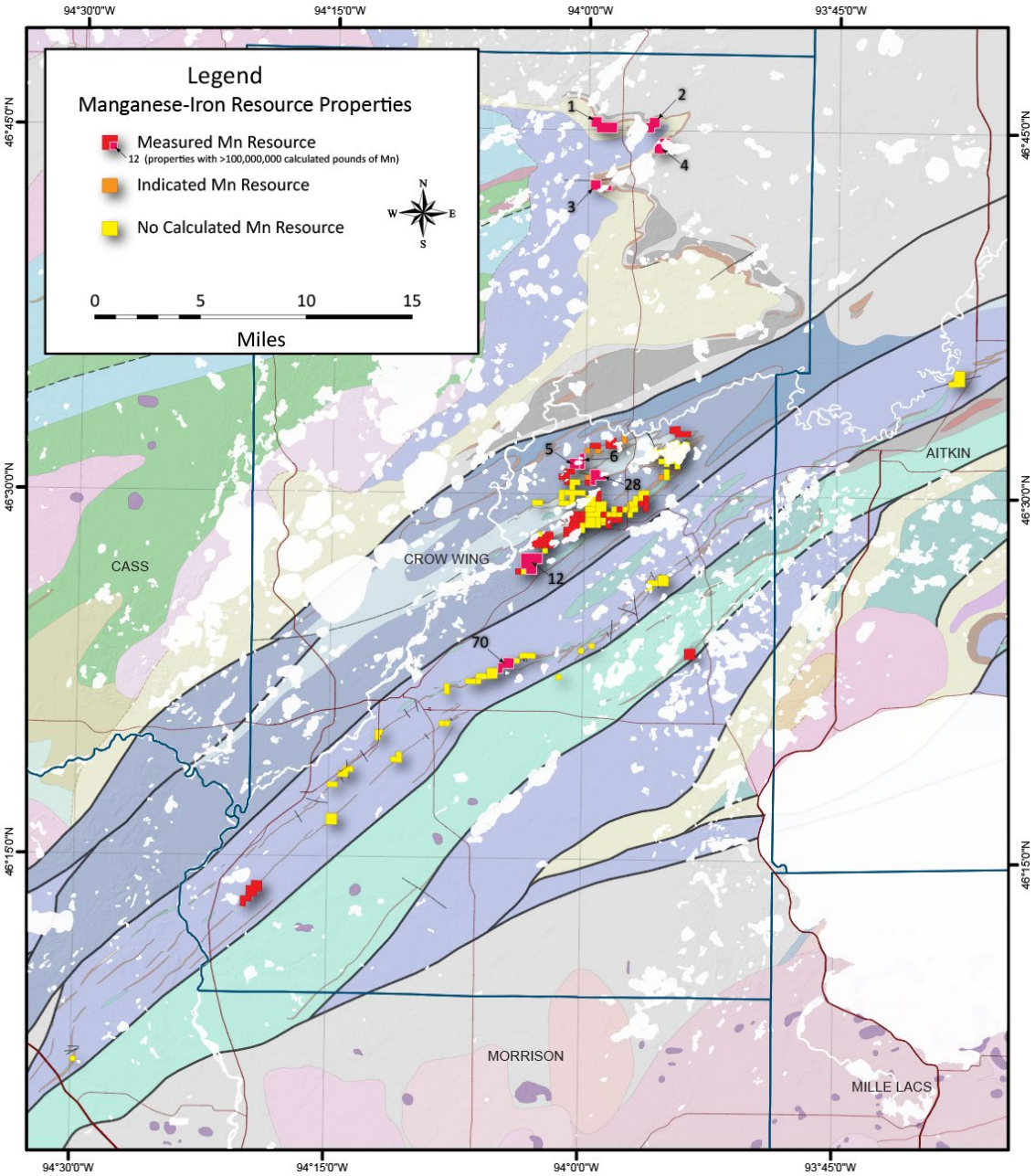


Figure 3-5. Bedrock geology and location map of properties outlined in reports by Strong (1959) and Beltrame et al. (1981) that includes manganese grade-tonnage estimates. Labeled parcels correlate with the MAP ID column in Table 3-2 and are those with an estimated resource greater than 100,000,000 pounds of manganese metal.

Penokean Orogeny

The Penokean orogeny began at about 1880 Ma when an oceanic arc, the Paleoproterozoic Pembine–Wausau terrane, collided with the southern margin of the Archean Superior (Laurentia) craton marking the end of a period of south-directed subduction. The docking of the buoyant craton to the arc resulted in a subduction jump to the south and development of back-arc extension both in the initial arc and adjacent craton margin to the north. Synchronous extension and subsidence of the Laurentia craton resulted in the development of broad shallow seas overlapping the Archean craton. The classic Superior-type banded iron-formations of the Lake Superior District, including those in the Marquette, Gogebic, Mesabi, and Gunflint Iron Ranges, formed in that sea. The newly established subduction zone caused continued arc volcanism until about 1850 Ma when a fragment of Archean crust, now the basement of the Marshfield terrane, arrived at the subduction zone.

The convergence of Archean blocks of the Superior and Marshfield cratons resulted in the major contractional phase of the Penokean orogeny. Rocks of the Pembine–Wausau arc were thrust northward onto the Superior craton causing subsidence of a foreland basin in which sedimentation began at about 1850 Ma in the south (Baraga Group rocks) and 1835 Ma in the north (Rove Formation). A thick succession of arc-derived turbidites constitutes most of the foreland basin-fill along with lesser volcanic rocks. In the southern fold and thrust belt, tectonic thickening resulted in high-grade metamorphism of the sediments by 1830 Ma. At this same time, a suite of post-tectonic plutons intruded the deformed sedimentary sequence and accreted arc terranes marking the end of the Penokean orogeny. A regional geologic map of the Penokean orogen, modified from Schulz and Cannon (2007), is given in Figure 3-5.

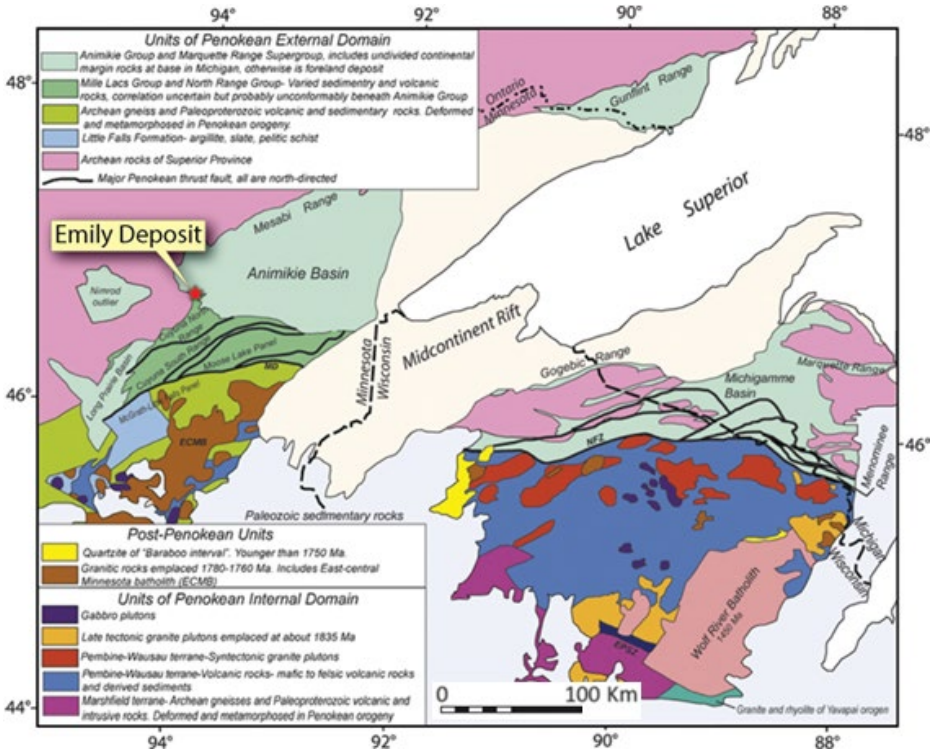


Figure 3-5. Generalized geologic map of the Penokean orogen. *Abbreviations*: ECMB - East-central Minnesota batholith; EPSZ - Eau Pleine shear zone; MD - Malmo discontinuity; NFZ - Niagara fault zone. Modified from Schulz and Cannon, 2007.

The Penokean deformation in Minnesota includes a southern intensely and complexly deformed series of thrust panels (Cuyuna North, Cuyuna South, Moose Lake, McGrath-Little Falls panels) that gives way northward to progressively more weakly and simply deformed rocks (Emily District) across a belt

about 100 km wide. Farther north strata in the Mesabi and Gunflint Iron Ranges are essentially undeformed (Holst, 1991). It should be noted that the "more weakly and simply deformed rocks" of the Emily District have been shortened ~250% into a series of shallowly east-plunging anticlines and synclines. Substantial progress has been made in deciphering the structure of the poorly exposed rocks of the Minnesota foreland through the use of aeromagnetic and gravity data and drillhole information. Southwick and Morey (1991) and Southwick et al. (1988) have presented syntheses of this information.

The complex thrust panels on the south, like comparable structures in Michigan, appear to be thin-skinned slices without Archean basement. However, as in Michigan, this area of thin-skinned thrusting is also the area where Archean-cored gneiss domes developed during post orogenic collapse of the Penokean orogen (Holm and Lux, 1996; Schneider et al., 2004). Farther north, basement-cover relations are not well known except for the Mesabi Range where Paleoproterozoic strata are mostly nearly flat lying above an undisturbed unconformity with Archean basement rocks. A schematic north-south geologic cross section of the Penokean orogeny in Minnesota, modified from Southwick and Morey (1991) is presented in Figure 3-6.

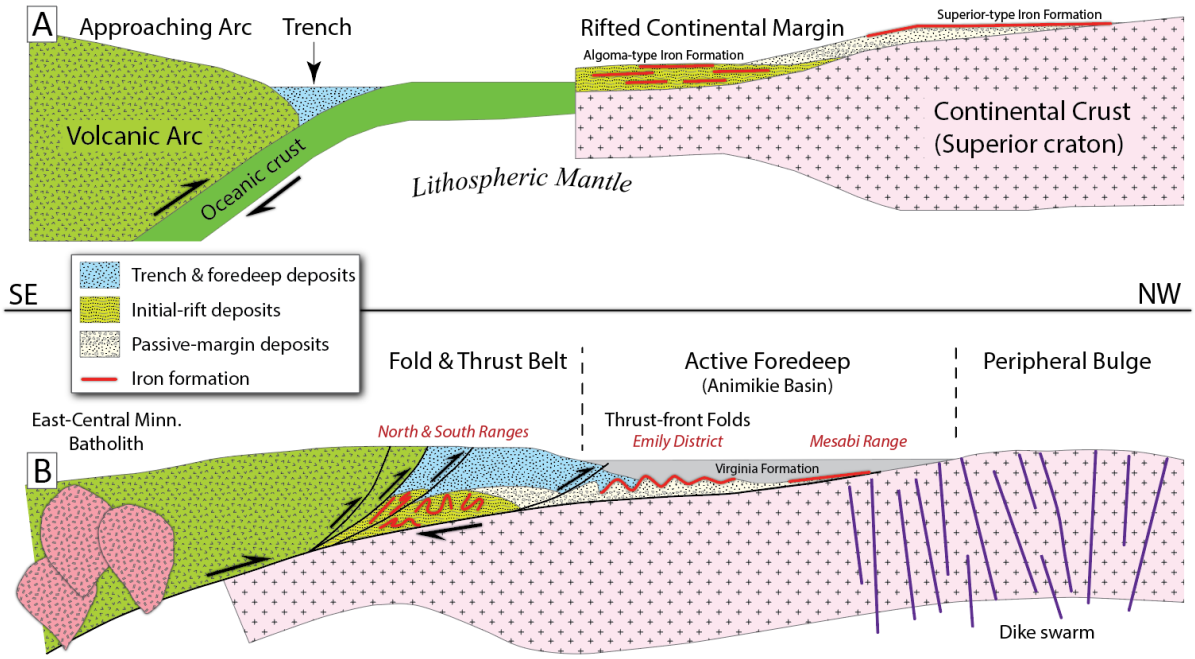


Figure 3-6. Schematic diagram illustrating the interpreted tectonic setting of the Penokean orogen in Minnesota. A) continental margin sedimentation, and B) thin-skinned thrusting and deformation related to the Penokean orogeny. Modified from Southwick & Morey, 1991.

Post Penokean Weathering and Erosion

Perhaps the most important component in the formation of the high-grade iron and manganese ores on the Mesabi and Cuyuna ranges is the vast amount of time (measured in hundreds of millions of years) upon which the newly-formed and uplifted Penokean mountains of the southern Laurentia craton weathered and eroded. As plate tectonic forces moved Laurentia across the globe to its current position on planet Earth, there were long periods of time when it resided within the tropical weathering zone (+30° to -30° latitude) near the Earth's equator. It is believed that the supergene enrichment of iron (to >60 wt.% elemental Fe) and manganese (to >50 wt.% elemental Mn) on the Mesabi and Cuyuna largely formed during the protracted periods of time that the area resided within the tropical weathering zone. A paleogeographic reconstruction of the location of Laurentia on planet Earth is given in Figure 3-7.

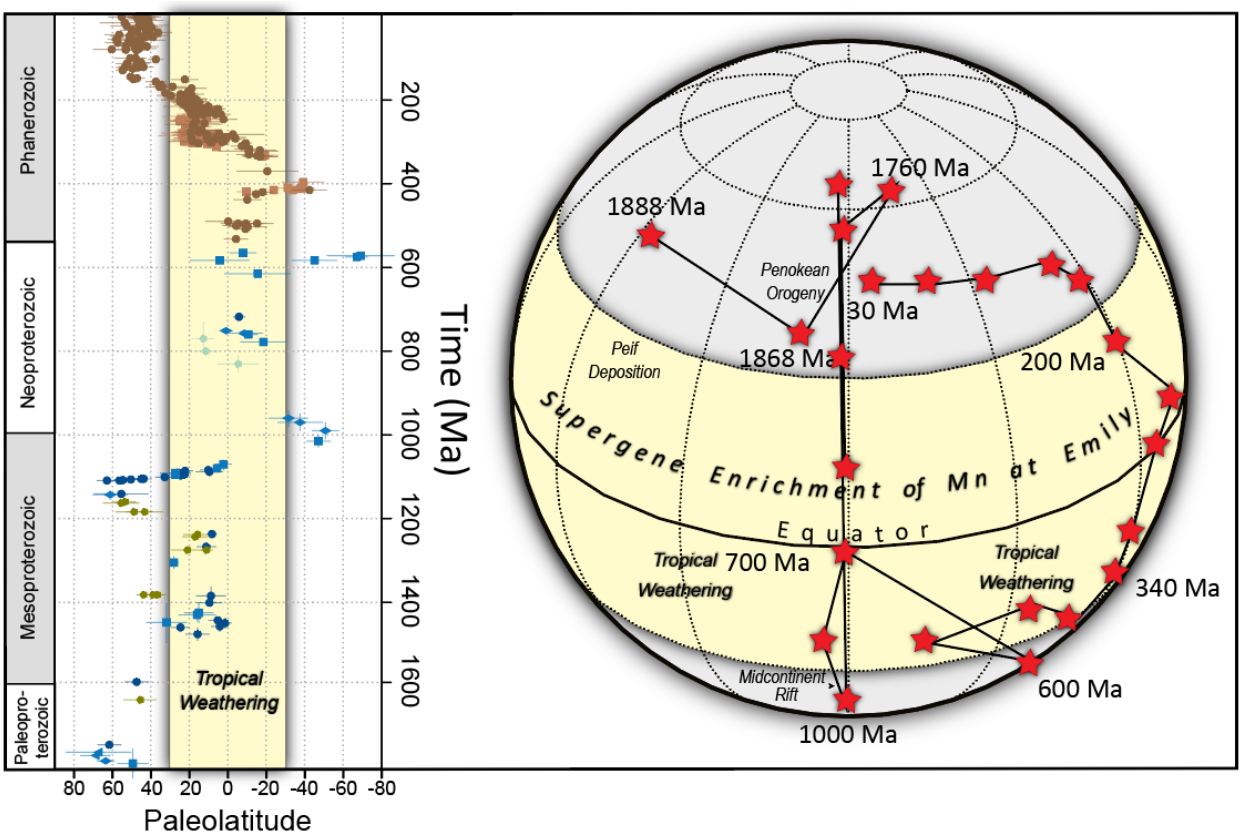


Figure 3-7. Paleogeographic reconstruction of the Laurentia craton from the Paleoproterozoic to present times.

FIELD TRIP STOPS

Four field trip stops have been selected to showcase selected geological features associated with supergene weathering of primary Paleoproterozoic Superior-type iron formation into high-grade of Fe and Mn ores. The locations of the field trip stops are shown in Figure 3-8 and briefly described below.

1) DNR drillcore library in Hibbing: Drillcore review of unoxidized Biwabik Iron Formation,
2) Emily deposit core shed: Drillcore review of high-grade supergene Mn ores, primary Mn-Fe carbonate-facies iron formation, Overlying Sudbury Impact breccias & accretionary lapilli?
3) Mary Ellen Mine: Walk into a historic natural-ore (hematite) open pit iron mine, sampling of the classic Mary Ellen stromatolites, and
4) Large roadcut of the partially oxidized Biwabik Iron Formation adjacent to the historic natural-ore Rouchleau Mine Complex.

Stop 1: DNR Drillcore Library, Hibbing Minnesota

Longitude/Latitude: 47.432412°N, -92.941811E

UTM NAD 83 Zone 15N: 504388E, 5253220N

At our first stop on this field trip, we will examine sections of two different drill cores of the Biwabik iron formation to directly compare depositional features to post-depositional features. The Drill Core Library is maintained by the Minnesota Department of Natural Resources, Lands and Minerals Division, and provides direct access for visitors to examine publicly owned geologic materials and exploration data. This incredible

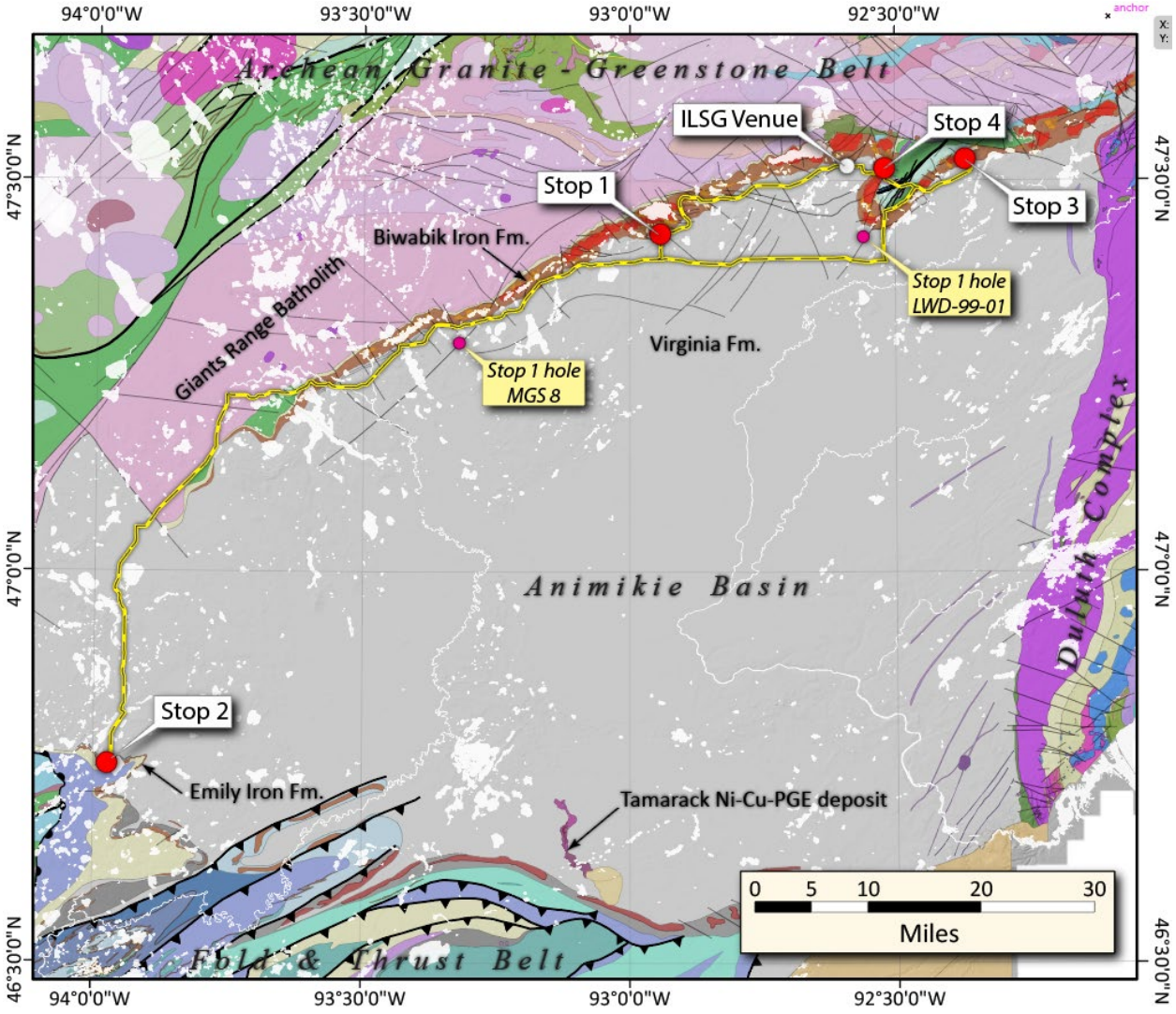


Figure 3-8. Location map of field trip stops and the collar location of the two drill holes looked at Stop 1.

repository contains over 7,000 mineral exploration cores, 1,500 roadway and bridge foundation cores, and 500 cores collected during scientific, governmental, and academic research, and their curation activities support researchers, exploration geologists, and engineers from around the world.

Depositional features and mineralogy in Precambrian chemical sedimentary rocks like iron formations have long been of interest to the scientific community as they may record information about Earth's early surface conditions. However, recovering data that links to depositional conditions requires the reconstruction of post-depositional mineral reactions and quantification of geochemical exchange. For this reason, the original mineralogy and geochemistry of iron formations has been the subject of numerous investigations.

Critical early investigations recognized the mineral greenalite - postulating its authigenic origin as a "chemical oceanic precipitate", and hypothesizing its role in forming the iron ore deposits in Minnesota, USA (Irving, 1886; Irving and Van Hise, 1892; Leith, 1903; Van Hise and Leith, 1911; Aldrich 1929; Gruner, 1946; Tyler, 1949; James, 1954; White, 1954; Goodwin, 1956; Gundarson and Schwartz, 1962; LaBerge; 1964). Key initial evidence for a primary or early origin for greenalite in the Superior craton included: (1) its abundance in low temperature, well-preserved assemblages, and comparative absence in metamorphosed iron formations in the same region (LaBerge, 1964); (2) the existence of submicroscopic

greenalite in the cores of circular to elliptical sand-sized grains as either the main mineral phase, <0.05 mm spherules, or as dusty nano-scale (submicroscopic) particles (Goodwin, 1956); intergranular relationships between phases where greenalite is crosscut by other phases in the same sample; (LaBerge, 1964; French, 1973; Klein and Fink, 1976), and even distribution throughout primary bedding (LaBerge, 1964). Recent mineralogical investigations (e.g, Duncanson et al., 2024, Muhling et al., 2025 and references therein) highlight that the earliest forming minerals in iron formation are commonly found within silica-cemented horizons, where abundant chert cement silicified the sediments at or near the sediment water interface. Such silica-cemented horizons preserve incomplete reactions and allow for identification of direct mineral relationships and local element exchange. Common mineral reactions observed in the Biwabik iron formation include the transformation of greenalite to minnesotaite, minnesotatite to stilpnomelane, greenalite to magnetite, siderite to magnetite, and magnetite to hematite. Of the mineral reactions that commonly occur in iron formation, transformations of Fe^{2+}-containing silicates like greenalite to mixed valence state minerals like magnetite and further oxidation of magnetite to hematite, contributed to formation of iron ores in the Biwabik.

To illustrate some of the many post-depositional reactions that occur in iron formations worldwide, we will examine a small section of two drill cores, MGS 8 from the western end of the Mesabi iron range, and LWD-99-01 from near the Virigina horn area (see Figure 3-8 for locations). LWD-99-01 clearly preserves depositional features, while MGS-8 documents abundant post-depositional oxidation throughout.

Stop 2: North Star Manganese Inc Drillcore Shed, Emily Minnesota

Longitude/Latitude: 46.753571°N, -93.973496E

UTM NAD 83 Zone 15N: 425650E, 5178240N

Historic exploration and drilling in the 1940's and 1950's by Pickands Mather and US Steel identified iron and manganese-bearing mineralization within the Emily Iron Formation. US Steel developed but did not implement a preliminary mine plan for mining of the Emily Deposit. Following approximately 50 years of inactivity, Cooperative Mineral Resources (subsidiary of Crow Wing Power) pursued a pilot mining operation using pressurized water that was ultimately unsuccessful. As a follow up investigation into the outcomes of pilot mining, a small-scale drill program was accomplished in 2010-2012.

A drilling program was designed and executed by Big Rock Exploration, LLC, in 2022-2023. A total of 29 drill holes were completed to extend mineralization and refine the previous resource estimates. A total of 13,107 feet of drilling was completed for this program. Data collected for this project includes lithological, structural, geotechnical, geochemical and geophysical data from the drill core.

Through interpretation of legacy, recent and new drilling data, Big Rock Exploration identified coherent zones of high-grade manganese mineralization (30 to ≥40 wt.% Mn) over a 1.25-kilometer strike length. Mineralization is comprised of horizons of secondary manganese oxide minerals, as well as locally present primary iron-manganese carbonate mineralization. An ore deposit model has been developed that incorporates the oxidation of primary thin-bedded manganese-iron carbonates into massive manganese oxide through early folding and prolonged periods of weathering, oxidation, and erosion. This ore deposit model and associated geological model have been used to support an updated and expanded mineral resource estimate (Table 3-3) for the Emily Deposit that was completed and published by Forte Dynamics (Hulse et al., 2024) on May 24, 2024.

We'll first begin the review of important geological features revealed in the four Emily Mn deposit drillholes on display in the core shed by elucidating our current understanding of the geology and structure for the whole Cuyuna Iron Range and then focus specifically on the stratigraphy and ore-forming processes at Emily through a series of figures and descriptive text written into a technical report (Steiner et al., 2024) and orally presented at the 2024 ILSG conference (Peterson and Steiner, 2024).

Table 3-3. Mineral resource estimate for the Emily Manganese deposit.

RESOURCE CLASS	CUTOFF (m%)	TONNES	DENSITY (g/cm3)	Mn (%)	Fe (%)	SiO_2 (%)
Indicated	15	4,264,430	3.08	22.34	21.70	25.77
	10	6,234,330	3.10	19.27	22.41	29.38
	5	14,474,660	2.98	12.06	22.20	38.02
Inferred	15	3,184,740	3.12	20.25	20.42	29.68
	10	4,914,670	3.15	17.50	20.44	32.29
	5	9,608,840	3.01	12.11	20.29	33.83

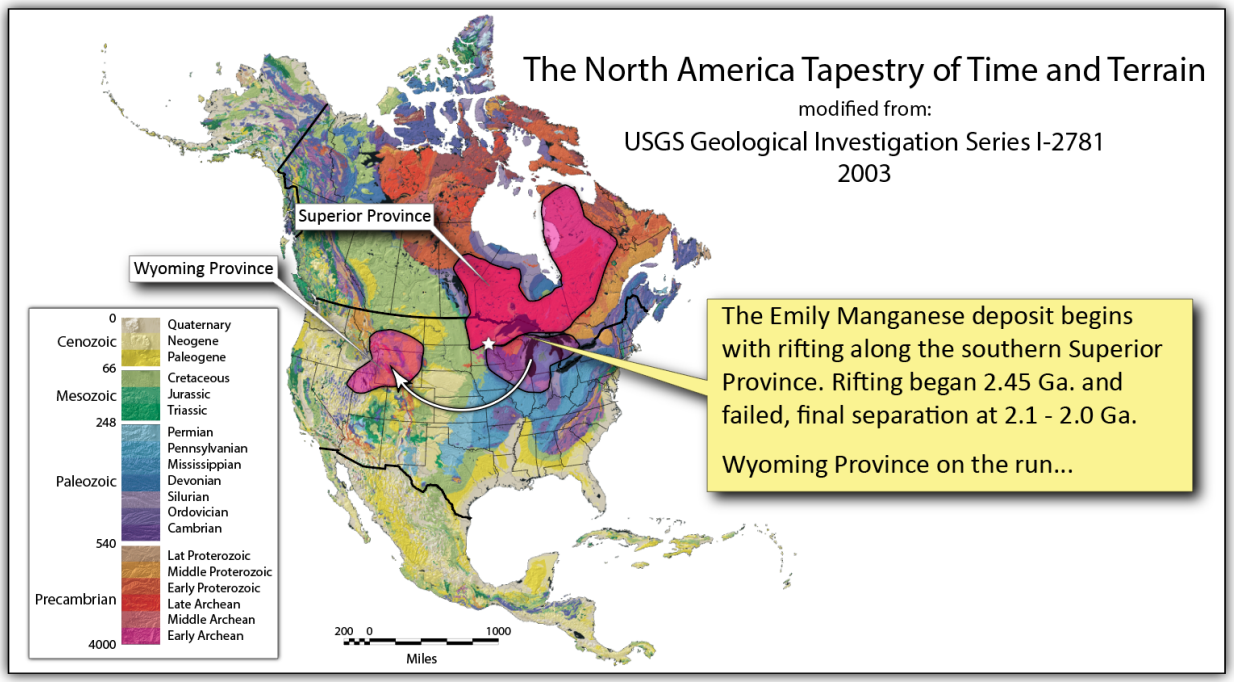


Figure 3-9. Continent-scale initial condition framework of Paleoproterozoic iron formations of Minnesota.

Initial Conditions

Deposition of Paleoproterozoic iron formations of the Lake Superior district all owe their origins to the ~2.4 – 2.1 Ga. rifting of the Wyoming Province craton off of the southern Superior Province craton (Figure 3-9). This rifting set the stage for the development of environments of deposition conducive to the formation of thick sequences of both Algoma- and Superior-type iron formations (Figure 3-10).

During the Penokean orogeny (see Figure 3-6) these variable environments of iron formation deposition were transposed northwestward via thin-skinned tectonics into a fold & thrust belt (Cuyuna North and South range thrust panels) over a series of thrust-front folds (Emily District) that was bounded by a basal decollement. Outcomes of the Penokean orogeny in the Cuyuna Range of central Minnesota are shown in an idealized cross sectional view Figure 3-11 and how ~1.8 billion years of erosion has left it today in Figure 3-12.

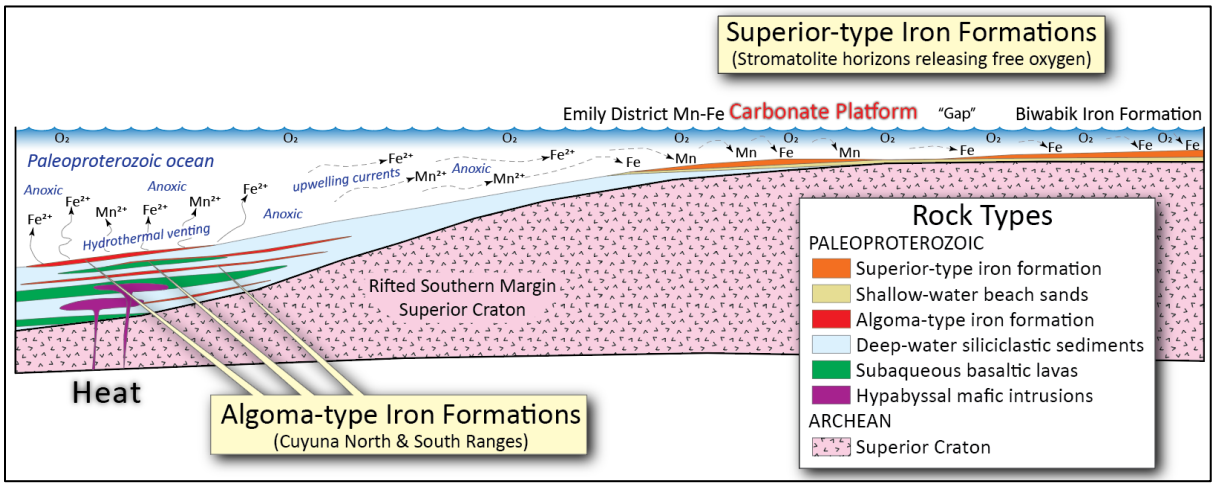


Figure 3-10. Schematic model for the variable environments of deposition of Paleoproterozoic iron formations of the Cuyuna and Mesabi ranges of Minnesota.

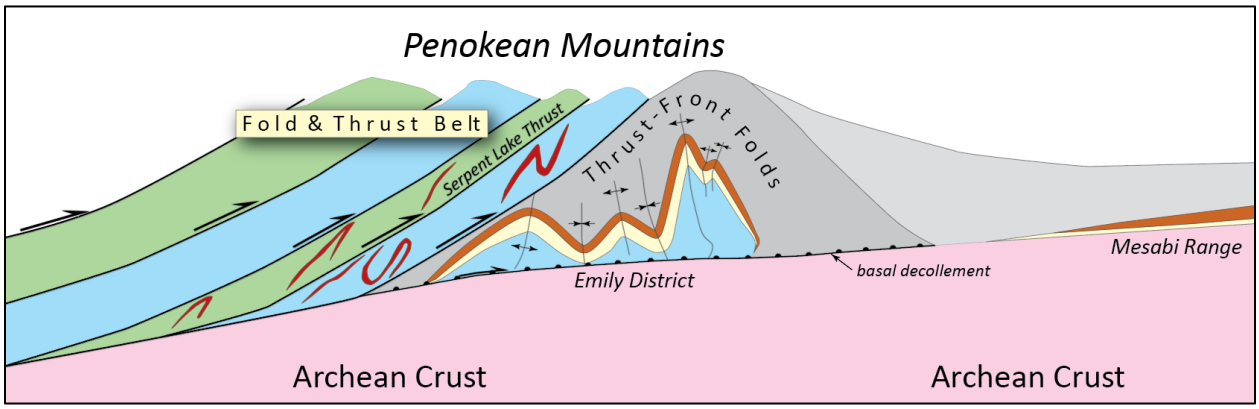


Figure 3-11. Idealized cross section of Minnesota's Penokean Mountains of central Minnesota approximately 1.83 billion years ago.

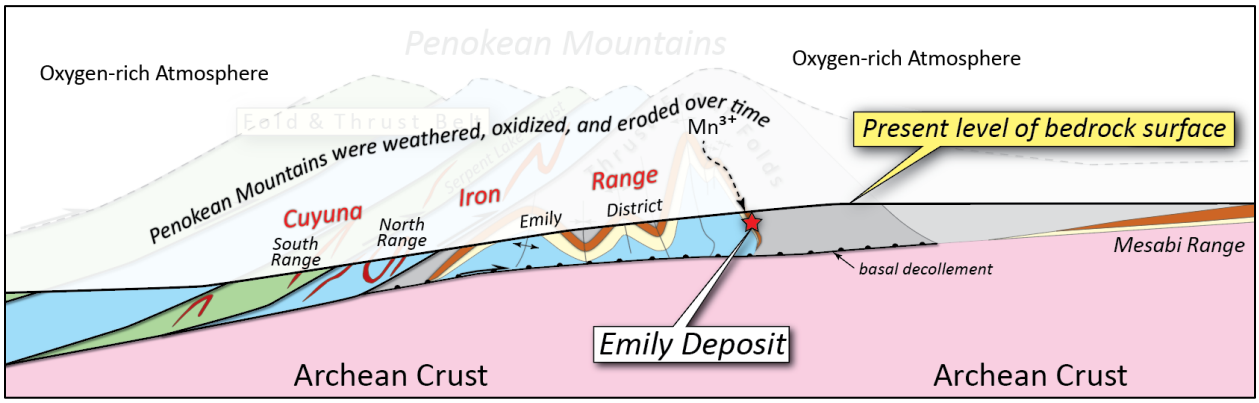


Figure 3-12. Schematic representation of the results of deep weathering and erosion of the Penokean Mountains in central Minnesota.

Geologic Maps

Geologic maps are the foundation upon which geologists interpret Earth processes and depict on a piece of paper the final outcomes of such processes in plan form. As such, the authors have added annotated bedrock geology map of the Cuyuna Range in Figure 3-13 and more specifically for the Emily District of the Cuyuna Range in Figure 3-14.

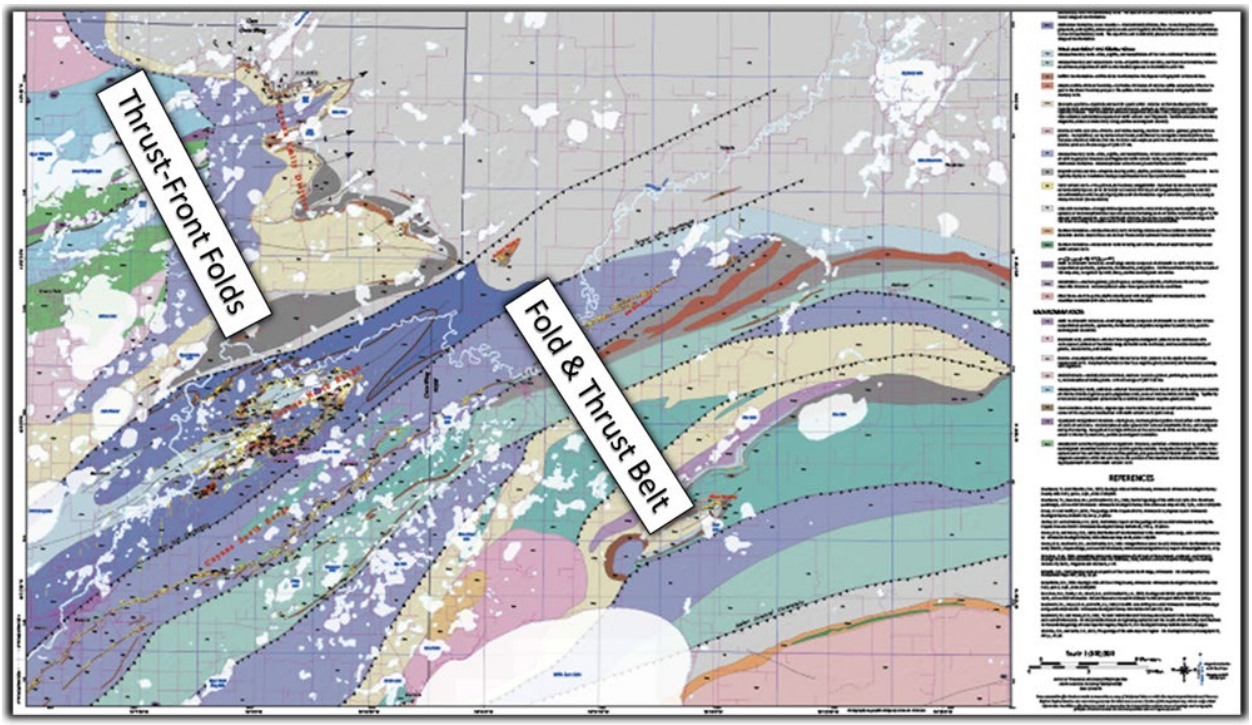


Figure 3-13. Annotated bedrock geologic map of a portion of the Cuyuna Range, central Minnesota. Clipped from the map of Peterson (2022).

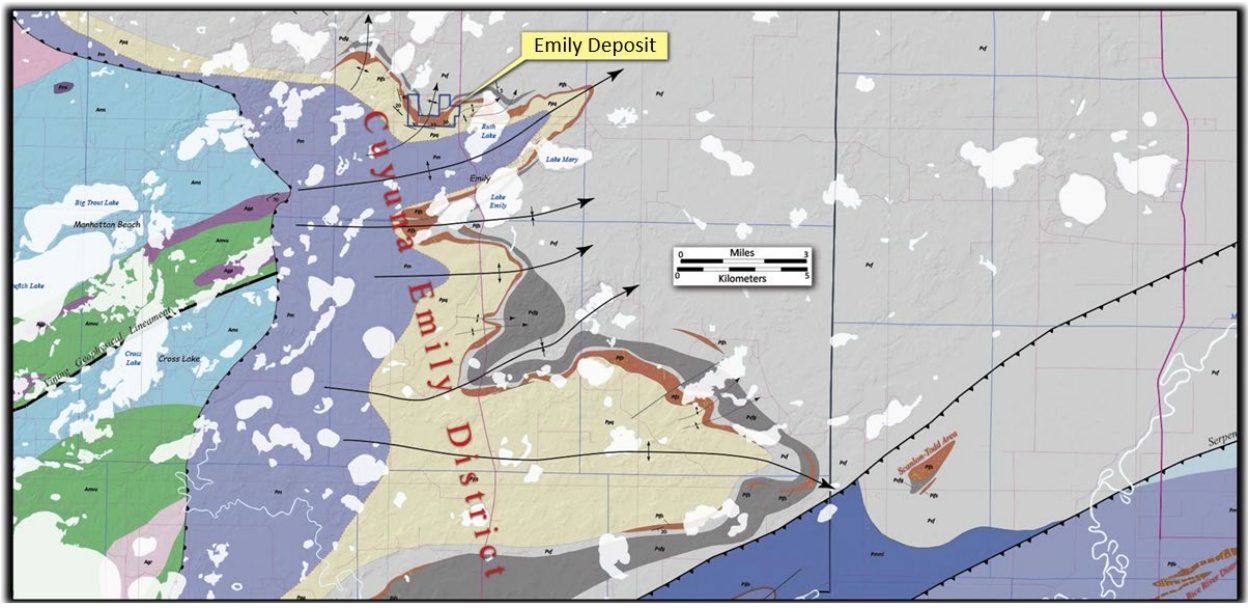


Figure 3-14. Annotated bedrock geologic map of the Emily District, Cuyuna Range, central Minnesota. Modified after Peterson, 2022.

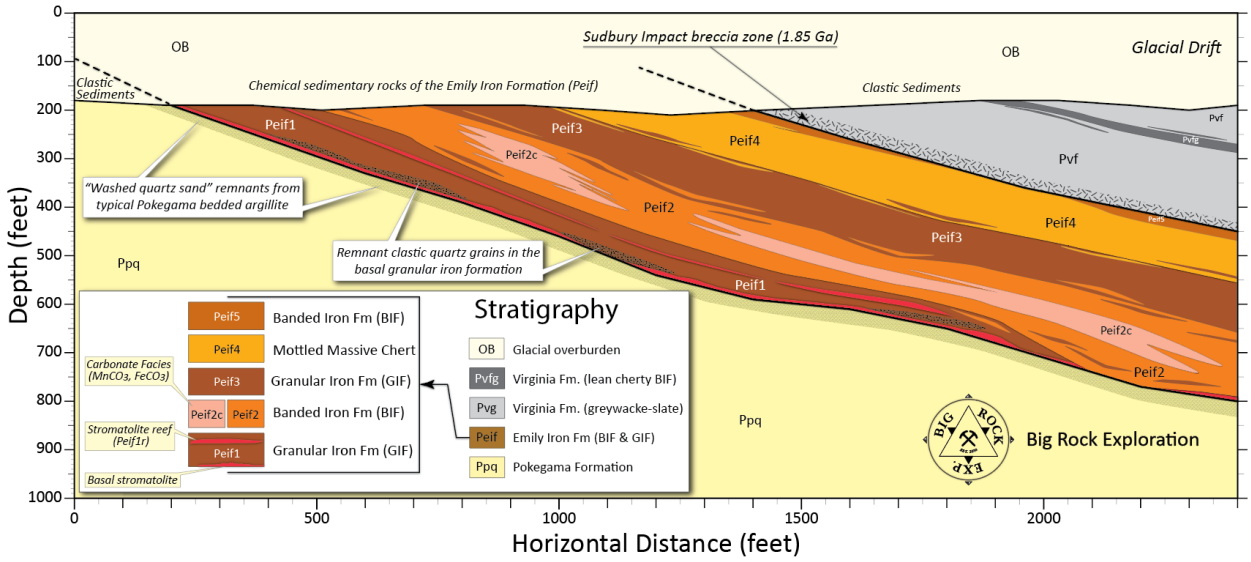


Figure 3-15. Schematic stratigraphic section through the Emily Manganese deposit, after Peterson & Steiner, 2024.

Stratigraphy

Relogging of historic drill core and logging of new core drilled during the 2023 exploration drilling program has led to the identification of a predictable stratigraphic sequence at the Emily Deposit (Fig. 3-15).

The four formations recognized at the Emily Deposit include three units of the Paleoproterozoic Animikie Basin unconformably overlain by Quaternary glacial drift. Descriptions of these stratigraphic units from the oldest to youngest are given below:

1. ***Pokegama Formation*** – White-grey, tan, or cream-colored indurated argillite and quartzite. The Pokegama formation at the Emily deposit is typically a clayey siltstone, though mudstones and quartz-arenites are common. Bedding is quite variable ranging from massive siltstones and quartz-arenites to thick, medium, and thin bedded or even finely laminated clayey-siltstones and mudstones. The Pokegama formation does not host significant manganese mineralization but when observed manganese minerals occur in trace amounts in veinlets or as small patches with iron oxides.
2. ***Emily Iron Formation*** – See below for subdivision descriptions.
3. ***Virginia Formation*** – Grey-brown in color, red when oxidized, fine-grained, well bedded clastic sediments commonly forming turbidite sequences. Fine-scale bedding, graded beds, and sandy lenses are common. Thin horizons of lean iron formation (subunit Pvif) composed of ferruginous chert occur locally. The basal 20-40 feet is characterized by highly disrupted and fragmented turbidite clasts sed in a poorly sorted massive matrix. This horizon has been hypothesized to be landslides associated with the Sudbury Impact.
4. ***Glacial Overburden*** – Unconsolidated glacial material including well sorted sands, lacustrine clays, and unsorted glacial till. The preservation of earthy hematite and saprolitic materials immediately below the basal angular unconformity indicates that overlying Laurentide ice sheet was not eroding its base in the immediate deposit area. Composition of the overburden is inferred from drill returns during tri-cone drilling.

Emily Iron Formation is further divided into five sub-units. Criteria for subunit designation requires that a given interval be sufficiently distinctive in petrologic character to be easily identified, and laterally extensive enough to be intercepted in multiple boreholes. Distinctive petrologic characteristics may be texture (e.g., banded or granular iron formation, composition (e.g., chert, carbonate), or unique

characteristics such as stromatolites. The subdivisions of the Emily Iron Formation are as follows from bottom to top:

1. ***Peif1*** – This unit is located as the base of the Emily Iron Formation lies conformably atop the Pokegama quartzite. The base is commonly cherty or stromatolitic before giving way to grain stones. The majority of the unit is a red-brown to black, granular iron formation (GIF) or ferruginous quartzose sandstone. The upper part (above the Peif1r marker, see below) is granular iron formation composed of silicious, hematitic granules that range from <1 to 2mm in size. Granular iron formation is weakly bedded. The lower part of Peif1 (below the Peif1r marker horizon) contains abundant quartzose sands cemented by iron oxides giving the rock a purple appearance. Sands are composed of well-rounded fine-grained quartz and are interbedded with granular iron formation. Manganese oxide mineralization is most intense within the Peif1 unit. Manganese oxides occur in multiple styles including massive Mn-oxide that replaces all original textures (may be within a bed or cross bedding), interstitial to grains (replacing the original iron cement?), and as veinlets. The most intense manganese oxide mineralization within Peif1 occurs adjacent to (above and below) the Peif1r marker horizon, though mineralization may occur throughout the unit. The lower Peif1 commonly exhibits a pock-mark texture when strongly mineralized. A thin stromatolite horizon (Peifbs) typically occurs at the base of Peif1.
2. ***Peif1r*** – This unit is located within the Peif1 unit. Usually <3m thick, the Peif1r is composed of fine-grained hematite-chert banded iron formation. The base of the Peif1r hosts distinctive digitate stromatolites.
3. ***Peif2*** – This unit lies conformably atop Peif1, usually gradually transitioning from granular iron formation (Peif1) to banded iron formation (Peif2) over a meter. The Peif2 is characterized by fine-grained well-bedded banded iron formation though the composition of the iron formation is variable. The most common composition for Peif2 is a hematite-chert banded iron formation, though this appears to be a secondary, altered composition. The primary composition is iron-manganese carbonate facies type iron formation. The carbonate facies are cream to greenish and gradually becomes red with increased oxidation. Fresh carbonate facies contain much more manganese than oxidized material, with the manganese found in rhodochrosite. This represents a very different manganese host than the oxide mineralization found in the granular iron formation units (Peif1 and Peif3).
4. ***Peif3*** – Peif3 is characterized by interbedded medium to fine grained GIF and fine grained, narrow BIF lenses. This unit lies conformably atop Peif2 where the contact is a graduation from BIF to GIF dominant facies. Both GIF and BIF are weakly to moderately strongly bedded and silicious in composition. Peif3 is commonly mineralized manganese oxides, only subordinate in manganese endowment to Peif1.
5. ***Peif4*** – White to grey, massive chert with mottled patches of iron-oxides. The sharp basal contact with the underlying Peif3 is often “sheared” possibly from bedding parallel slip. Some parts of the massive chert contain faint outlines of granules while most is simply massive white chert. The mottled iron oxides include large irregular pods and stringers, sometimes reaching a meter in width. Manganese is rarely found within the oxide pods.
6. ***Peif5*** – Well-bedded banded iron formation consisting of 2-5cm beds of chert and iron oxide in gradational contact with the underlying Peif4 massive chert. This unit is the least spatially consistent, due to a lack of drillhole intercepts and difficulty identifying it as a result of intense oxidation.

Supergene Enrichment of Manganese

The unique manganese endowment of the Emily Iron Formation is attributed to the primary deposition of Mn-carbonates in a shallow water environment (Figures 3-10, 3-16 and 3-17). However,

subsequent weathering, erosion, and oxidation has redistributed much of the manganese from the carbonate unit to other areas. The majority of the manganese mineralized material at the Emily deposit is composed of manganese oxides including manganite, jacobsite, and cryptolomene/hollandite. However, these phases are not the stable manganese phase predicted by geochemical modelling of early oceans (Mitra et al., 2022). Instead, manganese carbonates are the predicted stable phase. Therefore, the manganese oxide minerals that constitute the majority of the orebody must have formed at a later stage. The tectonics during and immediately after deposition of the Animikie basin sediments provide a plausible explanation for the extremely high-grade manganese oxide formation.



Figure 3-16. Carbonate facies iron formation where the gradual oxidation of primary carbonates can be observed from left to right. Note the increasingly hematite rich BIF from left to right.

Primary silicate and carbonate minerals in iron formations are well documented to be unstable under oxidizing, near surface conditions. For example, the formation of direct ship ores of the Biwabik Iron Formation on the Mesabi Iron Range has been ascribed to deep weathering of primary Fe-minerals (e.g., greenalite and siderite) over hundreds of millions or a billion years. The direct ship ores were composed of hematite and goethite. The Emily Iron Formation, having been deposited contemporaneously with the Biwabik Iron Formation, would have endured at least as much weathering over that period. The weathering and subsequent supergene enrichment of manganese is related to the hydrogeologic and geochemical interaction between interbedded banded (BIF) and granular (GIF) iron formation. Manganese in the Emily

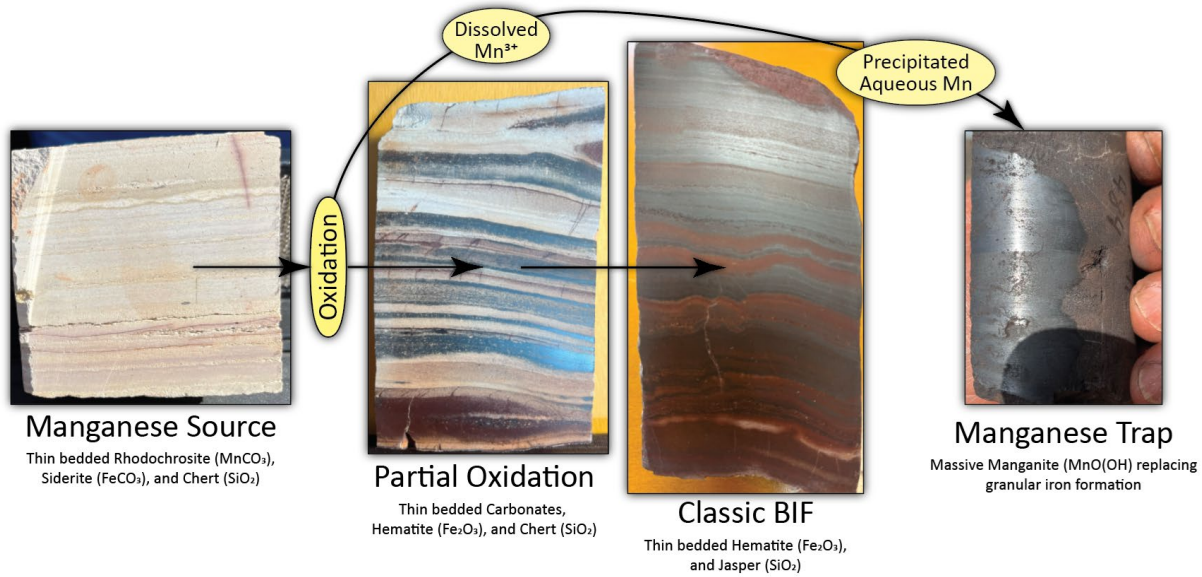


Figure 3-17. Emily deposit drill core that seemingly documents that the oxidation of carbonate-facies (rhodochrosite-siderite-chert) BIF generates classic thin-bedded hematite-jasper BIF as well as being the primary source of Mn^{3+} that forms the massive manganese oxide zones in permeable GIF horizons.

Iron Formation was originally co-precipitated with iron carbonate minerals (rhodochrosite $MnCO_3$ and siderite $FeCO_3$) within the banded iron formation lithotype (Peif2 subunit). Primary carbonates are observed at various stages of oxidation in several boreholes (e.g., NSC-23005). Like the Biwabik Iron Formation, the Emily Iron Formation underwent a protracted period of weathering and oxidation. Exposure of carbonate facies iron formation to oxidizing waters over that period is hypothesized to be the causative mechanism for supergene manganese enrichment at the Emily deposit. Oxidized meteoric water percolating through the carbonate iron formation reacts with and dissolves the carbonates, liberating manganese from rhodochrosite and converting siderite to hematite. The restite lithology appears very similar to hematite-rich banded iron formation (Fig. 3-17). The now manganese enriched waters redistribute manganese downslope to other subunits of the Emily Iron formation.

The second important litho-type, granular iron formation, is recognized as the primary manganese-oxide ore hosts at the Emily Deposit. Granular iron formation is composed of granules of varying compositions (e.g., Fe-silicate, chert, Fe-carbonates) with pore space found between the granules. That pore space creates permeability that drives fluid flow through the granular iron formation thereby moving and redepositing manganese from the enriched waters leaving the carbonate facies banded iron formation. The observations from drillcore logging at Emily indicate that manganese oxides are not found in significant concentrations within the banded iron formations, but manganese oxides are abundant in the granular iron formation.

The migration of manganese-rich waters from the banded iron formation into the granular units is the primary redistribution mechanism for manganese. Once manganese enriched waters enter the granular units, it is unclear by what mechanism the precipitation of manganese occurs. However, manganese oxide minerals are observed in the interstices between granules indicate direct precipitation from the pore fluids. It is unclear whether this interstitial manganese is the result of filling otherwise empty pore space if it is the result of replacement of prior GIF matrix. Additionally, pock marked textures in manganese-rich units suggest that granules may be replaced by the manganese-rich fluids, though the mechanism by which this may occur is unclear due to a lack of mineralogical constraints.

Stratigraphic and Structural Controls on the Distribution of Secondary Manganese

The compression associated with the Penokean Orogen uplifted the rocks Emily deposit. Folding and subsequent uplift of these originally shallow water subaqueous rocks into the Penokean mountains has important hydrogeological implications by greatly lowering the water table and exposing the Emily Iron Formation to oxidizing meteoric waters.

The Emily deposit is on the northernmost anticline of the Penokean fold and thrust belt, specifically within a parasitic syncline along the norther limb of the larger anticline. The structural geometry established during the Penokean provides a hydrogeologic “slope” that meteoric waters can migrate down under the influence of gravity. In particular, the parasitic syncline that hosts the Emily Deposit (see Figure 3-14), likely acted like a funnel or gutter that focused fluid flow through the rocks that now constitute the deposit. A schematic stepwise ore genesis model for the Emily deposit is presented in Figure 3-18.

On a deposit scale and within this structural setting, the two major litho-types play an important role in the movement of fluids due to their contrasting hydrogeological characteristics. In particular, the Peif1r stromatolite horizon represents an aquitard that seemingly focused fluid along its margins. The focusing of fluids along these margin manifests as exceptionally high Mn-grades (often massive manganese oxides) at the upper and lower contacts with flanks GIF of Peif1. Similarly, but to a lesser extent, the basal contact with the Pokegama formation and the contact between Peif2 and Peif3 represent areas of contrasting hydrogeologic characteristics that may concentrate mineralizing fluids. Both areas are observed to host massive manganese oxide mineralization, supporting such a relationship.

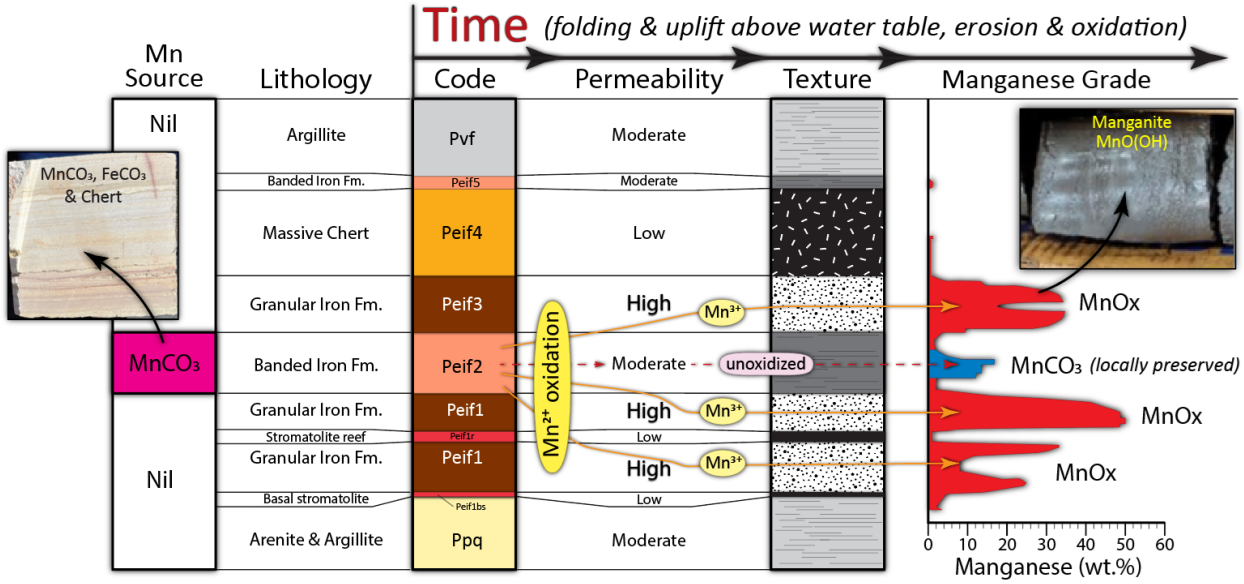


Figure 3-18. Emily deposit Mn-Oxide ore deposit model that incorporates stratigraphy, permeability, processes, and time, after Peterson & Steiner, 2024.

Drillholes on Display

Four drillholes from the 2023 exploration program at Emily will be on display for the 2025 ILSG field trip. These holes include:

1) **NSC-23002A -** high-grade Mn-oxide ores at the bedrock interface in Peif1,
2) **NSC-23004** - an almost complete stratigraphic section through the Emily IF,
3) **NSC-23005 -** Peif2 with carbonate facies IF and Sudbury Impact breccias in unit Pvf, and
4) **NSC-23050 –** The Western-most drillhole, nearly complete section of the Emily IF.

A detailed bedrock geology and drillhole location map of North Star Manganese Inc's Emily Project is presented in Figure 3-19, and striplogs of the four holes on display are given in Figures 3-20, 3-21, 3-22, and 3-23.

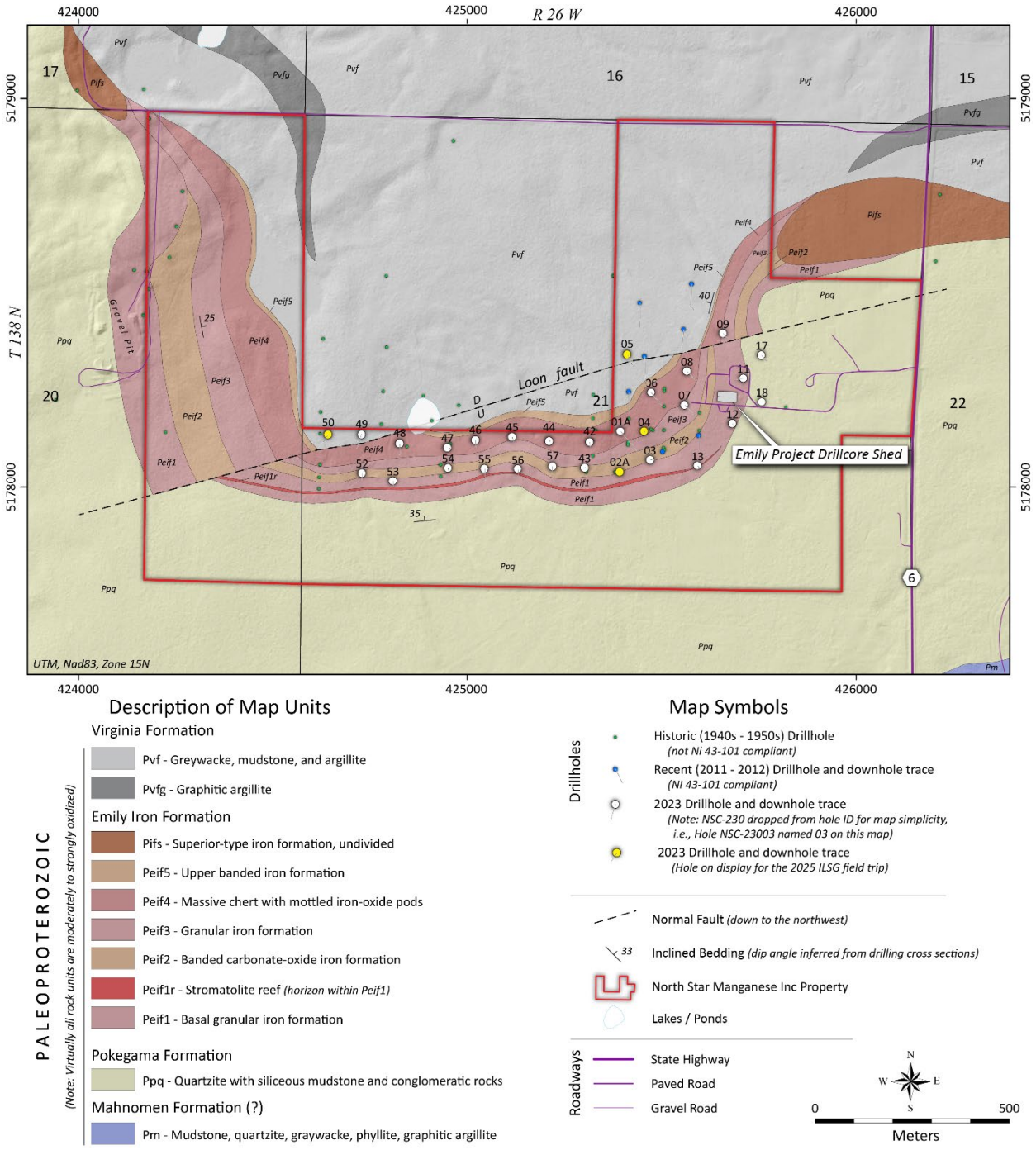


Figure 3-19. Detailed bedrock geology and drillhole location map of North Star Manganese Inc's Emily project. Note that the collar location of the four drillholes on display are highlighted by the small yellow circles. Modified after Steiner et al., 2024.

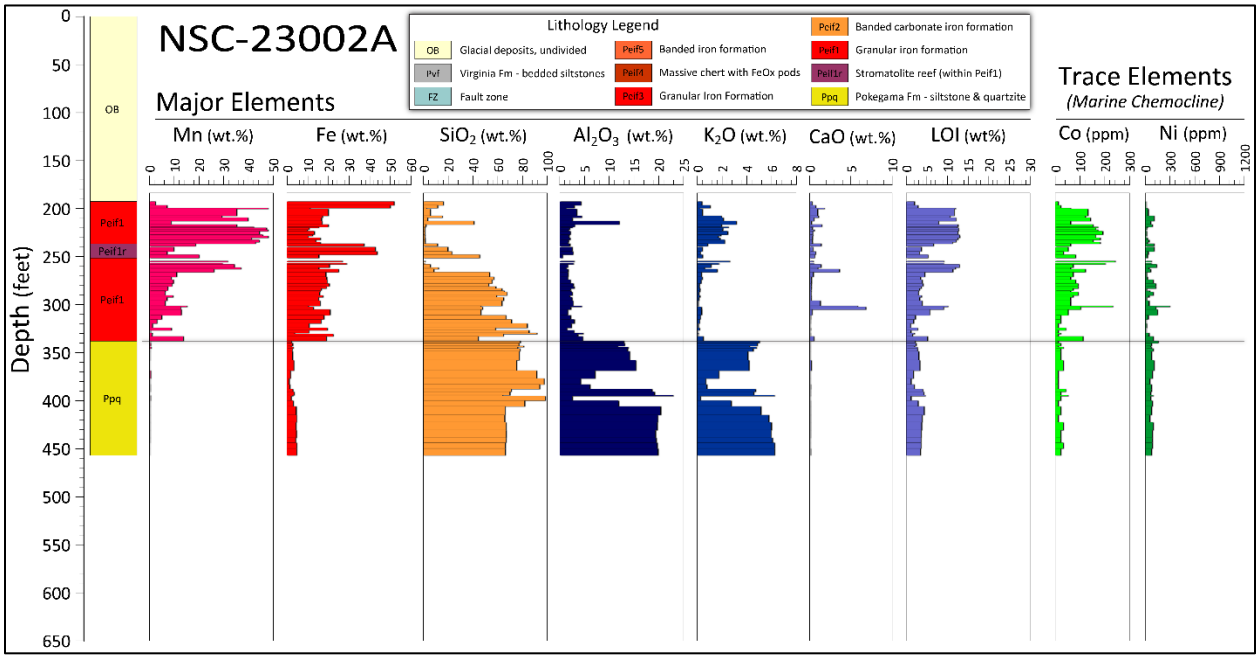


Figure 3-20. Striplog for drillhole NSC-23002A.

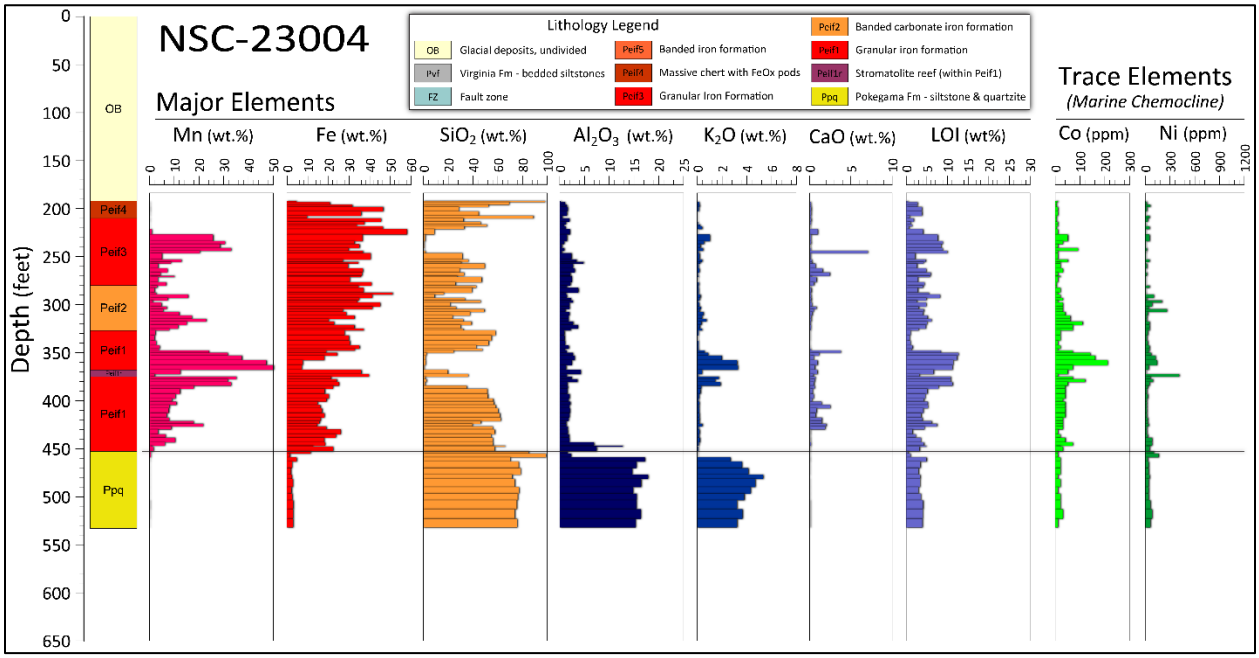


Figure 3-21. Striplog for drillhole NSC-23004.

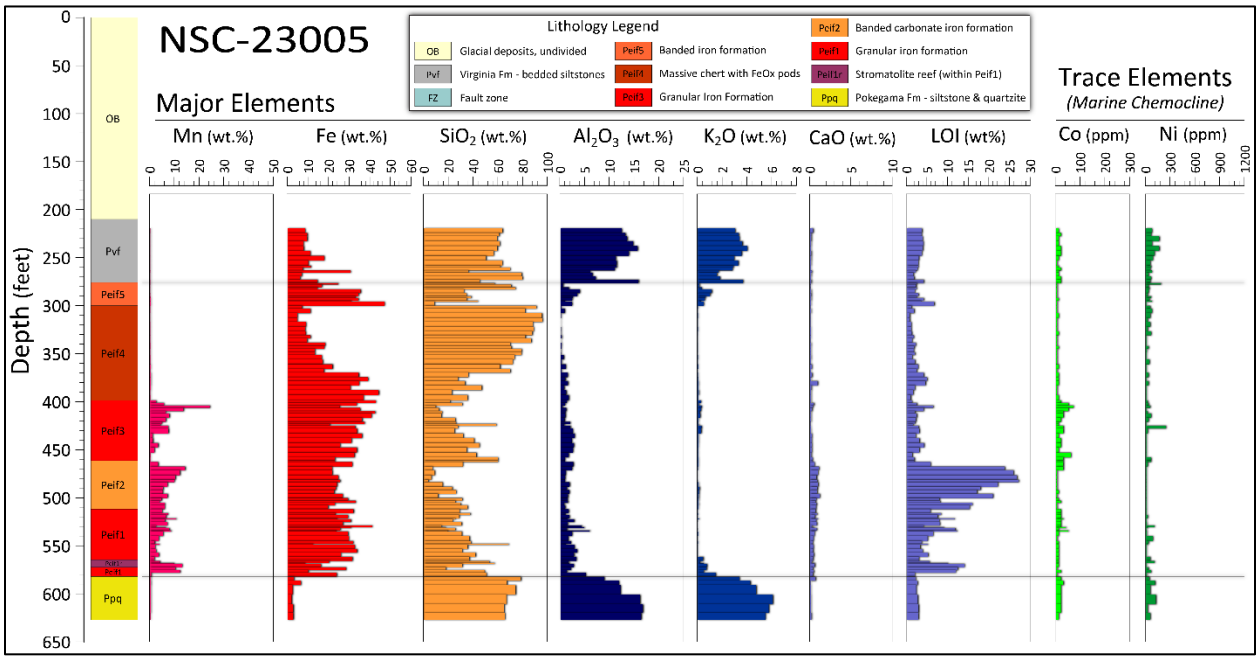


Figure 3-22. Striplog for drillhole NSC-23005.

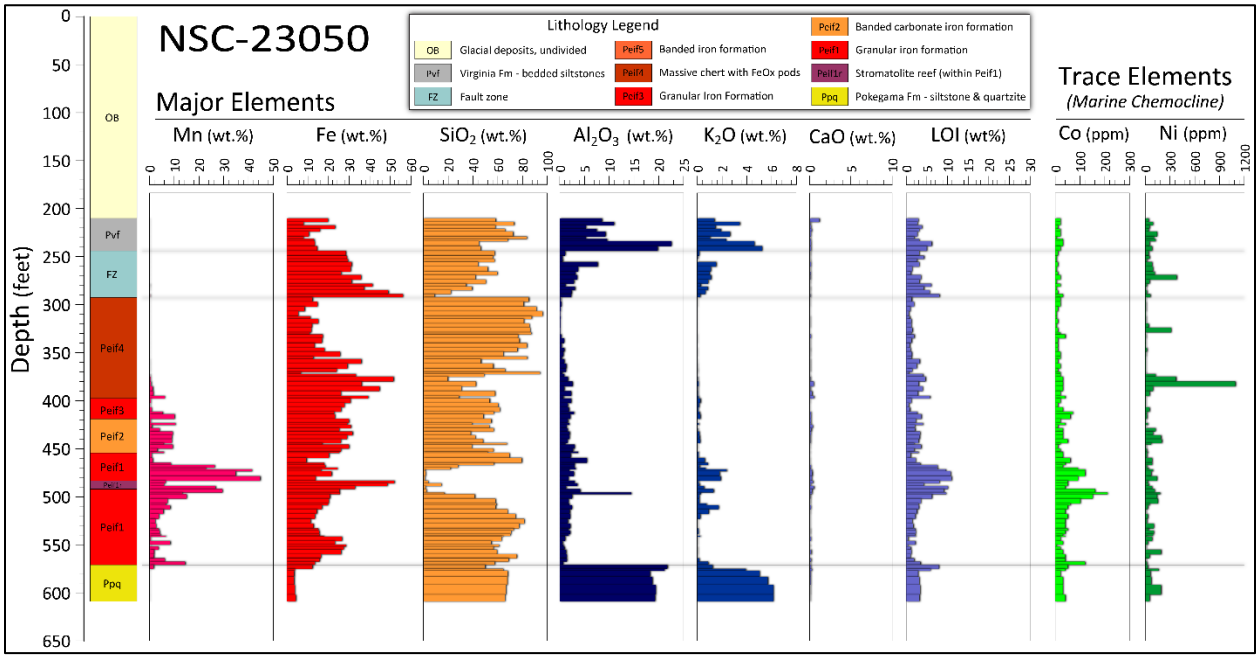


Figure 3-23. Striplog for drillhole NSC-23050.

Stop 3: Mary Ellen Mine, Biwabik Minnesota

Longitude/Latitude: 47.527677°N, -92.366645E

UTM NAD 83 Zone 15N: 547675E, 5264000N

The historic natural ore Mary Ellen mine (Figure 3-24) near Biwabik is probably most well-known today as the source of Mary Ellen Jasper, a world-class type-locality of Precambrian stromatolites. Rocks and polished slabs of stromatolites from the Mary Ellen mine can be found in natural history museums throughout the world, and you'll get to find and take-home pieces yourself during this field trip. According to several annual mining directories, the Stanley Iron Mining Company operated the Mary Ellen Mine between 1924 and 1928, with stockpile shipments occurring in 1929 and 1930. It actively mined the property again between 1948 and 1951. Beginning in 1952, the Pioneer Mining Company worked the mine, continuing to do so through 1961. The Pittsburgh Pacific Company operated it for one final year, in 1962. Its cumulative output of natural ore was 4,574,973 long tons, again according to an annual mining directory.

An interesting quote from the 2015 book titled: *Stromatolites Ancient, Beautiful and Earth-Altering*, by Bruce Stinchcomb & Bob Leis copied below strongly hints that some oxidation-related processes that formed the high-grade earthy hematitic iron ores were similar to those outlined for the high-grade manganese oxide ores at Emily. The quote is as follows, "In the early days of iron mining in Minnesota, the location of stromatolite material would indicate that an iron rich vein was close. The Mary Ellen Stromatolite material could be as much as 15 feet thick and would have to be removed before mining could commence. To the miners this material was considered a nuisance and a waste product."

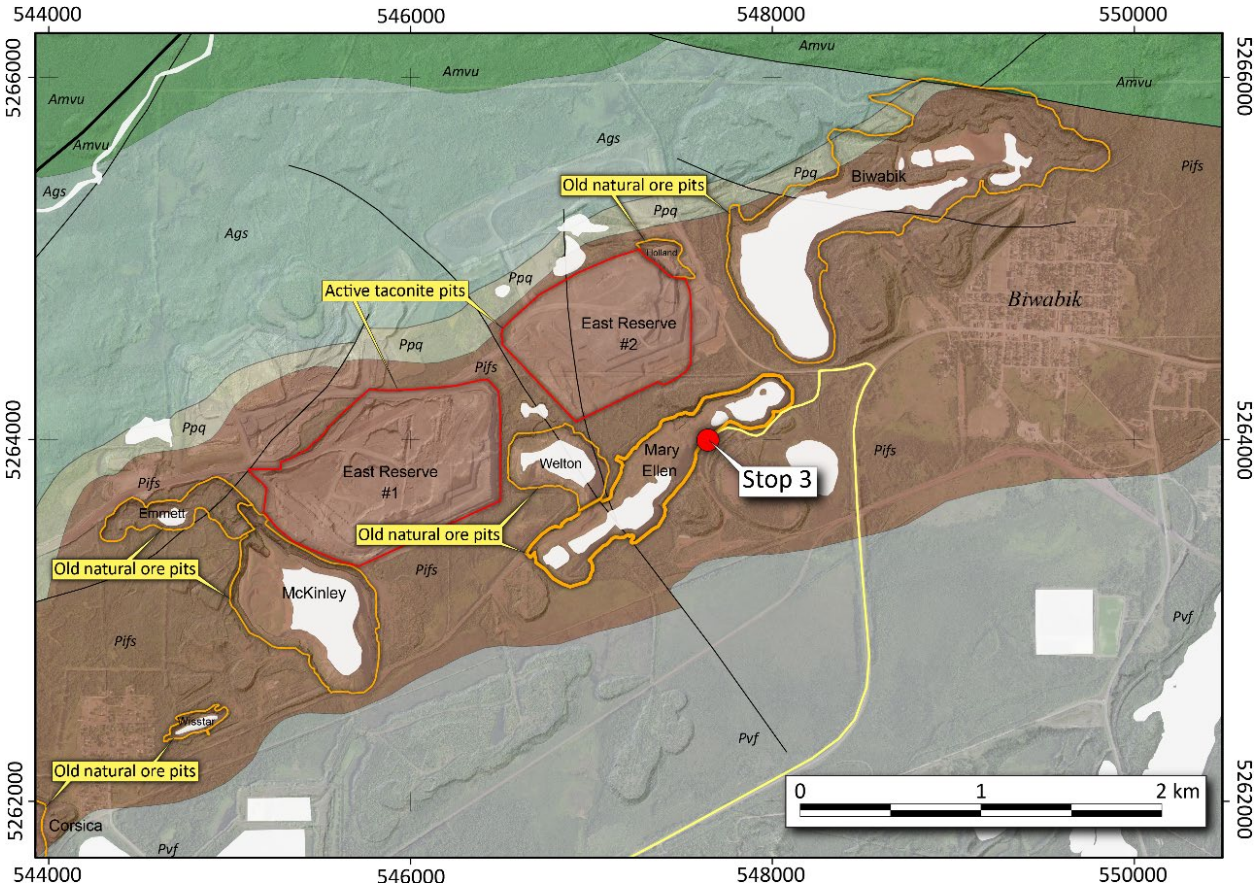


Figure 3-24. Simplified bedrock geology and iron mine map of the Mary Ellen mine area.

Stop 4: Rouchleau Mine Complex Bridge, Virginia Minnesota

Longitude/Latitude: 47.516178 °N, -92.518663 E

UTM NAD 83 Zone 15N: 536240 E, 5262640 N

The Thomas Rukavina Memorial Bridge carries U.S. 53 over the Rouchleau Mine pit connecting Virginia, Minnesota with other cities to the south. U.S. 53 continues through Virginia to International Falls and Canada; International Falls is about 100 miles (160 km) north of Virginia. The bridge, opened in 2017, was named after Tom Rukavina in 2021 following his death in 2019. Rukavina was a state legislator from the Iron Range. At 204 feet tall, it is the tallest bridge in Minnesota. This bridge carries a traffic volume of about 22,200 cars per day, making it one of the most-traveled highway segments on the Iron Range. The bridge also features a bike lane and pedestrian walkway (the Mesabi Trail) that leads to trails connecting Gilbert and Virginia.

In 1960, the state of Minnesota and the mining companies in the area came to an agreement that allowed the construction of U.S. 53 across lands held by the mining company without the state paying anything for the land. The agreement stipulated that after 1987, the state would be responsible for the costs involved with moving the roadway to allow for mining after given advance notice by the mining companies. The two owners of the land notified MnDOT of their intent to mine the site in 2010 which gave the state until 2017 to move the roadway. Cliffs Natural Resources, which had a nearby active mine, hoped to begin mining the site by 2017. After evaluating several more expensive options that involved longer bridges or routing US 53 across an active mine pit, an alignment was selected that resulted in the highest bridge in Minnesota. A route on level ground away from the mining formation was identified as too disruptive to development patterns in the area. The entire project estimated to cost $220 million with $159 million for construction of the bridge and diverted roadway. The bridge crosses the Rouchleau Mine pit.[9] The water filled pit also serves as Virginia's water supply. The final cost was $230 million with $30 million coming from the federal government and the remaining from the state. To prevent the need to move the bridge in the future, the state purchased the mineral rights for the land beneath roadway for $15 million.

References

Aftabi, A., Atapour, H., Mohseni, S., and Babaki, A., 2021, Geochemical discrimination among different types of banded iron formations (BIFs): A comparative review, Ore Geology Reviews, Volume 136.

Aldrich, H. R., 1929, The geology of the Gogebic Iron Range of Wisconsin: Wisconsin Geol. Survey Bull. 21, 279 p.

Beltrame, R.J., Holtzman, R.C., and Wahl, T.E., 1981, Manganese resources of the Cuyuna range, east-central Minnesota: Minnesota Geological Survey Report of Investigations 24, 22 p.

Berg, T., Peterson, D.M., and Sweet, G., 2022, The Emily Manganese Deposit, Crow Wing County, Minnesota: A mineral resource evaluation for North Star Manganese Inc, Big Rock Exploration technical report BRE-TR-2022-02, 33 pages, 3 appendices.

Dorr, J.VN., II, Crittenden, M.D., Jr., and Worl, RG., 1973, Manganese, in Probst, D.A., and Pratt, W.P., eds., United States Mineral Resources: U.S. Geological Survey Professional Paper 820, p. 385-399.

Duncanson S and 5 coauthors (2024) Reconstructing diagenetic mineral reactions from silicified horizons of the Paleoproterozoic Biwabik Iron Formation, Minnesota. American Mineralogist 109: 339-358, doi: 10.2138/am-2022-8776.

Goodwin, A.M., 1956, Facies relations in the Gunflint iron-formation: Ecox. GEOL., v. 51, p. 565-595.

Gruner, 1946, Mineralogy and geology of the Mesabi range: Iron Range Resources and Rehabilitation, St. Paul, Minn., 127 p.

Gunderson, J. N., and Schwartz, G. M., 1962, The geology of the metamorphosed Biwabik iron-formation, Eastern Mesabi District, Minnesota: Minnesota Geol. Survey Bull. 43, 139 p.

Hofstra, A.H., and Kreiner, D.C., Systems-Deposits-Commodities-Critical Minerals Table for the Earth Mapping Resource Initiative: U.S. Geological Survey Open-File Report 2020-1042, 24 p.

Holm, D.K., Lux, D.R., 1996, Core complex model proposed for gneiss dome development during collapse of the Paleoproterozoic Penokean orogen, Minnesota, Geology 24, 343–346.

Holst, T.B., 1991, The Penokean orogeny in Minnesota and Upper Michigan, U.S. Geological Survey Bulletin 1904-D, 10 pages.
Hulse, D.E., Irons, A., and Malhotra, D., 2024, Electric Metals (USA) Limited Emily Manganese Project, NI 43-101 Technical Report, Project No. 219001, Forte Dynamics, 89 pages.
Irving, R. D., 1886, Origin of the ferruginous schists and iron ores of the Lake Superior region: Am. Jour. Sci., v. 32 p, 255-272.
Irving and Van Hise, C. R., 1892, The Penokee iron-bearing series of Michigan and Wisconsin: U.S. Geol. Survey Mon. 19, 534 p.
James, H. L., 1954. Sedimentary facies of iron-formation. Economic Geology, 49(3), 235–293.
Klein, C., and Fink, R.P., 1976, Petrology of the Sokoman Iron Formation in the Howells River area, at the western edge of the Labrador trough: Economic Geology, v. 71, p. 453–487.
LaBerge, G.L., 1964, Development of magnetite in iron-formations of the Lake Superior Region: Econ. Geol., V. 59, p. 1313-1342.
Leith, C. K., 1903, The Mesabi iron-bearing district of Minnesota: U.S. Geol. Sur. Mono. 43, 316 p.
Lewis, W.E., 1951, Relationship of the Cuyuna manganiferous resources to others in the United States, in Geology of the Cuyuna Range Mining Geology Symposium, 3rd, Hibbing, Minnesota, Proceedings: Minneapolis, University of Minnesota, Center for Continuation Study, p. 30-43.
Marsden, R.W., 1972, Cuyuna district, in Sims, P.K., and Morey, G.B., eds., Geology of Minnesota: A centennial volume: Minnesota Geological Survey, p. 227-239.
Marsden, R.W., Emanuelson, J.W., Owens, J.S., Walker, N.E., and Werner, R.F., 1968, The Mesabi Iron Range, Minnesota, in Ridge, J.D. (ed.), Ore Deposits of the United States, 1933-1967: New York, American Institute of Mining, Metallurgical, and Petroleum Engineers, Inc., The Grafton-Sales Volume, v. 1, p. 518-537.
Mitra, Kaushik, Eleanor L. Moreland, Greg J. Ledingham, and Jeffrey G. Catalano, 2023, Formation of manganese oxides on early Mars due to active halogen cycling, Nature Geoscience 16, no. 2, p. 133-139.
Morey, G.B., 1978, Lower and Middle Precambrian stratigraphic nomenclature for east-central Minnesota: Minnesota Geological Survey Report of Investigations 21, 52 p., 1 pIate.
Morey, G.B., 1992, Chemical composition of the eastern Biwabik Iron Formation (Early Proterozoic), Mesabi Iron Range, Minnesota: Economic Geology, v. 87, p. 1649-1658.
Muhling, J., Brengman, L., & Johnson, J. Greenalite (2025, June issue): Cryptic mineral of ancient ferruginous oceans. Elements: Greenalite - Tiny crystal with a big story, Elements (in press).
Peterson, D.M., 2022, Bedrock geology and manganese mineral resource assessment map of the Emily Manganese Deposit, Big Rock Exploration map BRE-MAP-2022-02, 1:50,000 scale.
Peterson, D.M., and Steiner, A., 2024, The geology, history, and ore deposit model of the high-grade Emily Manganese Deposit, Cuyuna Range, Minnesota: Oral presentation, Institute on Lake Superior Geology conference, Houghton, Michigan.
Schmidt, R.G., 1963, Geology and ore deposits of Cuyuna North range, Minnesota: U.S. Geological Survey Professional Paper 407, 96 p.
Schneider, D.A., Holm, D.K., O'Boyle, C., Hamilton, M., Jercinovic, M., 2004, Paleoproterozoic development of a gneiss dome corridor in the southern Lake Superior region, U.S.A. *In:* Whitney, D.L., Teyssier, C., Siddoway, C.S. (Eds.), Gneiss Domes in Orogeny. Geol. Soc. Am. Spec. Pap. 380, pp. 339–357.
Schulz, K.J. and Cannon, W.F., 2007, The Penokean orogeny in the Lake Superior region, Precambrian Research, 157, p. 4–25.
Schulz, K.J., DeYoung, J.H., Jr., Seal, R.R., II, and Bradley, D.C., eds., 2017, Critical mineral resources of the United States - Economic and environmental geology and prospects for future supply: U.S. Geological Survey Professional Paper 1802, 797 p., https://doi.org/10.3133/pp1802.
Severson, M.J., Heine, J.J., and Patelke, M.M., 2009, Geologic and Stratigraphic Controls of the Biwabik Iron Formation and the Aggregate Potential of the Mesabi Iron Range, Minnesota: University of Minnesota Duluth, Natural Resources Research Institute, Technical Report NRRI/TR- 2009/09, 173 p. + 37 plates.
Southwick, D.L. and Morey, G.B., 1991, Tectonic imbrication and foredeep development in the Penokean orogen, east-central Minnesota; an interpretation based on regional geophysics and results of test drilling, U.S. Geological Survey Bulletin 1904-C, pp. C1–C17.
Southwick, D.L., Morey, G.B., and McSwiggen, P.L., 1988, Geologic map (scale 1:250,000) of the Penokean orogen, central and eastern Minnesota, and accompanying text: Minnesota Geological Survey Report of Investigations 37, 25 p., 1 pIate.

Steiner, A., Peterson, D.M., Berg, E., Solie, J., Larson, M., Schaefbauer, E., and Sweet, G., 2024, The North Star Emily Manganese Deposit: Observations, Interpretations, and Recommendations Following the Initial 2023 Drilling Campaign, Big Rock Exploration Technical Report BRE-TR-2023-01, 47 pages, 4 appendices, 1 plate.

Strong, R., 1959, Report on Geological Investigation of the Cuyuna District, Minnesota, 1949-1959, US Steel Internal Report, 318 pages.

Tyler, S.A., 1949, Development of Lake Superior soft iron ores from metamorphosed information: Geol. Soc. Am. Bull., v. 60, p. 1101-1024.

Van Hise, C. R., and Leith, C. K., 1911, Geology of the Lake Superior region. U.S. Geol. Survey Mon. 52, 641 p.

White, D. A., 1954, The stratigraphy and structure of the Mesabi Range, Minnesota: Minnesota Geol. Survey Bull. 38, 92 p.

Wolff, J.E., 1917, Recent geologic developments on the Mesabi Iron Range, Minnesota: American Institute of Mining and Metallurgical Engineers, Transactions, v. 56, p. 229-257.

FIELD TRIP 4

New Geological Insights into the Genesis of Iron Ores at Lake Vermilion – Soudan Underground Mine State Park

George J. Hudak[1,2,3], Zsuzsanna P. Allerton[1], and Annia Fayon[1]

[1]*Department of Earth and Environmental Sciences, University of Minnesota Twin Cities, 116 Church Street SE, Minneapolis, MN 55455*
[2]*Department of Earth and Environmental Sciences, University of Minnesota Duluth, 1114 Kirby Drive, Duluth, MN 55812*
[3]*George Hudak Geosciences P.L.L.C., Duluth, MN 55804*

Introduction

The Vermilion District of northeastern Minnesota contains one of the classic greenstone belts in the United States. The district comprises the southwestern part of the Wawa-Abitibi Terrane (Stott et al., 2007; Stott and Mueller, 2009) which encompasses Neoarchean metavolcanic, metasedimentary, and meta-intrusive rocks that extend northeastward through northwestern Ontario and Quebec (Figure 4-1). In Canada, this terrane hosts numerous volcanogenic massive sulfide deposits (e.g. Winston Lake, Geco, Noranda), gold-rich volcanogenic massive sulfide deposits (Horne (Noranda camp), Bousquet 2 – LaRonde 1, LaRonde-Penna; Mercier-Langevin et al., 2010), as well as a large number of lode (orogenic) gold deposits (for example, in the Hemlo, Timmins, and Kirkland Lake camps). The Vermilion District is known for its numerous, previously mined massive hematitic iron ore deposits (including the Pioneer Mine in Ely and the Soudan Mine in Soudan) which locally occur within regional extensive Algoma-type banded iron formations cut by Neoarchean shear zones. To date, no volcanogenic massive sulfide, gold-rich volcanogenic massive sulfide, or lode gold deposits have been discovered in the Vermilion District, although several studies (Peterson and Jirsa, 1999; Peterson, 2001; Hudak et al., 2002a; Peterson and Patelke, 2003; Hoffman, 2007; Hudak et al., 2007; Hudak et al., 2012; Lodge et al., 2013; Lodge et at., 2015; Thompson, 2015) have indicated that evidence for volcanic, hydrothermal, and structural processes associated with these types of mineral deposits is present throughout the Vermilion District.

The Vermilion District's iron ore mining heritage is currently preserved at Lake Vermilion / Soudan Underground Mine State Park located near Soudan, Minnesota as well as within several historic mines west of and within Ely, Minnesota. The Soudan mine operated from 1882 until December, 1962 and produced approximately 15.5 tons of hematic iron ore. With the donation of land and infrastructure associated with the former Oliver Iron Mining Division's Soudan Mine by United States Steel to the State of Minnesota in 1965, Soudan Underground Mine State Park was established. This state park currently preserves the historical surface and underground workings from, as well as the wilderness adjacent to, Minnesota's oldest iron ore mine, the Soudan Mine. The mine previously hosted several underground physics laboratories, including: 1) Soudan 1 (23rd level) which studied neutrino decay; 2) Soudan 2 (27th level), also to study neutrino decay; and 3) the MINOS (Main Injector Neutrino Oscillation Search) lab, which was built on the 27th level adjacent to Soudan 1 and studied the decay of neutrinos within the earth as they passed from Fermilab to Soudan. This popular tourist site continues to be the focus of a wide variety of research related to geology, geochemistry, hydrogeology, biology, biochemistry and physics.

Lake Vermilion/Soudan Underground Mine State Park is Minnesota's newest state park. In 2008, Minnesota State Legislature set aside $20 million in bonding authority to buy, plan, and develop the park, which is located immediately east of the former Soudan Underground Mine State Park. Lake Vermilion/Soudan Underground Mine State Park was established in June 2010 after over 3,000 acres land was purchased from U. S. Steel Corporation (Bakst, 2013). At the present time, considerable development

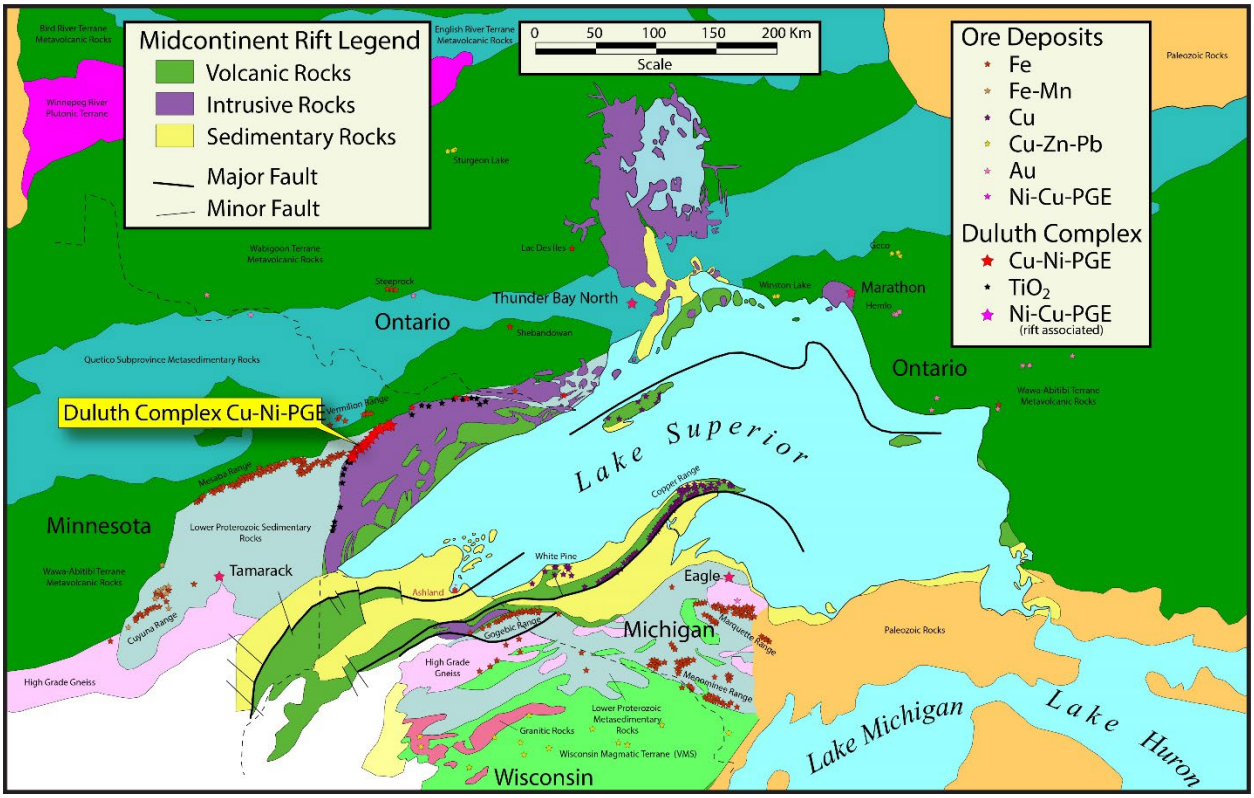


Figure 4-1. Regional geology of the Lake Superior region illustrating the wide variety of mineral deposit types (modified from Hudak and Peterson, 2014; D.M. Peterson, personal communication, 2013).

has taken place in the eastern part of the park, including the establishment of trails, roads, and campsites. The park boasts a rich natural and human history, including a wide variety of ~2.7 billion year old rocks that were formed by a wide variety of genetic process, abundant wildlife, as well as archaeological evidence for human habitation dating back over 6,000 years. Additionally, considerable evidence for recent (within the past 140 years) mineral exploration efforts can be readily identified in the park.

Since the late 1990's considerable geological research has been conducted in the region between Tower, MN (in the west) to Ely, MN (in the east) within the Vermilion District. Much of this research has been conducted to better understand the stratigraphy, structural geology, and economic geology of the belt. This research is summarized in several recent Institute on Lake Superior Geology (ILSG) field trips (Hudak et al., 2004; Jirsa et al., 2004; Peterson and Patelke, 2003; Larson and Mooers, 2009; Peterson et al., 2009a; Jirsa and Hillman, 2009; Peterson et al., 2009b), as well as in a few recent journal publications (Lodge et al., 2013; Lodge et al., 2015). In 2010 and 2011, students and faculty from the University of Minnesota Duluth Precambrian Research Center conducted new, 1:5000 scale mapping of this park and several maps and reports were produced (Radakovich et al., 2010; Vallowe et al., 2010; Heim et al., 2011; Baumgardner et al., 2013; Hudak et al., 2016; Peterson et al., 2016). These findings are summarized in Hudak et al., 2014. In addition, geologists from the Natural Resources Research Institute (NRRI), the Minnesota Geological Survey (MGS), and the University of Wisconsin Eau Claire produced a 1:10000-scale map of the park as well as a project report and accompanying spatial databases (Peterson et al., 2016; Hudak et al., 2016). Over the past several years, students and faculty from the University of Minnesota Twin Cities Advanced Field Camp have refined the geological map in an area approximately one-half mile east of the Soudan Mine headframe.

The results of these studies have provided a solid foundation for geological research that is currently taking place in Lake Vermilion/Soudan Underground Mine State Park (e.g.). Recent masters and doctoral studies from the University of Minnesota Duluth (Thompson, 2015) and the University of Minnesota Twin Cities (Allerton, in prep.; Allerton et al., 2024a; Allerton et al., 2024b; Allerton et al., in review) have focused their research on understanding the absolute age of massive hematite mineralization at the Soudan Mine. This is a problem that has baffled geoscientists for over a century (e.g. Gruner, 1926; Klinger, 1960). In addition, students and faculty from the University of Minnesota Twin Cities Advanced Field Camp have conducted more recent geological mapping (1:5000 scale) in an area approximately one-half mile east of the Soudan Mine headframe for the past several years. This mapping has led to minor reinterpretations of the geology in the central part of Lake Vermilion/Soudan Underground Mine State Park that was depicted by Peterson et al. (2016).

Recently, a grant from the Leaonardt Foundation was awarded to one of the co-authors (Fayon) to develop a new trail in the park that will focus on public education related to the ancient geology and geological processes that have taken place in the park. K-12 teachers are playing a major role in developing the curriculum and lessons that will be part of this trail project.

The goals of this field guide are to illustrate to field trip participants the wide variety of geological processes that have taken place within Lake Vermilion/Soudan Underground Mine State Park. Morning field trip stops will focus on understanding the stratigraphy, structure, hydrothermal alteration and mineralization closely associated with the Soudan iron orebodies. The afternoon will focus on observing both geological features of the massive hematite orebodies, as well as recent advances in our geochemical and geochronological understanding of these iron ore deposits in the Montana stope, located on the 27th level of the Soudan Mine.

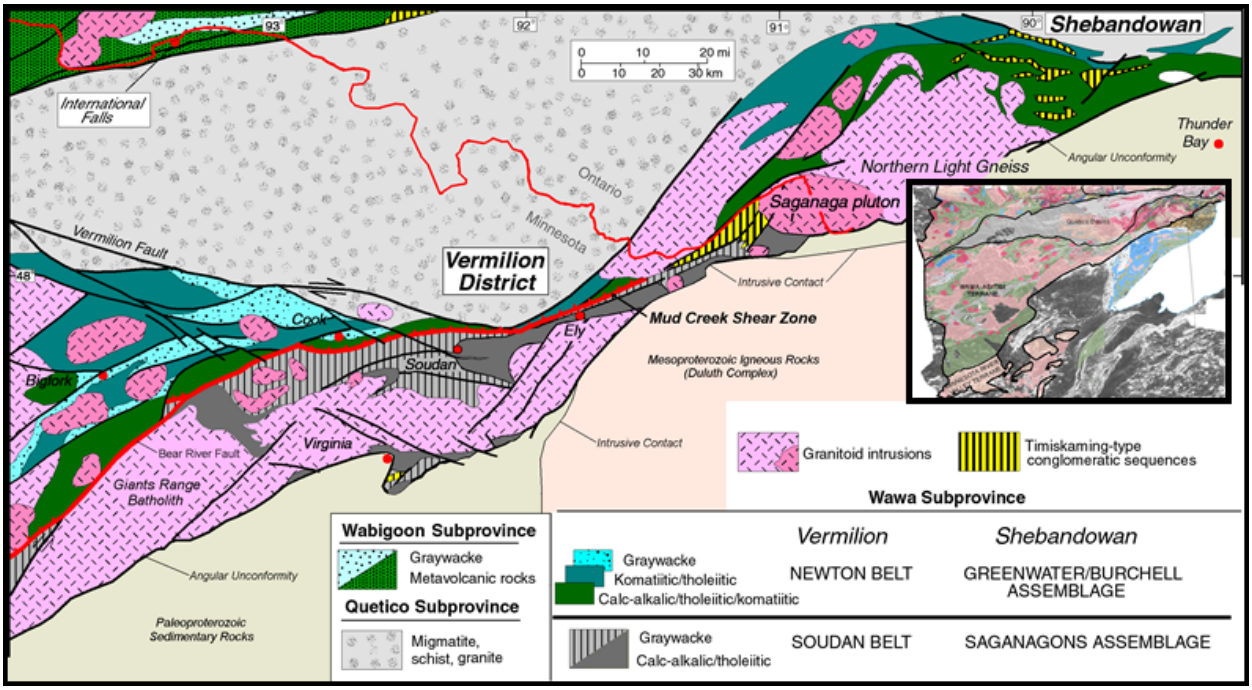


Figure 4-2. Simplified correlation map of Neoarchean assemblages in Minnesota and northwestern Ontario (after Peterson et al., 2001; Hudak and Peterson, 2014). Inset map illustrates location of the Wawa-Abitibi Terrane in Minnesota and northwestern Ontario (Stott et al., 2007). The Leach Lake structural discontinuity is illustrated in red. The red star symbols indicate location of Lake Vermilion State Park.

Regional Geologic Setting

A simplified regional geological map of the Neoarchean terranes of northeastern Minnesota and adjacent Ontario is presented in Figure 4-2. Supracrustal rocks in the Vermilion district consist of volcanic-dominated stratigraphic sequences of the Wawa Abitibi Terrane within the Superior Province of the Canadian Shield. Rocks of the Wawa Abitibi Terrane in northern Minnesota are divided based on stratigraphic and structural setting into: (1) the Soudan belt, to the south, and (2) the Newton belt, to the north (Jirsa et al., 1992; Southwick et al., 1998). The boundary between these contrasting structural panels can be traced geophysically across the width of Minnesota and was informally designated the Leech Lake structural discontinuity (Jirsa et al., 1992). In the region west and north of Lake Vermilion/Soudan Underground Mine State Park, the Leech Lake structural discontinuity occurs along the Mud Creek shear zone (Hudleston et al., 1988), small segments of the Vermilion and Wolf Lake faults (Sims and Southwick, 1985), and the Bear River fault (Jirsa et al., 1992).

The Soudan belt (Figure 4-3) contains large, broad generally east-west trending folds involving calc-alkalic and tholeiitic volcanic strata overlain by, and locally interlayered with, turbiditic rocks. In contrast, the Newton belt consists of elongate, northeast-trending, and mostly northward-younging volcanic and volcaniclastic sequences. Volcanic rocks of the Newton belt differ from those of the Soudan belt in containing locally abundant komatiite/basaltic komatiite flows and peridotite sills. The two belts are fault-bounded, and the relationships between stratigraphic units within each belt are largely conformable (although faults obscure contacts locally). In its eastern extension, the Soudan belt is continuous with the Saganagons assemblage in Ontario and terminates against the Saganaga pluton and Northern Light Gneiss. The Newton belt extends discontinuously eastward into the Shebandowan District of Ontario to form the Greenwater and Burchell assemblages. Intrusive rocks in both belts vary from gabbroic and felsic porphyries demonstrably related to volcanism, to large plutons emplaced post-tectonically. Both districts contain unconformable, Timiskaming-type sequences composed of calc-alkalic volcanic rocks, conglomerates, and finer grained sedimentary rocks.

Lithostratigraphic units in the western Vermilion district (Table 4-1) include: (1) the Lower member, Soudan Iron-Formation member, and Upper member (Upper Ely) of the Ely Greenstone Formation, the Lake Vermilion Formation (including the informally named Britt and Gafvert Lake sequences), and the Knife Lake Group of the Soudan belt; (2) the Bass Lake sequence (Peterson and Jirsa, 1999) and the Newton Lake Formation of the Newton belt; and, (3) syn- to post-tectonic granitoid intrusions of the Giants Range batholith, and a suite of post-tectonic alkalic stocks and plutons. Contacts between the different units are typically conformable, although considerable overlap in time and space is documented between volcanic and sedimentary sequences (Southwick, 1993). Regional chronostratigraphic correlations between the Vermilion district, the Wawa Greenstone (northwestern Ontario) and the Abitibi greenstone belt (eastern Ontario and Quebec) are indicated in Figure 4-4.

Geochronological information for supracrustal and intrusive lithologies in the Vermilion District is relatively sparse (Figure 4-4). Peterson et al. (2001) obtained a U-Pb zircon age date of 2722 ± 0.9 Ma from a quartz-phyric rhyolite dome in the Fivemile Lake Sequence of the Lower Member of the Ely Greenstone Formation. Lodge et al. (2013) obtained a U-Pb zircon date of 2689.7 ± 0.8 Ma for a Gafvert Lake Sequence dacitic tuff breccia that occurs approximately 2m north of the contact with the Soudan Iron-Formation member of the Ely Greenstone Formation. As well, Lodge et al. (2013) obtained detrital zircon dates ranging from 2680-2690 Ma from greywackes that comprise the Lake Vermilion Formation. This date confirms the source of the detritus in the Lake Vermilion Formation was derived locally from the volcaniclastic rocks comprising the Gafvert Lake Sequence. Jirsa et al. (2012) obtained a U-Pb age of 2690.7 ± 0.6 Ma for synvolcanic intrusions that cross-cut volcaniclastic rocks that comprise the Knife Lake Group. The upper part of the Knife Lake Group includes conglomerates which contain clasts derived from

Table 4-1. Lithostratigraphic units within the western Vermilion District (modified after Peterson and Jirsa, 1999; Peterson et al., 2009; Hudak et al., 2012).

Intrusive Rocks	
Late Intrusions	Plutons and stocks of syenite, monzonite, diorite, and lamprophyre. A U-Pb zircon age date of a non-foliated feldspar porphyry intrusion in the Newton belt is 2683 ± 1.4 Ma (Peterson et al., 2001).
Vermilion Granitic Complex	Granite, schist, amphibolite, and schist-rich migmatite
Giants Range Batholith	Granite, granodiorite, monzodiorite, and schist-rich migmatite. U-Pb zircon dates indicate a crystallization age ranging from 2640-2777Ma (Allerton et al., 2024a).
Supracrustal Rocks	
Newton Belt	
Newton Lake Formation	Tholeiitic and komatiitic basalt lava flows, intrusions, and clastic strata (deep subaqueous?)
Bass Lake Sequence	Tholeiitic basalt lava flows, iron-formation, and felsic porphyries (deep subaqueuous)
Soudan Belt	
Knife Lake Group	Graywacke, slate, conglomerate, and sheared equivalents
Lake Vermilion Formation	Graywacke, slate, dacitic tuff, minor conglomerate. Detrital zircons from planar bedded, normal-graded resedimented volcaniclastic rocks have U-Pb age dates of 2680-2690 Ma (Lodge et al., 2013; subaerial to subaquous)
Gafvert Lake Sequence	Dacitic to rhyodacitic tuff, lapilli-tuff, tuff-breccia, and iron-formation. Basal dacite tuff-breccia deposits in Lake Vermilion State Park have U-Pb age date of 2689.7 ± 0.8 Ma (Lodge et al., 2013; subaerial to subaqeous)
Britt Sequence	Tholeiitic basalt lava flows (deep subaqueous?)
Upper Member – Ely Greenstone	Tholeiitic basalt lava flows and iron-formation (deep subaqueous?)
Soudan Member – Ely Greenstone	Oxide-facies iron formation with intercollated basalt lava flows and felsic volcaniclastic rocks (deep subaqueous)
Lower Member – Ely Greenstone	Calc-alkaline and tholeiitic basalt-rhyolite lava flows, tuffs, epiclastic rocks, and minor iron-formation (shallow- to deep subaqueous)
Central Basalt Sequence	Calc-alkaline to tholeiitic sparsely amygdaloidal basalt and minor basaltic andesite lava flows with MORB-like or back arc basin-like chemical affinities within 100-200 meters of the overlying Soudan Member iron-formation; FII- and FIIIa-type felsic volcanic and volcaniclastic rocks (transition from shallow- to deep water environment)
Fivemile Lake Sequence	Calc-alkaline to transitional moderately to highly vesicular basalt and andesite lava flows and volcaniclastic rocks with arc-like chemical affinities: FI-, FII-, and FIV-type felsic volcanic and volcaniclastic rocks. Rhyolite dome at near Fivemile Lake has U-Pb age date of 2722.6 ± 0.9 Ma (Peterson et al., 2001). Epithermal-like zinc stringer mineralization is present near Fivemile Lake (Hudak et al., 2002a; interpreted as shallow subaqueous environment).
Eagles Nest Sequence	Algoma-type iron formation, basalt-andesite lava flows, hydrothermal exhalites, felsic tuffs.

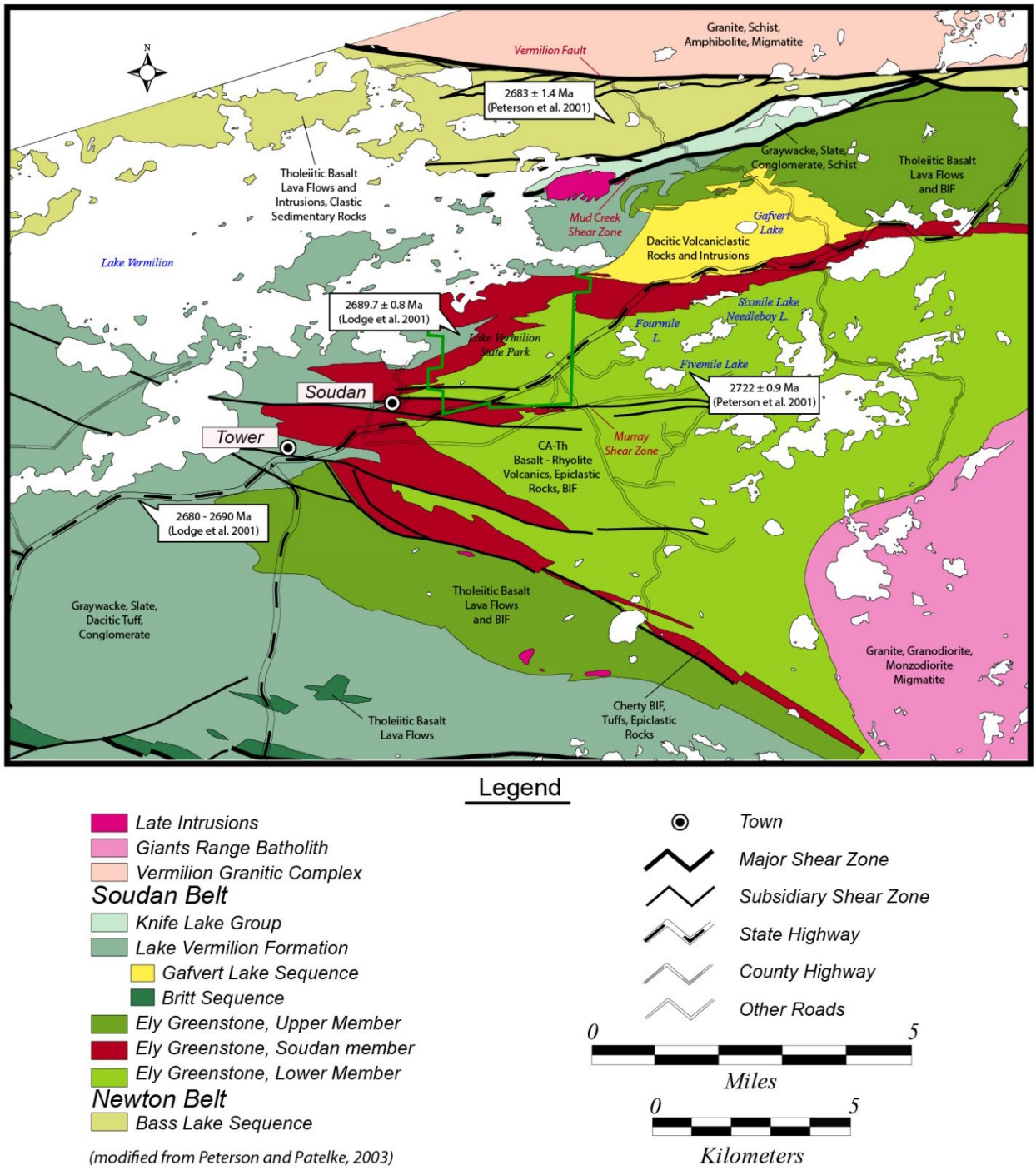


Figure 4-3. Generalized geology of the Soudan belt in the vicinity of the Tower-Soudan anticline (modified after Peterson, 2001; Hudak et al., 2014; Hudak and Peterson, 2014). Locations, ages, and sources of U-Pb ages dates within the district are noted in the callout boxes. Generalized lithologies for each of the groups, formations or sequences are also noted. The outline of the Lake Vermilion section of Lake Vermilion/Soudan Underground Mine State Park is shown in green.

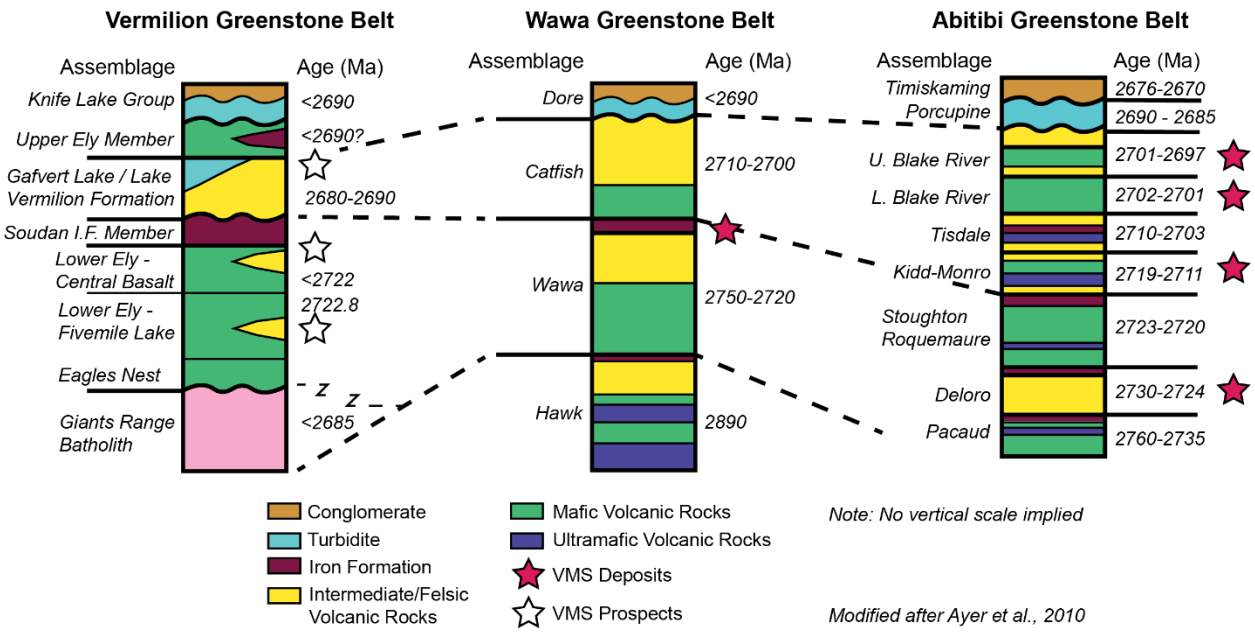


Figure 4-4. Regional chronostratigraphic correlations between the Vermilion district (Minnesota), the Wawa greenstone belt (northwestern Ontario), and the Abitibi greenstone belt (eastern Ontario and Quebec; after Ayer et al., 2010).

the Saganaga Tonalite, which has been dated by Driese et al. (2011) at 2690.83 ± 0.26 Ma. Peterson et al. (2001) also dated a non-foliated feldspar porphyry intruded into Newton Belt strata at 2683.1 +1/-4 Ma. This date provides a minimum age for the regional D_2 deformation event that is described below.

Structural Geology

The structural geology of the Vermilion District has been well described by Peterson et al. (2009). Periods of generally N-S directed compression resulted in three major regional deformation events in the Neoarchean terranes of northern Minnesota. The earliest deformation event (D_1) produced broad, locally recumbent folds within the Soudan belt and major fault zones throughout the region. In the Newton belt, D_1 was accommodated by thrust imbrication of large crustal blocks, resulting in mainly northward stratigraphic facing. Field relationships indicate that uplift, faulting, and the deposition of Timiskaming-type clastic sedimentary sequences in local fault-bounded basins occurred late in D_1 deformation (Jirsa, 2000). A large, map-scale structure related to D_1 deformation in the western Vermilion District is the Tower-Soudan Anticline, which is a west-plunging anticline within which the axis and plunge changes orientation along strike from nearly vertical in basalts to shallow NE plunging in the western sedimentary rocks. Axial-planar cleavage associated with this early fold typically is lacking, although Bauer (1985), Hooper and Ojakangas (1971), Hudleston (1976), and Jirsa et al. (1992) have described early cleavage (S_1) locally.

A second deformation event (D_2) associated with synchronous regional metamorphism resulted in foliation development and structures exhibiting dominantly dextral asymmetry. D_2 is constrained in the Vermilion District to the time period 2674 to 2685 Ma (Boerboom and Zartman, 1993), and between about 2680 and 2685 Ma in the Shebandowan (Corfu and Stott, 1998). Because D_2 deformation affected all the supracrustal rocks in the area and is reasonably constrained by geochronology, the regional foliation (S_2) can be used in the field to temporally relate other structural, intrusive, and deformation events. The relationship between S_2 fabric and shear structures indicates that most shearing occurred relatively late in the D_2 event. Major shearing that produced the Mud Creek and related shear zones is attributed to the late stages of D_2 dextral transpression (Peterson, 2001; Hudak et al., 2004; Peterson et al., 2009).

The third deformation event (D_3) is believed to be associated with the juxtaposition of the Wawa Abitibi and Quetico terranes (Peterson and Patelke, 2003). Structures associated with D_3 include abundant NE- and NW-trending faults that dissect the stratigraphic assemblages and include the NE-trending Waasa and Camp Rivard faults east of the Soudan Mine area, and the WNW-trending, crustal-scale Vermilion and related faults that form the Wawa-Quetico Subprovince boundary.

Geology of Lake Vermilion/Soudan Underground Mine State Park

Lake Vermilion State Park contains a variety of supracrustal and intrusive lithological units (Figure 4-5). Supracrustal rocks that can be observed in the park include the Lower Member of the Ely Greenstone Formation (both the Fivemile Lake and Central Basalt Sequences), the Soudan Member of the Ely Greenstone Formation, and the Gafvert Lake Sequence of the Lake Vermilion Formation. Additionally, a wide variety of syn- and post-volcanic mafic and felsic intrusive rocks and several varieties of sheared rocks crop out in the park (Peterson and Patelke, 2003; Radakovich et al., 2010; Heim et al., 2011; Hudak et al., 2016; Peterson et al., 2016). These various lithologies are described below.

Lithology

Supracrustal rocks in Lake Vermilion/Soudan Underground Mine State Park were described by Hudak et al. (2016) based on lithological types rather than lithostratigraphic members and/or formations. Their lithological descriptions are included below.

A summary of mafic supracrustal rocks that occur within the park include:

- undivided mafic volcanic rocks, including gray-green to green massive basalt, pillow basalt, basalt tuff, bedded scoria tuff and lapilli-tuff, and foliated basalt rocks
- massive basalt comprising green to dark green, aphyric to sparsely plagioclase-phyric basalt
- pillow basalt, including gray-green to green bun, mattress, and lobe morphologies using the pillow lava classification of Dimroth et al., (1978)
- basalt tuff, including green, massive to bedded, aphyric to sparsely plagioclase-phyric tuff.
- bedded scoria tuff and lapilli-tuff, composed of green, thin- to very thick-bedded, poorly-sorted, typically poorly-graded tuff and lapilli-tuff containing up to 65% <1-20cm scoria lapilli
- foliated basaltic rocks, made up of green, fine-grained, moderately to strongly foliated basalt comprising anastomosing bands of chlorite-rich phyllite separating domains of less deformed basalt

Felsic volcanic rocks within the park include:

- epiclastic, intermediate-felsic volcanic-derived sedimentary rocks, composed of light gray to brownish gray polymict volcaniclastic matrix-supported conglomerates and sandstones containing clasts of felsic volcanic and volcanic strata, oxide facies iron formation, and chert-rich iron formation.
- laminated felsic tuff, made up of white to dark gray, laminated- to very thinly bedded, aphyric to sparsely quartz- ± plagioclase-phyric dacite to rhyolite tuff.
- felsic tuff breccia, comprising light gray, very thickly bedded to massive, matrix-supported quartz- and plagioclase-phyric polymict dacite to rhyodacite tuff breccia containing 10-20% 1-10 cm quartz and plagioclase-phyric coherent dacite lapilli and blocks, 5-7% lens-shaped quartz- and plagioclase-phyric pumice lapilli up to 3 cm in diameter, 1% light- to dark-gray chert lapilli up to 3 cm in diameter, and 1-3% 0.5-5.0cm diameter black to dark gray to red magnetite-rich, hematite-rich, or jasper-rich banded iron formation lapilli.
- massive felsic lava flows composed of light gray to greenish gray, fine-grained, massive, aphyric to quartz-phyric rhyodacite to rhyolite lava flows.

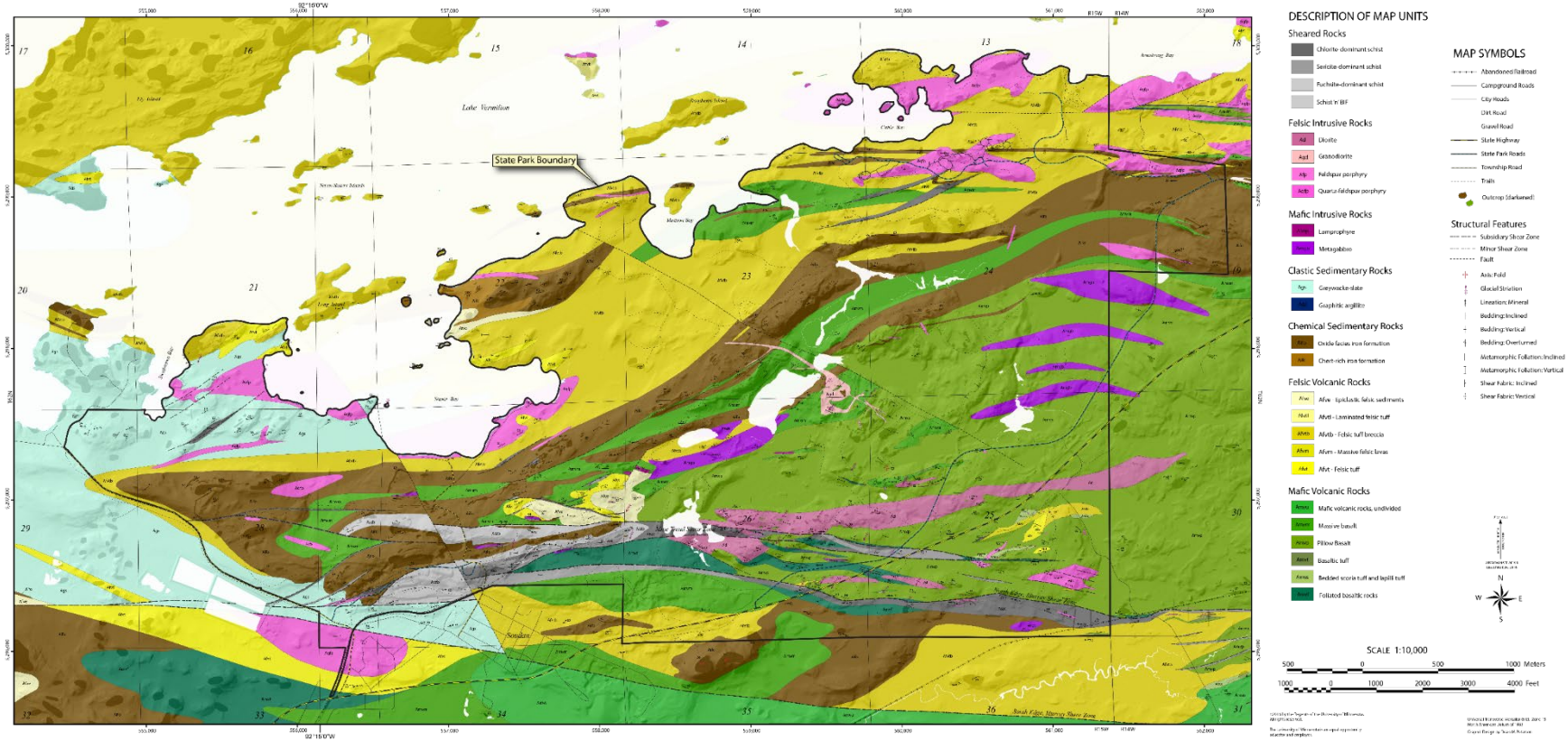


Figure 4-5. Geologic map of Lake Vermilion/Soudan Underground Mine State Park (after Peterson et al., 2016). Detailed maps showing locations of field trip stops are provided in Figure 4-8, and optional stops are shown in Figure 4-12.

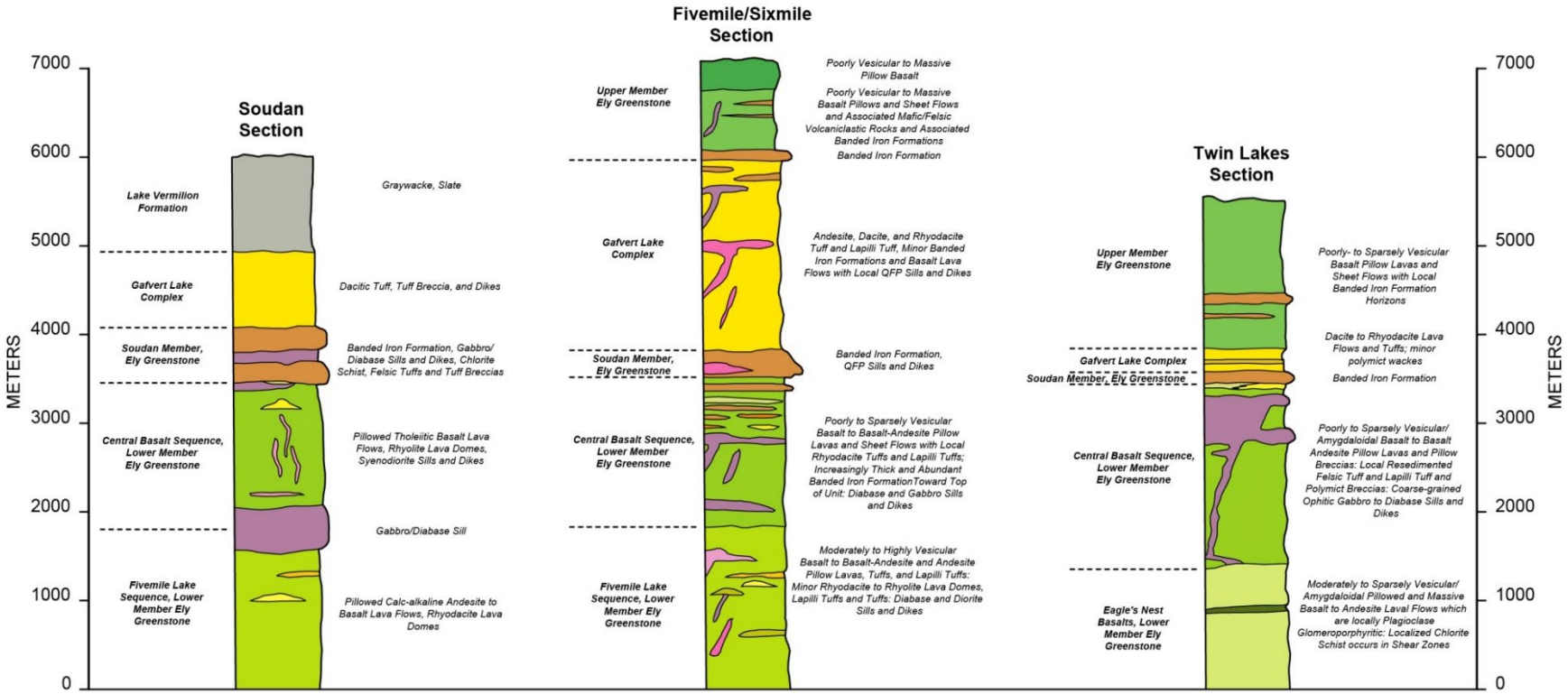


Figure 4-6. Regional stratigraphic correlations across the Vermilion District (after Hudak et al., 2012; Hudak et al., 2014; Hudak and Peterson, 2014). The sections are hung on the base of the Soudan Member of the Ely Greenstone Formation

- felsic tuff, made up of gray to tan, fine-grained, aphyric to quartz ± plagioclase-phyric rhyodacite to rhyolite tuff.

Clastic sedimentary rocks within the park include:

- graywacke-slate, made up of light gray, fine- to medium-grained, thin- to medium-bedded graywacke containing up to 3% <1-2mm quartz and plagioclase grains that are interbedded with dark gray, laminated to thin-bedded mudstone/slate.
- graphitic argillite, composed of dark gray to black, laminated to thin-bedded graphite-bearing argillite

Chemical sedimentary rocks that occur in the park include:

- oxide-facies iron formation, made up of black (magnetite-rich), dark gray (magnetite- and/or hematite-rich, red (jasper-rich or hematite-rich), or gray (chert-rich) laminated to medium-bedded, planar bedded to chaotically soft-sediment folded, banded iron formation. Hydrothermal alteration of the oxide-facies iron formations has resulted in the genesis of the massive hematite ores that make up the numerous iron ore lenses of the Soudan Mine (Gruner, 1926; Klinger, 1960; Thompson, 2015; Allerton, 2024a, 2024b).
- chert-rich iron formation, composed of light gray to black laminated to very thin bedded chert that is locally interbedded with subordinate laminated to very thin bedded oxide facies iron formation

Both mafic and felsic intrusive rocks have been identified in the park. Mafic intrusive rocks include:

- lamprophyre intrusions, including 1) massive gray-green intrusions containing scoria, chert and granite clasts within a fine- to medium-grained groundmass composed of up to 85% acicular amphibole; and 2) black, fine-grained massive hornblende-plagioclase-bearing intrusions containing up to 15% fine-grained hornblende needles and local rounded granite blocks greater than 25cm in diameter in a fine-grained gray-black to red groundmass (Peterson and Patelke, 2003).

Felsic intrusive rocks in the park include:

- diorite, comprising gray to gray-green, fine- to medium-grained, plagioclase- and hornblende-phyric equigranular diorite (actinolite pseudomorphs of hornblende are common)
- granodiorite, made up of whitish-pink to green-gray, medium-grained granodiorite and hornblende granodiorite that locally contains xenoliths of oxide-facied banded iron formation, chert, felsic epiclastic rocks, and mafic volcanic and volcaniclastic rocks
- feldspar porphyry, composed of white to whitish-pink, medium-grained, holocrystalline dacite with 5-12% 1-4mm subhedral to euhedral tabular plagioclase feldspar phenocrysts, and locally, 2-5% 1-3mm dark green actinolite pseudomorphs of hornblende (Radakovich et al., 2010)
- quartz feldspar porphyry, characterized by white to whitish-pink, light gray to pale green-gray porphyritic dacite and rhyodacite that contains 20-25% 1-5mm diameter subhedral to euhedral plagioclase feldspar phenocrysts and 5-15% 1-3mm diameter subhedral to euhedral pale gray to gray-blue quartz phenocrysts

Sheared rocks that crop out in Lake Vermilion/Soudan Underground Mine State Park include:

- chlorite-dominant schist, composed of dark green very fine- to fine-grained chlorite phyllite and schist (Peterson and Patelke, 2003)
- sericite-dominant schist, made up of pale yellow to yellow-gray to yellow-green very fine- to fine-grained sericite-bearing phyllite and schist (Peterson and Patelke, 2003)
- green mica (fuchsite)-dominant schist, comprising pale yellow to yellow gray, very fine- to fine-grained sericite-bearing phyllite that contains up to 20% emerald green disseminated porphyroblasts of green mica that are up to 5mm in length
- Schist ‘n’ BIF, an enigmatic unit made up of interlayered chlorite-dominant phyllite and schists and sericite-dominant phyllites and schists that contain lens-shaped clasts of oxide facies iron formation ranging from 1mm – 1 meter in length

Stratigraphic correlations across the central part of the Vermilion district are illustrated in Figure 4-6 (Hudak et al., 2012).

Structure

Three distinctive types of fault zones have been identified during geological mapping within Lake Vermilion/Soudan Underground Mine State Park. These structures include:

- Synvolcanic fault zones (D_0), which formed at the time of volcanism associated with the genesis of the volcanic rocks in the State Park, and which possess higher concentrations of synvolcanic hydrothermal alteration mineral assemblages proximal to the synvolcanic structures (see Gibson et al. (1999) and Hudak et al. (2014) for a detailed explanation of synvolcanic fault zones). Two potential synvolcanic fault zones have been described in the north-central part of the former Lake Vermilion State Park by Hudak et al. (2014);
- Shear zones that are associated with the regional D_2 deformation, and are characterized by linear zones of sheared rocks including chlorite-dominant schist, sericite-dominant schist, fuchsite (green mica)-dominant schist, and schist 'n' BIF. The Mine Trend and Murray shear zones (Peterson and Patelke, 2003; Peterson et al., 2016; Table 4-2) are examples of D_2-associated shear zones within the bounds of Lake Vermilion/Soudan Underground Mine State Park.
- Late faults are characterized by brittle deformation and associated offset of adjacent lithological units. Within Lake Vermilion/Soudan Underground Mine State Park, these D_3-associated structures are commonly expressed as northwest- to northeast-trending, minor displacement (generally less than one meter) brittle faults that offset sedimentary bedding and / or contacts between adjacent lithological units (D3-associated faults are clearly evident at field trip stop 1).

Table 4-2. Calculated displacements among the Mine Trend and Murray Shear zones (Peterson and Patelke, 2003). Ranges of values were calculated geometrically by using the average plunges of lineations associated with the shear zones, and two measured lines of possible correlative stratigraphy offset by the bounding shear zones. See Peterson and Patelke (2003) for further details.

		Calculated Displacement (Kilometers)		
Shear Zone	Lineation Plunge	Strike Slip	Dip Slip	Net Slip
Mine Trend Shear Zone	72.6°	2.1	6.7	7.0
	72.6°	1.0	3.2	3.3
Murray Shear Zone	71.0°	4.5	13.1	13.8
	71.0°	3.0	8.7	9.2

Measurements of other planar (e.g. bedding orientation, orientations of geological contacts, foliation measurements) and linear (e.g. mineral lineations, glacial striations) geological structures were recorded during field mapping, and are included on the new geologic map of Lake Vermilion/Soudan Underground Mine State Park (Peterson et al., 2016; see Figure 4-5).

Geochronology

Geochronological information for supracrustal and intrusive lithologies in the Vermilion District is relatively sparse (refer back to Figure 4-4). Peterson et al. (2001) obtained a U-Pb zircon age date of 2722 ± 0.9 Ma from a quartz-phyric rhyolite dome in the Fivemile Lake Sequence of the Lower Member of the Ely Greenstone Formation. Allerton et al. (2024a) obtained a crystallization age of 2708 ± 25 Ma for the Purvis Pluton, which intrudes the Eagles Nest Succession of the Lower Ely Member and has been interpreted as a synvolcanic intrusion (Peterson, 2001). The age of the Upper Member of the Ely Greenstone formation is currently unknown. Jirsa (2016) obtained an age of 2715.74 ± 0.50 Ma for a felsic volcanic

unit within the Newton Lake Formation (Boerboom, T. J., 2020). Lodge et al. (2013) obtained a U-Pb zircon date of 2689.7 ± 0.8 Ma for a Gafvert Lake Sequence dacitic tuff breccia that occurs approximately 2 meters north of the contact with the Soudan Iron-Formation member of the Ely Greenstone Formation. As well, Lodge et al. (2013) obtained detrital zircon dates ranging from 2680-2690 Ma from greywackes that comprise the Lake Vermilion Formation. This date confirms the source of the detritus in the Lake Vermilion Formation was derived locally from the volcaniclastic rocks comprising the Gafvert Lake Sequence.

The age of the orebodies at the Soudan Mine has eluded geologists for nearly a century. The genesis of the massive hematite orebodies was previously interpreted to be syn- or post-depositional to the formation of the Soudan Member of the Lower Ely Greenstone Formation (Gruner, 1926; Klinger, 1960; Thompson, 2015). Gruner (1926) believed the ores could be as young as the Mesoproterozoic Duluth Complex. Klinger (1960) found abundant evidence for post-iron formation depositional genesis of the massive hematite ores, but he could not determine a specific date for mineralization and concluded the orebodies were formed along with or after shear zones that are spatially associated with the ores. Thompson (2015) speculated based on geological, structural, and lithogeochemical data, that the ores were formed during the D_2 deformation, but could not determine a specific date for the massive hematite mineralization. Recent U/Pb and (U-Th)/He radiometric dating of hematite by Allerton (2024b) suggests the massive hematite orebodies at Soudan formed during Paleoproterozoic time (1640.8 ± 47.2 Ma – 1740.4 ± 72.5 Ma) and have been overprinted by a Mesoproterozoic hydrothermal event at approximately 1100 Ma (1093.1 ± 16.4 Ma).

Terminology Used for This Field Trip

The terminology used on this field trip will be consistent with the terminology used by Hudak et al. (2014) for their "Walk in the Park" ILSG field trip and is described below.

All stop locations for this field trip are given in Universal Transverse Mercator (UTM) coordinates, Zone 15N, using the North American Datum of 1983 (NAD83) as well as latitude/longitude. Section subdivisions read from smallest to largest quarter (e.g., "NW, SE" should be read "NW quarter of the SE quarter"). A geologic map with stop locations is given in Figure 4-8. A map of optional field trip stops is given in Figure 4-12.

It is important to note the terminology utilized in this field trip guide for: 1) volcaniclastic rocks; and 2) bedding characteristics. Use of consistent terminology is required to facilitate consistent and accurate describe these geological features.

Volcaniclastic rocks contain abundant volcanic material irrespective of their origin or depositional environment (Fisher, 1966). Such rocks can form directly from volcanic eruptions (whether subaerial or subaqueous), resedimentation of non-lithified volcanic deposits (for example, resedimentation of pyroclasts prior to lithification), or weathering and resedimentation of pre-existing lithified volcanic rocks.

Primary (juvenile) volcaniclastic particles result directly from eruptive processes, and are of three types:

- *Pyroclasts*, which form by explosive fragmentation of magma into particles (including ash, highly vesiculated glass (pumice, scoria), crystals and crystal fragments, and lithic fragments);
- *Hydroclasts*, which form by explosive interaction with external water (via phreatic (steam only) and/or phreatomagmatic (steam and magma) explosions) or by non-explosive quenching and granulation of lava (for example, the formation of hyaloclastite fragments on the margins of submarine lava flows or intrusions into wet sediments); and
- *Autoclasts*, which form by frictional breakage of moving viscous lava flows (for example, to form carapace breccias on the margins of subaerial lava flows).

Based on these different types of fragmentation, four types of primary volcaniclastic deposits have been identified by White and Houghton (2006):

- *Pyroclastic deposits*, which are generated from volcanic plumes and jets or pyroclastic density currents as particles first come to rest. Deposition mechanisms associated with these processes include suspension settling, traction, or *en masse* freezing;
- *Autoclastic deposits*, which are generated during effusive volcanism when lava cools and fragments as a result of thermal processes, or recently cooled lava breaks during flow. Deposition for these types of rocks is under the influence of continued lava flowage;
- *Hyaloclastite deposits*, which are generated during effusive volcanism when magma or flowing lava is chilled and fragmented due to contact with water. Deposition of such deposits is is influenced by the continued emplacement of the lava in the presence of water, and the thicknesses of the hyaloclastite deposits can be dictated by the temperature of the magma, the effusion rate, and the distance from the volcanic vent (Cas and Wright, 1987; Gibson et al., 1999; Newkirk et al., 2001); and
- *Peperite deposits*, which are generated when magma intrudes into unconsolidated clastic material and mingles with (generally wet) debris to form a volcaniclastic deposit (McPhie et al., 1993). Deposition of peperite deposits takes place essentially *in-situ*.

Secondary volcaniclastic particles are known as epiclasts:

- *Epiclasts* are lithic clasts and/or crystals derived from physical weathering and erosion of pre-existing lithified rocks. Epiclasts are volcaniclasts when the pre-existing rocks are volcanic.

The terminology for volcaniclastic rocks has historically been somewhat confusing because many different classification schemes have been developed (for example Fisher, 1961; Fisher 1966; Schmid, 1981; Cas and Wright, 1987; McPhie et al., 1993; White and Houghton, 2006), and different classification schemes are preferentially used in different parts of the world. As a result, the terminology relating to volcaniclastic rocks is commonly misused or misinterpreted. Four classification schemes that have been used most in the recent geological literature include:

- Fisher (1961, 1966) – Classification based on particle size, particle formation, or particle fragmentation mechanism;
- Schmid (1981) – Particle type within the deposit;
- Cas and Wright (1987) – Mode of fragmentation and deposition; *and*
- McPhie et al. (1993) – Transport and deposition mechanisms.

According to R. V. Fisher (1998), the difficulties with volcaniclastic rock classification can be understood because "volcaniclastic rocks are essentially igneous on the way up and sedimentary on the way down". In fact, Fisher's thesis advisor, when observing the volcaniclastic rocks that were the focus of his thesis studies, indicated that they were "the ugliest and most undistinguished rocks I've seen in my 30 years of petrology!" Classification is also especially difficult in ancient volcaniclastic rocks because key aspects of classification can be obscured by subsequent hydrothermal alteration, metamorphism and/or structural deformation (e.g. particle type, particle size) or because genetic processes cannot be ascertained unambiguously (e.g. transport and deposition mechanism, fragmentation mechanisms).

For this field trip guidebook, we will utilize Fisher's (1966) classification (Figure 4-7) for volcaniclastic rocks. This classification scheme is based on the relative proportions of ash-sized material (< 2mm), lapilli-sized material (2-64mm), and blocks/bomb sized material (>64mm) in the rock. Both Gibson et al. (1999) and Mueller and White (2004) suggest that this classification be used for field-based rock classification (mapping, diamond drill core logging, petrography) of ancient volcaniclastic deposits for the following reasons:

- The classification scheme is "field-user friendly" because it accommodates both the historically important pyroclastic rock names and enables comparison at both the hand sample and thin section scale (Mueller and White, 2004);
- It is a Wentworth-based scale, and thus enables comparison of volcaniclastic deposits to sedimentary deposits; and
- Rock classification does not require knowledge of the specific transport mechanism or depositional processes involved with the genesis of the deposit.

More recently, White and Houghton (2006) have developed a modified version of Fisher's (1966) volcaniclastic classification scheme (Figure 4-7). The scheme is essentially equivalent to the Fisher (1966) scheme, with the exception that the lapill-tuff field in the White and Houghton (2006) classification comprises the lapilli-tuff and lapillistone fields of Fisher's (1966).

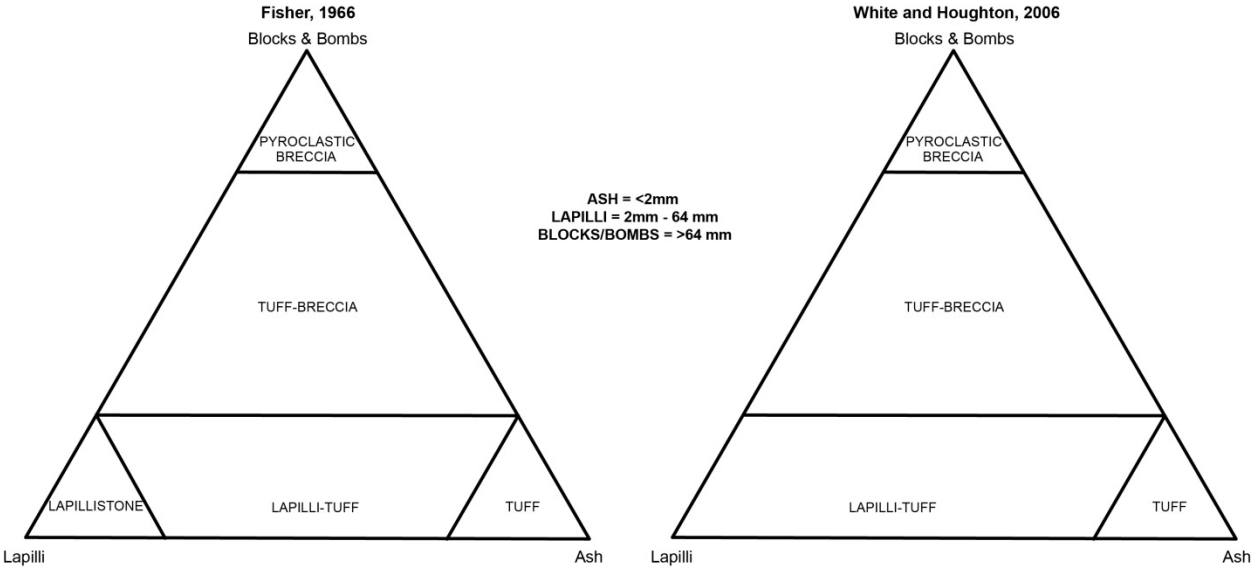


Figure 4-7. Volcaniclastic rock classification schemes of Fisher (1966) and White and Houghton (2006). This field trip guidebook will classify volcaniclastic rocks using Fisher's (1966) classification scheme.

Specific terms for bedding thicknesses are also used in this guidebook. The terminology for bedding thickness has been adopted from McPhie et al. (1993) and includes:

- Laminated <1 centimeters thick
- Very thinly bedded 1-3 centimeters thick
- Thinly bedded 3-10 centimeters thick
- Medium bedded 10-30 centimeters thick
- Thickly bedded 30-100 centimeters thick
- Very thickly bedded >100 centimeters thick

FIELD TRIP OVERVIEW

NOTE: This field trip will require hiking along trails and through the bush in Lake Vermilion/ Soudan Underground State Park and includes observations on the 27th level of the Soudan Mine. Hiking boots and safety eyewear are strongly encouraged as traverses in the park may encounter slippery conditions and vegetation which can cause eye injuries. Field trip participants should plan to wear a jacket and gloves while underground as the temperatures in this location are typically around 50°F (10°C).

Upon arriving at Lake Vermilion/Soudan Underground Mine State Park, we will park in the main parking lot located near the Park Manager's office. After a coffee break, we will strap on our hiking boots and spend the remainder of the morning making field trip stops in the central part of Lake Vermilion/Soudan Underground Mine State Park along a more-or-less north-south traverse. These field trip stops (Figure 4-8) will illustrate the stratigraphy, structural, and hydrothermal alteration features associated with the massive hematite ores at the Soudan Mine. We will then head back to the visitor center and have lunch overlooking one of the original Soudan Mine ore pits.

After lunch, we plan to continue the field trip by going underground. We will proceed to the mine shaft and travel 2341 feet underground to the 27th Level of the Soudan Mine. We will board a train (converted ore cars) and travel west for approximately three-quarters of a mile to the Montana Stope, the last active part of the mine. At this point we will climb vertically approximately 30 feet using a very tight spiral staircase. One in the Montana Stope, we will observe the massive hematite ore, the transitional region of non-ore iron formation, and will observe massive chlorite-rich schists associated with approximately east-west-trending D2-associated shear zones. Here we plan to discuss recent geological research that has been conducted to determine the absolute age of the massive hematite ores that reside there (Allerton et al., 2024a, 2024b; Allerton et al., in review). At the end of the tour we will proceed back down to the 27th level drift, board the train, and head back east through the drift to the shaft station where we will proceed back to the surface.

Field trip participants may not be able to access the 27th level of the Soudan Mine due to flooding that occurred during summer, 2024. Should this happen, afternoon field trip stops will investigate outcrops that illustrate the rarely exposed geological contact between the Soudan Member iron formation and Gafvert Lake Sequence tuffs, lapilli-tuff and tuff-breccias, Gafvert Lake Sequence tuffs and lapilli-tuffs, and subvolcanic intrusive rocks related to the Gafvert Lake Sequence that occur in the northeastern part of Lake Vermilion/Soudan Underground Mine State Park. Descriptions of these outcrops are included in a section below called "Optional Outcrop Stops" which have been taken from a recent ILSG field trip titled "Field Trip 2 - A Walk in the Park: Neoarchean Geology of Lake Vermilion State Park" (Hudak et al., 2014).

Following the completion of the field trip, we will board the vehicles and proceed back to the Mountain Iron Community Center, where the field trip will end.

FIELD TRIP

From the Mountain Iron Community Center, proceed 0.2west on Enterprise Drive S to Emerald Avenue. Turn north on Emerald Avenue and go 0.05 miles to Highway 169. Turn east on Hwy 160 and proceed 1.5 miles to the turn off for Hwy 169/Hwy 53N. Take Hwy169/Hwy53 approximately 6.1 miles, bear right, and continue north on Hwy1/169 toward Ely. Continue north/northeast on Hwy 1/169 for approximately 23.75 miles to the first turn-off to Soudan (this will be Main Street and you will see an ore car and a sign for the Soudan Mine at the intersection). Proceed north for 0.4 miles on Main Street, turn right, and continue on Main Street for approximately 0.9 miles until it intersects 1st Ave./Stuntz Bay Road. Turn north on 1st Ave/Stuntz Bay Road and proceed for approximately 0.4 miles until you see the dirt road (McKinley Park Road) that is the east entrance to the Soudan Mine. Turn west on the dirt road, go about 0.05 miles, and park near the Lake Vermilion/Soudan Underground Mine State Park Manager's office. Here

we will check in with the Manager. Turn left (south) on the dirt road and follow it around the old mine infrastructure, parking near the intersection of McKinley Park Road and Stuntz Bay Road (approximately 0.1 miles). From our vehicles parked at the intersection of Mckinley Park Road and Stuntz Bay Road, we will walk north approximately 175 meters up 1st Ave/Township Highway 4598 to field trip stop 1. Please walk against traffic as we proceed to and from this location.

Stop 1: Soudan Member Banded Iron Formation

Longitude/Latitude: 47.820074°N, -92.2365908°E

UTM NAD 83 Zone 15N: 557144E, 5296585N

(NOTE: From Peterson et al., 2009A; Hudak and Peterson, 2014)

The Soudan Member of the Ely Greenstone Formation is dominantly composed of laminated to thinly bedded Algoma-type oxide facies banded iron-formation, with subordinate, locally interstratified, sparsely amygdaloidal massive to pillowed basalt lava flows and resedimented felsic tuff deposits. Regionally, the stratigraphic thickness of the Soudan Member of the Ely Greenstone Formation varies from 50-3,000 meters, with an average stratigraphic thickness of approximately 700 meters (Peterson et al., 2009). Within Lake Vermilion State Park, the Soudan Member ranges in stratigraphic thickness from approximately 300 – 680 meters in thickness. Individual horizons of oxide-facies iron formation range from approximately 70-345 meters thick, whereas the Soudan basalt lava flow units range from approximately 60-300 meters in thickness.

This classic exposure of the Soudan member of the Ely Greenstone Formation lies on the north limb of the Tower-Soudan anticline approximately 75 meters north of the stratigraphic contact with the Lower member of the Ely Greenstone. The outcrop displays two generations of tight folding in delicate laminae of chert (creamy white), chert-hematite jasper (red), and magnetite-chert (black to silver-colored). The second generation of folds (F_2) is tectonic in origin, having subvertical axial surfaces that trend east, and steeply plunging axes. Most display Z-asymmetry. The earlier folds (F_{0-1}) appear to have been sharply refolded to produce complex interference patterns. Lundy (1985) studied folding at this locality and concluded that some of the apparent interference structures are the product of early-formed sheath folds that did not involve refolding by D_2. The F_1 structures are predominantly intrafolial, and exhibit a great variety of styles and orientations; implying they formed by layer-parallel, soft-sediment slumping (Fig. 4-9). Lundy's mapping of this outcrop is an interesting demonstration of how unraveling details at a single outcrop that led to recognition that D_1 deformation was not systematic here, but likely the result of soft sediment folding.

It is interesting to observe the rhythmic microlaminae (1 mm or so thick) in various cherty beds exposed here and speculate about the paleoenvironment - that is, whether these represent daily heating/cooling, tidal, climatic, annual, or some other repetitive influence (e.g. waxing/waning of a hydrothermal system) in the depositional environment. What is known about units of iron-formation in the Ely Greenstone, of which there are many, is that deposition occurred in deep water (below wave base) during periods of relative volcanic and tectonic quiescence by the slow subaqueous precipitation of chemical sediments.

The deep excavations in this area are the early workings of the Soudan iron mine, the first in Minnesota. The mine produced about 16 mt of high-grade hematite ore (60-63 percent ironconverted to a park. Although some early production came from open pits, most of the ore was extracted from underground workings that began here in 1900, and which now can be visited on guided tours. The mine previously housed several underground physics research facilities. These include Soudan 1 (23rd level) which studied neutrino decay; 2) Soudan 2 (27th level), also to study neutrino decay; and 3) the MINOS (Main Injector

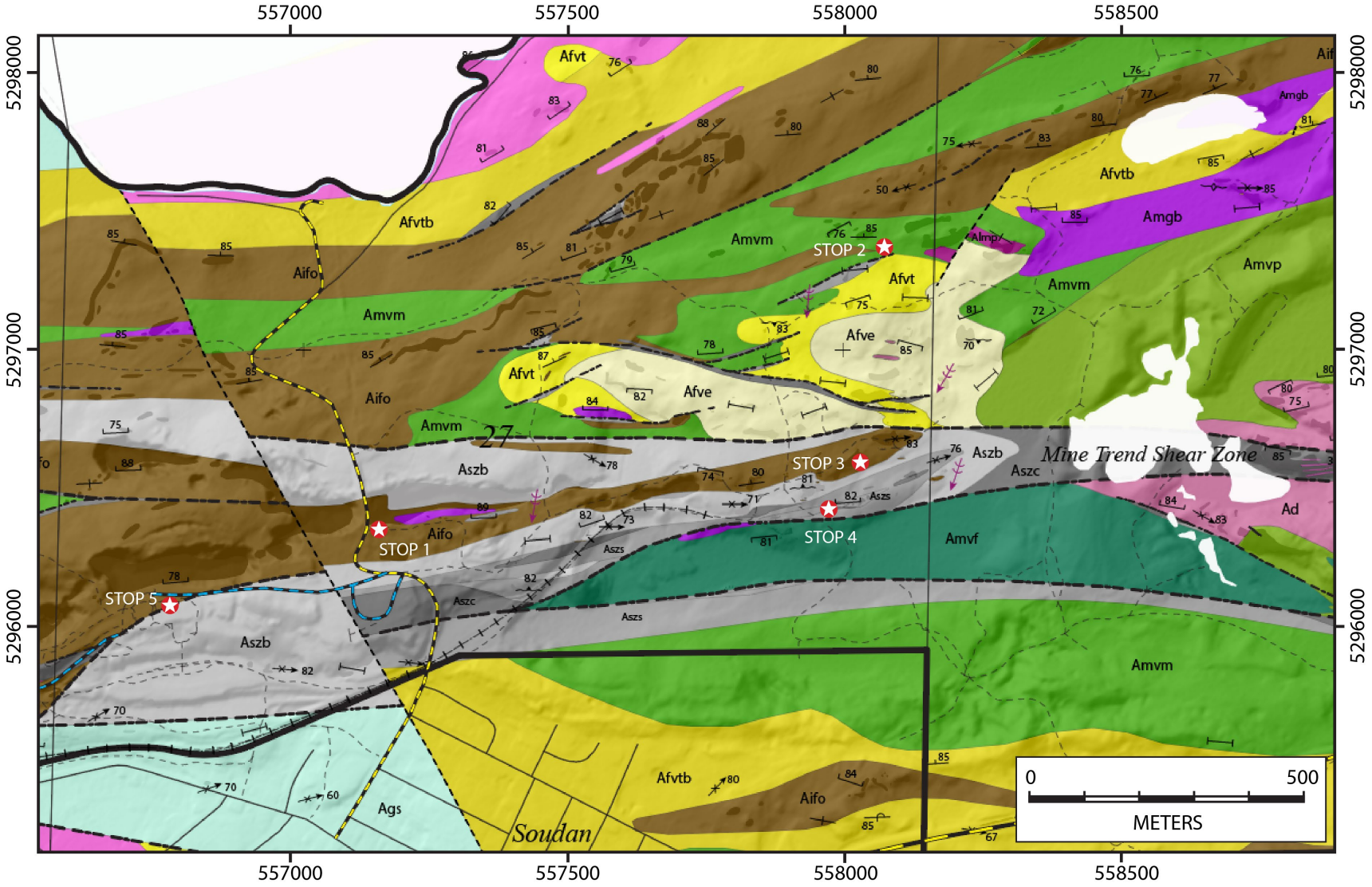


Figure 4-8. Geologic map of the central part of Lake Vermilion/Soudan Underground Mine State Park (after Peterson et al., 2016) illustrating locations of field trip stops. See Figure 4-5 for the description of map units.

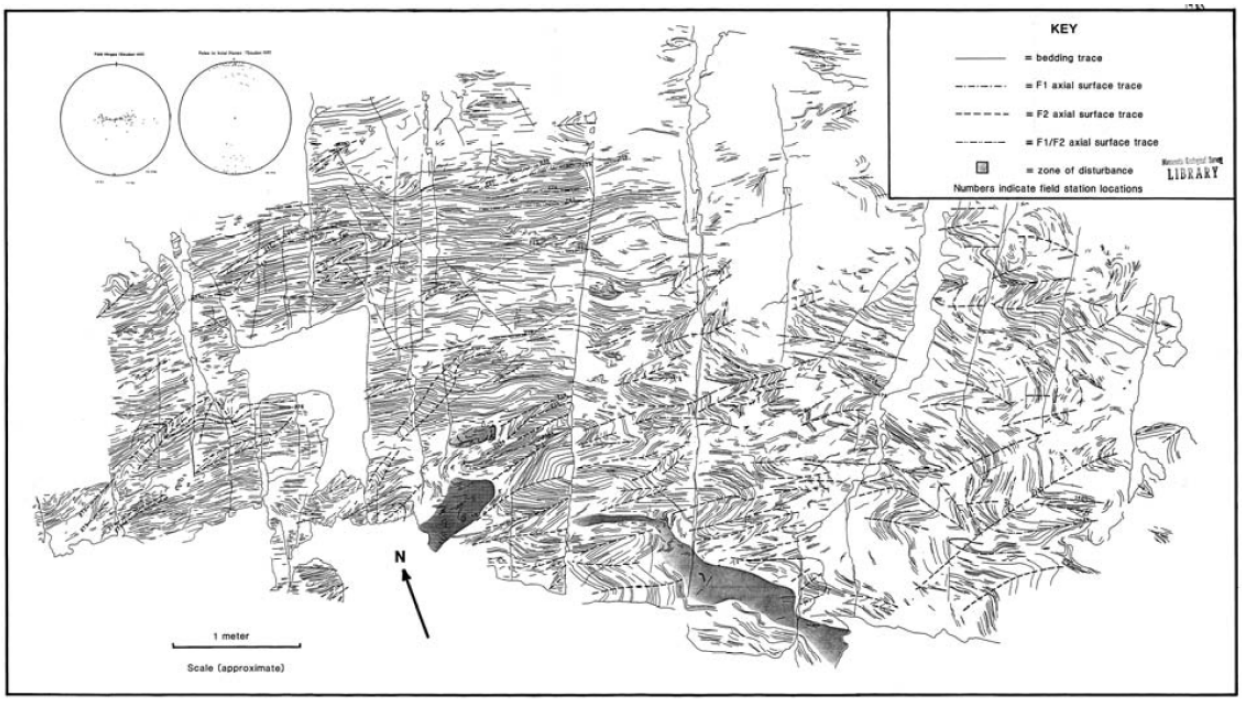


Figure 4-9. Outcrop map showing bedding trajectories and multiple generations of folds and faults (from Lundy, 1985). F_1 folds are non-systematic and include both nappe- and sheath fold geometries.

Neutrino Oscillation Search) lab, which was built on the 27th level adjacent to Soudan 1 and studied the decay of neutrinos within the earth as they passed from Fermilab to Soudan.

Follow the field trip leaders south along First Avenue/Township Highway 4598 to the blacktop-paved Mesabi Trail. Turn to the east and walk along the paved Mesabi trail for approximately 800m. There, turn north and proceed up the unpaved trail approximately 350 meters, where the trail intersects another trail that goes northeast. Turn right and proceed northeast along the trail for about 90 meters. We will then head into the bush and hike approximately 200 meters northeast to field trip stop 2.

Stop 2: Soudan Member Basalt Pillow Lavas

Longitude/Latitude: 47.82544775°N, -92.22434651°E

UTM NAD 83 Zone 15N: 558055E, 5297191N

Detailed mapping in the park by Peterson and Jirsa (1999), Peterson and Patelke (2003), Hoffman (2007), Radakovich et al. (2010), Vallowe et al. (2010), Heim et al. (2011), and Baumgardner et al. (2013) has shown that the Soudan member is dominantly composed of oxide facies iron formation horizons that are locally interlayered with massive and pillowed mafic lava flows and associated volcaniclastic rocks (e.g. pillow breccias). Basalt lava flows associated with the Soudan Member of the Lower Ely Greenstone Formation are characterized by a medium green to dark green color. They are typically aphyric- to sparsely plagioclase ± pyroxene (now actinolite)-phyric. Plagioclase phenocrysts vary from subhedral to euhedral tabular in morphology, are typically less than or equal to 1mm in length and are locally present in abundances up to 3%. Locally, 5-7% dark green actinolite pseudomorphs of pyroxene phenocrysts may be present. Where amygdaloidal, the unit contains up to 7% oval to round, light gray quartz-filled amygdules ranging from <1-4mm in diameter.

At this outcrop we will observe well-preserved 0.5-2m long, aphyric- to sparsely plagioclase-phyric, massive- to sparsely amygdaloidal bun- and mattress-shaped pillow lavas. These pillows dip steeply to the north and strike approximately east-west. Interpillow hyaloclastite is locally well-preserved and is

composed of <1-5mm chlorite-rich cuspate shards that are pseudomorphs of original volcanic glass formed by quenching of the mafic magma by water.

These pillow lavas share many characteristics with the underlying Central Basalt Sequence mafic lava flows that comprise the uppermost part of the Lower Ely Member of the Ely Greenstone Formation. Such characteristics include exceptional preservation of primary volcanic textures, medium- to dark green color, sparsely plagioclase ± pyroxene-phyric, and low vesicularity. Based on these features, the Soudan Member pillow basalts at this location and are interpreted to have formed in a "deep water" (e.g. below wave based) volcanic environment.

Proceed approximately 200 meters southwest to the northeast-southwest trending trail. Walk approximately 90 meters southwest to intersect the main north-south trail that intersects the Mesabi Trail. Walk approximately 350 meters south back to the paved Mesabi Trail. Turn to the east and follow the field trip leaders through the bush for about 140 meters to field trip stop 3.

Stop 3: Soudan Member Oxide Facies Banded Iron Formation

Longitude/Latitude: 47.82139974°N, -92.225809591°E

UTM NAD 83 Zone 15N: 557990E, 5296775N

Within Lake Vermilion/Soudan Underground Mine State Park, the Soudan Member oxide-facies banded iron-formation is generally planar laminated to medium-bedded, with black magnetite-rich horizons, light gray to black chert horizons, red to blueish-black hematite-rich horizons, and red jasper horizons defining the bedding. Locally, very tight, chaotically oriented folds, resulting from syn-depositional soft sediment deformation and subsequent tectonic deformation, are present. As indicated above, these iron formation deposits are locally intimately interbedded with basalt lava flows such that mapping individual iron-formation and basalt horizons is often impossible at 1:5000 scale (Peterson and Patelke, 2003; Hudak and Peterson, 2014; Hudak et al., 2016).

This outcrop is composed of slightly- to moderately hematite-altered Soudan member oxide facies banded iron formation. The rock varies from locally non-magnetic to slightly magnetic due to alteration of magnetite to hematite/martite. Such alteration is common in areas within a few hundred meters of massive hematite ore and is commonly found in close proximity to D_2-associated shear zones. The closest previously mined massive hematite orebody was located approximately 250 meters west-southwest of this location in an existing mine pit. D_2-associated shear zones have been identified approximately 25 meters north and south of this outcrop.

Here, the oxide-facies banded iron formation comprises interlayered planar horizons of gray oxide-rich (hematite ± magnetite), red jasper-rich, and pale white (silica (chert)-rich that are laminated, thinly bedded, and locally medium bedded. Bedding orientations generally strike more or less east-west, although locally contorted layers may vary significantly in strike direction. Dips are generally steep (>75°) to the north, although locally dips may be steep to the south.

Follow the field trip leaders southwest for about 85 meters to field trip stop 4.

Stop 4: Mine Trend Shear Zone "Schist 'n' BIF"

Longitude/Latitude: 47.82126659°N, -92.22607876°E

UTM NAD 83 Zone 15N: 557725E, 5296740N

The "Schist 'n' BIF" units at this location (Figure 4-10) are composed of sheared rocks comprising chlorite schist that are interlayered with, and locally contain fragments of red, jasper-rich banded iron formation and light gray to white chert. The chlorite schist is fine-grained (<1 mm) with a tan (chlorite-ankerite) to green (chlorite-rich) weathered surface. Common minerals include chlorite, ankerite, sericite,

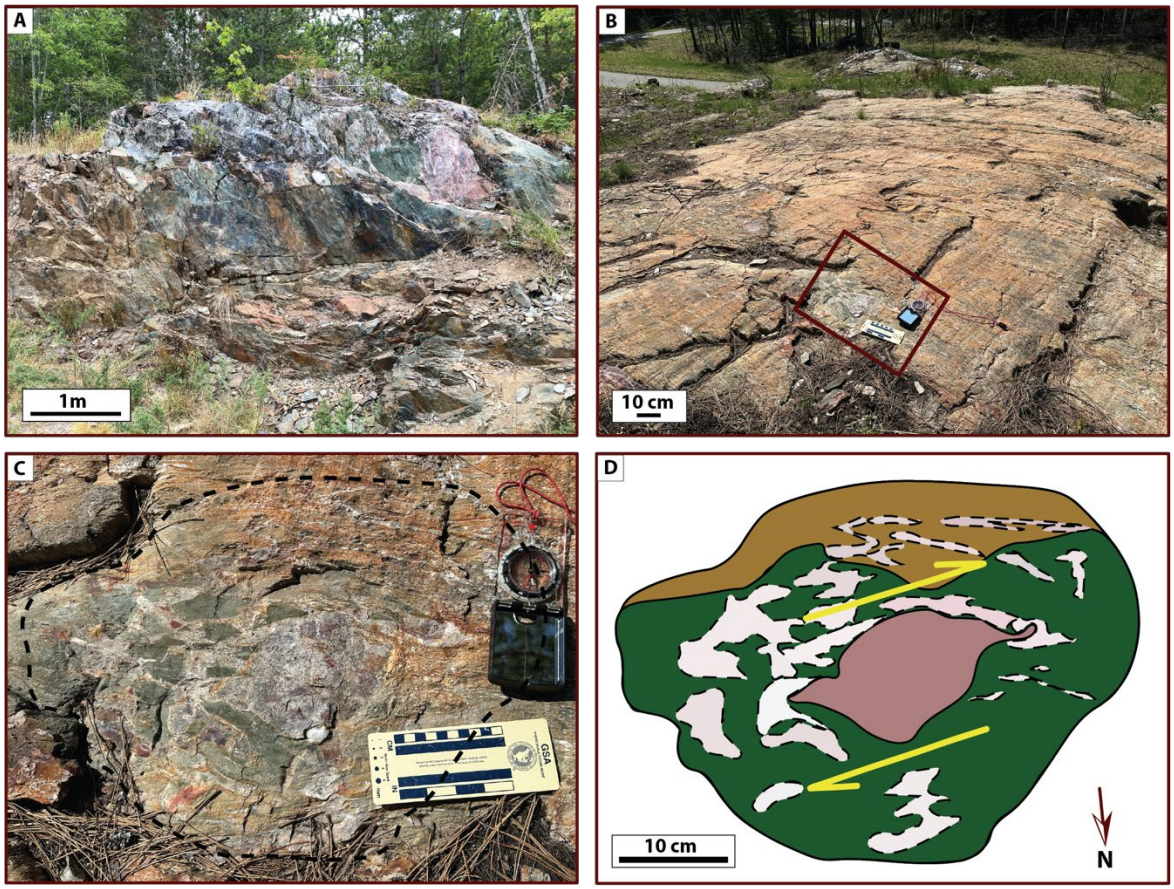


Figure 4-10. Photographs of outcrop exposures at Stop 4. A) Image is showing the southern face of the "Schist 'n' BIF" unit. The greenish tan rock is chlorite schist, and the red and white layers are banded iron formation. B) This image is north of image A and is the near horizontal exposure of the "Shist 'n' BIF" outcrop. The dark red inset in this figure is the location of the photographic in Figure 4-10C. C) This image shows a sigma clast of banded iron formation enclosed by chorite schist. Although the banded iron formation pieces are locally broken off, the clast can be traced, and a sketch of the clast is shown in Figure 4-10D). D) Sketch of a somewhat intact banded iron formation clast (dark pink) surrounded by silicates and other chert fragments (light pink) and enclosed by green and tan chlorite ± ankerite schist.

and siderite. Banded iron formation fragments occur as clasts or thin bedded layers between foliation planes of the schist. The foliation here strikes east-west and dips near-vertically. The previously mentioned D_2 associated shearing has a dextral or right lateral sense of shear that is approximately east-west trending on a regional scale, although locally sinistral shear sense indicators are present locally.

This outcrop is located southwest of the previously visited oxide facies banded iron formation.

The construction of a new paved road in 2020 exposed the now southern face of the unit (Figure 4-10A), providing access to three planes for structural measurements. The shear plane (Figure 4-10B) contains banded iron formation/chert clasts that serve as kinematic indicators and are located conveniently under our feet due to the dip of the schist layers. Outcrop-scale kinematic indicators of sigma and delta clasts (Figures 4-10C and 4-10D) trend mostly east-west with dextral sense of shear, mimicking regional deformation trends.

Follow the field trip leaders and walk west-southwest for approximately 800 meters along the paved Mesabi back to First Avenue/Township Highway 4598. We will then proceed back to the vehicles and head to the

main parking lot for the Soudan Mine. We will eat lunch at the Soudan Mine visitors' center (bathrooms are available in the visitors' center).

Stop 5: Soudan Underground Mine Shaft

Longitude/Latitude: 47.82126659°N, -92.22607876°E

UTM NAD 83 Zone 15N: 556765E, 5296536N

Following lunch, we will watch a short video, pick up hard hats from state park staff, and proceed to the Soudan Mine shaft. **Make sure to bring a jacket and gloves underground as the temperature there is approximately 50°F (10°C).** Once in the cages, we will travel 2341 feet underground to the 27th Level of the Soudan Mine. After exiting the cage we will board a train (converted ore cars) and travel west for approximately three-quarters of a mile to the Montana Stope, the last active part of the mine. **It is important for everyone's safety to stay in the train car for the duration of the trip, and to not raise your hands while traveling in the train car.** At this point we will exit the train, and after a short walk, climb vertically approximately 30 feet using a very tight spiral staircase to the Montana Stope.

The Montana Stope is the last active part of the Soudan Mine. Thompson (2015) conducted detailed mapping of the Montana ore zone (Figure 4-11) and noted the presence of several rock types, including:

- Chlorite-dominant schist, which locally replaces sericite-dominant schist proximal to the ore (unit 5c)
- Chlorite + sericite schist, which locally replaces sericite-dominant schist (unit 5cs)
- Sericite-dominant schist composed of sericite + paragonite ± pyrophyllite that has a mylonitic texture and occurs intermediate to ore breccia zones (unit 5s)
- Sericite-dominant schist that is locally silicified and occurs in well foliated zones at the margins of ore bodies that locally contain disseminated iron-rich chlorite domains (unit 5sc)
- Hematite ore, predominantly composed of specular hematite with microplaty hematite occurring locally within fractures and vugs (unit 4o)
- Hematite ore breccia, composed of hematite-rich banded iron formation and brecciated massive hematite ore with abundant milky "bull" quartz and disseminated sulfides (pyrite ± chalcopyrite; unit Fbx)
- Hematite-jasper banded iron formation, which retains many of its primary sedimentary textures and represents an intermediate rock between fresh Soudan Member oxide facies banded iron formation and the altered hematite-rich iron ore (unit 4a)

The absolute age and geological processes associated with the genesis of the Soudan (and other Vermilion district) massive hematite ores have baffled geoscientists for over a century (e.g. Gruner, 1926; Klinger, 1960). Gruner (1926) proposed that massive hematite mineralization occurred after deposition and lithification of the Soudan Member oxide facies banded iron formation and proposed that the mineralization occurred resulted from alteration of the original banded iron formation by ascending upwelling hydrothermal solutions that oxidized most of the iron, dissolved quartz, and precipitated secondary carbonates and sulfides. He did not specify an exact age for this mineralization process.

Klinger (1960) noted the close association of massive hematite ore zones at the Soudan Mine to faults (shear zones) within the mine. He states that "the orebodies occur in the iron formation and their dimensions are controlled by its structure". He also noted that the massive hematite ores showed little evidence of deformation and concluded that "a second generation of hematite appears to post-date structural movements which occurred after the main ore-forming period. These movements, and later hematite, are

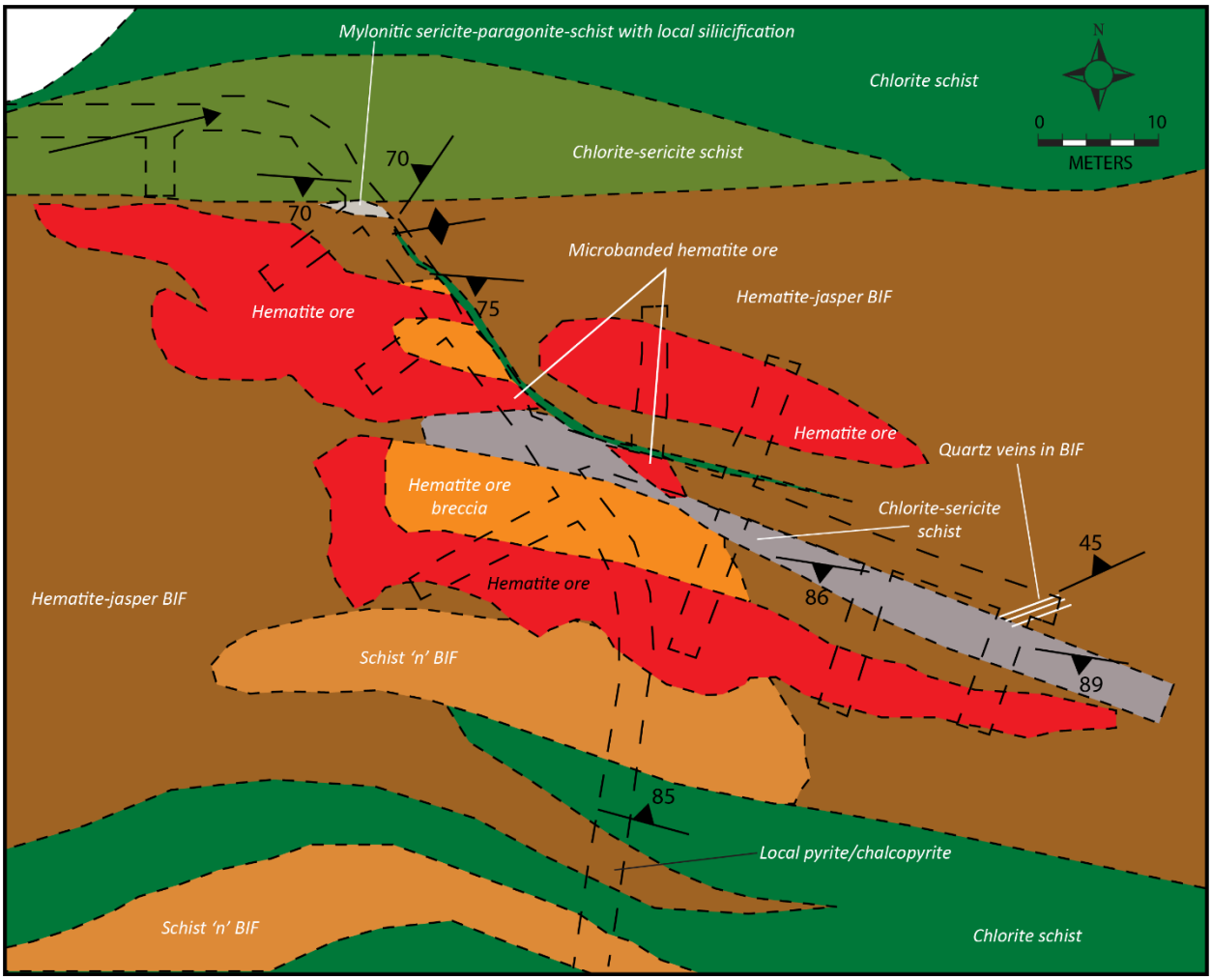


Figure 4-11. Geological map of the Montana stope (modified from Thompson, 2015).

both later in time than a sericite rock that has been dated at 1.67 billion years by the A40/K40 method". He also indicated that "at least some of the hematite is younger than 1.67 billion years" and concluded that the ores were "post-Huronian to pre-Keewenawan" in age.

Recent masters and doctoral studies from the University of Minnesota Duluth (Thompson, 2015) and the University of Minnesota Twin Cities (Allerton, in prep.; Allerton et al., 2024a; Allerton et al., 2024b; Allerton et al., in review) have focused their research on understanding the absolute age of massive hematite mineralization at the Soudan Mine.

Based on detailed mapping, petrographic studies, and lithogeochemical studies, Thompson (2015) suggested that the massive hematite ores at Soudan were formed from a multi-stage process involving alteration of the original oxide-facies banded iron formation by a fluid-dominated synvolcanic sea-floor hydrothermal system followed by interaction with hydrothermal metamorphic fluids associated with the subduction of strata within the Vermilion district. Therefore, his model for the genesis of the Soudan massive hematite ores suggests a Neoarchean age ranging from the time of the original deposition of the oxide-facies banded iron formations (~2720 Ma) to the time spanning the D_2 deformation (2674-2685 Ma (Boerboom and Zartman, 1993) which is likely associated transpression and the development of the D_2 shear zones in which the ores occur.

New research (Allerton et al., in review) utilizing petrographic observations and electron microprobe analyses shows that the massive hematite ore can be divided further into two distinct ore

textures comprising: 1) homogenous microcrystalline hematite-martite; and 2) heterogenous microcrystalline hematite. The fine-grained microcrystalline hematite-martite (martite comprises hematite pseudomorph replacing magnetite) locally contains minute vug spaces and larger fractures that are filled by microplaty hematite and silicates. The heterogeneous ore contains a minor amount of metallic and/or earthy microcrystalline hematite, but is predominantly composed of coarser-grained microplaty hematite and silicates. Microcrystalline hematite-martite predates microplaty hematite and silicates based on crosscutting relationships. U-Pb radiometric dating of hematite was used to establish the timing of ore mineralization at ca. 1.8-1.6 Ga. Our new model for the genesis of Soudan massive ore suggests that hydrothermal alteration related to mineralization is coeval with orogenic events generated by Proterozoic terrain accretion and associated magmatism.

Additional geochemical analyses involving mass-balance calculations and Fe stable iron isotopes indicate that the upgrade of BIF to hematite ore was a two-stage process. Dense microcrystalline hematite-martite matrix yielding a homogeneous texture was produced during the first stage. The second stage resulted in the formation of a heterogeneous texture containing microplaty hematite and silicates in larger vugs and fractures in the microcrystalline hematite-martite ore.

At the end of this stop, we will proceed back to the 27th level drift using another tight spiral staircase. We will board the train and proceed east back to the shaft station where we will board the cages and return to the surface. At the surface, we will reboard the vehicles and proceed back to the Mountain Iron Community Center via the directions below.

From our parking spot at Soudan Mine, proceed down the hill on McKinley Park Road for approximately 0.4 miles to the intersection with Main Street. Turn south and drive for approximately 0.4 miles to the intersection with Hwy 1/169. Turn west and Hwy 1/169 and drive for about 23.7 miles and merge onto Hwy 53/169 South. Follow Hwy 1/169 the intersection with Hwy 53/Hwy 169. Merge on to Hwy 169 south and proceed for 1.5 miles to Emerald Avenue. Turn south and proceed on Emerald Avenue for approximately 0.1 mile. Turn east and proceed for approximately 0.2 miles back to the Mountain Iron Community Center.

OPTIONAL OUTCROPS

The following field trip stop descriptions have been taken from the 2014 ILSG Field Trip 2 "A Walk in the Park – Neoarchean Geology of Lake Vermilion State Park" (Hudak et al., 2014). A map showing the locations of the optional field trip stops is shown in Figure 4-12.

From the original parking spot near the Manager's office at Soudan Mine, proceed approximately 0.2 miles south on Stuntz Bay Road/1st Avenue to the intersection with Jasper Street. Go southeast on Jasper Street for about -.5 miles to the intersection of Hwy 1/169. Proceed east on Hwy 1/169 for 0.75miles to Vermilion Park Drive (this is the eastern entrance to Lake Vermilion/Soudan Underground Mine State Park and allows access to campsite near Cable Bay). Turn north on to Vermilion Park drive and proceed for 2.9 miles to Old Hwy 169. Turn west (left) on to Old Hwy 169 and follow it for 0.8 miles to Vermilion Ridge Road. Turn west on Vermilion Ridge Road and proceed for approximately 0.5 miles. Turn right and park near the restroom east of Cable Bay.

We will depart the vehicles here and walk across the street to the Crosscut Trail. walk southeast along the Crosscut Trail for about 2200 meters. We will then take a short hike (approximately 30 meters) up the hill to Stop 6o.

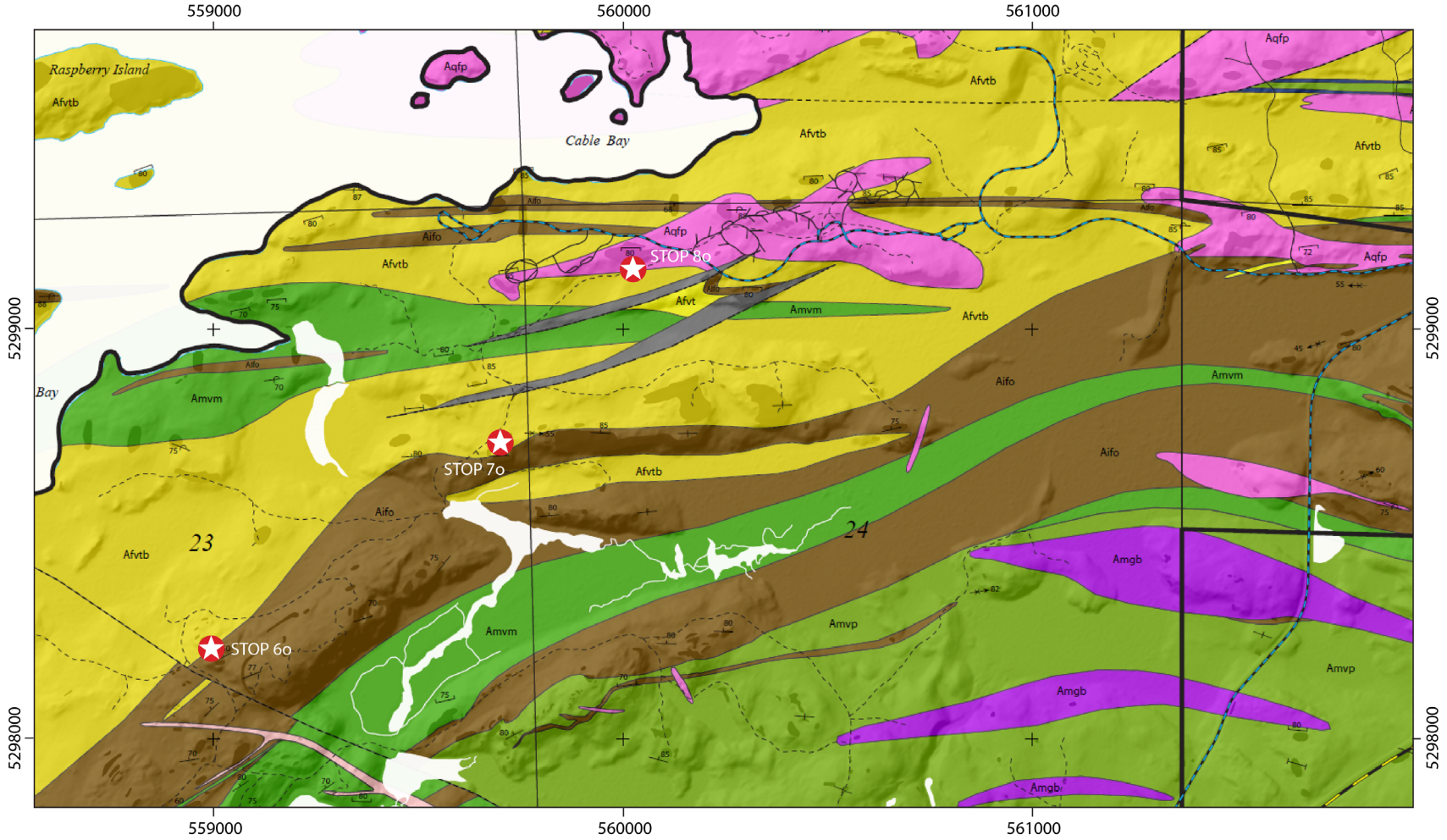


Figure 4-12. Geologic map of the northeastern part of Lake Vermilion/Soudan Underground Mine State Park (after Peterson et al., 2016) illustrating locations of optional field trip stops. See Figure 4-5 for the description of map units.

Stop 6o (Optional)" Contact" Between Soudan Member Banded Iron Formation and Gafvert Lake Sequence Rhyodacite Polymict Lapilli-tuff/Tuff-breccia

Longitude/Latitude: 47.834710°N, -92.211647°E

UTM NAD 83 Zone 15N: 558,995E / 5,298,230N

Here we will see one of the few places where the nature of the contact between the Soudan Iron-Formation Member oxide facies iron-formation and the overlying dacitic to rhyodacitic volcaniclastic rocks associated within the informally named Gafvert Lake Sequence can be observed (Figure 4-13). The Gafvert Lake Sequence (mapped as the "Upper Sequence" by Peterson and Patelke, 2003; Radakovich et al., 2010: and Heim et al., 2011) comprises dacitic to rhyodacitic volcaniclastic and epiclastic rocks that are locally interbedded with Algoma-type banded iron-formation and chert deposits. This sequence is part of the Lake Vermilion Formation. Within Lake Vermilion State Park, the overall stratigraphic thickness of the Gafvert Lake Sequence is up to approximately 1300 meters thick, with individual felsic volcaniclastic deposits having stratigraphic thicknesses ranging from approximately 75 – 400 meters thick, and individual Algoma-type oxide facies banded iron formations and associated massive- to bedded chert deposits ranging from 25-250 meters and up to 175 meters in stratigraphic thickness, respectively. Northwest of the Soudan Mine, the Gafvert Lake Sequence is locally interlayered with, and overlain by, greywacke deposits associated with the Lake Vermilion Formation.

Within Lake Vermilion State Park, several lithofacies comprise the Gafvert Lake Sequence. The basal member of this sequence comprises massive, very-thickly bedded, quartz- and plagioclase-phyric polymict dacitic to rhyodacitic tuff, lapilli-tuff, and tuff-breccia deposits. These light gray, non-sorted, non-graded, matrix-supported deposits contain 3-8% 1-2mm (rare 3mm) pale gray anhedral to subhedral quartz phenocrysts, 10-15% <1-2mm subhedral to euhedral tabular plagioclase phenocrysts, and a wide variety of lapilli- to block-sized clasts including: 1) 10-20% 1-10 cm quartz- and plagioclase-phyric coherent dacite to rhyodacite lapilli and blocks; 2) 5-7% $\leq$3cm diameter pale gray-green lens-shaped, locally quartz- and plagioclase-phyric pumice lapilli; 3) up to 1% dark gray to light gray angular chert lapilli ranging from 0.5-3cm in diameter; and 4) 1-3% 0.5-5cm dark gray to black to red magnetite-rich, hematite-rich, or jasper-rich banded iron formation lapilli. These deposits are overlain by, and interbedded with, light gray, matrix-supported, non-sorted and non-graded quartz- and plagioclase-phyric dacitic to rhyodacitic tuff deposits (Figure 4-14) which contain 10-25% 1-3mm subhedral to euhedral tabular plagioclase phenocrysts, 1-3% 1-3mm subhedral to anhedral, commonly broken, quartz phenocrysts, as well as 10-15% subangular quartz- and plagioclase-phyric coherent dacite to rhyodacite lapilli and up to 5% locally quartz- and plagioclase-phyric pumice lapilli. Spectacular felsic epiclastic deposits comprising polymict volcaniclastic conglomerates and lithic sandstones are also present in the Gafvert Lake Sequence and crop out west of Lake Vermilion State Park in Stunz Bay (Radakovich et al., 2010).

Based on regional mapping, Sims and Southwick (1980), Southwick (1993), and Southwick et al. (1998) have suggested that the contact between the underlying Soudan Iron-Formation Member of the Ely Greenstone Formation and the overlying Lake Vermilion Formation is locally an unconformity. Geochronological work in the Vermilion District (Peterson et al., 2001. Lodge et al., 2013), combined with detailed field mapping in the limited number of locations where the contact between the Soudan Iron-Formation Member and the Lake Vermilion Formation occurs, bears out this interpretation. Based on field relationships recognized by Radakovich et al. (2010), Lodge et al. (2013) collected a sample of the basal part of the Gafvert Lake polymict dacite- to rhyodacite lapilli-tuff / tuff-breccia deposits that occur at this outcrop in order to determine the age of volcanism of the Gafvert Lake Sequence relative to the ages of the Lower and Soudan Iron-Formation members of the Ely Greenstone Formation. Zircons from the sample of polymict rhyodacite tuff-breccia from this outcrop approximately 2m north of the contact with the Soudan Iron-Formation Member at this field trip stop produced a high precision U-Pb date of 2689.7 ±0.8 Ma using

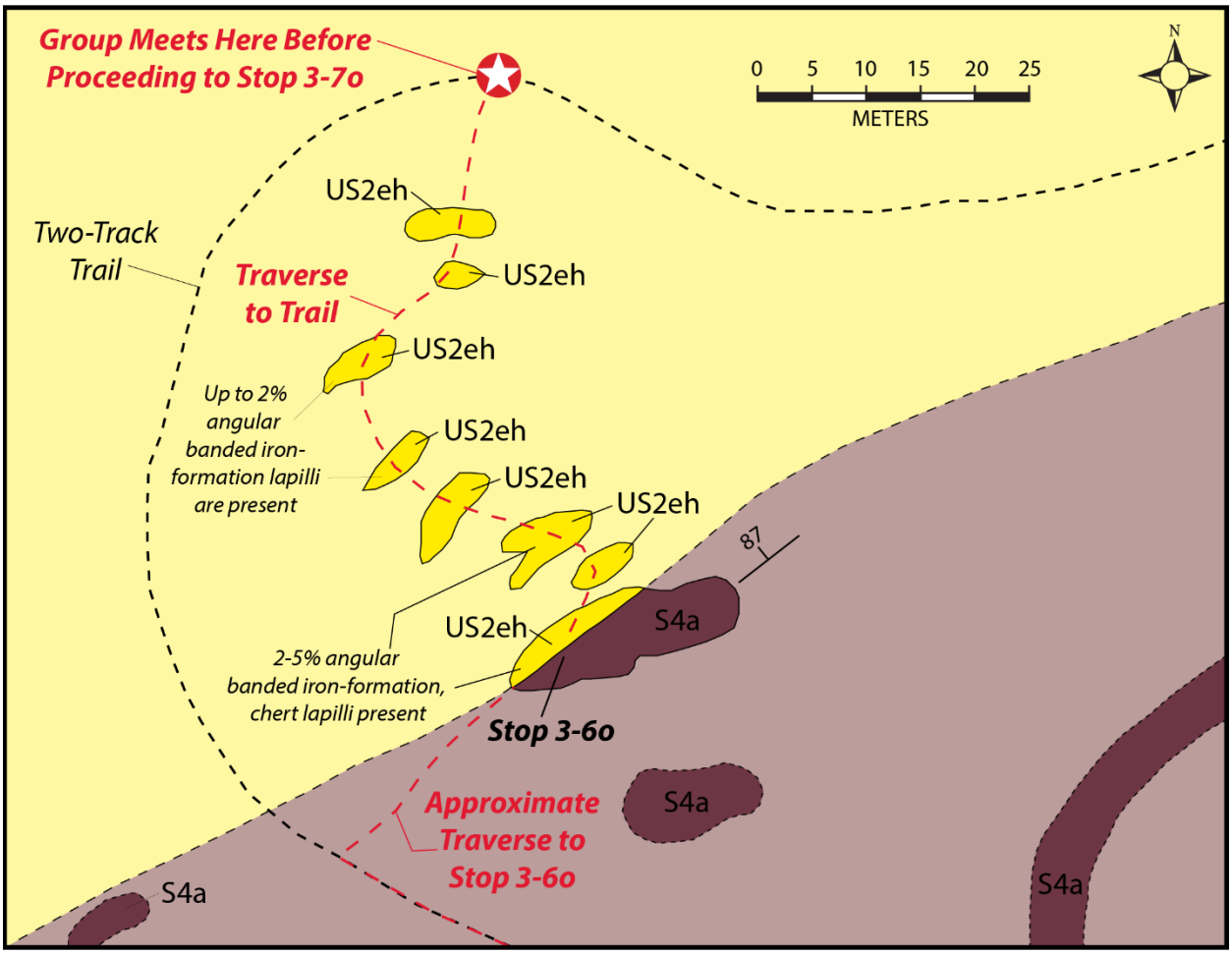


Figure 4-13. Detailed (1:5000 scale) map (after Hudak et al., 2014) illustrating the disconformable contact between the Soudan Member Algoma-type banded iron-formation (unit S4a) and the Gafvert Lake Sequence quartz- and plagioclase-phyric polymict dacite-rhyodacite tuff-breccia / lapilli-tuff deposits (unit US2eh). We will start our investigation where Stop 6o is indicated, and traverse along the bedding and are locally folded. path indicated by the red dashed line over a series of outcrops. We will assemble on the two-track trail where indicated by the star symbol before proceeding to Stop 7o.

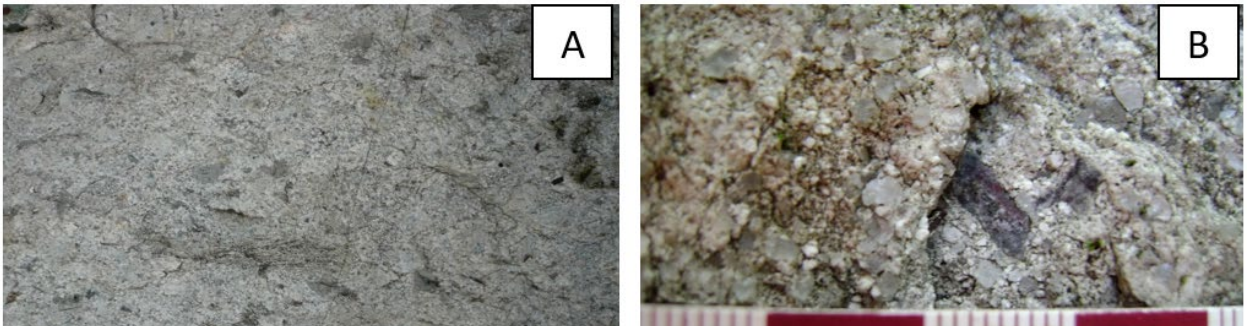


Figure 4-14. Quartz- and plagioclase-phyric polymict dacite-rhyodacite tuff-breccia / lapilli-tuff from the Gafvert Lake Sequence. A) Typical appearance of very thickly bedded quartz- and plagioclase-phyric polymict dacite-rhyodacite lapilli-tuff. B) Close-up of unit illustrating tannish-white subhedral to euhedral tabular plagioclase phenocrysts, gray to gray-blue anhedral quartz phenocrysts, and 1cm diameter angular accidental fragment composed of jasper-rich banded iron formation.

hermal ionization mass spectrometry (Lodge et al., 2013). Given that the basal Gafvert Lake Sequence deposits contain angular intraclasts of chert and banded iron formation, and that there appears to be no intense structural fabric in either the Soudan Iron-Formation Member or the Gafvert Lake volcaniclastic rocks, Lodge et al. (2013) interpreted the contact here to represent a disconformity, a type of unconformity characterized by strata that are essentially parallel on either side of the erosional or non-depositional surface.

Several outcrops occur at this location (refer back to Figure 4-13). The largest part of the outcrop, which extends east up the hill, is composed of laminated to medium bedded Soudan Iron-Formation Member. Alternating magnetite-rich horizons, chert horizons, and jasper horizons display planar bedding and are locally folded. Moving toward the northwest part of this outcrop, we observe a small break in the outcrop exposure. This break occurs directly above the contact between the Soudan Member iron formation (to the south) and the Gafvert Lake volcaniclastic rocks (to the north). In this area, note the lack of deformation in both lithological units. The lack of structural deformation at this contact, as well as geochronological data obtained from the Gafvert Lake volcaniclastic rocks near this contact (Lodge et al., 2013), supports the interpretation of a disconformity.

Moving to the northwest, we observe the basal several meters of the Gafvert Lake Succession volcaniclastic rocks. Here, the rock is composed of a very thickly bedded quartz- and plagioclase-phyric polymict dacite-rhyodacite tuff-breccia / lapilli-tuff. The rock is characterized by up to 5% 1-3mm diameter subhedral to euhedral gray to blue-gray quartz phenocrysts and locally, 5-10% subhedral to euhedral light gray to tan tabular plagioclase phenocrysts set in a fine-grained quartzo-felspathic matrix that is locally sericite altered. Accidental fragments comprising laplli-sized light gray to grayish black angular to subangular chert, gray to dark gray subangular to angular banded iron formation (Figure 4-14), and rare angular to subangular reddish brown jasper fragments are present. As well, juvenile fragments comprising lapilli- to locally block-sized pumice are present. Lapilli- to block-sized accessory fragments of quartz- and plagioclase-phyric coherent dacite and rhyodacite are also present, in abundances up to 5%. As we move northwest then north down the hill, we will traverse several outcrops composed of Gafvert Lake Sequence tuff-breccia and lapilli-tuff deposits.

We will traverse northwest then north down the hill (as shown in Figure 4-13) for about 80 meters back to the Crosscut Trail. We will then head northeast along the Crosscut Trail for approximately 900 meters. We will then traverse southeast through the bush for about 45 meters to Stop 7o.

Stop 7o (Optional): Gafvert Lake Sequence Tuffs and Lapilli -tuffs

Longitude/Latitude: 47.838875°N, -92.202496°E

UTM NAD 83 Zone 15N: 559,675E / 5,298,700N

We will stop here to observe several small outcrops of the Gafvert Lake Sequence tuffs and lapilli-tuffs. These deposits comprise very thickly bedded, light gray, quartz- and plagioclase-phyric dacitic to rhyodacitic tuffs and lapilli-tuffs. The light gray recrystallized matrix generally contains 10-15% <1-2mm subhedral to euhedral tabular plagioclase phenocrysts which locally appear to be broken, as well as 3-8% <1-2mm pale gray anhedral, locally broken, anhedral to subhedral quartz phenocrysts. Various types of lapilli may be observed, including: 1) 10-20% 1-3cm diameter quartz- and plagioclase-phyric coherent dacite to rhyodacite lapilli; 2) 5-7% ≤3cm diameter pale gray green, lens-shaped, locally quartz- and plagioclase-phyric pumice lapilli; 3) ≤1mm dark gray to light gray angular chert lapilli ranging from 0.5-3cm in diameter; and 4) 1-3% 0.5-5cm dark gray to black magnetite-rich banded iron formation lapilli.

We will traverse northwest for about 45 meters back to the Crosscut Trail. We will then proceed northeast along the Crosscut Trail for approximately 750 meters, then turn north for about 35 meters to Stop 8o.

Stop 8o (Optional): Quartz- ± Plagioclase-phyric Rhyodacite Sill (informally named the Gafvert Lake Intrusive Complex)

Longitude/Latitude: 47.843117°N, -92.197887°E

UTM NAD 83 Zone 15N: 560,015E / 5,299,175N

At this location we will observe a spectacular light gray, massive, quartz- ± plagioclase-phyric coherent rhyodacite which, based on regional mapping (Peterson and Jirsa, 1999; Peterson, 2001; Hudak et al., 2002b; Heim et al., 2011) comprises a sill-dike complex that extends from the northern extents of Lake Vermilion State Park over 20km eastward to Mitchell Lake. This intrusion is most prevalent in the vicinity of Gafvert Lake, where it comprises several sills and dikes that intrude into the thickest section of Gafvert Lake Sequence volcaniclastic rocks. Based on the distribution of sills and dikes, coherent-facies Gafvert Lake Sequence deposits, and an abundance of coarse polymict breccias in this region, Peterson (2001) has interpreted this area to be the remnants of a stratovolcano that produced the Gafvert Lake Sequence dacitic to rhyodacitic volcaniclastic rocks. For this reason, this unique quartz-feldspar porphyry intrusion has been informally named the Gafvert Lake Intrusive Complex (GLIC). Lithogeochemical work recently completed at the University of Wisconsin Eau Claire (Schwierske et al., 2014; Figure 4-15) indicates that the GLIC and Gafvert Lake volcaniclastic rocks have very similar major, trace and rare earth element characteristics suggesting that they may be genetically related. However, geochronological studies will need to be performed to determine unambiguously if the GLIC and Gafvert Lake volcaniclastic rocks are indeed genetically related.

The GLIC comprises light gray, massive, quartz ± plagioclase-phyric coherent rhyodacite. The light gray aphanitic groundmass contains 3-7% gray to light blue subhedral rounded to euhedral square quartz phenocrysts that range from 3-10mm in diameter, and 2-10% pale gray to tan, subhedral to euhedral tabular plagioclase phenocrysts ranging from 1-4mm in length. A variety of xenoliths may be found in this intrusion, including: 1) brown mudstone lapilli; 2) green to gray-green massive and/or amygdaloidal basalt lapilli; and 3) light gray aphyric coherent rhyodacite lapilli. In the field, the presence of large 5mm-10mm diameter gray to blue gray quartz phenocrysts distinguishes the GLIC from other quartz-feldspar-porphyry intrusions in the Vermilion District.

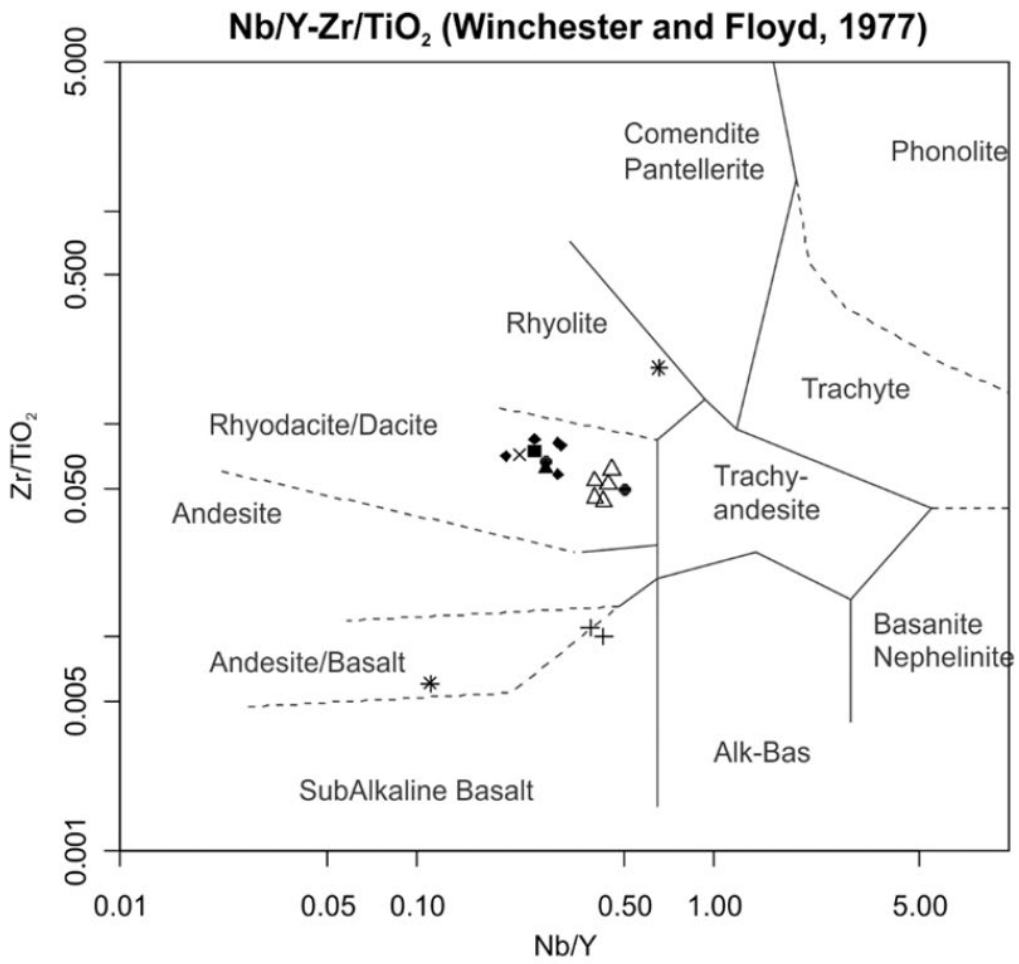


Figure 4-15. Chemical classification of various lithologies within Lake Vermilion State Park (Schwierske et al., 2014) using the immobile element classification scheme of Winchester and Floyd (1977). Open triangles represent samples from a quartz- ± plagioclase-phyric rhyodacite/dacite sill in the northeastern part of Lake Vermilion State Park. The black squares, large black diamonds, and small black diamonds represent various Gafvert Lake Succession volcaniclastic and epiclastic rock units.

We will return to the Crosscut Trail and proceed northeast on the trail back to the vehicles.

Upon loading the vehicles, we will return to the Mountain Iron Community Center. Travel east on Vermilion Ridge Road for approximately 0.5 miles to the intersection with Old Highway 169. Turn right (south) and continue east on Old Highway 169 for 0.8 miles. Turn south at the intersection with Vermilion Park Drive and proceed south for 2.9 miles to the intersection with Hwy 1/169. Turn west and Hwy 1/169 and drive for about 25.4 miles and merge onto Hwy 53/169 South. Follow Hwy 1/169 the intersection with Hwy 53/Hwy 169. Merge on to Hwy 169 south and proceed for 1.5 miles to Emerald Avenue. Turn south and proceed on Emerald Avenue for approximately 0.1 mile. Turn east and proceed for approximately 0.2 miles back to the Mountain Iron Community Center.

END OF FIELD TRIP

Acknowledgements

The authors would like to thank Jim Essig (Manager, Lake Vermilion/Soudan Underground Mine State Park), James Pointer (former Interpretive Supervisor, Lake Vermilion/Soudan Underground Mine State Park), and Jim DeVries (Assistant Manager, Lake Vermilion/Soudan Underground Mine State Park) for their assistance over the past two decades while the authors have conducted research, teaching, and numerous field trips within the park.

References

Allerton, Z., in prep., Thermal and Hydrothermal Effects of Proterozoic Events in the Archean Terrain of Northeastern Minnesota: unpublished Ph. D. dissertation, University of Minnesota Twin Cities.

Allerton, Z., Hudak, G., Teyssier, C., Fayon, A., Daniŝik, M., Courtney-Davies, L, and Larson, P., 2024b, Geochronology campaign in northeastern Minnesota: Institute on Lake Superior Geology, Proceedings Volume 70, Part 1 – Program and Abstracts, p. 2-3.

Allerton, Z., Hudak, G., Teyssier, C., Fayon, A., Daniŝik, M., Courtney-Davies, L, and Larson, P., 2024b, Geochronology and geochemistry of hematite ore in northeastern Minnesota: Institute on Lake Superior Geology, Proceedings Volume 70, Part 1 – Program and Abstracts, p. 4-5.

Allerton, Z. P., Courtney-Davies, L., Daniŝik, M., Hudak, G. J., Teyssier, C., Mitchell, J. T., and Larson, P., in review, Hematite double-dating defines Proterozoic mineralization and thermal history of Archean banded iron formations, NE Minnesota, USA: submitted to *Geology*.

Ayer, J. A., Goutier, J., Thurston, P. C., Dube, B., and Kamber, B. S., 2010, Tectonic and Metallogenic Evolution of the Abitibi and Wawa subprovinces: Summary of Field Work and Other Activities, 2010, Ontario Geological Survey Open File Report 6260, p. 3-1 – 3.6.

Bakst, B., 2013, Minnesota's Lake Vermilion State Park evolving at a cautious pace: TwinCities.com, Pioneer Press, http://www.twincities.com/localnews/ci_23939683/lake-vermilion-state-park-minnesotas-newest-evolving-at.

Bauer, R. L., 1985, Correlation of early recumbent and younger upright folding across the boundary between an Archean gneiss belt and greenstone terrane, northeastern Minnesota: Geology, v. 13, p. 657-660.

Baumgardner, M., Brown, N., Jacobson, A., Kendall, J., Ostwald, C., Schriner, N., White, J., and Peterson, D., 2013, Bedrock geologic map of the Gafvert Lake area, St. Louis County, northeastern Minnesota: Precambrian Research Center Map Series, PRC/Map-2013-04, 1:10,000 scale.

Boerboom, T. J., 2020, D-07, Geochronology Database: Minnesota Geological Survey – Open Data Site, https://mngs-umn.opendata.arcgis.com/datasets/d7903b83244a4878bcfb31f362bf5787_0/explore?location=46.147285%2C-92.317888%2C7.04.

Boerboom, T. J., and Zartman, R. E., 1993, Geology, geochemistry, and geochronology of the central Giants Range Batholith, northeastern Minnesota: Canadian Journal of Earth Science, v. 30, p. 2510-2522.

Cas, R. A. F., and Wright, J. V., 1987, Volcanic Successions – Modern and Ancient: George Allen and Unwin, London, 528 p.

Corfu, F. and Stott, G. M., 1998, Shebandowan greenstone belt, western Superior Province: U-Pb ages, tectonic implications, and correlations: Geological Society of America Bulletin, v. 110, p. 1467-1484.

Dimroth, E., Cousineau, P., Leduc, M., and Sanschagrin, Y., 1978, Structure and organization of Archean subaqueous basalt flows, Rouyn-Noranda area, Quebec: Canadian Journal of Earth Sciences, v. 15, p. 902-918.

Driese, S. G., Jirsa, M. A, Ren, M., Brantley, S. L., Sheldon, N. D., Parker, D., and Schmitz, M. D., 2011, Neoarchean paleoweathering of tonalite and metabasalt: Implications for reconstructions of 2.69 Ga early terrestrial ecosystems and paleoatmospheric chemistry: Precambrian Research, v. 189, p. 1-17.

Fisher, R. V., 1961, Proposed classification of volcaniclastic sediments and rocks: Geological Society of America Bulletin, v. 72, p. 1409-1414.

Fisher, R. V., 1966, Rocks composed of volcanic fragments and their classification: Earth Science Reviews, v. 1, p. 287-298.

Fisher, R. V., 1998, Out of the Crater: Princeton University Press, 180 p.

Gibson, H. L., Morton, R. L., and Hudak, G. J., 1999, Submarine volcanic processes, deposits, and environments favorable for the location of volcanic-associated massive sulfide deposits: Reviews in Economic Geology, v. 8, p. 13-51.

Gruner, J. W., 1926, Hydrothermal alteration of iron ores of the Lake Superior type – a modified theory: Economic Geology, v. 32, p. 121-130.

Heim, N., Scott, H., Kilduff, R., Rahtz, C., Vial, A., Young, S., Mahr, C., and Hudak, G., 2011, Preliminary bedrock geology map of the eastern part of Lake Vermilion State Park, St. Louis County, NE Minnesota: Precambrian Research Center Map Series Map PRC/Map – 2010-01, 1:5000 scale.

Hoffman, A. T., 2007. Lithostratigraphy, Hydrothermal Alteration, and Lithogeochemistry of Neoarchean Rocks in the Lower and Soudan Members of the Ely Greenstone Formation, Vermilion District, NE Minnesota: Implications for Volcanogenic Massive Sulfide Deposits: unpublished M. S. thesis, University of Minnesota – Duluth, 295 p.

Hooper, P., and Ojakangas, R., 1971, Multiple deformation in the Vermilion District, Minnesota: Canadian Journal of Earth Sciences, v. 8, p. 423-434.

Hudak, G. J., Heine, J., Hocker, S. M., and Hauck, S., 2002b, Geological mapping of the Needleboy Lake – Sixmile Lake area, northeastern Minnesota: a summary of volcanogenic massive sulfide potential: Natural Resources Research Institute Report of Investigation NRRI/RI-2002/14, 15 p.

Hudak, G.J., Heine, J., Jirsa, M.A., and Peterson, D.M., 2004, Field Trip 1 - Volcanic stratigraphy, hydrothermal alteration, and VMS potential of the Lower Ely Greenstone, Fivemile Lake to Sixmile Lake area: 50th Annual Meeting, Institute on Lake Superior Geology, Proceedings Volume 50, Part 2 – Field Trip Guidebook, p. 1-45.

Hudak, G. J., Heine, J., Lodge, R. W. D., and Jansen, A., 2012, Recent developments understanding the volcanic, magmatic, tectonic, and metallogenic evolution of the Ely Greenstone Formation, Vermilion District, NE Minnesota: Geological Association of Canada – Mineralogical Association of Canada, Abstracts and Program, v. 35, p. 59.

Hudak, G. J., Heine, J., Newkirk, T., Odette, J., and Hauck, S., 2002a, Comparative geology, stratigraphy, and lithogeochemistry of the Fivemile Lake, Quartz Hill, and Skeleton Lake VMS occurrences, Vermilion district, NE Minnesota: A report to the Minerals Coordinating Committee, DNR, Minerals Division, State of Minnesota: Natural Resources Research Institute Technical Report NRRI/TR-2002/03, 390 pages.

Hudak, G. J., Hoffman, A. T., Peterson, D. M., and Heine, J., 2007, Recent developments understanding the volcanic, magmatic, tectonic, and metallogenic evolution of the Ely Greenstone Formation, Vermilion District, NE Minnesota: 53rd Annual Meeting, Institute on Lake Superior Geology, Proceedings Volume 53, Part 1 – Program and Abstracts, p. 42-43.

Hudak, G. J., and Peterson, D. M., 2014, Non-Ferrous Mineralization Associated with the Wawa-Abitibi Terrane and Duluth Complex Cu-Ni-PGM Deposits, Northeastern Minnesota: Society of Economic Geologists, Guidebook Series, v. 47, 150 p.

Hudak, G. J., Peterson, D. M., Radakovich, A, Pignotta, G., Schwierske, K., and the students from the 20120-2013 Precambrian Research Center Field Camp, 2016, Bedrock Geology of Lake Vermilion/Soudan Underground Mine State Park: Natural Resources Research Institute Technical Report NRRI/TR-2016-20, 23 p.

Hudak, G. J., Radakovich, A., Pignotta, G., and Schwierske, K., 2014, Field Trip 2 – A Walk in the Park – Neoarchean Geology of Lake Vermilion State Park: Institute on Lake Superior Geology, Proceedings Volume 60, Part 2 – Field Trip Guidebook, p. 37-75.

Hudleston, P. J., Schultz-Ela, D., and Southwick, D. L., 1988, Transpression in an Archean greenstone belt, northern Minnesota: Canadian Journal of Earth Sciences, v. 25, p. 1060-1068.

Hudleston, P.J., 1976, Early deformational history of Archean rocks in the Vermilion district, north-eastern Minnesota: Canadian Journal of Earth Sciences, v. 13, p. 579-592.

Jansen, A. C., Hudak, G. J., Heine, J. J., and Peterson, D. M., 1999, Lithogeochemical evaluation of Neoarchean mafic volcanic rocks comprising the footwall to the Soudan Member of the Ely Greenstone Formation, northeastern Minnesota: 55th Annual Meeting, Institute on Lake Superior Geology, Proceedings Volume 55, Part 1 – Program and Abstracts, p. 46-47.

Jirsa, M. A., 2000. The Midway sequence: a Timiskaming-type pull-apart basin deposit in the western Wawa Subprovince, Minnesota: Canadian Journal of Earth Sciences, v. 37, p. 1-15.

Jirsa, M.A., 2016, Preliminary geologic maps of Lake and St. Louis counties, northeastern Minnesota: Minnesota Geological Survey Open File Report OFR 16-4, https://conservancy.umn.edu/items/a68ec090-cf02-463a-8fcb-e3c05926d80e.

Jirsa, M. A., Boerboom, T. J., Green, J. C., Miller, J. D., Morey, G. B., Ojakangas, R. W., and Peterson, D. M., 2004, Field Trip 5 – Classic outcrops of northeastern Minnesota: 50th Annual Meeting, Institute on Lake Superior Geology, Proceedings Volume 50, Part 2 – Field Trip Guidebook, p. 129-169.

Jirsa, M., and Hillman, M., 2009, Field Trip 4 – Pioneer Mine (Miners Lake) Canoe Excursion: 55th Annual Meeting, Institute on Lake Superior Geology, Proceedings Volume 55, Part 2 – Field Trip Guidebook, p. 110-115.

Jirsa, M. A., Starns, E. C., and Schmitz, M. D., 2012, Bedrock geologic map of the 2006 Cavity Lake forest fire area, Boundary Waters Canoe Area Wilderness, northeastern Minnesota: Minnesota Geological Survey Miscellaneous Map M-193, 1:24,000 scale.

Jirsa, M.A., Southwick, D.L., and Boerboom, T.J., 1992, Structural evolution of Archean rocks in the western Wawa subprovince, Minnesota: refolding of precleavage nappes during D2 transpression: Canadian Journal of Earth Sciences **29**:2146-2155.

Klinger, F. L., 1960, Geology and ore deposits of the Soudan Mine, St. Louis County, Minnesota: unpublished Ph. D. dissertation, University of Wisconsin, Madison, 96 p.

Larson, P., and Mooers, H., 2009, Field Trip 2 – Glacial geology of the Vermilion Moraine: 55th Annual Meeting, Institute on Lake Superior Geology, Proceedings Volume 55, Part 2 – Field Trip Guidebook, p. 81-99.

Lodge, R.W.D., Gibson, H. L., Stott, G. M., Franklin, J. M., and Hudak, G. J., 2015, Geodynamic setting, crustal architecture, and VMS metallogeny of ca 2720 Ma greenstone belt assemblages of the northern Wawa Subprovince, Superior Province, Canadian Journal of Earth Sciences, v. 52, p. 196 – 214.

Lodge, R. W. D., Gibson, H. L., Stott, G. M., Hudak, G. J., Jirsa, M. A., and Hamilton, M. A., 2013, New U-Pb geochronology from the Timiskaming-type assemblages in the Shebandowan and Vermilion greenstone belts, Wawa Subprovince, Superior Craton: Implications for the Neoarchean development of the southwestern Superior Province: Precambrian Research, v. 235, p. 264-277.

Lundy, J. R., 1985, Clues to structural history in the minor folds of the Soudan Iron Formation, northeastern Minnesota: Unpublished M. S. thesis, University of Minnesota, Minneapolis, 144 p.

McPhie, J., Doyle, M., and Allen, R., 1993, Volcanic Textures: A Guide to the Interpretation of Textures in Volcanic Rocks: CODES Key Centre, University of Tasmania, Hobart, Tasmania, 198 p.

Mercier-Langevin, P., Hannington, M. D., Dubé, B., and Bécu, V., 2010, The gold content of volcanogenic massive sulfide deposits: Mineralium Deposita, v. 46, p. 509-539.

Mueller, W. U., and White, J. D. L., 2004, 4.2 – Terminology of Volcanic and Volcaniclastic Rocks: *in* Eriksson, P. G., Altermann, W., Nelson, D. R., Mueller, W. U., and Catuneanu, O., (eds.), The Precambrian Earth: Tempos and Events: Developments in Precambrian Geology, v. 12, Elsevier, Amsterdam, p. 273-277.

Newkirk, T., Hudak, G. J., and Hauck, S. A., 2001, Preliminary lava flow morphology studies at the Five Mile Lake VMS prospect, Vermilion District, NE Minnesota: Implications for volcanic processes, volcanic paleoenvironments, and VMS exploration [abstract/poster]: Geological Society of America Abstracts and Programs V. 33, No. 6.

Peterson, D. M., 2001, Development of Archean lode-gold and massive sulfide deposit exploration models using geographic information system applications: targeting mineral exploration in northeastern Minnesota from analysis of analog Canadian mining camps: unpublished Ph. D. dissertation, University of Minnesota, Duluth, Minnesota, 503 p.

Peterson, D. M., Gallup, C., Jirsa, M. A., and Davis, D. W., 2001, Correlation of Archean assemblages across the U.S.- Canadian border: Phase I geochronology: 47th Annual Meeting, Institute on Lake Superior Geology, Proceedings Volume 47, Part 1 – Programs and Abstracts, p. 77-78.

Peterson, D.M., Hudak, G.J., Radakovich, A., Pignotta, G., and Schwierske, K., 2016, Geologic Map of Lake Vermilion/Soudan Underground Mine State Park: Precambrian Research Center Map PRC/Map-2016-01, 1:10,000 scale.

Peterson, D. M., and Jirsa, M.A., 1999, Bedrock geologic map and mineral exploration data, western Vermilion district, St. Louis and Lake Counties, northeastern Minnesota: MGS Miscellaneous Map M-98, scale 1:48,000.

Peterson, D., Jirsa, M., and Hudak, G., 2009a, Field Trip 7 – Architecture of an Archean Greenstone Belt: Stratigraphy, Structure, Mineralization: 55th Annual Meeting, Institute on Lake Superior Geology, Proceedings Volume 55, Part 2 – Field Trip Guidebook, p. 178-215.

Peterson, D. M., and Patelke, R. L., 2003, National Underground Science and Engineering Laboratory (NUSEL): Geological site investigation for the Soudan Mine, northeastern Minnesota: Natural Resources Research Institute Technical Report NRRI/TR-2003/29, 88 p.a

Peterson, D. M., and Patelke, R. L., 2004, Field Trip 7 – Economic geology of Archean gold occurrences in the Vermilion District, northeast of Soudan, Minnesota: 50th Annual Meeting, Institute on Lake Superior Geology, Proceedings Volume 50, Part 2 – Field Trip Guidebook, p. 200-226.

Peterson, D. M., Pointer, J., and Marshak, M., 2009b, Field Trip 3 – Soudan Iron Mine and Physics Lab Tour: 55th Annual Meeting, Institute on Lake Superior Geology, Proceedings Volume 55, Part 2 – Field Trip Guidebook, p. 100-109.

Radakovich, A. L., Parent, C. T., Partridge, M. E., Ritts, A. D., Pierce, R., and Hudak, G. J., 2010, Reconnaissance bedrock geological map of the northern part of Soudan Underground Mine State Park and the northwestern part of Lake Vermilion State Park, St. Louis County, Minnesota: Precambrian Research Center Map Series Map PRC/Map – 2010-04, 1:5000 scale.

Schmid, R., 1981, Descriptive nomenclature and classification of pyroclastic deposits and fragments; recommendations of the IUGS subcommission on the systematics of igneous rocks: Geology, v. 9, p. 41-43.

Schwierske, K.L., Pignotta, G. S., and Hudak, G. J., 2014, The 2.7 billion year old Mt. St. Helens of northern Minnesota: Petrography, geochemistry, and economic significance of the Neoarchean Gafvert Lake Sequence: 60th Annual Meeting, Institute on Lake Superior Geology, Proceedings Volume 60, Part 1 – Programs and Abstracts, p. 113-114.

Sims, P. K., and Southwick, D. L., 1985, Geologic map of Archean rocks, western Vermilion district, northern Minnesota: U. S. Geological Survey, Miscellaneous Investigations Map I-1527, scale 1:48,000.

Southwick, D. L., (compiler), 1993, Bedrock geologic map of the Soudan-Bigfork area, northern Minnesota: Minnesota Geological Survey, Miscellaneous Map M-79, scale 1:100,000.

Southwick, D. L., Boerboom, T. J., and Jirsa, M. A., 1998, Geologic setting and descriptive geochemistry of Archean supracrustal and hypabyssal rocks, Soudan-Bigfork area, northern Minnesota: implications for metallic mineral exploration: Minnesota Geological Survey, Report of Investigations 51, 69 p.

Stott, G., Corkery, T., Leclair, A., Boily, M., and Percival, J., 2007, A revised terrane map for the Superior Province as interpreted from Aeromagnetic Data: 53rd Annual Meeting, Institute on Lake Superior Geology, Proceedings Volume 53, Part 1 – Program and Abstracts, p. 74-76.

Stott, G. and Mueller, W., 2009, Superior Province: The nature and evolution of the Archean continental lithosphere: Precambrian Research, v. 168, p. 1-3.

Thompson, A., 2015, A Hydrothermal Model for Metasomatism, of Neoarchean Algoma-Type Banded Iron Formation to Massive Hematite Ore at the Soudan Mine, NE Minnesota: unpublished M. S. Thesis, University of Minnesota Duluth, 59 p.

Vallowe, A. M., Thalhamer, E. J., Rhoades, D. L., and Peterson, D. M., 2010, Surface and subsurface geologic maps of the Soudan Underground Mine State Park, St. Louis County, northeastern, Minnesota: Precambrian Research Center Map Series Map PRC/Map – 2010-01, 1:2500 and 1:5000 scale.

White, J. D. L., and Houghton, B. F., 2006, Primary volcaniclastic rocks: Geology, v. 34, no. 8, p. 677-680.

Winchester, J. A., and Floyd, P. A., 1977, Geochemical discrimination of different magma series and the differentiation products using immobile elements: Chemical Geology, v. 20, p. 325-343.

FIELD TRIP 5

Neoarchean Alkalic Intrusions in the Wawa and Quetico Subprovinces

Terry Boerboom (retired)[1] and Amy Radakovich[1]

[1] *Minnesota Geological Survey, College of Science and Engineering, University of Minnesota, 2609 Territorial Road, St. Paul, MN 55114*

This field trip will visit several alkalic intrusions that have been mapped from a combination of outcrop, drilling, and geophysical data. Refer to Figure 5-1 for the pluton names and generalized regional geology. The stop descriptions are very brief, but a more thorough description of each pluton (as well as others not visited on this trip) are contained in the introductory text.

These plutons were emplaced mainly into the Lake Vermilion Formation which is composed of volcanogenic sedimentary rocks sourced from Gafvert Lk rhyodacite tuff (2689.7±0.8 Ma) and also likely from felsic tuffs at the south limb of the Britt structure (2689.6±0.5 Ma). The **Linden pluton** has an age of 2681.00±0.29 Ma, and the **Lost Lake pluton** an age of 2675.1±0.5 (Boerboom et al., 2022). These ages are slightly older than the large Shannon Lake granite (2674±5 and 2674±27; Boerboom and Zartman 1993), and straddle two ages obtained on the Britt granodiorite (2681±4 and 2685±4 Ma; Boerboom and Zartman 1993). The **Idington pluton** is intruded by the Shannon Lake granite, consistent with the aforementioned age dates. The suite of alkalic plutons we will visit are located mainly in the Wawa subprovince but one (Gheen) is in the Quetico subprovince and will include the **Side Lake, Morcom, Linden, Gheen, Idington, and Lost Lake** plutons (Figure 5-1). All of these intrusions are similar in mineralogy with varied ratios of perthitic to antiperthitic feldspar and Na-plagioclase, hence are divided into those that are more syenitic vs. monzodioritic. All contain Na-rich aegirine/aegirine-augite with variable proportions of primary and secondary-deuteric hornblende, titanite, biotite, and minor oxides and apatite. Textures vary from uniformly medium-coarse grained to strongly and coarsely porphyritic, and they typically exhibit a flow-foliation defined by feldspar and subprismatic pyroxene and/or hornblende. All except the Linden are multi-phase with variations from ultramafic pyroxenite/hornblendite to intermediate syenite/monzodiorite, with relatively minor late-phase felsic phases; where multi-phase they generally show complex and conflicting intrusive relationships between the various phases.

The following discussion, modified from Minnesota Geological Survey Report of Investigations 43 (Boerboom, 1994), covers the plutons we will visit as well as others that we will not visit. Note that some of the ideas presented in this report may have been modified or discredited based on newer geochronological data.

ALKALIC PLUTONS OF NORTHEASTERN MINNESOTA

Minnesota Geological Survey Report of Investigations 43

By

T. Boerboom

ABSTRACT

A series of alkalic plutons in northeastern Minnesota intrude metamorphosed sedimentary and volcanic rocks in the Wawa and Quetico subprovinces of the Archean Superior Province. The plutons generally fall into one of three categories-a syenitic clan, a monzodioritic clan, and a granitic clan. The main rock phases of the syenitic and monzodioritic clans are strongly porphyritic, coarse-grained, green and pink, quartz-poor syenite and diorite. Na-rich pyroxene is the predominant mafic mineral in these intrusions, and titanite is prominent in hand sample. Some of the syenitic intrusions contain melanite garnet, and at least one contains the feldspathoids nepheline and cancrinite. The granitic intrusions consist of variably porphyritic, coarse-grained, pink granite and monzonite, with hornblende as the dominant mafic mineral. Whereas these granitic plutons tend to be uniform in texture and composition, the syenite and monzodiorite plutons are characterized by abrupt internal variations in rock type ranging from dark-colored pyroxenite to light-pink leucocratic granite, syenite, and trondhjemite.

The alkalic plutons range in size from 1.5 to 60 mi^2 (3.9 – 155 km^2) are oval to amoeboid in shape and elongate to the northeast, and are eroded to middle and upper levels. All of the alkalic plutons produce positive aeromagnetic anomalies; outcrops, although limited, confirm that these anomalies reflect the shapes of the plutons. Several unexposed plutons, whose shapes are inferred from aeromagnetic data, have been verified by test drilling. Field relationships show that these plutons are post-tectonic.

Although chemical data are not available for all of the plutons, those with analyses plot as alkalic in terms of $Na_2O + K_2O$ vs SiO_2, but as mainly calc-alkalic on an AFM diagram. The syenitic and monzodioritic clans are generally neither nepheline-normative to neither quartz- nor nepheline-normative, with the exception of minor leucocratic phases. All are characterized by steep REE patterns and exceptionally high concentrations of Ba and Sr.

INTRODUCTION

Recent mapping in northern and northeastern Minnesota, including the Koochiching-Itasca-Beltrami County area (Jirsa and Boerboom, 1990) and western St. Louis County (Jirsa and others, 1991), has delineated several previously unrecognized subalkalic to alkalic plutons. This report summarizes the lithological and intrusive relationships of several of these alkalic intrusions and briefly summarizes their geochemical characteristics. Some plutons in this group, such as the Snowbank and Kekekabic stocks and the Daisy Bay and Dead River plutons have been previously described (Geldon, 1972; Sims and Mudrey, 1972) and are not included in this report. Others (Coon Lake, Linden, Lost Lake plutons) have been briefly described in the literature (Sims and others, 1970, 1972; Sims and Mudrey, 1972), but are detailed here, as are others which have no published information or were unknown (Fig. 5-1A). Alkalic rock complexes similar to these are well known in Ontario (for example Sage, 1988a, 1988b, 1988c), but few have been described from Minnesota. Several other small alkalic plutons are inferred from aeromagnetic data, but are not exposed or have not been drilled (Jirsa and others, 1991).

Characteristics of the Alkalic Rock Suite

The alkalic intrusions fall into three general categories – a syenitic group comprising the Coon Lake, Linden, Gheen, and Baudette plutons; a monzodioritic group including the Side Lake, Morcom, Idington, and Cook plutons; and a granitoid group containing the Bello Lake, Stingy Lake, and Rice River plutons (Fig. 5-1). Although most classify into one of the three clans, the many phases in each pluton (Table 5-1) produce considerable overlap. The syenitic and monzodioritic intrusions consist mainly of medium- to coarse-grained, porphyritic, pink and green syenite and monzodiorite, whereas the granitoid intrusions are typically medium-grained, variably porphyritic, pink quartz monzonite or granodiorite. The syenite and especially the monzodiorite plutons contain multiple erratic melanocratic to felsic phases with aegirine-augite as the predominant mafic mineral, whereas the granitoid plutons generally lack multiple phases, are more uniform in texture, and contain mainly hornblende as the mafic phase.

Most of the alkalic plutons intrude metamorphosed volcanic and sedimentary rocks in the western Wawa subprovince, but some are within the Quetico subprovince (Card and Ciesielski, 1986; Fig. 5-1A). All were emplaced in the latest stages of the last major regional deformational event (Jirsa and others, 1992) or after it. Several of the alkalic plutons are cut by northwest-trending Late Proterozoic diabase dikes of the Kenora-Kabetogama swarm, which have been dated al 2,125 Ma (Rb-Sr; Beck, 1988) *[NOTE: more recent U-Pb geochron ages of ca. 2067 -2070 Ma (Chamberlain and others, 2015; Schmitz and others 2006; Wirth and others , 1995)*. The plutons are exposed at various levels, and many, such as the Gheen, Side Lake, and Lost Lake, are exposed close to their roof zones. All of the alkalic plutons produce positive aeromagnetic anomalies which generally conform to the pluton shape (Fig. 5-1B).

The major-element geochemistry of the alkalic plutonic rocks varies greatly as a result of their diverse mineralogy. However, except for minor proportions of felsic differentiates, they are low in SiO2 (49-62 wt. % for syenites, 47 to 58 wt. % for monzodiorites, 61-70 wt. % for granites; Table 5-2), and are mostly metaluminous to weakly peralkalic in composition (Fig. 5-2). The syenitic and monzodioritic rocks are generally quartz-free to nepheline-normative, whereas the granite from the Bello Lake pluton is mostly quartz-normative (Fig. 5-3). Except for one of the granites and a leucocratic differentiate of the Idington pluton, all plot as alkalic in terms of Na20 + K20 vs Si02, but as calc-alkalic to weakly alkalic on an AFM diagram. In all the plutons, Ba and Sr are in general highly enriched, but vary between the different phases. However, the Coon Lake pluton although slightly enriched, is surprisingly low in Ba and Sr, considering its extremely alkalic composition. The Linden pluton is extremely enriched in Ba and Sr, with Ba values of up to 13,000 ppm and Sr values up to 8,100 ppm reported from company drill cores. Chondrite-normalized REE patterns for the syenites and monzodiorites are fairly consistent, with moderately steep slopes and negligible Eu anomalies *(Fig. 5-6)*. No REE data are available for any of the granitoid plutons.

Table 5-1 (next page). Modal analyses of alkalic plutonic rocks; results in volume percent. Linden analyses from Sims and others (1972, p. 161); samples with KIB and CD prefixes from drill cores, all others from outcrops. Pyroxene includes aegirine to augite; *n,* points counted; est, estimate

	Bello Lake			Coon Lake		Gheen		Idington				Linden		
Sample	KIB-7	KIB-39	KIB-40	DL-61	KIB-6	C027	C029	C551X	C552B	C650	C561A	Gnw7A	Msw2A	Gnw7-2
Quartz	20		3			tr			41		2	tr		
K-feldspar	43	32	46	50	79	8	61	26	3	tr	3	77.6	56.2	37.1
Plagioclase	32	53	40	9	tr	21	7	29	55	32	88	1.9	5.6	0.4
Pyroxene		8		5	2	12		31		49		16.8	25.9	57.1
Hornblende	2	1	8			46	19			8	6			
Biotite	1	1	tr	tr		7		5		7			4.1	0.4
Muscovite					tr									
Chlorite	tr	1	tr			4		4		tr				
Epidote	tr		tr							tr				
Apatite	tr	tr	tr	tr	tr	1	2	2		2	1	0.8	1.1	2.7
Sphene		1	tr	tr	tr	1	3	2		2		2.9	3.7	2.3
Opaques	2	3	3	tr		tr	2			tr	1		3.4	
Calcite, Fl*				tr	tr	tr	5		2 Fl*		1			
Nepheline				33	15									
Cancrinite				2	2									
Melanite					2									
n	est	est	est	1143	est	1368	1114	989	1157	999	946			

	Linden	L-Sat	Side Lake		Side Lake satellites					Morcom		Stingy	Rice R.	Cook
Sample	Gnw-7B	CD-4	1242	C706B	C533A	C534A	C543A	C564A	C603A	CD-7**	CD-7	CD-9	CD-17	CD-19
Quartz												26	13	
K-feldspar	56.3	28	31	tr	13	2	28	1	29	7	20	22	30	
Plagioclase	0.9	52	30	65	47	33	55	44	20	54	55	47	43	67
Pyroxene	27.1	16	17	22		26		30	47	21	5			
Hypersthene			14	8										
Hornblende		2			34	16	9	3		8	8	3	6	
Biotite	9		7	4	1		3	20	1	7	10		1	
Muscovite														
Chlorite					1	14	3		1			1	4	
Epidote						5	1			1		1	2	183
Apatite	5.2	1	tr	tr	2	2	1	1	0.5					tr
Sphene	1.5	2			2	I	1	1	0.5		1		0.5	tr
Opaques			1						1					tr
Calcite										1			0.5	tr
n		1166	1151	est	976	1188	947	1115	1137	988	1152	836	960	est

***** Fluorite in sample C552B; ** Poikilitic and non-poikilitic phases, sample CD-7; **L-Sat** is intrusion beween Linden and Gheen

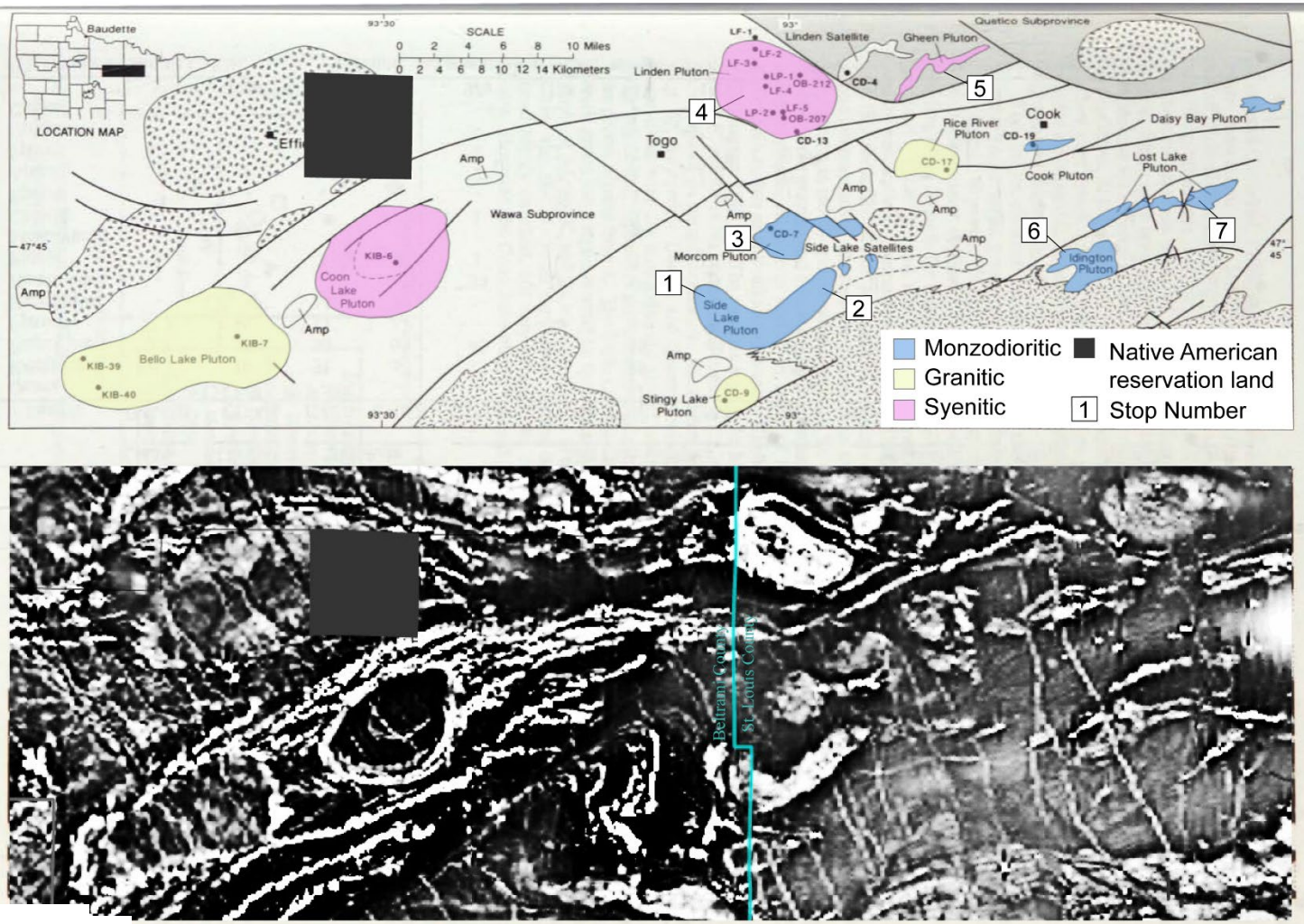


Figure 1-1. ure 1. Geologic and aeromagnetic maps. (A) Simplified geologic map of a part of northern Minnesota (inset), with plutons discussed in this paper named. Heavy black lines, faults. Single-line pattern, Giants Range batholith; double-line pattern, miscellaneous granite plutons not part of the alkalic suite. Dashed lines: In Coon Lake pluton, boundary between weak and strong magnetic anomalies; in Side Lake pluton, boundary of intercalated monzonite and schist linking pluton and satellites; in Idington pluton, extent of Shannon Lake granite intrusion. Amp, alkalic plutons inferred only from aeromagnetic data. (B) Lower image, first vertical derivative shaded-relief aeromagnetic map of same area. Approximate range ± 1,500 nT/km. Modified from RI-43 for 2025 ILSG field trip.

SYENITIC PLUTONS

Most of the syenitic plutons are northwest of the other plutons (Fig. 5-1A). The Gheen and Baudette plutons are within the Quetico subprovince, the Coon Lake pluton is in the Wawa subprovince, and the **Linden pluton** straddles the subprovince border.

These plutons are distinguished by a preponderance of K-rich perthite, typically as trachytic, blocky phenocrysts in an aegirine-rich groundmass, or an amphibole-rich groundmass in the case of the Gheen pluton. The Gheen and Linden plutons contain quartz, chlorite, apatite, epidote, titanite, opaque oxides, and pyrite as ubiquitous but generally minor constituents. The Coon Lake pluton differs from all others in that it contains substantial nepheline and cancrinite; the Baudette pluton lacks both feldspathoids and quartz. Melanite garnet is present in the Coon Lake and Baudette plutons, and in some phases of the Linden. A distinctive phase of spotted monzodiorite with centimeter-size poikilitic feldspar enclosing pyroxene, hornblende, plagioclase, biotite, and sphene is present in both the Linden and Gheen plutons and in plutons of the monzodiorite clan. Although the Gheen and parts of the Linden plutons are texturally similar to rocks of the monzodiorite clan, they differ by having phenocrysts of pink perthite instead of gray antiperthite.

Trachytic fabric in the syenitic intrusions conforms to the pluton edges and dips steeply toward the pluton centers. However, outcrops are generally limited to the pluton borders, and the Baudette and Linden satellite intrusions are seen only in drill core. Aeromagnetic signatures correspond with intrusion shapes, whether it be a consistent oval like the Baudette, Coon Lake, and Linden plutons, or irregular and amoeboid like the Gheen and Linden satellite plutons (Fig. 5-1B).

Coon Lake Pluton

The Coon Lake pluton (Fig. 5-l; Jirsa, 1990; Jirsa and Boerboom, 1990) is a 48-mi^2 subcircular pluton which intrudes mafic to felsic volcanic rocks metamorphosed to greenschist grade. A narrow aureole of amphibolite-grade metamorphism accompanied pluton emplacement. The pluton has a strongly magnetic border and internal lithological zonation is indicated by a circular, weakly positive magnetic anomaly within the pluton. Its north and northeast edges are exposed in scattered outcrops, and a single 10-foot-long vertical drill core was obtained from the pluton center (Boerboom and others, 1989).

The main rock type in the exposed and cored portions of the Coon Lake pluton is pink to gray, medium- to very coarse grained, slightly to strongly porphyritic nepheline syenite, 50-79% microperthite, 15-33% nepheline {Ne_{76-80}) 2-5% aegirine ($Ac_{23}Wo_{18}En_7Fs_{52}$), and as much as 9% plagioclase, 2% cancrinite, and 3% melanite, together with accessory sphene, apatite , biotite, magnetite, muscovite , and zircon (Tables 5-1 and 5-3, Fig. 5-7). Minor proportions of pyroxenite occur in ill-defined dikelets. String- and braid-textured microperthite forms rectangular crystals with minor inclusions of aegirine, sphene, cancrinite, and nepheline. Nepheline is typically anhedral but locally euhedral, up to 2 mm in size, and ranges from fresh to moderately altered to an unknown fibrous mineral of low birefringence. Prismatic, grass- green aegirine formed early in the crystallization sequence and is trachytic. Plagioclase and cancrinite are interstitial, the latter as colorless, highly birefringent fibrous grains. Melanite garnet forms subhedral, dark-brown grains up to 1 cm across with inclusions of aegirine and altered feldspar. In places the syenite consists of trachytic, purplish-brown, rectangular perthite crystals up to 7 cm in length, with minor nepheline, melanite, biotite, and aegirine. A syenite dike that cuts mafic volcanic rocks outboard of the main pluton contains an estimated 1% scolecite and a trace of blue corundum. Netlike anastomosing veinlets of white nepheline parallel to the vertical trachytic fabric of the feldspar in drill core from the center of the pluton imply that a late influx of volatiles affected the magnetic signature of the pluton's interior.

Table 5-2. Major- and select minor-element geochemical analyses of alkalic rocks [Major elements in wt% oxides, minor elements in ppm, blank – nod determined. See Boerboom 1994 for more information.

	Bello Lake			Coon Lake				Gheen			Morcom
Sample	**KIB-7**	**KIB-40**	**KIB-39**	**KIB-6**	**CLP-1**	**I-561A**	**DL-61**	**C029**	**C027**	**12, IC-2**	**CD-7**
SiO2	69.7	63.9	60.2	57.7	62.3	60.3	55.65	56	49.2	49.65	58.5
Al2O3	15.7	17.4	17.2	17.8	18.9	22.4	21.88	14.1	9.52	9.27	l5.4
CaO	1.87	2.16	3.55	5.45	0.33	1.69	1.65	6.48	12.3	13.08	5.01
MgO	0.51	1.28	1.85	0.42	0.35	0.28	1.01	2.55	10.5	8.89	3.58
Na2O	5.67	6.13	6.3	5.75	5.32	7.1	8.12	3.57	1.51	2.38	5.9
K2O	3.51	4.47	4.4	5.8	9.3	4.13	7.28	6.56	2.4	1.71	3.8
Fe2O3t	1.84	3.32	3.94	2.71	2.18	2.54	3.67	6.19	10.2	11.76	5.22
FeO	0.4	1	1	0.3	1.6	1.7	6.08	3.2			
Fe2O3c	1.4	2.21	2.83	2.38	0.76	1.78	5	1.66			
MnO	0.04	0.07	0.08	0.07	0.05	175 ppm	0.08	0.12	0.16	0.56	0.1
TiO2	0.2	0.35	0.42	0.26	0.18	0.19	0.44	0.71	0.88	0.89	0.48
P2O5	0.09	0.18	0.32	0.11	0.02	<10 ppm	0.08	1.03	0.33	0.06	0.29
LOI	0.7	0.77	1	2.77	0.85	1.31	0.37	1.85	2.39	1.99	1.08
Total	100.2	100.4	99.8	99.6	100.1	100.1	100.38	99.9	99.5	99.93	99.7
Rb	165	135	129	100	246	132	100	120	60	79	
Sr	1210	1340	2180	3700	1300	806	926	2520	290	1470	
Y	<10	41	17	81	<10	10	2	47	14	<10	
Zr	90	303	253	64	118	404	119	331	84		
Nb	<10	14	14	15	24	27		24	13		
Ba	1340	1470	1970	2530	676	500	215	3710	697		
Ni					8	<l	7	78	94		
Cu				11.2	8.7	9.8	16	5.5	40.8		
Zn				8.18	70.3	46.3	30	84.5	80.1	Cs	
Cs					9	3	4.5	1	2		
La					17.5	79.3	27	130	20.8		
Ce					33	130	58	328	46		
Pr						12.8					
Nd					11	39.7	33	186	24		
Sm					1.7	5.5	5.1	34.7	5.7		
Eu					0.4	1.45	1.21	9.3	1.9		
Gd						3.9					
Tb					<0.5	0.5	0.4	2.3	0.7		
Dy						2.6					
Ho						0.49					
Er						1.4					
Tm						0.5					
Yb					0.2	1.4	0.65	2.3	1.7		
Lu					<0.1	0.19	0.1	0.2	0.2		
Hf					4	9	4	8	3		
V					20	45					
Cr	22	26	36	<10	10	29	11	67	630		
Li					18	74	39	<10	<10		
B					30	41	<10	<10	<10		
F						160	850				

	Idington					Linden		L'ndn Sat	Side Lk-Sat	Side Lake		Cook
Sample	**C552B**	**10, IC2-**	**11, IC-2**	**C650A**	**C551X**	**8, IC-2**	**MN-10**	**CD-4-92**	**C564A**	**1242**	**C706B**	**CD-19**
SiO2	74.5	47.27	50.27	48.3	54	60.21	57.1	62.2	52.2	55.2	53.5	53.6
Al2O3	14.8	6.99	7.61	7.24	13.1	16.28	10.2	15	11.7	14.6	15.4	17.7
CaO	0.08	20.49	13.87	16.6	8.16	4.76	10.1	4.09	9.89	7.38	7.68	7.59
MgO	0.09	9.18	7.92	9.58	4.56	2.21	4.43	1.62	7.08	6.89	6.25	3.26
Na2O	8.8	1.91	2.41	2.12	4.24	3.78	2.64	6.57	4.04	3.42	3.79	5.4
K2O	1.08	0.89	3.63	1.23	3.86	6.32	6.52	4.73	2.22	2.95	2.21	1.79
Fe2O3t	0.51	9.15	10.68	IO.IO	7.05	4.29	6.51	3.98	10.3	7.93	8.37	7.07
FeO		5.44	7.04	6	3.3	1.62	2.83	1.4			5.7	2.6
Fe2O3c		3.1	2.86	3.43	3.38	2.49	3.36	2.42			2.04	4.18
MnO	0.03	0.3	0.2	0.19	0.13	0.08	0.15	0.09	0.19	0.14	0.15	0.13
TiO2	0.03	0.67	1.51	1	0.96	0.56	0.64	0.48	0.81	0.77	0.76	0.71
P2O5	0.02	1.62	1.46	1.25	0.75	0.23	1.07	0.24	0.45	0.39	0.39	0.36
LOI	0.16	1.33	0.84	0.77	1.23	0.73		0.54	1.08	0.23	0.47	1.54
Total	100.1	99.28	99.91	98.6	98.5	99.76	99.1	99.9	100.2	100.2	99.3	99.5
Rb	97			59	57		164	94	67	60	31	39
Sr	43			772	1770		2924	510	1080	1030	1190	1950
y	<10			37	26			10	<10	20	20	<10
Zr	36			262	181			246	102	30	82	110
Nb	30			15	9			14	21	10	2	15
Ba	81			817	1830		3574	2290	985	1220	1530	882
Ni	<1			76	64				57		61	
Cu	1.5			185	54.9				108		20.4	
Zn	28.6			125	120				128		108	
Cs	7			9	1				2		1	
La	5.9			164	134				50.6		43.2	
Ce	10			348	278		406		101		88	
Pr				41.4	30.8						11.3	
Nd	<5			171	124		183		46		48.8	
Sm	0.2			27.9	19.2		28.1		8.9		9.3	
Eu	0.2			6.99	5.14		6.62		2.4		2.81	
Gd				18.2	11.8		16.6				6.4	
Tb	<0.5			2	1.3				0.6		0.8	
Dy				8.8	6.4						4.1	
Ho				1.46	1.01						0.73	
Er				3.2	1.9						1.8	
Tm				0.3	0.2						0.2	
Yb	<0.2			2.6	1.6		1.53		1.4		1.6	
Lu	<0.1			0.32	0.22		0.262		0.2		0.23	
Hf	2			7.6	5				4		2.2	
V	<10			256	148				210		208	
Cr	4			140	120				80		180	
Li	<10			231	76				84		26	
B	20			14	14				<10		<10	
F				2900	1400						680	

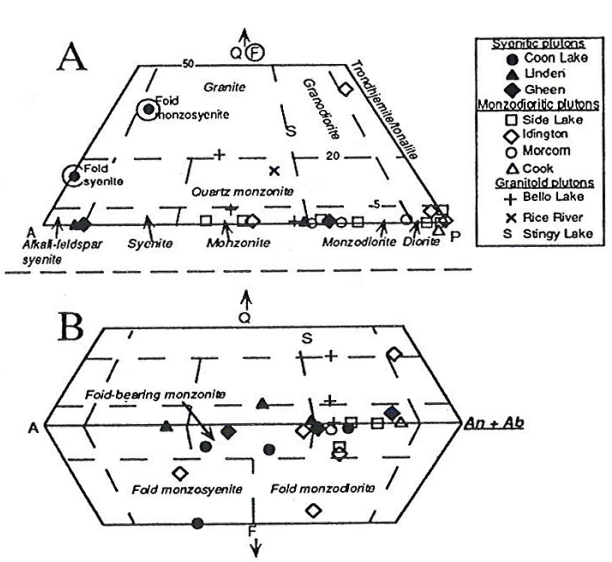


Figure 5-3. Modal (A) and normative (B) compositions of the alkalic plutonic rocks. Compositional fields from Streckeisen (1973), except "P" corner, which consists of albite and anorthite, used here to emphasize variations in K content. Q, quartz; F, feldspathoids; A, alkali feldspars; P, plagioclase. Circled symbols are feldspathoidal, not quartz.

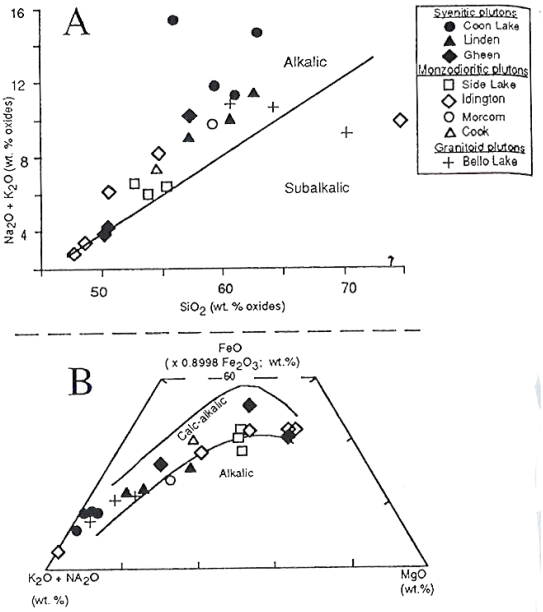


Figure 5-4. Geochemical discrimination diagrams. (A) Alkalic versus subalkalic discrimination diagram; modified from Irvine and Baragar (1971). (B) AFM diagram for the alkalic plutonic rocks; modified from Barker and Arth (1976).

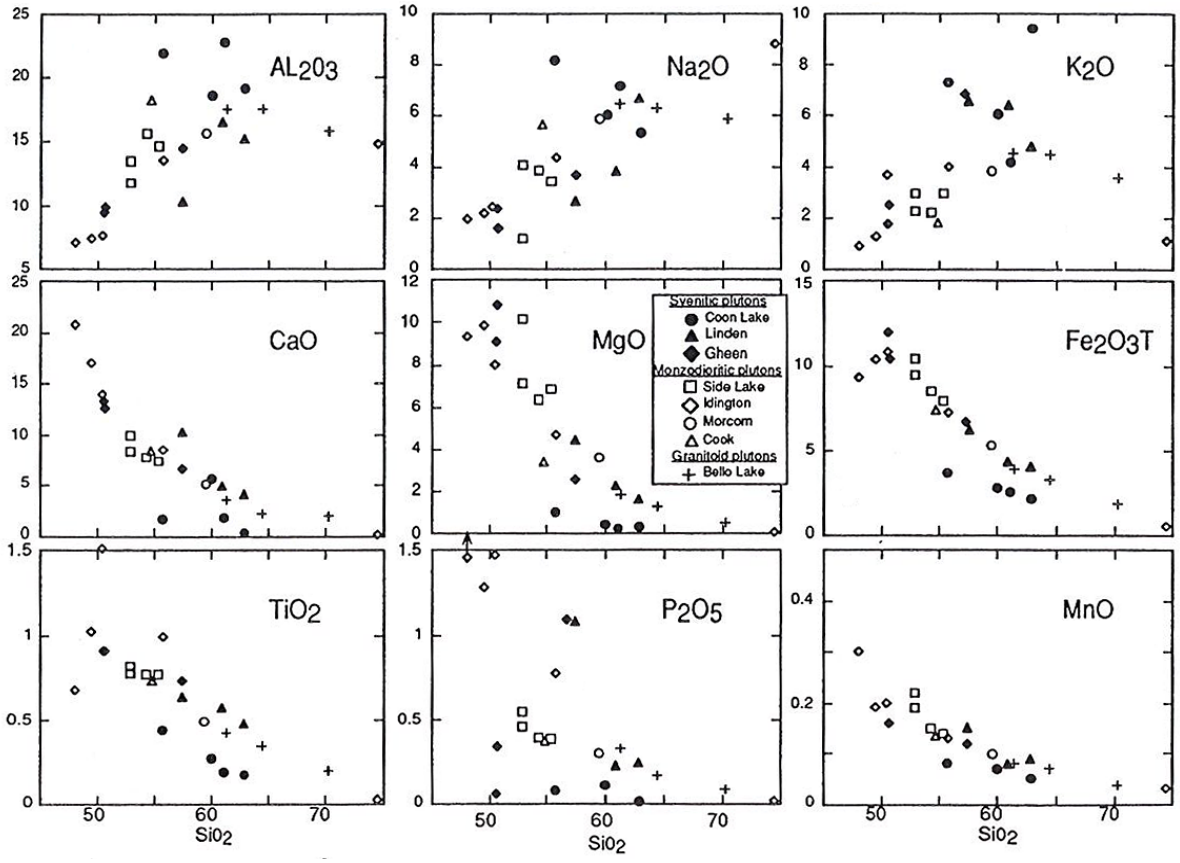


Figure 5-5. Harker diagrams for the alkalic plutonic rocks, in wt % oxides recalculated to no loss on ignition.

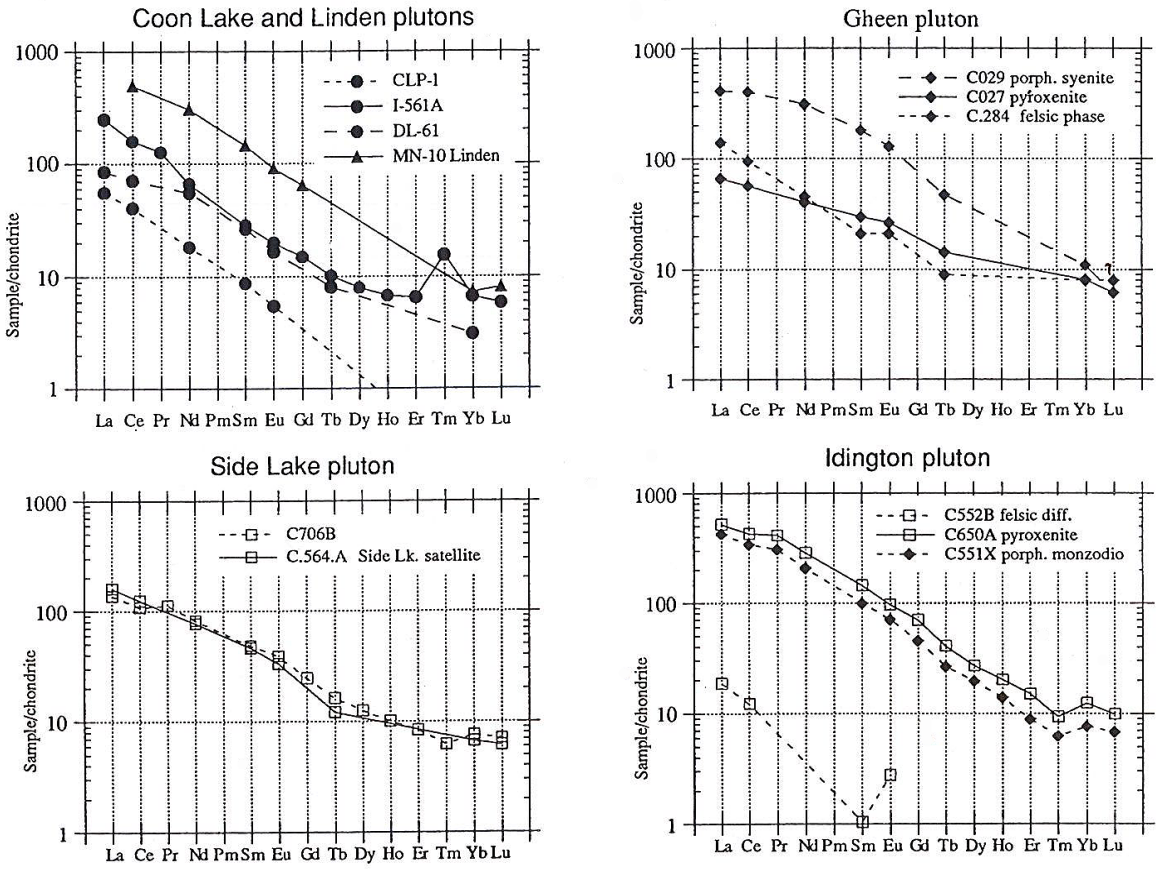


Figure 5-6. Chondrite-normalized rare-earth-element patterns for the alkalic plutonic rocks for which analyses are available.

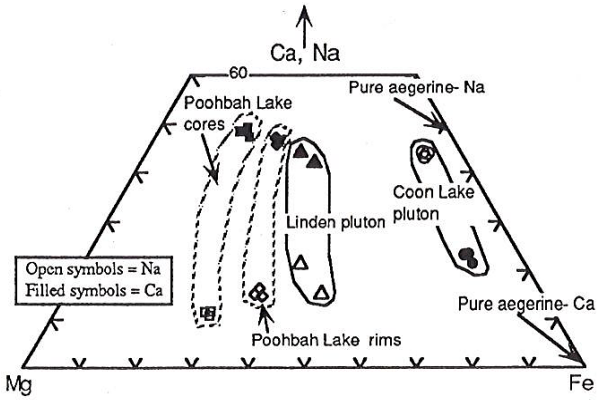


Figure 5-7. Pyroxene compositions from the Coon Like and Linden plutons. Pyroxene compositions from Poohbah Lake (Sage, 1988a) and compositions of pure aegirine (Deer and others, 1966, p. 107) shown for comparison.

Table 5-3. Microprobe analyses of minerals from the Coon Lake and Linden plutons. [Linden results from Sims and others (1972). Chemical analyses in weight percent oxides. Cancrinite totals low due to abundance of volatiles. Table is continued on next page.

	Aegirine					Biotite				Sphene		
	Coon Lake			Linden		Coon Lake		Linden		Coon Lake		Linden
SiO_2	51.49	51.62	51.8	53	46.85	37.16	35.69	44	43	30.01	30.65	31
TiO_2	0.58	0.54	0.48	0.5	2.13	2.66	3.13	0.5	0.5	37.17	34.62	31
Al_2O_3	1.35	1.34	1.38	1	2.5	13.96	12.34	11	13	0.55	0.57	3.5
FeO	25.43	25.36	25.74	14.8	16.97	21.02	18.42	18	14	2.06	2.34	3
MnO	0.33	0.41	0.44		0.31	1.13	1.11			0.01	0.06	
MgO	1.96	2.00	1.85	8.6	8.17	9.32	10.03	14	16.2	0.02	0.02	
CaO	6.74	6.92	6.29	18.8	17.85	0	0.01			26.51	25.44	29
Na_2O	9.74	9.51	9.88	3.5	2.49	0.14	0.22	1	1	0.29	0.33	3.3
K_2O	0.00	0	0.00	0.5	0.5	9.21	9.34	10.5	11.5	0.01	0.01	
Cr_20_3	0.00	0.02	0.00		nd	0.01	0			0.00	0	
Total	97.62	97.70	97.85	100.7	99.84	94.60	90.28	99.0	99.20	96.62	94.04	100.80
	Number of cations based on 6 oxygen					Number of cations based on 24 oxygen						
Si	2.1	2.1	2.1	2.02	1.88	6.31	6.33	6.96	6.71	4.89	5.11	4.91
Ti	0.02	0.02	0.01	0.01	0.06	0.34	0.42	0.06	0.06	4.55	4.34	3.69
Al	0.06	0.06	0.07	0.04	0.12	2.79	2.58	2.05	2.39	0.11	0.11	0.65
Fe	0.87	0.86	0.87	0.47	0.57	2.98	2.73	2.38	1.83	0.28	0.33	0.40
Mn	0.01	0.01	O.D2	0	0.01	0.16	0.17			0.00	0.01	
Mg	0.12	0.12	0.11	0.49	0.49	2.36	2.65	3.3	3.77	0.01	0.01	
Ca	0.29	0.3	0.27	0.77	0.77	0	0.00	0.00	0.00	4.63	4.54	4.92
Na	0.77	0.75	0.78	0.26	0.19	0.05	0.08	0.31	0.3	0.09	0.11	1.01
K	0	0	0	0.02	0,03	1.99	2.1I	2.12	2.29	0.00	0.00	
Cr	0	0	0			0.00	0.00	0.00	0.00	0.00	0.00	

Table 5-3 continued

	Exsolved albite	Perthite					Nepheline					Cancrinite		
		Coon Lake				Linden	Coon Lake					Coon Lake		
SiO_2	72.37	63.422	66.725	67.493	66.235	61.5	46.153	46.641	48.068	46.297	45.345	37.455	37.613	37.472
Al_2O_3	19.868	15.347	17.527	18.889	18.612	19	33.061	34.701	35.152	34.217	33.123	28.053	26.956	28.416
BaO	0.000	0.000	0.132	0.000	0.104		0.000	0.000	0.000	0.028	0.000	0.122	0	0
CaO	0.031	0.000	0.018	0.001	0.000	0.5	0.084	0.076	0.116	0.102	0.484	5.583	5.432	5.348
Na_2O	10.58	0.646	3.055	3.785	0.716	1.5	15.947	14.848	13.198	15.917	13.574	18.776	18.468	18.201
K_2O	1.268	12.139	12.521	12.016	15.932	15.8	6.186	6.211	5.877	6.133	6.068	0.04	0.052	0.206
Total	104.118	91.553	99.977	102.185	101.598	99.8	101.43	102.476	102.412	102.693	98.594	90.029	88.52	89.643
		Number of cations based on 8 oxygen					Number of cations based on 32 oxygen					No. of cations based on 12 O		
Si	3.03	3.13	3.04	3	3.01	2.92	8.67	8.62	8.79	8.59	8.70	3.02	3.08	3.02
Al	0.98	0.89	0.94	0.99	1	1.06	7.33	7.56	7.58	7.48	7.49	2.67	2.6	2.7
Ba	0	0	0.01	0	0.01		0	0	0	0.01	0	0.01	0	0
Ca	0	0	0	0	0	0.03	0.02	0.02	0.02	0.02	0.10	0.48	0.48	0.46
Na	0.86	0.06	0.27	0.33	0.06	0.14	5.81	5.32	4.68	5.72	5.05	2.94	·2.93	2.85
K	0,07	0.76	0.73	0.68	0.92	0.96	1.48	1.46	1.37	1.45	1.49	0	0.01	0.02

Linden Pluton

The Linden pluton [**2681.00±0.29 Ma**] and its smaller satellite to the east intrude mafic to felsic volcaniclastic and sedimentary rocks that are metamorphosed to the sillimanite grade at the north edge of the pluton and to chlorite grade at the southern edge. A narrow amphibolite-grade metamorphic aureole surrounds the pluton (Jirsa and others, 1992), as is evident in drill core LF-1 (Fig. 5-1). In this core, thin syenitic dikelets cut biotite-amphibole schist that has centimeter-thick green bands dominated by bright-green sodic amphibole and brown bands dominated by biotite. The country rock here is of sillimanite grade, and the aureole along the north edge of the Linden pluton may reflect retrogression. Sims and others (1972), who describe amphibolite-grade contact metamorphism of mafic volcanic rocks adjacent to the western margin of the pluton, suggest that the foliation at a high angle to the regional fabric is the result of forcible pluton emplacement.

The Linden pluton is roughly 54 mi^2 in size and elongate to the northwest, whereas the satellitic intrusion is about 4.5 mi^2 in size and elongate to the northeast (Fig. 5-1). Exposures are limited to the pluton edges, but ten drill cores from the pluton were obtained by various private and governmental agencies. Records of these cores and the cores themselves are on file at the Minnesota Department of Natural Resources, Division of minerals in Hibbing. A summary of the cores is given in Table 5-4. The LP-series of drill cores were subsequently examined by Himmelberg (1973), and thin sections from these cores were briefly reexamined in conjunction with this report. The LP-series descriptions are directly from company logs, and the OB- series descriptions are from the Minnesota Department of Natural Resources, Division of Minerals (Martin and others, 1988). The target of company drilling is not known, but complete metals analyses, together with Na, K, Al, Ca, Ba, and Sr abundances, were obtained by the explorationists. The satellite intrusion is not exposed, but one short drill core was obtained by the Minnesota Geological Survey (Meints and others, 1993).

The main Linden pluton is generally uniform in composition within the exposed portions and in the drill cores. The typical phase consists of trachytic, variably porphyritic, salmon-pink and greenish-black, medium-to coarse-grained aegirine-augite syenite with conspicuous dark-brown sphene and centimeter-scale elliptical pyroxenite clots. As reported by Sims and others (1972), and confirmed here, the dominant minerals of the syenite are braid-textured perthite and dark-green aegirine-augite ($Ac_7Wo_{41}En_{26}Fs_{25}$, Table 5-3 and Fig. 5-7), with variable but lesser amounts of plagioclase, sphene, apatite, biotite, hornblende, magnetite, and epidote. Modal analyses and compositions of selected minerals are summarized in Tables 5-1 and 5-3. Complete descriptions of exposures are given in Sims and others (1972), and the drill cores are summarized in Table 5-4.

Textures in the groundmass of drill holes CD-13 (Meints and others, 1993) and LF-2 are suggestive of cataclasis, yet other features in these cores, such as tabular plagioclase, blocky pseudomorphic biotite and epidote (presumably after pyroxene), and euhedral diamond-shaped sphene, show no evidence of brittle deformation. Thus the granoblastic fabric of the groundmass is most likely the result of plastic flow deformation of a viscous, mostly crystallized magma, in conjunction with late deuteric fluids. Drill hole CD-4 in the Linden satellite also contains zones of moderately sheared syenite characterized by rounded, rolled feldspar phenocrysts, suggestions of C- S fabric, and streaky pink and gray segregations. Shear bands <I inch to 10 feet thick are foliated parallel to the trachytic fabric of unsheared portions, and the mineralogy of the sheared rock in thin section is identical to that of the undeformed portions (Table 5-1). As is the case in the Linden pluton proper, the annealed texture implies that deformation occurred in a hot,

semiplastic state, under near-magmatic temperatures. These submagmatic deformation features are also present in the Idington and Coon Lake plutons.

Gheen Pluton

The Gheen pluton, some 3 miles east of the Linden pluton, intrudes sillimanite-grade metasedimentary rocks. It is currently exposed **at** a high level, and its magnetic signature conforms to the long, sinuous, northeast- elongate shape deduced from scattered outcrops along the length of the body. Local trachytic fabric defined by tabular perthite phenocrysts is steep and subconformable to the pluton contacts and the pluton shape at both map and outcrop scale is subcordant to the schistosity of the host supracrustal rocks.

The pluton is chiefly mesocratic, pink and dark-green, porphyritic syenite and ranges to dark-greenish-black, coarse-grained pyroxenite and leucocratic, pink, coarse- grained alkali-feldspar syenite. Conflicting internal intrusive relationships are common, with melanocratic phases occurring both as inclusions and as dikes in the porphyritic phase. However, pink leucosyenite dikelets cross all other phases. Mesocratic syenite phases contain 1- to 3-cm tabular perthite phenocrysts in a groundmass of fibrous amphibole, euhedral sphene, blocky oxides, stubby prismatic apatite, and minor calcite and epidote. Trace amounts of dark-green pyroxene are present, but most has been deuterically altered to bright-green fibrous amphibole. Calcite occurs both in irregular veinlets with amphibole and as magmatic, interstitial grains against sharp comers of feldspar phenocrysts. The melanocratic monzodiorite phase consists predominantly of relict pale-green pyroxene up to 2.5 mm across and lesser amounts of sericitized plagioclase, fine-grained, euhedral sphene, and apatite. The pyroxene is variably replaced by euhedral, pale-green hornblende. Biotite occurs as brown books within hornblende, and is slightly altered to chlorite. Unaltered microperthite occupies a late anhedral interstitial position.

Sills of pink, leucocratic, coarse-grained syenite up to 10 feet wide emanate from the Gheen pluton and cut adjacent metasedimentary rocks. This phase is characterized by irregular microcline phenocrysts in a seriate groundmass of macroscopically identified, pink microcline, fine-grained biotite, and minor white albite. Local planar miariolitic cavities lined with K-feldspar crystals are consistent with the interpretation that the pluton is exposed at a high level.

The Gheen pluton differs from the other alkalic intrusions by its pervasive deuteric alteration and relatively abundant chalcopyrite. Modal analyses of the melanocratic and porphyritic mesocratic phases are listed in Table 5-1 and shown on Figure 5-3.

Table 5-4. Descriptions of cores from the Linden pluton; Dominant lithology in bold type.

Drill Hole	Description	Mineralogy
LF-2	Pink, slightly porphyritic, medium-grained homogeneous leuco alkali-feldspar syenite. Trachytic foliation defined by aligned mafic minerals. Feldspar varies from coarse blocky phenocrysts with recrystallized edges to granoblastic groundmass.	**Perthite,** biotite, muscovite, aegerine, melanite, sphene, calcite, epidote, oxides, pyrite.
LF-3	Dark-gray, slightly porphyritic, fine- to medium-grained heterogeneous poikilitic syenite to monzonite. Poikilitic feldspar encloses pyroxene, biotite, and sphene. Weak trachytic fabric defined by aligned pyroxenes and feldspar oikocrysts. Feldspathic dikelets and aegirine veinlets.	**Microperthite** that grades to **antiperthite, pyroxene, biotite,** sphene, apatite
LF-4	Light-grayish-white, medium-grained, granular to hypidiomorphic hornblende monzonite with 1-cm mafic segregations. Deuteric pyroxene alteration.	**Perthite, antiperthite, hornblende-biotite-oxide** clusters after pyroxene, epidote, sphene, apatite, calcite in brittle veinlets.
LF-5	Light-pinkish-gray, medium- to coarse-grained, moderately porphyritic syenite; 2- to 4-cm mafic segregations of slightly porphyritic, euhedral aegirine in groundmass of feldspar, hornblende, sphene, etc.	**Perthite, aegirine,** sphene, apatite, oxides, hornblende, biotite, chlorite.
OB-207	Pinkish-gray, coarse-grained, trachytic, aegirine syenite.	**Perthite, aegirine-augite,** biotite, sphene, apatite, oxides.
OB-212	Coarse-grained, green and pink, trachytic syenite. Deuteric alteration of mafic minerals.	Red-stained **perthite,** fine granular **plagioclase,** stilpnomelane after biotite, chlorite after hornblende or pyroxene, leucoxene after sphene.
LP-1	Pink, coarse-grained syenite with erratic distribution of mafic minerals. Contains a 1-foot-wide dike of melasyenite (biotite pyroxene-carbonate).	Very coarse **feldspar,** 7-80% aegirine, sphene. Not described.
LP-2	Upper 20 feet, leucosyenite with 75-90° dipping trachytic fabric; rest is pink and green mesocratic syenite with biotite segregations.	Not described
CD-13	Pink and green, coarse-grained, weakly trachytic syenite with annealed cataclastic texture. Microperthite phenocrysts, pyroxene altered to tabular clusters of biotite plus epidote. Foliated matrix of fine-grained plagioclase.	**Microperthite, plagioclase, biotite, epidote,** melanite, sphene, sericite.
CD--4 Linden Satellite	Gray, coarse-grained, trachytic, porphyritic syenite with narrow pink and green, fine-grained shear bands. Granoblastic-recrystallized texture in shear bands grades into unsheared rock, contains rolled feldspar phenocrysts. Sheared portions of same mineralogy as unsheared.	In unsheared portion, tabular **perthite** rimmed by granular **plagioclase,** zoned euhedral **aegirine-augite** rimmed by pale-green fibrous amphibole. Apatite, chlorite, sphene, allanite, oxides.

Baudette pluton, Lake of the Woods County

The Baudette pluton is not exposed, but is seen in a drill core obtained by the Minnesota Geological Survey (hole 1986-CUSMAP-1; Mills and others, 1987). It is located 8 miles south of the town of Baudette, in Lake of the Woods County, and intrudes felsic schists. As judged from geophysical data, the pluton is approximately 1 mile long and half a mile wide, but the best resolution of available geophysics is only 1:250,000 (USGS data in Chandler, 1991).

The core consists of coarse-grained, green and pink, porphyritic garnet-biotite syenite. Trachytoid phenocrysts of pink perthite up to 2 cm long with irregular granular borders are in a groundmass of green biotite, melanite garnet, plagioclase, lesser epidote, sphene, and aegirine- augite, and accessory apatite and zircon or monazite. The brownish-yellow melanite varies from small euhedral crystals to large granular masses enclosed within coarser green biotite. The biotite varies greatly in grain size from fine-grained mats to medium-grained books with a decussate intergrown fabric.

MONZODIORITE CLAN

The monzodioritic group includes the **Side Lake, Morcom, Idington, Lost Lake**, and Cook plutons, as well as the Daisy Bay pluton (Sims and Mudrey, 1972), which is shown on Figure 5-1 but not discussed here. All are within the Wawa subprovince, adjacent to the north edge of the Shannon Lake granite phase of the Giants Range batholith (Jirsa and others, 1991).

These plutons tend to be irregular in shape and elongate to the northeast, parallel to the regional *D2* fabric (Jirsa and others, 1992) of the supracrustal country rocks. The rock is largely pink and green porphyritic monzodiorite, but varies erratically to dark-green pyroxenite and pink granite, granodiorite, and Na-rich trondhjemite. The pyroxenite tends to occur in small irregular pods and segregations, whereas the felsic differentiates occur in thin, straight dikes and in larger segregations. In addition, the monzodiorite group contains minor dark-green poikilitic phases in which antiperthite is grown over pyroxene, sphene, apatite, and hornblende.

Porphyritic phases typically have strong trachytoid fabrics, defined by aligned feldspar phenocrysts that are subconformable to the borders but more erratic in the centers of the intrusions. The typical porphyritic phase is characterized by coarse, blocky, pink to gray phenocrysts of Na-rich antiperthite in a groundrnass of predominantly fine-grained euhedral aegirine-augite, along with sphene, perthite, polygonal plagioclase, lesser proportions of hornblende, biotite, apatite, epidote, chlorite, opaque oxides, and rare quartz. Feldspar phenocrysts are typically antiperthitic, but range from albitic plagioclase to strongly perthitic K-feldspar. The normative composition is commonly midway between the K-rich and Na-rich end members in contrast to the compositions implied by point counting, because of difficulties in properly quantifying modal abundances of the strongly exsolved feldspars (Fig. 5-3B).

Idington Pluton

The Idington pluton is located in west-central St. Louis County near the former village of Idington. Its irregular horseshoe shape, roughly 8 mi^2 in size, is elongate to the northeast (Fig. 5-1). Trachytic foliations are predominantly northeast-oriented, subcordant to the pluton boundary, and dip generally more than 70°. However, exposures are limited to central parts of the pluton, where trachytic fabrics are less likely to conform to the pluton shape. The pluton has a rather irregular magnetic anomaly (Fig. 5-1), but the magnetic pattern has been somewhat obscured by a 150-foot-wide, strongly magnetic diabase dike and possibly by late north-trending brittle faults. No contact relationships with country rocks were observed, except at the southwestern edge of the pluton, where it is intruded by the 2,674-Ma Shannon Lake granite of the Giants Range batholith (Jirsa and others, 1991; Boerboom and Zartman, 1993).

Rock types in the Idington pluton are consistent in mineralogy but extremely erratic in modal proportions. Mesocratic, porphyritic pyroxene monzonite predominates, but dark-green aegirine-augite pyroxenite is common, and a small proportion of pink, sodic leucotrondhjemite occurs in aplopegmatite dikes 1 to 10 cm wide in the heart of the pluton. A mappable segregation of leucotrondhjemite exposed at the pluton's northeast corner contains minor flat-lying vuggy fractures lined with purple fluorite and a dark brown translucent tetragonal mineral tentatively identified as zircon or cassiterite.

Modal analyses from four samples of the Idington pluton (porphyritic phase-C.551.X, pyroxenite phase- C.650.A, and two felsic differentiates-C.552.B and C.561.A) are listed in Table 5-1. In the porphyritic phase, feldspar phenocrysts are mostly gray, rectangular, 1- to 4- cm crystals of coarsely exsolved antiperthite, but small intergrown polygonal grains of plagioclase and perthite also are abundant in the groundmass. Aegirine-augite crystals are prismatic, weakly pleochroic, and zoned with darker green rims. Apatite inclusions are common near the edges of pyroxene crystals. Euhedral, dark-brown sphene is prominent in hand sample and is microscopically associated with biotite. Melanocratic diorite is medium to coarse grained, with trachytically aligned aegirine-augite prisms in a groundmass dominated by fresh, zoned, anhedral plagioclase. Hornblende in this phase occurs as dark-green patches of secondary origin within pyroxene and as larger subpoikilitic grains with inclusions of apatite, pyroxene, and plagioclase. Green biotite forms clusters of euhedral blocky grains aligned parallel to the trachytic fabric. Sphene is mostly euhedral, but locally is subpoikilitic-anhedral and partially encloses pyroxene and other mafic minerals. Accessory minerals include allanite and secondary chlorite, calcite, and epidote. The leucocratic differentiate contains albitic feldspar as large as 40 cm across, which is characterized by graphic Intergrowths with quartz. Aplitic parts of the leuco-phase contain radial-plumose sheaves of albite as long as 3 cm.

The erratic distribution between phases, which typifies exposures of this intrusion, can be documented on an outcrop scale to have formed by filter-pressing of a mafic liquid out of a feldspar-phenocryst slurry. The groundmass in the porphyry is identical to the melanocratic pyroxenite, which occurs as irregular amoeboid to net-vein segregations as large as several feet. However, at the southwestern end of the pluton, cumulus modal layering is also present in the form of melanocratic layers tens of centimeters thick interlayered with mesocratic, porphyritic diorite. This diorite itself shows layering by changes in phenocryst size and abundance and trachytoid foliation parallel to layering. The layering and trachytic fabric have been drag-folded into widely spaced, crosscutting ductile shear bands, which lack cleavage or schistosity, but instead have an annealed, granoblastic habit similar to that in the Linden pluton. Pink granite pegmatite dikelets (Shannon Lake granite?) commonly occupy these shear planes. In these bands, elliptical deformed relict feldspar phenocrysts are recrystallized into granoblastic aggregates, and the pyroxenes have been replaced by bright-green hornblende. The annealed textures and lack of through-going fabric development imply that ductile deformation, recrystallization, and annealment, caused by self-induced strain during emplacement or the last vestiges of regional deformation, occurred while the rock was still hot.

In a series of exposures along Highway 53 at the south edge of the Idington pluton a sharp line of demarcation exists whereby outcrops of Shannon Lake granite have inclusions only of Idington monzodiorite north of an east-west line, and those south of it have inclusions only of granodiorite derived from the Britt pluton, an early, D_2-deformed intrusion (Jirsa and others, 1991, 1992). This implies that the earlier intrusive contact of the Idington pluton into the Britt granodiorite was overprinted but preserved by upward stoping of the Shannon Lake granite (Boerboom and Zartman, 1993).

Side Lake Pluton

The long, arcuate Side Lake pluton, roughly 27 mi^2 in dimension, extends eastward from Side Lake in western St. Louis County. The pluton crops out only at its very western and eastern limits. Two exposed satellitic plugs off the eastern tip of the main pluton (Fig. 5-1) are identical in mineralogy to, and

conterminous with, the eastern end of the Side Lake pluton. These satellites have complex intrusive relationships with the country rocks, and are described in a separate section below. The main pluton intrudes metamorphosed basaltic volcanic and felsic sedimentary **rocks** along most of its length. It is just north of the Shannon Lake granite, but intrusive relationships with the granite are unknown because of lack of exposure. Crosscutting Proterozoic diabase dikes have lowered the magnetism along their length, in contrast to the Idington pluton, where the diabase dikes have enhanced the magnetism.

Rocks from the exposures of the Side Lake pluton range from mesocratic biotite-hypersthene-clinopyroxene diorite on the west to hornblende monzodiorite on the east Trachytic fabrics in most outcrops are generally conformable to the margins of the pluton. Segregations of melanocratic pyroxenite to hornblendite occur throughout the intrusion, but are more abundant to the west, where they occur as irregular dikelets, segregations, and small inclusions in mesocratic diorite. In addition, dikes of diorite and pyroxenite up to 150 feet wide, which emanate from the western margin of the pluton, are parallel to the pluton boundary and intrude metabasaltic rocks. These dikes are clearly discordant to the regional metamorphic fabric in the intruded basalts; some of them contain wispy felsic stringers parallel to their walls produced by flow segregation. Thin, straight, late-stage pink granitic to syenitic dikelets are common within and adjacent to the pluton.

Mesocratic, medium-grained, pinkish-gray diorite, which predominates at the western end, contains 5-10% tiny euhedral grains of pleochroic pale-pink to green hypersthene, and at least 20% euhedral, pale-green clinopyroxene with light-colored rims. These pyroxenes range in size from less than 1 to 3 mm; the hypersthene is generally finer grained, and the clinopyroxene is variably phenocrystic. Plagioclase is the predominant feldspar. A sample from the pluton 200 feet from the western contact contains strongly zoned, subhedral, trachytic plagioclase, with fuzzy grain boundaries. Another thin section 500 feet from the contact has fine-grained granoblastic plagioclase, orthoclase, and quartz between larger augite phenocrysts. Apatite is abundant as fine-grained euhedral prismatic grains included within pyroxene and feldspar. Oxides occur both within augite as wormy blebs of apparent secondary origin and as scattered blocky, fine-grained crystals. Sphene is rare or lacking at the western end. Brown biotite is a generally minor component at the western end of the pluton, but in some outcrops composes up to 5% of the rock. It locally forms vertically oriented poikilitic plates that are up to 2 cm long and oriented parallel to the trachytic fabric of the monzodiorite.

The eastern outcrops consist of moderately heterogeneous, medium- to coarse-grained, pink and green pyroxene-hornblende monzodiorite. Here moderately developed trachytic foliation plunges 20-30° to the souL'1west, down the axis of the pluton. Fine-grained, centimeter-sized, angular cognate xenoliths of mafic monzodiorite, in addition to dark-green mafic stringers, are common.

Side Lake Pluton Satellites

Two small plugs are exposed northeast of the Side Lake pluton. One, about 1/4 mile east of the Side Lake pluton, is round and 3/4 mile in diameter. It consists of medium- to coarse-grained, trachytic, weakly porphyritic, green and pink hornblende-pyroxene monzodiorite. Subhedral 5-mm orange-white antiperthite and scattered 2-mm aegirine-augite phenocrysts are set in a fine-grained groundmass of green prismatic pyroxene, fine-grained anhedral feldspar of unknown composition, minor hornblende, and brownish-green biotite mostly replaced by chlorite. Apatite, biotite, opaques (oxides and pyrite), and sphene each compose about 1% (Table 5-1). Clots and irregular segregations of pyroxenite are common, as are late dikelets of pink syenite up to 10 cm wide which cut across trachytic fabrics. The trachytic fabric is locally variable and inconsistent in orientation, but generally has a shallow southwest plunge toward the main Side Lake pluton.

The next satellite is a horseshoe-shaped body, 0.75 mi^2 in size, located 1.5 miles east of the Side Lake pluton (Fig. 5-1). Its linear trachytic fabrics are subconformable to the edges of the plug, and again plunge shallowly southwest toward the Side Lake pluton. This small intrusion is highly varied in

texture and mafic content, but dark-green poikilitic diorite and white leucocratic monzodiorite with small inclusions of pyroxenite predominate. The poikilitic diorite has 1-cm, oval-shaped antiperthitic to perthitic poikilitic feldspar with inclusions of aegirine-augite, biotite, sphene, and apatite. The long axes of the poikilitic feldspars and prismatic pyroxenes are parallel and define a primary trachytic fabric. The dark poikilitic phase is sharply cut by sills of the white monzodiorite. However at one location, the two rocks are commingled in a pillow-like fashion that suggests mixing of immiscible liquids. Thus the field relationships, as well as mineralogy, indicate that the dark poikilitic and leucocratic phases are comagmatic.

Relationship of Satellitic Intrusions to the Side Lake Pluton

Their similar lithological and textural attributes and aligned trachytic fabrics imply that the Side Lake pluton and the two satellites are derived from a common source at depth to the west. Further evidence of comagmatism is the presence of numerous thin anastamosing sills of white monzodiorite, identical to the white phase in the small plugs, which are parallel to the schistosity of the surrounding metasedimentary country rocks and intercalated with them. The intercalated monzodiorite and schist define a mappable unit along a discrete zone (dashed area on Fig. 5-1 that links the two satellitic plugs to the Side Lake pluton. This zone continues past the eastern satellite for at least 2.5 miles, where it merges back into a magnetic anomaly interpreted as another alkalic intrusion (Jirsa and others, 1991).

At the intersection of Highway 73 and the Sturgeon River east of the Side Lake pluton, the intercalated monzodiorite and metasedirnentary rocks are transected by a late, north-trending brittle shear zone, which has minimal offset but has reduced the rocks to a fine-grained cataclasite.

Morcom Pluton [Thin section CD-7]

The Morcom pluton is just north of the Side Lake pluton and may be related to it at depth, because a large positive gravity anomaly underlies the area between the two. The Morcom pluton, which intrudes metasedimentary rocks, has a bulbous shape with a long narrow appendage to the east (Fig. 5-1). Scattered outcrops exist at the eastern limit of the pluton, and a drill core was obtained from the western end, near the north side. Trachytic foliation near the southeast edge dips 80°N, and at the eastern tip plunges 40°SW. In the drill core the foliation dips 40-45°, presumably toward the pluton center. Rock types are similar in the Morcom pluton, the eastern Side Lake pluton and its satellites, and the Idington pluton. However, the major-element geochemistry of the Morcom is very similar to that of the Linden pluton (Fig. 5-5). The drill core consists of multiphase, medium-grained, weakly porphyritic biotite-hornblende-pyroxene monzodiorite, with a trachytoid foliation defined by alignment of plagioclase phenocrysts and prismatic mafic minerals. Dark-green, poikilitic monzodiorite occurs in the core as 15-cm inclusions or layers; small miariolitic cavities lined with fine-grained crystalline biotite, pyroxene, and pyrite are also present. Late brittle slickensided faults and fractures, oriented obliquely to foliation, locally transect the core. Feldspar compositions vary from clean plagioclase with narrow twin lamellae to untwinned plagioclase, and from antiperthite to perthite, the latter confined to anhedral grains in the groundmass. Euhedral, light-green, aegirine-augite has hornblende rims and alteration patches; hornblende is also present as subhedral to prismatic, brownish- to bluish-green grains with patchy color zonation and rare deuteric overgrowths of colorless actinolite. Biotite is dark green and pleochroic, and is associated with hornblende. Accessory minerals include sphene, allanite, apatite, epidote, calcite, and minor secondary oxides within pyroxene. The nonpoikilitic and poikilitic phases have similar mineralogy (Table 5-1).

Exposures at the eastern tip of the pluton consist of pink to gray, medium-grained monzodiorite with abundant 5- to 10-cm, elongate xenoliths of foliated felsic to pelitic schist, together with cognate xenoliths of fine-grained melanocratic monzodiorite. Some of the intrusive-breccia xenoliths are themselves an intrusive breccia. Pink monzonitic dikelets are abundant and cut all the earlier intrusive phases and xenoliths. The monzodiorite contains scattered sericitized plagioclase phenocrysts in a fine-grained groundmass consisting of up to 5% quartz intergrown with granular K-feldspar and plagioclase,

along with hornblende, actinolite, sphene, chlorite, apatite, and minor oxides and secondary calcite. Melanocratic clots are of similar mineralogy but with a higher proportion of mafic minerals. Elsewhere at the eastern terminus, the rock lacks xenolithic inclusions but is still heterogeneous and cut by late, pink felsic differentiates. This inclusion- free monzodiorite has a trachytic fabric defined by aligned feldspars and mafic clots, and is similar in mineralogy to the core from the western end of the pluton.

Lost Lake Pluton (2675.1±0.5 Ma)

The Lost Lake pluton, the "pluton southwest of Lost Lake" of Sims and Mudrey (1972), was described as a circular pluton composed of heterogeneous syenite with a local, conspicuously porphyritic facies, a pegmatitic facies with miariolitic cavities, and small bodies of pyroxene- biotite lamprophyre. They noted that the borders of the pluton tend to be quartzose and contain small angular inclusions of metagraywacke and slate of the Lake Vermilion Formation.

Based on detailed remapping, the authors have redefined the shape of the pluton as a long, sinuous and bulbous, northeast-trending body that is 1 mile or less wide but approximately 9 mi^2 in size. The eastern tip of the pluton lies 1/4 mile south of Lost Lake, and the western terminus is just south of Angora on State Highway 53, about half a mile north of the Idington pluton (Fig. 5-1). The uniform magnetic signature of the pluton has been lowered locally by late, north-south, brittle faults which have minimal offset. The western end of the Lost Lake pluton is not exposed and its shape is inferred from aeromagnetic data, whereas the central portion is well exposed, and scattered outcrops exist over the eastern end, mainly adjacent to more resistant crosscutting Proterozoic diabase dikes. Two mappable intrusions of quartz monzonite 1/4 mile in diameter occur adjacent to the main body (Jirsa and others, 1991). These small plugs are similar in composition to leucocratic dikes within the main pluton, and are related to the pluton.

Subvertical trachytic fabric, which is defined by both phenocrysts and elongate poikilitic feldspar, strikes generally northeast, subparallel to the length of the intrusion. The small, separate bodies of pink monzonite also possess a northeast-oriented trachytic fabric, defined by orbicular clots of biotite, disseminated biotite, or aligned feldspar crystals.

The Lost Lake pluton is mineralogically similar to the Idington and eastern Side Lake plutons, but contains a higher proportion of pink leucocratic phases. The main rock types range from pink and green, porphyritic monzodiorite to dark-green, poikilitic biotite-pyroxene monzodiorite to pink monzonite, syenite, and quartz monzonite. Pyroxenite occurs in small segregations, in the same fashion as in the Idington pluton. In general, the poikilitic and porphyritic phases are earliest and are cut by the pink rock varieties. Small dikes of pink granitic pegmatite cut all other rock types, but it is unclear whether these dikes are related to the pluton or are from an external source, such as the Shannon Lake granite of the Giants Range batholith. The pink monzodiorite and syenite differentiates are medium grained, equigranular to weakly porphyritic, and commonly aplitic to pegmatitic, with pyroxene, hornblende, and biotite as the predominant mafic phases.

The two small felsic plugs of quartz monzonite to granodiorite contain a mafic mineral assemblage of varied proportions of biotite, chlorite, and hornblende, and up to 30% quartz. The margins of these plugs contain abundant inclusions of felsic volcanic country rocks up to 15 feet across which were clearly deformed prior to incorporation, and small dikes emanating from these plugs cut across fold axes in the supracrustal rocks. One of the plugs contains a unique medium-grained, pink, orbicular granodiorite with trachytically aligned discs of black, concentrically foliated biotite that are as much as 0.5 cm thick and 5 cm long. The biotite orbs which contain intergrown sphene, apatite, plagioclase, quartz, and magnetite, compose as much as 15% of the rock. The orbicular rock grades into a non-orbicular phase with the same proportion of biotite, but as medium-grained, uniformly disseminated flakes. In addition to the typical phases, related rocks in the small plugs include coarse-grained, dark-green biotite-hornblende lamprophyre; green poikilitic monzodiorite; and pink monzonitic pegmatite.

Cook Pluton

The Cook pluton (Cook Airport pluton on Southwick, 1993), 1 mile south of the town of Cook (Fig. 5-1), is inferred from aeromagnetic data to be 1.5 mi^2 in size, elongate to the east. No outcrops of this pluton are known, but a drill hole in the western margin of the pluton recovered core of uniformly coarse-grained, peppery, dark-greenish-black and light-green, epidote-altered hornblende-biotite diorite. Strong trachytic foliation, which is defined by tabular plagioclase and mafic minerals, dips 50° from horizontal. One fine-grained cognate xenolith, 1 cm x 3 cm in size, is present near the bottom of the 10-foot core. The rock has a primary hypidiomorphic-granular texture, but pervasive, small euhedral crystals of secondary epidote are overprinted on all primary minerals, preferentially in the cores of plagioclase, and as fine-grained granular masses in biotite. Pale-green hornblende is rimmed by green biotite, and zoned plagioclase is clean and well-twinned, despite the pervasive epidote alteration. Accessory minerals include apatite, sphene, oxides, calcite, and interstitial orthoclase. Scattered late, brittle fractures which dip as much as 20° from horizontal are lined with coarse, lineated chlorite, pink-altered feldspar, and a crust of epidote and white carbonate. The pristine trachytic igneous texture and lack of metamorphic fabric indicate that the pervasive epidotization is the result of deuteric alteration, rather than regional metamorphism.

GRANITOID PLUTONS

The granitoid group includes the Stingy Lake, Rice River, and Bello Lake plutons, all within the Wawa subprovince. These plutons tend to be oval in shape and elongate to the northeast. Rocks in this group are characterized by substantial quantities of quartz and are vaguely to strongly porphyritic and trachytic. Hornblende is the predominant mafic phase, along with biotite and rare pyroxene. These plutons are considered part of the alkalic group on the basis of their similarity to the other alkalic plutons in size, shape, high Ba and Sr content, magnetic signature, and trachytic fabric.

Stingy Lake Pluton

The Stingy Lake pluton is a 9 mi^2 circular pluton located 3 miles south of Sturgeon Lake, adjacent to the Giants Range granite, and is inferred to intrude mafic volcanic rocks (Fig. 5-1). Although unexposed, its round shape is well defined by its aeromagnetic anomaly (magnetic rim and nonmagnetic core). A 10-foot drill core was obtained from the northwest side of the pluton (Meints and others, 1993). The intrusion is cut by two Proterozoic diabase dikes.

The rock in the core is uniformly coarse-grained, porphyritic, pink granodiorite to quartz monzodiorite. Tabular phenocrysts of string-and-braid microperthite up to 7 mm long, together with weakly zoned plagioclase up to 2 mm long having narrow twin lamellae and weakly sericitized cores, define the 45°-dipping trachytoid foliation. The perthite contains small blocky plagioclase inclusions, and the areas between abutting perthite grains are also stuffed with small blocky plagioclase grains. Light-gray anhedral interstitial quartz with shadowy extinction has been recrystallized into coarse polycrystalline aggregates. Hornblende is mostly altered to green biotite, epidote, and granular oxides; however, fresh, dark-green, euhedral hornblende is locally preserved within quartz and feldspar. Accessory minerals include blocky primary oxides, sphene, zircon, and apatite (Table 5-1). Late closely spaced, vertical brittle fractures lined with epidote and chlorite are pervasive in the 10-foot core.

Rice River Pluton

The Rice River pluton, about *5* miles west of Cook, intrudes metamorphosed sedimentary rocks. It is inferred to be approximately 15 mi^2 in size, although its magnetic signature (Fig. 5-1B) of magnetic rim and nonmagnetic core is irregular and overprinted at the western edge by a north- trending Proterozoic diabase dike. A drill hole in the magnetic eastern rim of the pluton recovered core of gray, coarse-grained, porphyritic quartz monzonite to monzodiorite. Steeply inclined trachytic foliation is

defined by euhedral, strongly zoned, 1- to 2-cm perthite phenocrysts and small elliptical melanocratic clots that are fine-grained cognate xenoliths. Groundmass to the phenocrysts consists of 3- to 6-mm subhedral microcline, zoned plagioclase, hornblende, and anhedral interstitial quartz; the phenocrysts are rimmed by fine-grained plagioclase and myrmekitic quartz-feldspar intergrowths. Plagioclase grains are heavily sericitized, preferentially in the cores. Hornblende is weakly zoned and slightly altered to biotite, chlorite, and opaques. Euhedral sphene, allanite rimmed by epidote, and secondary calcite occur in minor proportions. Scattered chlorite-pyrite veinlets dip 5-10° from horizontal and occupy brittle fractures; some have slickensides that dip shallowly in the fracture planes.

Bello Lake Pluton

The Bello Lake pluton (Jirsa, 1990; Jirsa and Boerboom, 1990) is just southwest of the Coon Lake pluton. It is approximately 60 mi^2 in size, elongate to the northeast parallel to the regional strike of the mafic to felsic supracrustal rocks that it intrudes. The Bello Lake pluton is unexposed, but three 10-foot drill cores were obtained by the Minnesota Geological Survey, two near the western end, and one near the eastern end of the pluton (Fig. 5-1). The intrusion is magnetically quiet relative to the mafic volcanic rocks around it, but the pluton margins are strongly magnetic locally.

As judged from the cores, the Bello Lake pluton is uniform in color and texture, but moderately variable in composition, ranging from pyroxene monzonite to hornblende granite. The pyroxene-bearing phase occurs close to the pluton margin, whereas the hornblende monzonite occurs near the center of the pluton at its western end, and the hornblende granite is near the eastern end of the pluton. Data are insufficient to properly judge spatial variation of rock types, but the observed distribution suggests that the pluton may be zoned from a pyroxene-bearing phase at the rim, to a more differentiated, quartz-bearing phase near the center.

Pyroxene monzodiorite near the pluton border (KIB-39; Table 5-1) is green and pink, medium grained, and seriate in texture with a strong trachytic fabric defined by rectangular, zoned plagioclase and subhedral, weakly uralitized augite crystals. Accessory oxides, sphene, hornblende, chlorite, biotite, and apatite all formed late in the crystallization sequence, and tend to occur together.

Green and pink, medium-grained, slightly porphyritic hornblende monzonite (KIB-40; Table 5-1) on the western side of the pluton contains subhedral-prismatic hornblende and small phenocrysts of grayish-pink, blocky microperthite in an allotriomorphic-granular to weakly seriate groundmass of plagioclase, perthite, and minor quartz. This rock is similar to the pyroxene monzodiorite in hole KIB-39, except that hornblende occupies the position of pyroxene.

Hornblende granite from the eastern part of the pluton (drill hole KIB-7; Table 5-1) is characterized by strongly zoned, blocky plagioclase with sericitized cores surrounded by poikilitic microperthite. Myrmekitic feldspar-quartz intergrowths occur along perthite-plagioclase grain boundaries. Quartz is coarse and anhedral interstitial, and hornblende forms dark-green, irregular grains with abundant tiny quartz inclusions near the edges and granular oxide inclusions in the cores. Accessory green biotite, epidote, and chlorite are associated with hornblende as alteration products, and blocky apatite crystals are associated with mafic phases.

PETROGENETIC AND GEOCHRONOLOGICAL STUDIES

Arth and Hanson (1975), using data on major, trace, and rare earth elements, and isotopic data from the Linden pluton, concluded that the magma formed from 5 to 10% partial melting of a mixed eclogite and garnet peridotite source at mantle depth. Stern and others (1989) believe that the Linden originated by partial melting of a LILE- enriched mantle peridotite at shallow depths under hydrous conditions created by mantle metasomatism from rapid subduction of oceanic

lithosphere. However, they have lumped the Linden pluton in with the "sanukatoid suite," a very broad suite of rocks of variable size, timing, and associations throughout the Superior Province.

The age of D_2 deformation of the supracrustal rocks at the southern edge of the area from Cook to Side Lake (Jirsa and others, 1991) was bracketed by U-Pb zircon geochronology to between 2,685 and 2,669 Ma (Boerboom and Zartman, 1993). The alkalic plutons lack significant D_2 fabrics, and thus could not have been emplaced until approximately 2,669 Ma. ***[NOTE: This has been discredited by the new ages of 2681.00±0.29 Ma on the Linden and 2675.1±0.05 Ma on the Lost Lake plutons – Boerboom and others, 2022]*** The Idington pluton is intruded by a granite pegmatite inferred to have originated from the Shannon Lake granite, which was dated by Boerboom and Zartman (1993) at 2,674 ± 5, or a minimum of 2,669.

Catanzaro and Hanson (1971) obtained a discordant Pb^{207}/Pb^{206} age of 2,740 ± 10 Ma on sphene from the Linden pluton. Prince and Hanson (1972) obtained a similar age of 2,740 Ma, based on a Rb/Sr isochron through apatite and two whole-rock samples. These older ages on the Linden pluton relative to the younger age implied for the Idington pluton indicate that the syenitic rocks may be slightly older than the monzodioritic group, or that pluton emplacement may have progressed from north to south. Clearly, modern high-precision U-Pb zircon dates on the alkalic plutons are needed. ***[NOTE: Recent age of $^{207}Pb/^{206}Pb$ 2681.00±0.29 Ma (Boerboom and others, 2022)]***

CONCLUSIONS

The alkalic intrusions in northern Minnesota can be generally subdivided into a syenitic group, a monzodioritic group, and a granitoid group. The syenitic plutons are somewhat north of the monzodioritic intrusions, whereas the granitoid plutons are interspersed with the monzodiorites. Although these groups differ in mineralogy, they are all similar in terms of size, texture, map pattern, geochemistry (e.g., high Ba and Sr), aeromagnetic signature, and timing of emplacement All of the alkalic plutons have porphyritic textures, and the syenitic and monzodioritic plutons typically contain abrupt phase transitions from predominantly mesocratic, porphyritic rocks to dark-green pyroxenites and pink felsic differentiates. The granitoid plutons are more uniform in composition and texture.

The plutons are eroded to various levels. The northeastward-elongation and en-echelon map pattern of the Gheen and Lost Lake plutons and the eastern Side Lake pluton and its satellites indicate exposure at high levels, whereas the broad, rounded map shapes of the Linden, Coon Lake, and Bello Lake plutons indicate a deeper level of erosion. The map patterns of the relatively well exposed Side Lake, Idington, and Lost Lake plutons indicate a similar style of emplacement, in which the plutons have penetrated the supracrustal rocks to different levels. The Side Lake pluton plunges to the west, as indicated by the deeper level of erosion at the western end of the pluton and the west-plunging linear trachytic fabrics in the Side Lake satellites. This westward plunge may be either a primary emplacement feature or the result of tilting of the pluton prior to unroofing.

Several other plutons of alkalic affinity are suggested by the aeromagnetic data, but they are not exposed and their existence has not been verified by drilling.

ACKNOWLEDGMENTS

Field work and geochemical analyses for this project were funded by the Minerals Diversification Program administered by the Minerals .Coordinating Committee for the Minnesota Legislature. The Minerals Division of the Minnesota Natural Resources Research Institute (also supported by the Minerals Diversification Program) coordinated the analytical work for several of the geochemical samples.

FIELD TRIP STOPS

These stop descriptions are brief – see introductory section for more detail about the individual plutons.

Directions: To stop 1: Drive west on Highway 169 to Highway 5 at Chisholm • go ~15 miles north on Hwy. 5 to road 915/McCarthy Beach road the •go west on McCarthy Beach road between Side and Sturgeon Lakes, this turns into Link Lake trail—stay on for a total of ~7 miles to small trail (491988, 5283636) • walk SW on trail ~ 1000' / 300m and go W-SW to ridge where there are some peeled outcrops. Work your way back NE along top of ridge for more outcrop back to road.

Stop 1. (**NAD83: 491723, 5283344) (47.70606°, -93.10680°)** Side Lake pluton – multiphase Side Lake Pluton ultramafic to felsic.

NEXT: Head back east on Link Lake Trail • at about one mile turn left on Beatrice Lake road at sharp bend in trail. • Take Beatrice Lake road ~1.7 miles to intersection with Snake Trail and turn right. • Follow Snake Trail ~2.5 miles to Hwy. 5. • Go right/south on Hwy. 5 for ~1.8 miles. • Go left on Hwy. 65/Perch Lake road for 1.7 miles then • take a left / north on Dean Forest Road (268). • Follow Dean Forest Road (276) ~4.6 miles through a series of jogs to a small road on the right / south (Mud Hole Road # 276). • Drive ~500 feet and park next to knob on the west side of the road (504781, 5284935), go up on outcrop knob to east. Multiple peels.

Stop 2. (NAD83: 504781, 5284935) (47.71778°, -92.93625°) Roof zone of Side Lake Pluton. Many dikes of multiphase monzonitic rocks cut high-grade garnet-staurolite-sillimanite bearing metasedimentary rocks of the Lake Vermilion Formation. Some dikes may be unrelated tonalite. One smaller outcrop near road along south edge of knob has 3-5 x 7-15 cm mafic enclaves in quartz tonalite to monzonite. This lies in what is interpreted as the roof zone of the Side Lake Pluton.

NEXT: Go back to road # 276 • turn right / east and drive ~3.4 miles to Highway 73. • Turn left / north on Hwy 73 for 4 miles to Hwy. 22 • turn left / west for 3 miles to road 931. • Turn left / south on 931 for 0.5 miles to crest of small hill, outcrop in the east side of road.

Stop 3. ***Private Property please be respectful*** (**NAD83: 504882, 5290921) (47.77164°, -92.93484°)** Morcom Pluton – Monzdioritic intrusive breccia of widely variable grain size bearing many inclusions of different phases of itself that range from intermediate-porphyritic to ultramafic. One thin section was made from this outcrop and in it the mafic phase is dominantly hornblende, in contrast to samples from other parts of the pluton which contain abundant green Na-pyroxene in addition to hornblende. Sphene, magnetite, and apatite are also relatively abundant.
This pluton is not well exposed with only a few outcrops in this vicinity on the east end and a drill hole on the west end; extent outlined via aeromag data.

NEXT: Head back east to Hwy. 73 • turn left / north for 5 miles to Highway 1 • Turn left / west on Hwy. 1 for 3.4 miles to large outcrop ridge and find a safe place to park...

Stop 4. Linden Pluton **(NAD83: 504222, 5301045) (47.86273°, -92.94355°)** ***(2681.00±0.29 Ma)*** Brownish-pink medium- to coarse-grained, strongly foliated, moderately porphyritic pyroxene syenite. Tabular crystals of gray perthite and prismatic dark green pyroxene phenocryst are surrounded by a pink groundmass composed mainly of fine granular albitic plagioclase. The foliation (and weak subvertical lineation), interpreted as magmatic, is defined by the phenocrysts of microcline and

pyroxene, and dips steeply to the northwest parallel to the pluton margin. The syenite also contains cm-scale ellipsoidal ultramafic pyroxenite enclaves that are flattened parallel to the main foliation. Dominantly composed of perthitic alkali feldspar, albitic plagioclase, and dark-green prismatic aegirine-augite ($Ac_7Wo_{41}En_{26}Fs_{25}$, Table 5-3 and Fig. 5-7), with lesser amounts of sphene, apatite, biotite, hornblende, magnetite, and epidote. Relatively coarse reddish-brown titanite/sphene is readily visible in hand sample. Plagioclase is generally restricted to the groundmass as very fine-grained granoblastic grains.

In thin section the pyroxene is very fresh, bright green, sub-euhedral, and weakly zoned with roundish lighter green cores. Sphene forms small euhedral crystals, apatite forms thick irregular to subprismatic crystals, and minor proportions of biotite form strongly pleochroic light brown to deep brownish-green irregular books commonly intergrown with or included in pyroxene. Strongly aligned perthitic orthoclase forms blocky-rectangular crystals up to 7mm in length that are commonly Carlsbad-twinned. The groundmass matrix between the orthoclase and pyroxene is composed of fine-grained granoblastic feldspar that appears to have undergone brittle deformation; however within this granulated matrix are pristine pyroxene, sphene, and apatite crystals that show no evidence of shearing or rotation. This coupled with the apparent lack of shear bands on the outcrop implies that the granulation of the groundmass may have occurred during emplacement by semi-plastic deformation during upward flowage of the magma.

Just north of the highway at the lowermost east end of this outcrop is an old adit that goes straight into the hillside; not sure as to when or why this was made.

NEXT: Head back east on Hwy. 1 to Hwy. 73 • turn left / north for 5.2 miles to Highway 53. • Hang a right (go SW) on Hwy. 53 for 2 miles to where there are outcrops on the northeast side of the road. There is a driveway adjacent to this outcrop (on the north end) that would be a good place to park.

Stop 5. **********WATCH OUT FOR TRAFFIC THIS IS A BUSY ROAD**********
Gheen Pluton **(NAD83: 515162, 5306034) (47.90745°, -92.79711°)**

The Gheen pluton is a spectacular example of multi-phase magma mingling textures. Strongly and coarsely porphyritic pyroxene syenite grades into, is cut by, and has inclusions of, medium-grained dark green hornblende gabbro to pyroxenite. Pink aplite and pegmatite forms the latest phase as small dikes that cross the other phases, and seems to have preferentially permeated the more mafic phases. Bluish chloritic slickenside surfaces look similar to those in the Linden pluton.

The phenocrysts in the porphyritic phase at this stop are composed of braid-textured perthite to antiperthite in a matrix of bluish-green hornblende and prismatic actinolitic amphibole, abundant sphene, magnetite, and apatite, and anhedral to subpoikilitic saussuritized plagioclase. The aphyric mafic phases are composed varied combinations of pale green augite magmatic hornblende, secondary actinolitic amphibole, biotite, and accessory sphene, apatite, magnetite, and calcite.

NEXT: Continue southeast on Hwy. 53 for about 14 miles, through the town of Cook, to County Road 467. • Turn left / east for 0.6 miles then veer right to stay on 467. Continue on 467 to railroad crossing; from there go another 0.75 miles to Forest Road 258D • Either drive or walk south on this road for 0.5 mile to an outcrop on the left / east in an overgrown clearcut, next to a logging trail that goes east.

Stop 6. Idington Pluton **(NAD83: 529108, 5287200) (47.73752°, -92.61175°)**

The Idington (eye-ding-ton) pluton as not been dated, but it is intruded by the 2,674-Ma Shannon Lake granite along the southwestern margin of the pluton.
This pluton is characterized by its coarsely porphyritic character as dramatically shown at this stop, and the phenocrysts are typically aligned by magmatic flow (trachytoid) in a crystal mush. In places the phenocrysts are randomly oriented, and in others oriented in a circular fashion that implies they were caught in an eddy. The mafic matrix is composed dominantly of aegirine or aegirine-augite and commonly has been squeezed out (i.e. filter-pressed) of the crystal mush to form small to large (10's of meters) zones of an ultramafic phase. White 'aplite' dikes and some larger segregations cut the syenite and pyroxenite phases; these are interpreted as late residual differentiated melts that were squirted around through the semi-solid pluton.
Very fine, delicate compositional zonation is visible in some of the phenocrysts here at this stop, where the rock is properly weathered.
For a more thorough description of the pluton as a whole refer to the appropriate section of the introduction.
The strikingly porphyritic syenite at this stop is typical of the Idington pluton although the phenocrysts are larger than normal. The phenocrysts are composed of perthite / antiperthite and

NEXT: Go back north to the main road (467) and head east for 2.25 miles then follow road around bend to north (turns into County road 381) • Continue on 381 for 2.75 miles to Highway 1 • Turn right / east on Hwy. 1 for 3.25 miles to County Road 361 • Turn left / north and drive 1.5 miles to a small flat outcrop in the east ditch. There are also outcrops along the road on the way here one can stop at.

Stop 7. Lost Lake Pluton **(NAD83: 537263, 5293105) (47.79023°, -92.50248°)** ***2675.1±0.5 Ma***

The Lost Lake pluton is an irregularly-shaped intrusion that elongate to the east-northeast.
The small outcrop in the road ditch shows mafic pyroxene-rich enclaves in pink syenitic phase. Outcrops nearby in the woods to the east demonstrate many different phases ranging from uniform pink to coarsely porphyritic to dark green and ultramafic.
The ultramafic phases/enclaves in the road ditch outcrop are composed primarily of deep green (in thin section) aegirine as small equant to subprismatic crystals, a lesser proportion of larger blocky to subpoikitic biotite, and accessory sphene and apatite in a groundmass of poikilitic calcite (it fizzes) and minor sodic plagioclase. The pink portion is composed of allotriomorphic-granular mosaic of anhedral sodic plagioclase, perthite to antiperthite (commonly poikilitic), prismatic green aegirine, apatite, biotite, and interstitial calcite.
At this stop we also will display some drill core from the Lost Lake pluton which demonstrates the multiple phases and diversity within this unit.

NEXT: End of trip. Go back south to Highway 1 then east to Highway 169, then south back to Mountain Iron. Thank you for attending.

REFERENCES CITED

Arth, J.G., and Hanson, G.N., 1975, Geochemistry and origin of the early Precambrian crust of northeastern Minnesota: Geochimica et Cosmochimica Acta, v. 39, p. 325-362.

Barker, J.G., and Arth, J.G., 1976, Generation of trondhjemite-tonalite liquids and Archean bimodal trondhjemite-basalt suites, Geology, v. 4, p. 596-600.

Beck, J.W., 1988, Implications for Early Proterozoic tectonics and the origin of continental flood basalts, based on combined trace element and neodymium/strontium isotopic studies of mafic igneous rocks of the Penokean Lake Superior belt, Minnesota, Wisconsin, and Michigan: Unpublished Ph.D. dissertation, University of Minnesota, Minneapolis.

Boerboom, T.J., Jirsa, **M.A.,** Southwick, D.L., Meints, J.P., and Campbell, F.K., 1989, Scientific core drilling in parts of Koochiching, Itasca, and Beltrami Counties, north-central Minnesota, 1987-1989: Summary of lithological, geochemical, and geophysical results: Minnesota Geological Survey Information Circular 26, 159 p.

Boerboom, T.J., and Zartman, R.E., 1993, Geology, geochemistry, and geochronology of the central Giants Range Batholith, northeastern Minnesota: Canadian Journal of Earth Sciences, v. 30, p. 2510-2522.

Boerboom, T.J., Block, Amy Radakovich, Jirsa, M.A., Chandler, V.W., and Peterson, D.M., 2022, Bedrock Geology, pl. 2 of Jirsa, M.A., project manager, Geologic Atlas of Lake County, Minnesota: Minnesota Geological Survey County Atlas C-54, pt. A, 6 pls., scale 1:200,000

Card, K.D., and Ciesielski, A., 1986, **DNAG** #1. Subdivisions of the Superior Province of the Canadian Shield: Geoscience Canada, v. 13, p. 5-13.

Catanzaro, E.J., and Hanson, G.N., 1971, U-Pb ages for sphene in northeastern Minnesota-northwestern Ontario: Canadian Journal of Earth Sciences, v. 8, p. 1319-1324.

Chamberlain, K.R., Boerboom, T.J, and Bleeker, W., 2015: 2070 Ma dyke of southern Superior Province: a test of the radiating dyke model for the Kenora-Kabetogama/Fort Frances swarm, *in* Reconstruction of supercontinents back to 2.7 Ga using the large igneous province (LIP) record: with implications for mineral deposit targeting, hydrocarbon resource exploration, and earth system evolution; Supercontinent.org report number A194, 9 p.

Chandler, V.W., 1991, Aeromagnetic map of Minnesota: Minnesota Geological Survey State Map Series S-17, scale 1:500,000.

Deer, W.A., Howie, R.A., and Zussman, J, 1966, An introduction to the rock-forming minerals: London, Longman Group Limited, 528 p.

Geldon, A.L., 1972, Petrology of the larnprophyre pluton near Dead River, *in* Sims, P.K., and Morey, G.B., eds., Geology of Minnesota: A centennial volume: Minnesota Geological Survey, p. 153-159.

Himmelberg, G.R., 1973, Geologic descriptions of drill core from greenstone belts in northeastern Minnesota: Minnesota Geological Survey Open-File Report

Irvine, T.N., and Baragar, W.R.A., 1971, A guide to the chemical classification of the common volcanic rocks: Canadian Journal of Earth Sciences, v. 8, p. 523-548.

Jirsa, M.A., 1990, Bedrock geologic map of northeastern Itasca County, Minnesota: Minnesota Geological Survey Miscellaneous Map M-68, scale 1:48,000.

Jirsa, **M.A.,** and Boerboom, T.J., 1990, Bedrock geologic map of parts of Koochiching, Itasca, and Beltrami Counties, north-central Minnesota: Minnesota Geological Survey Miscellaneous Map series M-67, scale 1:250,000 /

Jirsa, **M.A.,** Boerboom, T.J., Chandler, **V.W.,** and McSwiggen, P.L., 1991, Bedrock geologic map of the Cook to Side Lake area, St. Louis and Itasca Counties, Minnesota: Minnesota Geological Survey Miscellaneous Map Series M-75, scale 1:48,000.

Jirsa, **M.A.,** Southwick, D.L., and Boerboom, T.J., 1992, Structural evolution of Archean rocks in the western Wawa subprovince Minnesota: Refolding of pre- cleavage nappes during D_2 transpression: Canadian Journal of Earth Sciences, v. 29, p. 2146-2155.

Martin, D.P., Meyer, G.N., Lawler, T.L., Chandler, V.W., and Malmquist, K.L., 1988, Regional survey of buried glacial drift geochemistry over Archean terrane in northern Minnesota: Minnesota Department of Natural Resources, Division of Minerals Report 252, v. 1, 74 p.; v. 2, 386 p.

Meints, J.P., Jirsa, **M.A.,** Chandler, **V.W.,** and Miller, J.D., Jr., 1993, Scientific core drilling in parts of Itasca, St. Louis, and Lake Counties, northeastern Minnesota, 1989-1991: Summary of lithologic, geochemical, and geophysical results: Minnesota Geological Survey Information Circular 37, 159 p.

Mills, SJ., Southwick, D.L., and Meyer, G.N., 1987, Scientific core drilling in north-central Minnesota: Summary of 1986 lithologic and geochemical results: Minnesota Geological Survey Information Circular 24, 48 p.

Prince, L.A., and Hanson, G.N., 1972, Rb-Sr isochron ages for the Giants Range granite, northeastern Minnesota: Geological Society of America Memoir 135, p. 217-225.

Ruotsala, A.P., and Tufford, S.P., 1965, Chemical analyses of igneous rocks: Minnesota Geological Survey Information Circular 2, 87 p.

Sage, R.P., 1988a, Geology of carbonatite-alkalic rock complexes in Ontario: ·Poohbah Lake alkalic rock complex, district of Rainy River: Ontario Geological Survey Study 48, 68 p.

Sage, R.P., 1988b, Geology of carbonatite-alkalic rock complexes in Ontario: Sturgeon Narrows and Squaw Lake alkalic rock complexes, district of Thunder Bay: Ontario Geological Survey Study 49, 117 p.

Sage, R.P., 1988c, Geology of carbonatite-alkalic rock complexes in Ontario: Wapikopa Lake alkalic rock complex, district of Kenora: Ontario Geological Survey Study 52, 63 p.

Schmitz, M.D., Bowring, S.A., Southwick, D.L., Boerboom, T.J., and Wirth, K.R., 2006, High-precision U-Pb geochronology in the Minnesota River Valley subprovince and its bearing on the Neoarchean to Paleoproterozoic evolution of the southern Superior Province: Geological Society of America Bulletin, v. 118, p. 82-93.

Sims, P.K., and Mudrey, M.G., Jr., 1972, Syenitic plutons and associated lamprophyres: *in* Sims, P.K., and Morey, G.B., eds., Geology of Minnesota: A centennial volume: Minnesota Geological Survey, p. 140-152.

Sims, P.K., Morey, G.B., Ojakangas, R.W., and Viswanathan, S., 1970, Geologic map of Minnesota, Hibbing Sheet: Minnesota Geological Survey, scale 1:250,000.

Sims, P.K., Sinclair, D., and Mudrey, M.G., Jr., 1972, Linden pluton: *in* Sims, P.K., and Morey, G.B., eds., Geology of Minnesota: A centennial volume: Minnesota Geological Survey, p. 160-162.

Southwick, D.L., 1993, Geologic map of Archean bedrock, Soudan to Bigfork area, northern Minnesota: Minnesota Geological Survey Miscellaneous Map Series M-79, scale 1:100,000.

Stern, R.A., Hanson, G.N., and Shirey, S.B., 1989, Petrogenesis of mantle-derived LILE-enriched Archean monzodiorites and trachyandesites (sanukitoids, in southwestern Superior Province: Canadian Journal of Earth Sciences, v. 26, p. 1688-1712.

Streckeisen, A.L., 1973, Plutonic rocks: Classification and nomenclature recommended by the IUGS Subcommission on the Systematics of Igneous Rocks: Geotimes, v. 18, no. 10, p. 26-30.

Wirth, K.R., Vervoort, J.D., and Heaman, L.M., 1995, Nd isotopic constraints on mantle and crustal contributions to 2.08 Ga diabase dykes of the southern Superior Province (abstract), Program & Abstracts for the Third International Dyke Conference, Sept. 4-8, 1995, Jerusalem, Israel, A. Agnon, G. Baer, 84, 1995.

FIELD TRIP 6

Unique Keweenawan Inclusion (Colvin Creek) in the Duluth Complex

Mark Severson (retired)[1,2], Allison Severson[3] and Laurie Severson (retired)[4]

[1](1988–2012) Natural Resources Research Institute, University of Minnesota, Duluth, 5013 Miller Trunk Hwy, Duluth, MN 55811
[2](2013–2018) Previously Teck American, then Teck Resources Unlimited, now NewRange (joint venture between Teck and PolyMet Mining Inc.)
[3]Minnesota Geological Survey, College of Science and Engineering, University of Minnesota, 2609 Territorial Road, St. Paul, MN 55114
[4]Earth Science Teacher, Woodland Middle School, ISD 709, Duluth, MN 55811

In memory of Richard Patelke

1957-2011



"Well, it ain't my truck"

INTRODUCTION

Magnetic basalt inclusions within the Duluth Complex were first described by Bonnichsen (1974). Most of that description pertained to limited outcrops in what is now informally referred to as the South Colvin Creek Hornfels (Fig.6-1). Later, Tyson (1976) looked at four basalt inclusions including three non-magnetic basalt inclusions in railroad cuts to the north, as well as the South Colvin Creek Hornfels. He concluded that the South Colvin Creek Hornfels was different and theorized that the magnetic basalts were derived from weathered and oxidized basalt flows, correlative with the North Shore Volcanic Group, and metamorphosed by the Duluth Complex. This field trip will visit the North Colvin Creek Hornfels (NCCH), shown in Figure 6-1, which is better exposed, contains several internal mappable units, and was first described by Severson and Hauck (1990). There they found a unique very fine-grained and cross-bedded unit, of gabbroic composition, within the inclusion. They initially theorized that the NCCH was formed as a result of magmatic currents (a concept they no longer support). It was also theorized that the cross-bedded unit represents a portion of a shear zone (Ojakangas and Holst, pers. com., sited in Patelke (1996)). This theory is also no longer deemed viable. Lastly, Patelke (1996) mapped and described the NCCH in more detail and proposed that it was an inclusion containing both metavolcanic and metasedimentary rocks that can be correlated with the North Shore Volcanic Group. This field trip will visit the NCCH which is referred to simply as the Colvin Creek Inclusion for the remainder of this guide. The thesis by *Patelke (1996) is the source of almost all of this guide.*

GEOLOGIC SETTING

The Colvin Creek inclusion is a large inclusion (2,500 X 800 meters), associated with a magnetic high, that has been rotated to a near vertical position and exhibits stratigraphic tops to the northwest as defined by pipe amygdules, sheeted amygdules, local convoluted flow bases and flow tops, and cross-bedding. Patelke (1996) subdivided the inclusion into five major mappable units that include: two granoblastic, fine-grained metavolcanic units; two gabbroic sill units that bound the inclusion on the north and south; and a 350-meter-thick, cross-bedded, granoblastic, fine-grained metasedimentary unit of gabbroic composition. Overall, the inclusion strikes about N60°E with dips of 70-90° to the northwest. The entire inclusion has been metamorphosed to pyroxene grade facies and rotated to a subvertical position by the Duluth Complex. According to Miller and Severson (2005), the Colvin Creek inclusion is situated near the bottom of a “heterogeneous upper troctolitic cumulate” of the Partridge River intrusion (PRI).

Geochemical work by Patelke (1996) indicate that metamorphism of the magnetic metabasalt units was isochemical and that they are probably equivalent to intermediate olivine tholeiites of the North Shore Volcanic Group (NSVG). The metasedimentary rocks are more problematic in that they are not analogous to any of the interflow sandstones of the NSVG as described by Jirsa (1980, 1984). At about 350 meters thick they are as thick as the total measured section of the NSVG interflow sedimentary rocks and show: no rock fragments; NO quartz, no conglomeratic horizons, and no intercalated volcanic rocks. Patelke (1996) suggested that the cross-bedded rocks were most likely deposited in a restricted basin as an eolian sediment that was derived from a strictly basaltic terrain – thus no quartz. Similar inclusions of cross-bedded sediments with a gabbroic composition have been found at six locations within the Duluth Complex (i.e., geologic maps of the Babbitt SE and Babbitt SW quadrangles). Patelke (1996) thought that the informal “Phantom Lake sandstone,” an inclusion in the Whyte Quadrangle to the north of Two Harbors, was the most similar to the sediments in the Colvin Creek inclusion. While Patelke (1996) felt that these two units were similar, he concluded that neither of them can be strictly correlated with any other of the interflow sandstones in the Keweenawan system.

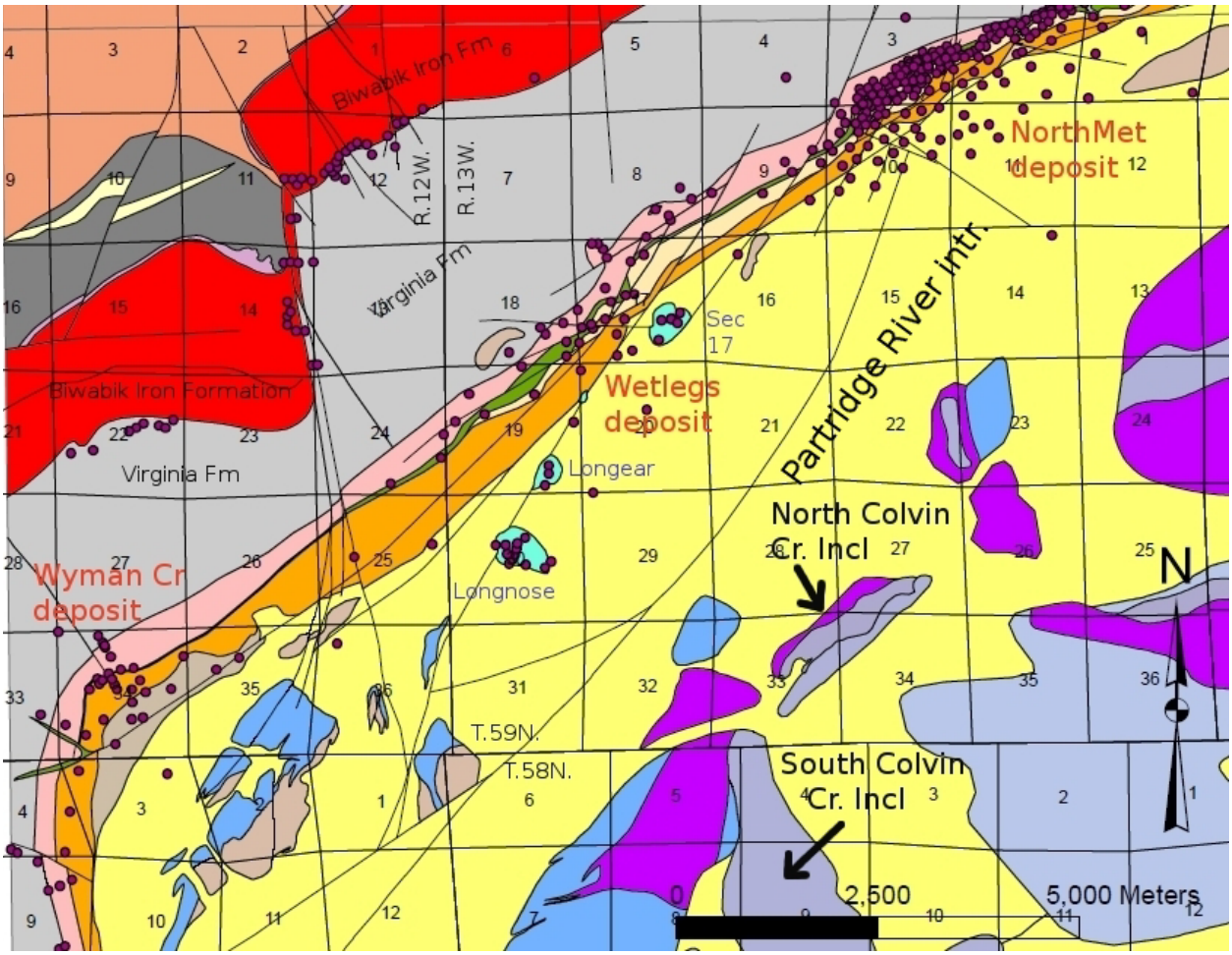


Figure 6-1. Generalized geologic map of a portion of the Partridge River intrusion showing locations of the Colvin Creek Hornfels inclusions (gray) relative to the known Cu-Ni deposits. Base map from Miller and others (2001).

GEOLOGY OF THE COLVIN CREEK INCLUSION

Patelke (1996) mapped six major units associated with the Northern Colvin Creek Hornfels inclusion (exposed in Sections 27, 28, 33, and 34, T.59N., R.13W.). These units are briefly described below, and their distribution is shown in the geology map of Figure 6-2. The six units are, from south to north (also stratigraphically younging to the north) labeled as: MCC, AMG, AA, XBB, and GOG. These names are acronyms for field textures observed by Severson and Hauck (1990), and while these are not appropriate rock names, Patelke (1996) retained them in his thesis.

MCC (Massive Colvin Creek unit)

The MCC unit is a plagioclase-augite-oxide (titanomagnetite>ilmenite) rock, with local orthopyroxene and/or olivine, that under Phinney's classification system (1972) is an oxide-bearing gabbro to augite troctolite. The MCC displays a massive, fine- to medium-grained texture similar to the units that stratigraphically overlie it but also shows primary decussate igneous texture. It is variably ophitic, and locally porphyritic. Granoblastic triple point junctions are reasonably well developed where the feldspar is

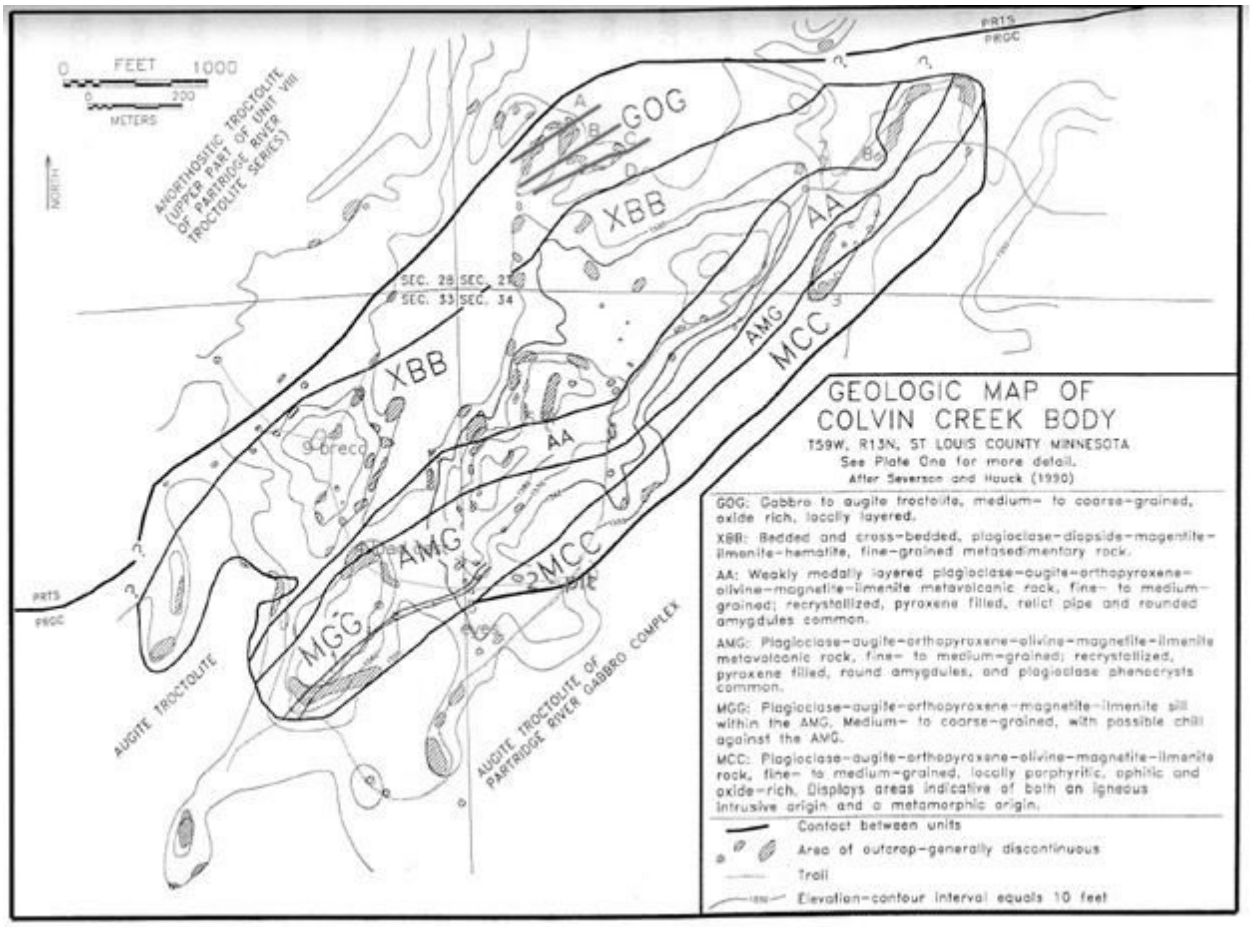


Figure 6-2. Geology of the Northern Colvin Creek inclusion from Patelke, 1996.

equant. Locally, there are ovoid clots of granular plagioclase that could be interpreted as amygdule infillings. The bottom contact of the MCC unit is not exposed. The upper contact with the AMG unit consists of rock types attributable to both MCC and AMG units within a 3-meter zone. For this reason, Patelke (1996) suggests that the MCC was injected sill-like and was mixed into the AMG while both were in a plastic state. Unfortunately, this particular exposure will not be visited during this trip.

AMG (Amygdaloidal Gabbro unit)

The AMG is stratigraphically above the MCC unit and is interpreted to be a subaerial metavolcanic unit with recrystallized amygdules. The rock is classed as an oxide melagabbro to augite troctolite. In the vast majority of the exposures, it is fine- to medium-grained and composed of plagioclase, augite, and oxide (titanomagnetite>ilmenite) with local orthopyroxene and poikilitic olivine. The AMG unit shows a persistent fine-grained, polygonal-granoblastic, sugary texture. In a few instances this texture is interrupted by clusters of plagioclase and by rounded to amoeboidal clot-like segregations of augite; both of which are lengthened parallel to the overall strike of bedding. These layers of pyroxene-rich segregations are interpreted to be recrystallized amygdules within relict volcanic flowtops. In areas of outcrop with common pyroxene-rich layers, the spacing of layers indicates flow thicknesses of 0.5 to 3.5 meters. The upper contact with the AA unit is exposed in only one outcrop (Fig. 6-3 - not visited this trip) wherein a black pyroxene-magnetite rich convoluted flowtop of the AMG is overlain by the base of a flow in the AA unit.



Figure 6-3. Contact between the AMG (bottom, dark) and AA (top, light) units. The dark portion of the image is related to increased pyroxene and oxide content and interpreted to be a rubbly flow top that is abruptly overlain by the AA unit.

MGC (Medium-Grained Gabbro unit)

The MGC is a sill of very limited extent in the SW end of the Colvin Creek inclusion (Fig. 6-2). The rock is a medium- to coarse-grained orthopyroxene-bearing anorthositic gabbro according to the classification system of Phinney (1972). The sill crosscuts only the AMG unit, exhibits apparent chilled margins, and is estimated to be about two meters thick. Exposures of this unit will not be visited.

AA (Amoeboidal Augite unit)

The AA unit overlies the AMG unit and is also a fine- to medium-grained, massive, granoblastic magnetic basalt unit. At the outcrop scale, the AA is distinguished from the AMG by increased amounts pyroxene-filled avoids (amygdules) and by elongate pyroxene segregations that are interpreted as recrystallized pipe amygdules. Petrographically, the AA and AMG are very similar. Mineralogy consists of plagioclase, diopsidic augite, and titanomagnetite>ilmenite with local orthopyroxene (a major constituent in one outcrop). Plagioclase has a bimodal grain distribution consisting of fine-grained equant to stubby grains (0.25-1 mm) and patchy distributed laths (2-7 mm).

The modal layering within this unit is defined by pyroxene stringers and ovoid clots that are interpreted to define both lava flow bases and amygdaloidal tops. Individual flows range from 0.5 to several meters thick. Elongate pyroxene masses lying perpendicular to strike are thought to be recrystallized pipe amygdules near the flow base (Fig. 6-4).



Figure 6-4. Two flow units in the AA unit. Base of a single flow (6 inches to left of hammer head) with recrystallized, coalescing upward-trending pipe vesicles. Black wavy lines in extreme upper right of photo is the base of a third lava flow. The location of this outcrop is not documented.

"Pyroxene interval"

At the very top of the AA unit is a 0-2 meter thick, black, melagabbro unit, or "pyroxene interval" as mapped by Patelke (1996) in a few scattered outcrops. This unit consists of fine- to coarse-grained ferrosalite pyroxene and plagioclase. At one locality this unit contains: 1-10% brown garnet, 2-5% ilmenite>>titanomagnetite, and trace amounts of cordierite and hercynite. At one exposure (Fig. 6-5 – to be visited), there are several "veins" of potassium feldspar masses (up to 20-40 cm long by 1-10 cm wide), or tension gashes according to Patelke (1996). These "veins" are perpendicular to, and truncated by, the upper contact with the overlying XBB unit. The base of the XBB unit often exhibits a trough-like morphology downwards towards these feldspar masses. At several locations where this "pyroxene interval" is present, Patelke (1996) thought that there was some evidence of left-lateral tectonic movement. The tension gashes are one of his lines of evidence. Overall, Patelke (1996) thought that the "pyroxene interval" represents a deeply weathered flow top or soil developed on the AA unit and the effects of faulting are secondary.

At another outcrop along the contact between the AA and XBB units (Stop 5 - to be visited), the "pyroxene interval" is absent. In its place are several sigmoidal-shaped pyroxene-rich lenses. Patelke (1996) thought that these lenses were developed along a bedding parallel fault.



Figure 6-5. "Pyroxene Interval" (bottom 2/3rds of photo) between the AA and XBB units. Note convolute contact and k-spar-filled "tension gashes" as described by Patelke (1996).



Figure 6-6. Typical cross-bedding exhibited by the XBB unit in a flat-laying outcrop.

XBB (Cross-Bedded Belt)

To the north of, and overlying the magnetic basalt units, is the Cross-Bedded Belt unit of roughly gabbroic composition. The rock is composed of fine-grained (1mm average) plagioclase-diopside-orthopyroxene-titanomagnetite>ilmenite with minor amount of orthopyroxene, hematite, hercynite, and geikielite. The rock exhibits beautiful bedding, cross-bedding (Fig. 6-6), density graded modal layering, and concave upward cross-beds along with scour and fill structures. Throughout the unit are localized minor biotite. There are several intervals, 0.5-3.0 meters thick, that are located near the base of the XBB that contain poikiloblastic pyroxene, up to several inches long (Fig. 6-7) that appear to have grown along bedding planes.

The density graded modal layering consists of oxide- and pyroxene-rich basal layers grading upward into plagioclase-rich layers. Grain size for any individual mineral (1 mm) remains constant throughout the bed thickness. Angles of bedding and cross-bedding change over short distances in most outcrops. In some areas, the bedding exhibits a weak convolution or deformation (Fig. 6-7); possibly due to either soft sediment deformation and/or partial melting by the Duluth Complex.

GOG (Gabbro-Olivine Gabbro unit)

A gabbro to olivine gabbro unit, labelled as GOG, bounds the Colvin Creek inclusion at its upper (northwest) contact. The GOG was classed as a unit of the inclusion because it contains contact parallel layering (as does the inclusion) and shares strike-length and general tabular form with the other units of the inclusion. The GOG is medium to coarse-grained and composed of plagioclase (37-72%), augite (9-42%), olivine (0-23%), ilmenite (3-12%), and titanomagnetite (2-8%).

The GOG unit is best exposed at the northwest end of the Colvin Creek inclusion where four contact-parallel zones were described by Severson and Hauck (1990) and by Patelke (1996). These zones (Fig. 6-2) are: A. weakly modally layered granular-textured augite troctolite zone with a plagioclase foliation B. phenocryst-rich gabbroic zone with anorthositic inclusions up to 5 inches across; C. a zone of heterogeneous gabbroic rocks with local inch-scale layering and cross-bedding (Fig. 6-8) indicative of magmatic currents; and D. a zone of anorthositic gabbro grading upward to gabbro with olivine gabbro interbeds. The trend of all of these zones parallel the contact trends of the underlying Colvin Creek inclusion. Unfortunately, this unit is too far away to bushwhack to gain access and visit during this trip.



Figure 6-7. Poikiloblastic pyroxene (black squares) in XBB unit. Note strange convolutions of bedding.



Figure 6-8. Rhythmic layering in GOG unit (subzone C) consisting of alternating olivine-rich and olivine-poor layers. Upper massive gabbro (hammer) truncates bed sets.

Common Characteristics of Colvin Creek Hornfels

Listed below are characteristics common to all rock types of the Colvin Creek Hornfels:

- All of the units are strongly magnetic and microscopically exhibit polygonal/granoblastic triple point junctions
- Thin veins and later pods of pyroxene and/or massive magnetite are locally common. They are arranged in both parallel sets and discontinuous cross-cutting stringers
- Thin, brown hornblende and/or orthopyroxene rims around titanomagnetite are commonly seen in thin-section
- Sericitized plagioclase is seldom seen
- Olivine, where present, is usually fresh and never serpentinized
- Biotite is generally absent except in the XBB just above the "pyroxene interval"
- The titanomagnetite is titanium-rich and the ilmenites are magnesium-rich.

FIELD TRIP STOPS

Access starting from Mountain Iron will be heading south on Highway 53 through Virginia. Shortly after crossing the Tony Rukavina Bridge, over the Rouchleau Mine, turn and head east on Road 135 through the towns of Gilbert, Biwabik, and Aurora. Within Aurora, turn right at the stop sign and head south on CSAH 100, cross the railroad tracks, proceed to a stop sign and turn left on CSAH 110. Proceed to Hoyt Lakes on this highway. Within Hoyt Lakes continue straight through two stop signs and head out of town on Highway 110 (also called Skibo Vista Road). for about 4 miles. Just after passing the Bird Lake Recreation area, turn left onto road UT9235 (also called 569/Skibo Rd). Proceed down this road about 2.7 miles, cross the railroad tracks and continue east for another 1.9 miles. Turn left (north) on **forest road 113** (yellow "share the road" sign at this intersection). Go 5.9 miles **north on 113** to an unmarked logging road (another yellow "share the road" sign at this intersection). Turn left on unmarked logging road (Figure 6-9) and head west about 1.5 miles depending on road conditions. Turn vehicles around, park as best as possible, and walk about 0.2 miles to the west (through an old beaver pond) to the first stop. Locations of the trip stops are shown in Figures 6-9 and 6-10.

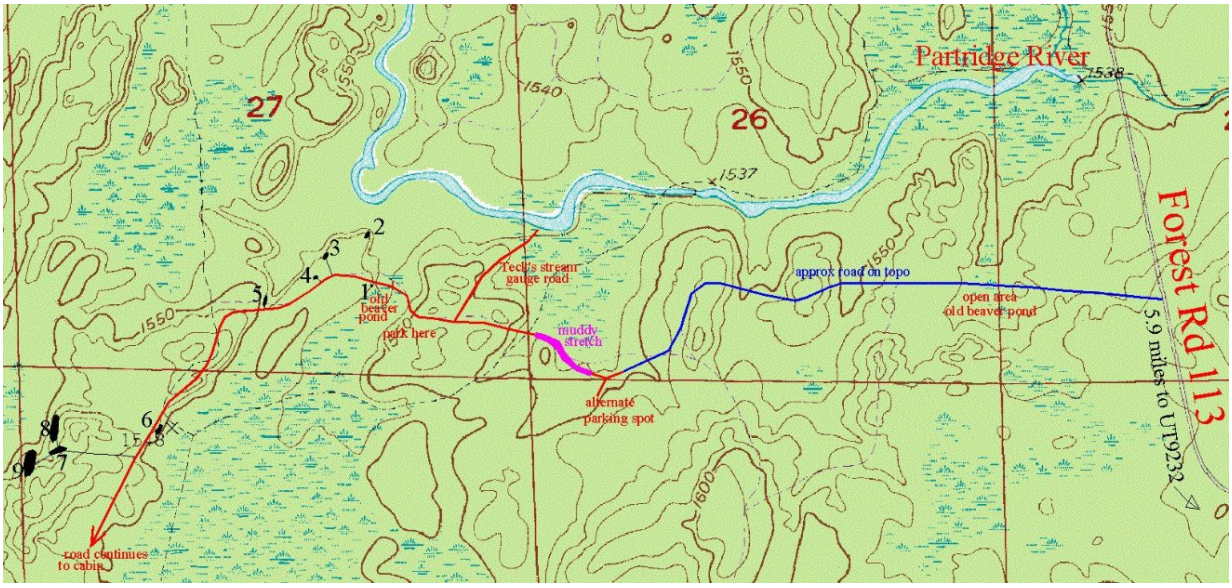


Figure 6-9. Access to Colvin Creek hornfels area and trip stops via remote logging road.

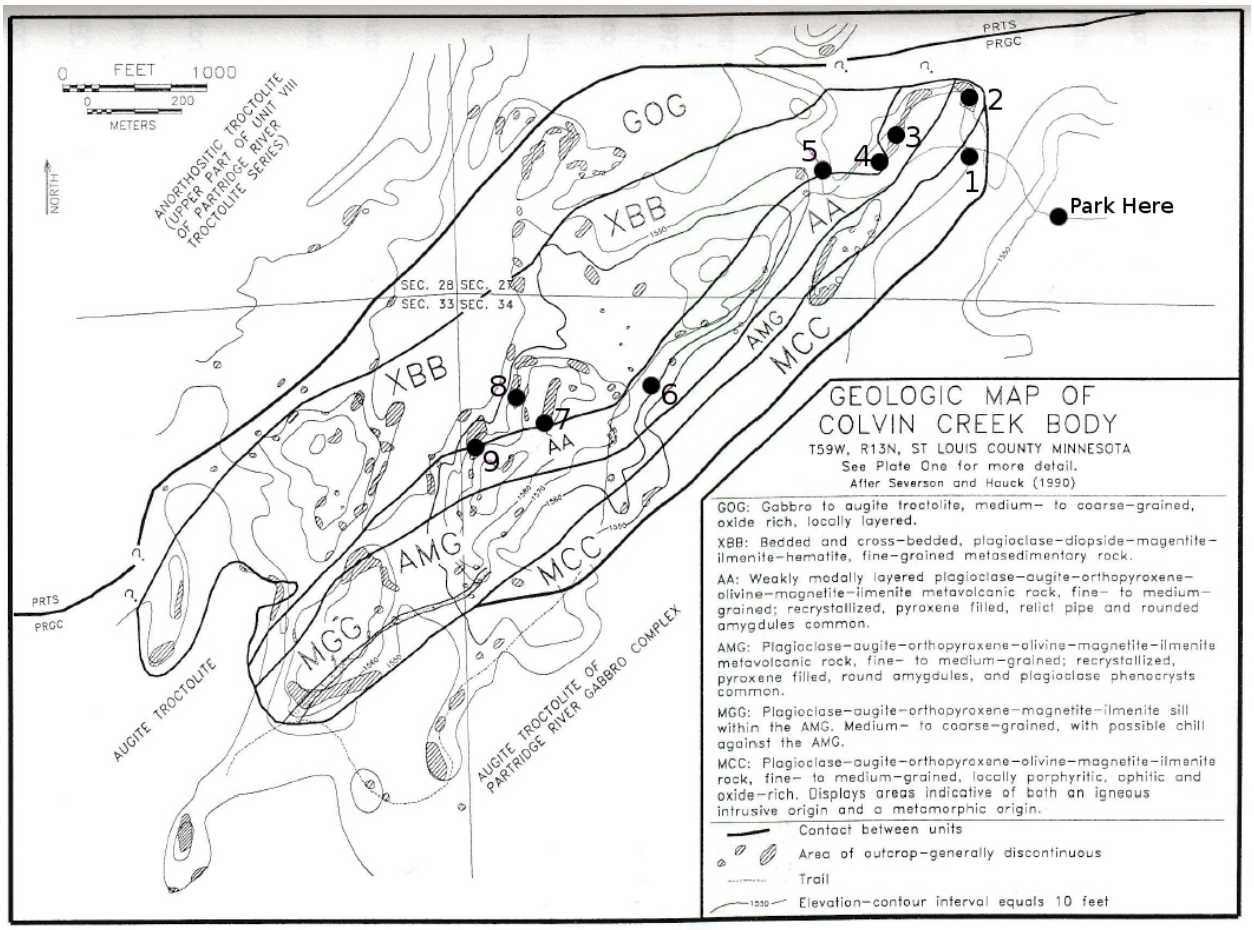


Figure 6-10. Field trip stops (black dots) relative to mapped geology (modified from Patelke, 1996).

Stop 1: **MCC (Massive Colvin Creek unit) (NAD83: 577246E/5268002N) (47.56084°, -91.97315°)**

The MCC unit at this exposure is enigmatic. The rock is massive, lacks modal layering and regular concentrations of minerals. It is classed as a gabbro to augite troctolite composed of plagioclase, augite, orthopyroxene, olivine, and oxide (titanomagnetite>ilmenite). It is fine- to medium-grained with granoblastic triple point junctions. Locally, there are clots of granular plagioclase that could be interpreted as amygdule infillings, as in the overlying basaltic units. However, the MCC also displays primary decussate igneous textures, is variably ophitic, and locally porphyritic. For this reason, the distinction between the MCC and overlying AMG are often unclear. Patelke (1996) felt that the portions of the MCC were injected sill-like into the base of the inclusion while they were both in a plastic state.

Directions: Continue down the road for about 2 minutes to a flagged trail off to the north. Follow the trail for another 5 minutes to Stop 2.

Stop 2: AMG (Amygdaloidal Gabbro unit) (NAD83: 577230E/5268130N) (47.56199°, -91.97334°)

At first glance, the AMG unit at this exposure is similar to the previous stop in that it consists mostly of massive, fine- to medium-grained "oxide gabbro." However, within this exposure are several localized dark-gray, very fine-grained internal patches of basalt, that contain unquestionable plagioclase-filled amygdules. These patches exhibit gradational contacts with the surrounding medium-grained "oxide gabbro." Thus, both fine-grained basalt and medium grained "gabbro" are present here (best seen after peeling a large area of the exposure). It is unknown whether these basalt patches represent true inclusions or are remnant unmetamorphosed patches in a rock that has undergone various degrees of partial melting to produce the "gabbroic" portions.

Directions: Return to fork in flagged trail and continue north a few minutes to Stop 3.

Stop 3: AA (Amoeboidal Augite unit) (NAD83: 577094E/5268083N) (47.56159°, -91.97515°)

The AA unit overlies the AMG unit and is also a fine- to medium-grained, massive, granoblastic magnetic basalt unit. At the outcrop scale, the AA is similar to the AMG except for zones that contain common pyroxene-filled ovoids (recrystallized amygdules) and by pyroxene-rich horizons that are interpreted as sheeted amygdules and/or flow tops. Petrographically, the AA and AMG are very similar. Mineralogy consists of plagioclase, diopsidic augite, and titanomagnetite>ilmenite. Several basalt flows can be distinguished in portions of this outcrop based on massive flows grading upward (northward) into amygdule-rich basalt that in turn grades into pyroxene-rich flow tops. Individual flows range from over several meters to less than one meter thick. Note the presence of a cluster of coarse-grained pyroxene with minor K-spar (similar features will be seen at stop 6).

Directions: Return to road and proceed further west for about 1-2 minutes to another flagged trail leading to the north. The Stop 4 exposure is about 100 feet north of the road on this trail.

Stop 4: XBB Unit (Cross-Bedded Belt) (NAD83: 577065E/5268019N) (47.56101°, -91.97555°)

To the north of, and overlying the magnetic basalt units, is the Cross-Bedded Belt unit of roughly gabbroic composition. This is the first of several exposures of the XBB unit that will be viewed during this trip. The rock is composed of fine-grained (1mm average) plagioclase-diopside-orthopyroxene-titanomagnetite>ilmenite. The rock exhibits beautiful bedding, cross-bedding, density graded modal layering, and concave upward cross-beds along with scour and fill structures. Note that NO quartz has ever been noted in this unit!

There appears to be small-scale convolutions in the bedding trends that may be related to either soft-sediment slump or folding during intrusion of the Duluth Complex and subsequent rotation of the Colvin Creek inclusion. The location of this exposure along a curved mapped contact (Fig. 6-9) suggests that there is a small open fold between the AA and XBB units as suggested by Patelke (1996).

Directions: Return to the road and head 3 minutes to the west to Stop 5 (about 50 feet north of the road).

Stop 5: Contact of XBB and AA units (below photo) **(NAD83: 576907E/5267935N) (47.56028°, -91.97767°)**

Both the AA and XBB units are present in this exposure. At the southern end of the exposure is a massive basalt unit that grades upward (northward) into a rock that contains abundant pyroxene-filled amygdules, which in turn, contains several pyroxene-rich lenses that represent sheeted amygdules and flow tops. Several flows are defined in the outcrop and the contact with the XBB unit is well defined (see Fig. 6-11). The overlying XBB unit consists of a fine-grained gabbroic rock with bedding planes similar to the previous stop but actual cross-bedding is not as striking. In regard to the contact between the two units, the intervening "pyroxene interval" is largely absent except for thin irregular pyroxene-rich lenses that display sigmoidal shapes. Patelke (1996) thought that sigmoidal-shaped pyroxene-rich lenses were developed along a bedding parallel fault with left-lateral movement. At the extreme north end of the exposure is an irregular, cross-cutting, massive oxide vein up to 3 inches wide.



Figure 6-11. Contact between AA (left) and XBB (right) units with very poorly defined "pyroxene interval" in the contact zone. Note sigmoidal shapes of pyroxene layers at the contact. To the left of the contact (not in photo) are 2-3 trough-shaped zones (less than 2x3 feet) that contain bedded sediments similar to the XBB unit. Whether these zones are sedimentary interbeds or enfolded patches is unknown.

Directions: Return to the road and proceed further west for about 10 minutes to Stop 6 on the southern edge of the road. On the way to Stop 6 there are numerous pavement road-crop exposures that consist mostly of massive magnetic basalt with local amygdules.

Stop 6: AA (Amoeboidal Augite Unit) (NAD83: 576560E/5267549N) (47.55684°, -91.98234°)

This outcrop is situated about 2,000 feet down the road from Stop 5 and serves more as a rest and regrouping stop. At this locale, the unit is massive and grades upwards (toward the road) into typical amygdaloidal basalt.

Directions: Proceed down the road 350 feet and follow a flagged trail through the woods for about 840 feet westward (10 minutes).

Stop 7: Contact of XBB & underlying AA unit (NAD83: 576259E/5267482N) (47.55628°, -91.98636°)

This is the best exposure of "pyroxene interval" along the contact (see Figure 6-5 and description in text). Perpendicular to the contact, and wholly within the "pyroxene interval," are at several "vein-like" potassium feldspar veins (up to 20-40 cm long by 1-4 cm wide) and a mass about 4 ft long by 1.5 ft wide. Patelke (1996) felt that the veins are tension gashes formed by lateral movement along the contact. The contact between the XBB and "pyroxene interval" exhibits some folding (soft-sediment?) with small-scale V-shaped troughs projecting downward into the "pyroxene interval." Some of these troughs exhibit truncated bedding of the XBB against the "pyroxene interval" At one of the "V's", biotite, garnet and cordierite have been identified by Patelke (1996). At the extreme east end of the exposure, it appears that a bed of the XBB is folded(?) downward into the "pyroxene interval." Patelke (1996) thought that the "pyroxene interval" represents a deeply weathered flow top or soil developed on the AA unit.

Directions: At the west end of the Stop 7 exposure proceed northward for short distances (<100 feet) to several outstanding outcrops of the XBB unit of Stop 8.

Stop 8: XBB Unit (Cross-Bedded Belt) (NAD83: 576248E/5267546N) (47.55685°, -91.98649°)

Numerous exposures of beautifully cross-bedded XBB unit are present on the top of this hill. The rock is a very fine-grained granoblastic rock with a general modal composition of oxide-bearing anorthositic gabbro to gabbroic anorthosite. It is composed of plagioclase, diopsitic augite, and various iron-titanium-manganese oxides making up to 8-15% of the rock, NO quartz has ever been documented. As shown in Figures 6-6, 6-7 and 6-11, the rock is bedded and cross-bedded, exhibits density graded modal layering, concave upward cross beds, and scour and fill features. Some of the cross-beds show an unusually high angle of repose over very short distances possibly related to the environment of deposit (aeolian).



Figure 6-12. Classic exposure of the XBB unit. Bedding tops to the north (right).

Directions: Return to Stop 7 and proceed west for about 5 minutes to large exposures of the XBB and AA units. Note that between stops 8 and 9 is a glacial erratic of the GOG unit with stupendous inch-scale layering. This erratic is a good example of the GOG unit (otherwise inaccessible on this field trip).

Stop 9: AA (Amoeboidal Augite Unit) (NAD83: 576167E/5267425N) (47.55578°, -91.98759°)

After crossing over a large outcrop of the XBB unit, proceed southward a short distancer to a large tip over exposure (uprooted and wind-fallen tree) of the AA unit consisting of multiple basalt flows with ropey tops. This outcrop is present near the upper contact of the unit and small exposures of the XBB are present to the north and west. Pipe vesicles are present in one small area of the AA unit. Also present is a very small exposure of the "pyroxene interval."

Directions: Return to vehicles. Return to Mountain Iron Community Center (47.51869°, -92.58997°).

References

Bonnichsen, B., 1972, Southern Part of the Duluth Complex. In: Sims, P.K. and Morey, G.B. (eds), Geology of Minnesota – A Centennial Volume, Minnesota Geological Survey, p. 361-388.

Jirsa, M.A., 1980, The Petrology and Tectonic Significance of Interflow Sediments in the North Shore Volcanic Group, Northeastern Minnesota, unpublished M.S. Thesis, University of Minnesota Duluth, 125 pages.

Jirsa, M.A., 1984, Interflow Sedimentary Rocks in the Keweenawan North Shore Volcanic Group, Northeastern Minnesota: Minnesota Geological Survey, Report of Investigations 30, 20 p.

Miller, J.D., Green, J.C., Severson, M.J., Chandler, V.W., and Peterson, D.M., 2001, Geological map of the Duluth Complex and related rocks, Northeastern Minnesota; Minnesota Geological Survey, Miscellaneous Map M119, scale 1:200,000.

Miller, J.D., Jr. and Severson, M.J., 2002, Geology of the Duluth Complex in Miller, J.D., Jr., Green, J.C., Severson, M.J., Chandler, V.W., Hauck, S.A., Peterson, D.M., and Wahl, T.E., 2002a, Geology and mineral potential of the Duluth Complex and related rocks of northeastern Minnesota: Minnesota Geological Survey Report of Investigations RI-58, p. 106-143.

Miller, J.D., Jr. and Severson, M.J., 2004, Geology and Mineralization of the Western Contact of the Duluth Complex, Partridge River and South Kawishiwi intrusions, Northeastern Minnesota: Institute on Lake Superior Geology, 50th Annual Meeting, Duluth, MN, Part II: Field Trip Guidebook, p. 227-258.

Miller, J.D., Jr. and Severson, M.J., 2005,

Patelke, R.L., 1996, The Colvin Creek Body, A Metavolcanic and Metasedimentary Mafic Inclusion in the Keweenawan Duluth Complex, northeastern Minnesota: unpublished M.S. Thesis, University of Minnesota, 232 p.

Phinney, W.C., 1972, Duluth Complex, history and nomenclature, in Sims, P. K., and Morey, G. B., eds., Geology of Minnesota: A Centennial Volume: Minn. Geol. Survey, pp. 333-334.

Severson, M.J., and Hauck, S.A., 1990, Geology, geochemistry, and stratigraphy of a portion of the Partridge River intrusion: Natural Resources Research Institute, University of Minnesota-Duluth, Technical Report, NRRI/GMIN-TR-89-11, 236p. (with plates).

Tyson, R. M., 1976, Hornfelsed Basalts in the Duluth Complex: unpublished M.S. Thesis, Cornell University, Ithaca, New York, 85 p.

FIELD TRIP 7

Classic Outcrops of Northeastern Minnesota

Dean M. Peterson[1] and George J. Hudak[2,3]

[1]*Big Rock Exploration, 2505 W. Superior St., Duluth, MN 55806*
[2]*George Hudak Geosciences P.L.L.C., Duluth, MN 55804*
[3]*Department of Earth and Environmental Sciences, University of Minnesota Twin Cities, 116 Church Street SE, Minneapolis, MN 55455*

Introduction

This field trip will investigate a wide variety of Neoarchean, Paleoproterozoic and Mesoproterozoic rocks that illustrate the diversity of Precambrian rocks in northeastern Minnesota. The field trip is an updated version of "Field Trip 5 – Classic Outcrops of Northeastern Minnesota" that was run during the 50th Annual Meeting of the Institute on Lake Superior Geology that took place in Duluth, Minnesota during May, 2004. As such, several of the field trip stop descriptions in this guidebook are derived from this earlier field trip guide, with updates based on recent geological studies.

Generalized Stratigraphy of Northeastern Minnesota

Neoarchean Vermilion District

Supracrustal rocks in the Vermilion district consist of volcanic-dominated stratigraphic sequences of the Wawa-Abitibi Terrane within the Superior Province of the Canadian Shield. Rocks of the Wawa-Abitibi Terrane in northern Minnesota are divided on the basis of stratigraphic and structural setting into: (1) the Soudan belt, to the south, and (2) the Newton belt, to the north (Jirsa et al., 1992; Southwick et al., 1998). The boundary between these contrasting structural panels can be traced geophysically across the width of Minnesota and was informally designated the Leech Lake structural discontinuity (Jirsa et al., 1992). In the region west and north of the Lake Vermilion State Park, the Leech Lake structural discontinuity occurs along the Mud Creek shear zone (Hudleston et al., 1988), small segments of the Vermilion and Wolf Lake faults (Sims and Southwick, 1985), and the Bear River fault (Jirsa et al., 1992). A simplified regional geological map of the Neo-Archean terranes of northeastern Minnesota and adjacent Ontario is presented in Figure 7-1.

The Soudan belt (Figures 7-1 and 7-2) contains large, broad folds involving calc-alkalic and tholeiitic volcanic strata overlain by, and locally interdigitated with, turbiditic rocks. In contrast, the Newton belt consists of elongate, northeast-trending, and mostly northward-younging volcanic and volcaniclastic sequences. Volcanic rocks of the Newton belt differ from those of the Soudan belt in containing locally abundant komatiitic flows and peridotitic sills. The two belts are fault-bounded, and the relationships between stratigraphic units within each belt are largely conformable (although faults obscure contacts locally). In its eastern extension, the Soudan belt is continuous with the Saganagons assemblage in Ontario and terminates against the Saganaga pluton and Northern Light Gneiss. The Newton belt extends discontinuously eastward into the Shebandowan District of Ontario to form the Greenwater and Burchell assemblages. Intrusive rocks in both belts vary from gabbroic and felsic porphyries demonstrably related to volcanism, to large plutons emplaced post-tectonically. Both districts contain unconformable, Timiskaming-type sequences composed of calc-alkalic volcanic rocks, conglomerates, and finer grained sedimentary rocks.

Lithostratigraphic units in the western Vermilion district (Table 7-1) include: (1) the Lower member, Soudan Iron-Formation member, and Upper member (Upper Ely) of the Ely Greenstone

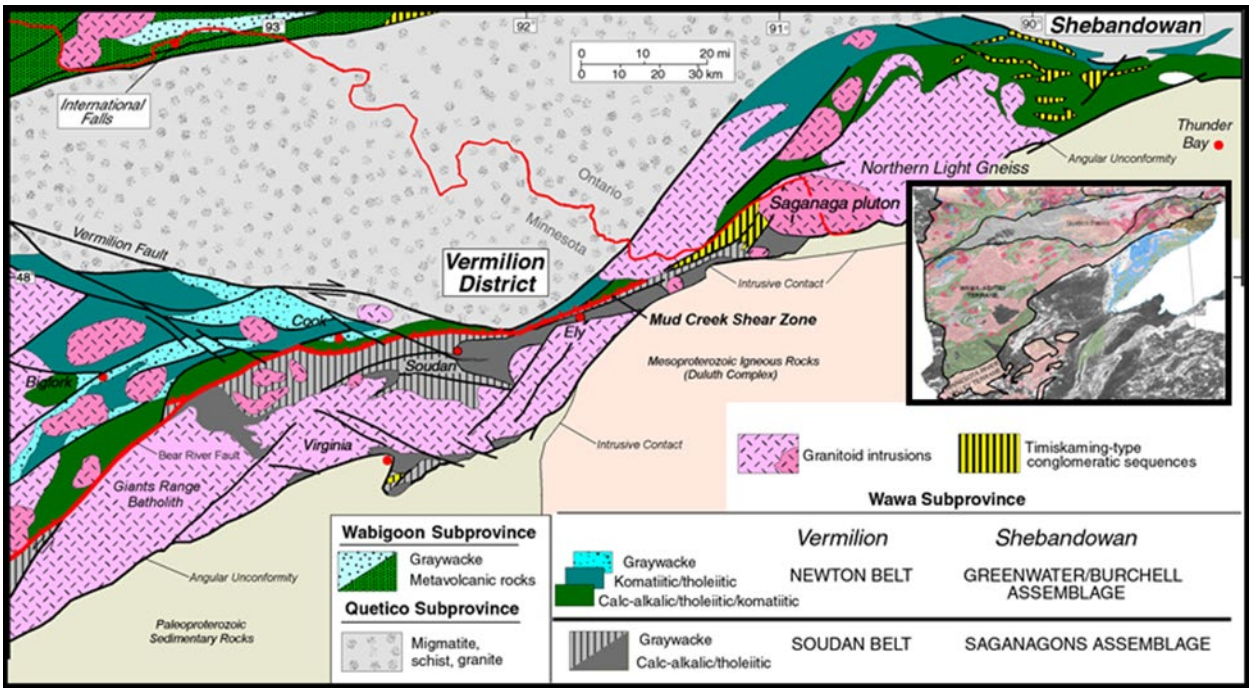


Figure 7-1. Simplified correlation map of Neoarchean assemblages in Minnesota and northwestern Ontario (after Peterson et al., 2001). Inset map illustrates location of the Wawa-Abitibi Terrane in Minnesota and northwestern Ontario (Stott et al., 2007). The Leach Lake structural discontinuity is illustrated in red.

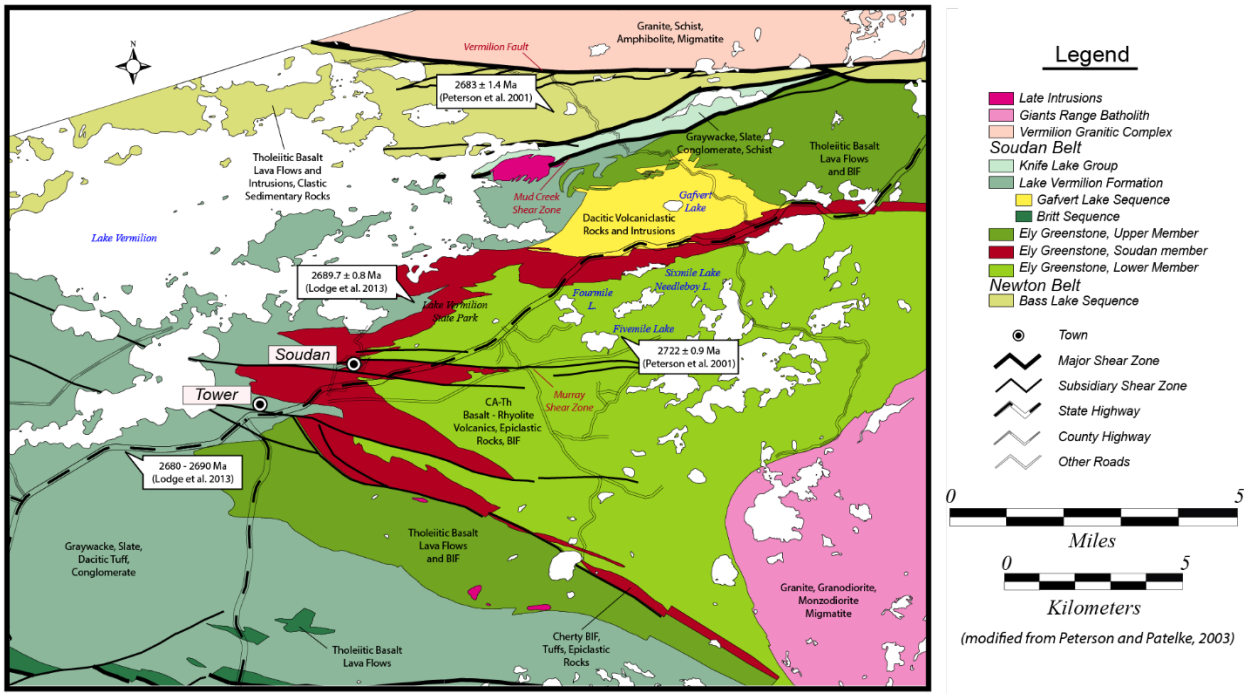


Figure 7-2. Generalized geology and geochronology of the Vermilion District in the vicinity of the Tower-Soudan anticline (modified after Peterson, 2001; Hudak et al., 2014).

Formation, the Lake Vermilion Formation (including the informally named Britt and Gafvert Lake sequences), and the Knife Lake Group of the Soudan belt; (2) the Bass Lake sequence (Peterson and Jirsa, 1999, Peterson, 2001) and the Newton Lake Formation of the Newton belt; and, (3) syn- to post-tectonic granitoid intrusions of the Giants Range batholith, and a suite of post-tectonic alkalic stocks and plutons. Contacts between the different units are typically conformable, although considerable overlap in time and space is documented between volcanic and sedimentary sequences (Southwick, 1993). Regional chronostratigraphic correlations between the Wawa Greenstone (northwestern Ontario) and the Abitibi greenstone belt (eastern Ontario and Quebec) are indicated in Figure 7-3.

Geochronological information for supracrustal and intrusive lithologies in the Vermilion District is relatively sparse (Figure 7-3). Peterson et al. (2001) obtained a U-Pb zircon age of 2722 ± 0.9 Ma from a quartz-phyric rhyolite dome in the Fivemile Lake Sequence of the Lower Member of the Ely Greenstone Formation. Allerton et al. (2024a) obtained a crystallization age of 2708 ± 25 Ma for the Purvis Pluton, which intrudes the Eagles Nest Succession of the Lower Ely Member, and has been interpreted as a synvolcanic intrusion (Peterson, 2001). The age of the Upper Member of the Ely Greenstone formation is currently unknown. Jirsa (2016) obtained an age of 2715.74 ± 0.50 Ma for a felsic volcanic unit within the Newton Lake Formation (Boerboom, T. J., 2020). Lodge et al. (2013) obtained a U-Pb zircon age of 2689.7 ± 0.8 Ma for a Gafvert Lake Sequence dacitic tuff breccia that occurs approximately 2m north of the contact with the Soudan Iron-Formation member of the Ely Greenstone Formation. As well, Lodge et al. (2013) obtained detrital zircon ages ranging from 2680-2690 Ma from greywackes that comprise the Lake Vermilion formation. These dates confirm the source of the detritus in the Lake Vermilion Formation was derived locally from the volcaniclastic rocks comprising the Gafvert Lake Sequence.

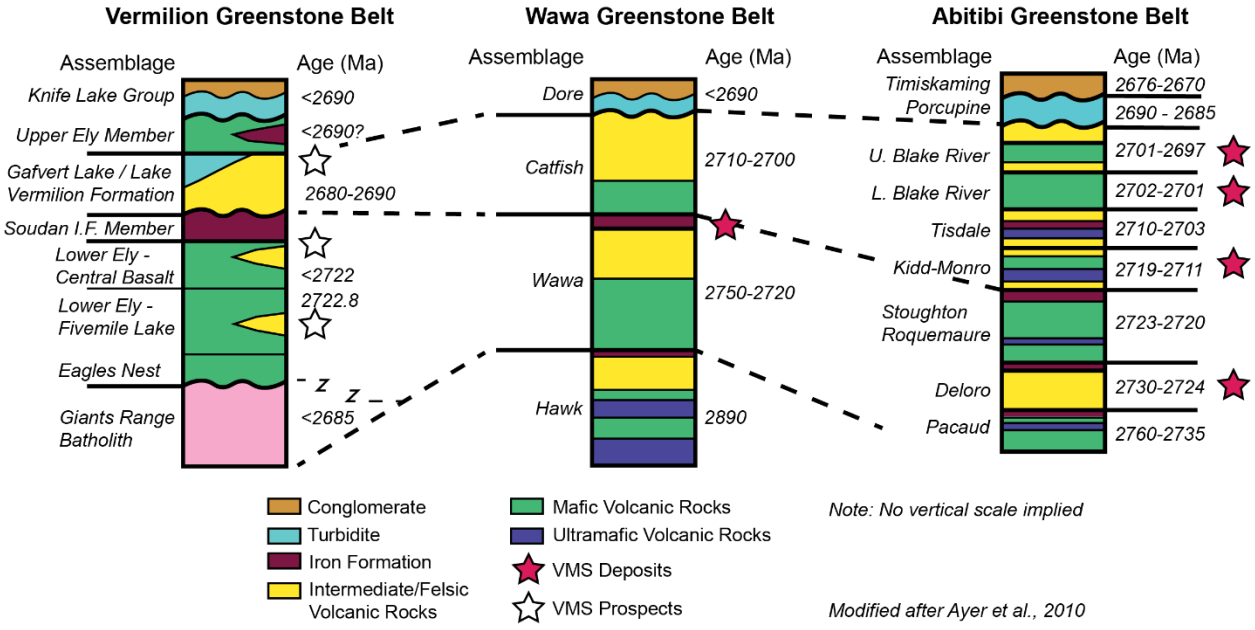


Figure 7-3. Regional chronostratigraphic correlations between the Vermilion district (Minnesota), the Wawa greenstone belt (northwestern Ontario), and the Abitibi greenstone belt (eastern Ontario and Quebec; after Ayer, 2010).

Table 7-1. Lithostratigraphic units within the western Vermilion District (modified after Peterson and Jirsa, 1999; Peterson et al., 2009; Hudak et al., 2012).

Intrusive Rocks	
Late Intrusions	Plutons and stocks of syenite, monzonite, diorite, and lamprophyre. A U-Pb zircon age date of a non-foliated feldspar porphyry intrusion in the Newton belt is 2683 ± 1.4 Ma (Peterson et al., 2001).
Vermilion Granitic Complex	Granite, schist, amphibolite, and schist-rich migmatite
Giants Range Batholith	Granite, granodiorite, monzodiorite, and schist-rich migmatite. U-Pb zircon dates indicate a crystallization age ranging from 2640-2777Ma (Allerton et al., 2024a).
Supracrustal Rocks	
Newton Belt	
Newton Lake Formation	Tholeiitic and komatiitic basalt lava flows, intrusions, and clastic strata (deep subaqueous?)
Bass Lake Sequence	Tholeiitic basalt lava flows, iron-formation, and felsic porphyries (deep subaqueous)
Soudan Belt	
Knife Lake Group	Graywacke, slate, conglomerate, and sheared equivalents
Lake Vermilion Formation	Graywacke, slate, dacitic tuff, minor conglomerate. Detrital zircons from planar bedded, normal-graded resedimented volcaniclastic rocks have U-Pb age dates of 2680-2690 Ma (Lodge et al., 2013; subaerial to subaqueous)
Gafvert Lake Sequence	Dacitic to rhyodacitic tuff, lapilli-tuff, tuff-breccia, and iron-formation. Basal dacite tuff-breccia deposits in Lake Vermilion State Park have U-Pb age date of 2689.7 ± 0.8 Ma (Lodge et al., 2013; subaerial to subaqueous)
Britt Sequence	Tholeiitic basalt lava flows (deep subaqueous?)
Upper Member – Ely Greenstone	Tholeiitic basalt lava flows and iron-formation (deep subaqueous?)
Soudan Member – Ely Greenstone	Oxide-facies iron formation with intercalated basalt lava flows and felsic volcaniclastic rocks (deep subaqueous)
Lower Member – Ely Greenstone	Calc-alkaline and tholeiitic basalt-rhyolite lava flows, tuffs, epiclastic rocks, and minor iron-formation (shallow- to deep subaqueous)
Central Basalt Sequence	Calc-alkaline to tholeiitic sparsely amygdaloidal basalt and minor basaltic andesite lava flows with MORB-like or back arc basin-like chemical affinities within 100-200 meters of the overlying Soudan Member iron-formation; FII- and FIIIa-type felsic volcanic and volcaniclastic rocks (transition from shallow- to deep water environment)
Fivemile Lake Sequence	Calc-alkaline to transitional moderately to highly vesicular basalt and andesite lava flows and volcaniclastic rocks with arc-like chemical affinities: FI-, FII-, and FIV-type felsic volcanic and volcaniclastic rocks. Rhyolite dome at near Fivemile Lake has U-Pb age date of 2722.6 ± 0.9 Ma (Peterson et al., 2001). Epithermal-like zinc stringer mineralization is present near Fivemile Lake (Hudak et al., 2002a; interpreted as shallow subaqueous environment).
Eagles Nest Sequence	*Algoma-type iron formation, basalt-andesite lava flows, hydrothermal exhalites, felsic tuffs.*

The upper part of the Knife Lake Group includes conglomerates which contain clasts derived from the Saganaga Tonalite, which has been dated by Driese et al. (2011) at 2690.83 ± 0.26 Ma. Jirsa et al. (2012) obtained a U-Pb age of 2690.7 ± 0.6 Ma for synvolcanic intrusions that cross-cut volcaniclastic rocks that comprise the Knife Lake Group. Peterson et al. (2001) also dated a non-foliated feldspar porphyry intruded into Newton Belt strata at 2683.1 +1/-4 Ma. This date provides a minimum age for the regional D_2 deformation event that is described below.

The age of the orebodies at the Soudan Mine were previously interpreted to be syn- or post-depositional to the precipitation of the Soudan Member of the Lower Ely Greenstone Formation (Gruner, 1926; Klinger, 1960; Thompson, 2015). Recent U/Pb and (U-Th)/He radiometric dating by Allerton (2024b) suggest the massive hematite orebodies at Soudan formed during Paleoproterozoic time (1640.8 ± 47.2 Ma – 1740.4 ± 72.5 Ma) and have been overprinted by a Mesoproterozoic hydrothermal event at approximately 1100 Ma (1093.1 ± 16.4 Ma).

Structural Geology

The structural geology of the Vermilion District has been well described by Peterson et al. (2009) and is reproduced below.

Periods of generally N-S directed compression resulted in three major regional deformation events in the Neoarchean terranes of northern Minnesota. The earliest deformation event (D_1) produced broad, locally recumbent folds within the Soudan belt and major fault zones throughout the region. In the Newton belt, D_1 was accommodated by thrust imbrication of large crustal blocks, resulting in mainly northward stratigraphic facing. Field relationships indicate that uplift, faulting, and the deposition of Timiskaming-type clastic sedimentary sequences in local fault- bounded basins occurred late in D_1 deformation (Jirsa, 2000). A large, map-scale structure related to D_1 deformation in the western Vermilion District is the Tower-Soudan Anticline, which is a west-plunging anticline within which the axis and plunge changes orientation along strike from nearly vertical in basalts to shallow NE plunging in the western sedimentary rocks (Figure 7-2). Axial-planar cleavage associated with this early fold typically is lacking, although Bauer (1985), Hooper and Ojakangas (1971), Hudleston (1976), and Jirsa et al. (1992) have described early cleavage (S_1) locally.

A second deformation event (D_2) associated with synchronous regional metamorphism resulted in foliation development and structures having largely dextral asymmetry. D_2 is constrained in the Vermilion District to the time period 2674 to 2685 Ma (Boerboom and Zartman, 1993), and between about 2680 and 2685 Ma in the Shebandowan (Corfu and Stott, 1998). Because D_2 deformation affected all of the supracrustal rocks in the area and is reasonably constrained by geochronology, the regional foliation (S_2) can be used in the field to temporally relate other structural, intrusive, and deformation events. The relationship between S_2 fabric and shear structures indicates that most shearing occurred relatively late in the D_2 event. Major shearing that produced the Mud Creek and related shear zones is attributed to the late stages of D_2 dextral transpression.

Structures related to the third deformation event (D_3), which led to juxtaposition of the Wawa Abitibi and Quetico terranes (Peterson and Patelke, 2003) include abundant NE- and NW-trending faults that dissect the stratigraphic assemblages. Named structures related to D_3 include the NE-trending Waasa and Camp Rivard faults east of the Soudan Mine area, and the WNW-trending, crustal-scale Vermilion and related faults that form the Wawa-Quetico Subprovince boundary.

Paleoproterozoic Superior Type Iron Resources of the Mesabi Iron Range

Superior type iron formation resources of Minnesota are exemplified by the long-standing mining of iron resources of the Biwabik Iron Formation along the length of the Mesabi Iron Range. The Mesabi Iron Range is largely located in St. Louis and Itasca counties and has been the most important iron ore district in the United States since ~1900. The Mesabi Iron Range is 120 miles long, averages one to two miles wide, and is comprised of rocks of the Paleoproterozoic Animikie Group. The Animikie Group on

the Mesabi Iron Range consists of three major conformable formations: Pokegama Formation at the base; Biwabik Iron Formation in the middle; and the overlying Virginia Formation. On the Mesabi Iron Range, these three formations generally dip gently to the southeast at angles of 3-15 degrees.

Since the early 20th century, the Biwabik Iron Formation has been subdivided into four informal members referred to as (from bottom to top): Lower Cherty member, Lower Slaty member, Upper Cherty member, and Upper Slaty member (Wolff, 1917). The cherty members are typically characterized by a granular (sand-sized) texture and thick-bedding (beds ≥ several inches thick); whereas the slaty members are typically fine-grained (mud-sized) and thin-bedded (≤1 cm thick beds). The cherty members are largely composed of chert and iron oxides (with zones rich in iron silicate minerals), while the slaty members are composed of iron silicates and iron carbonates with local chert beds. Both cherty and slaty iron-formation types are interlayered at all scales, but one rock type or the other predominates in each of the four informal members, and they are so-named for this dominance Severson et. al. (2009).

Leached and iron enriched direct ores (or natural ores) were the first materials mined, with the first shipments beginning in 1892, from strongly oxidized pockets along fault and fracture zones and the blanket oxidation of the iron formation at the surface. Taconite, which is the material that is mined today using magnetic separation methods, constitutes most of the iron formation and pertains to the hard, non-oxidized portions of the iron-formation. Production has been dominantly controlled by vertically integrated steelmakers since 1901, and therefore the mining and utilization of these ores have been dictated largely by US ironmaking capacity and demand. The taconite typically contains 30-35% iron and 40-50% SiO_2, plus other components (Morey, 1992). The Biwabik Iron Formation is around 175-300 feet thick in the extreme eastern end of the Mesabi Iron Range at Dunka Pit, 730-780 feet thick in the central Mesabi Iron Range/Virginia Horn area near Eveleth, around 500 feet thick in the western Mesabi Iron Range near Coleraine, and eventually exhibits a "nebulous ending about 15 miles southwest of Grand Rapids" (Marsden et al., 1968) on the extreme western end of the Mesabi Iron Range.

Maps of currently active taconite mining operations on the Mesabi Iron Range are presented in Figure 7-4.

Mesoproterozoic Duluth Complex

The Duluth Complex and associated intrusions of Keweenawan age (~1.1 billion years) in northeastern Minnesota constitute one of the largest mafic intrusive complexes in the world, second only to the Bushveld Complex of South Africa (Miller et al., 2002). These rocks cover a 2,200 square mile (5,700 square km) arcuate area associated with the two strongest gravity anomalies (+50 and +70 milligals) in North America, implying intrusive roots over 8 miles (13 km) deep (Allen and others, 1997). The comagmatic flood basalts and intrusive rocks underlying much of northeastern Minnesota were emplaced during development of the Mesoproterozoic Midcontinent rift, which can be traced geophysically from exposures in the Lake Superior region along a 1250 mile (2,000 km) long, segmented, arcuate path to Kansas and Lower Michigan. The Duluth Complex is defined as the more or less continuous mass of mafic to felsic plutonic rocks that extends for >170 miles (275 km) in an arcuate fashion from Duluth nearly to Grand Portage (Figure 7-5). It is bounded by a footwall of Paleoproterozoic sedimentary rocks and Archean granite-greenstone terranes (Peterson and Severson, 2002), and a hanging wall largely of comagmatic, rift-related flood basalts and hypabyssal intrusions of the Beaver Bay Complex. In genetic terms, the Duluth Complex is composed of multiple discrete intrusions of mafic to felsic tholeiitic magmas that were episodically emplaced into the base of a volcanic edifice between 1108 and 1098 Ma.

The geology of the Duluth Complex and adjacent areas has been described in two major publications by the Minnesota Geological Survey (MGS). These include a 1:200,000 scale regional bedrock geological map of northeastern Minnesota (Miller et al., 2001), and a comprehensive written description of the geology depicted on this map (Miller et al., 2002), commonly referred to as the "bible" by geologists working on Duluth Complex geology. Within the nearly continuous mass of intrusive igneous rock forming the Duluth Complex, four general rock series are distinguished on the basis of age, dominant lithology, internal structure, and structural position within the complex.

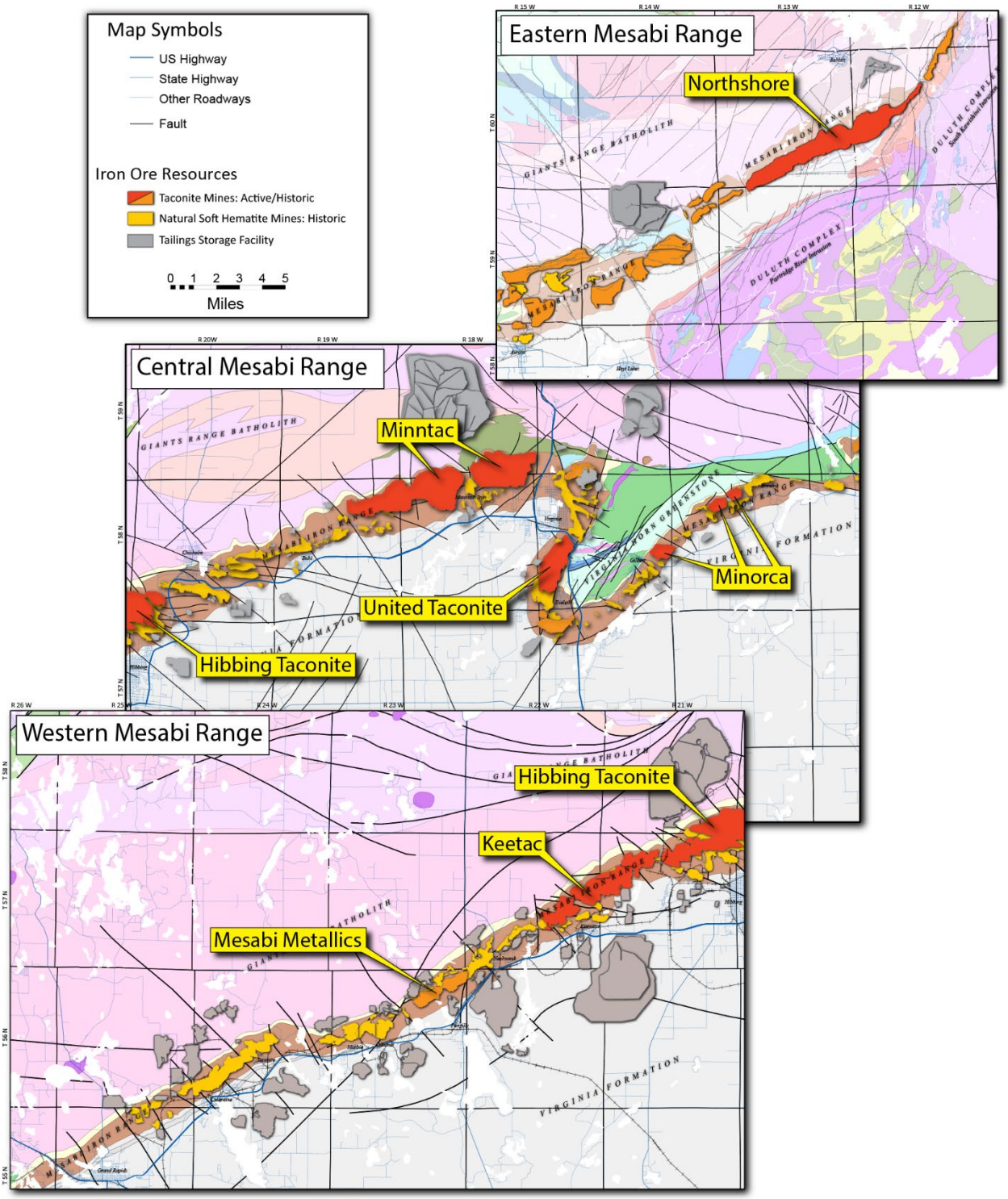


Figure 7-4. Bedrock geology and iron mining features of the Mesabi Iron Range.

Felsic series—*Massive granophyric granite and smaller amounts of intermediate rock that occur as a semi-continuous mass of intrusions strung along the eastern and central roof zone of the complex, that were emplaced during early-stage magmatism (~1108 Ma).*

Early gabbro series—*Layered sequences of dominantly gabbroic rocks that occur along the northeastern contact of the Duluth Complex, emplaced during early-stage magmatism (~1108 Ma).*

Anorthositic series—*Structurally complex suite of foliated, but rarely layered, plagioclase-rich gabbroic anorthosite emplaced throughout the complex during main stage magmatism (~1099 Ma).*

Layered series—*Suite of stratiform troctolitic intrusions that comprises at least 11 variably differentiated mafic layered intrusions that occur mostly along the base of the Duluth Complex. These intrusions were emplaced shortly after the Anorthositic series (~1099 Ma).*

South Kawishiwi Intrusion

The South Kawishiwi intrusion (SKI), together with the similar sized Partridge River intrusion (PRI) immediately to the south, are most renowned for hosting the largest tonnage of Cu-Ni sulfide mineralization in the world (Naldrett, 1997). The realization that the SKI hosts vast quantities of Cu-Ni mineralization over 50 years ago has led to the publication of numerous geologic maps, (Green et al., 1966, Bonnichsen, 1974, Foose and Cooper, 1974, Miller et al., 2001, Peterson, 2002e, f, Peterson et al., 2004, Peterson, 2006b, Peterson et al., 2006), articles (Bonnichsen et al., 1980, Weiblen and Morey, 1980, Ripley, 1986, Chandler and Ferderer, 1989, Lee and Ripley, 1996, Hauck et al., 1997, Peterson, 2001b) theses (Weiblen, 1965, Vislova, 2003, Marma, 2003, Gal, 2008, White, 2010), and reports (Phinney, 1969, Phinney, 1972, Listerude and Meineke, 1977, Morey and Cooper, 1977, Foose, 1984, Dahlberg, 1987,

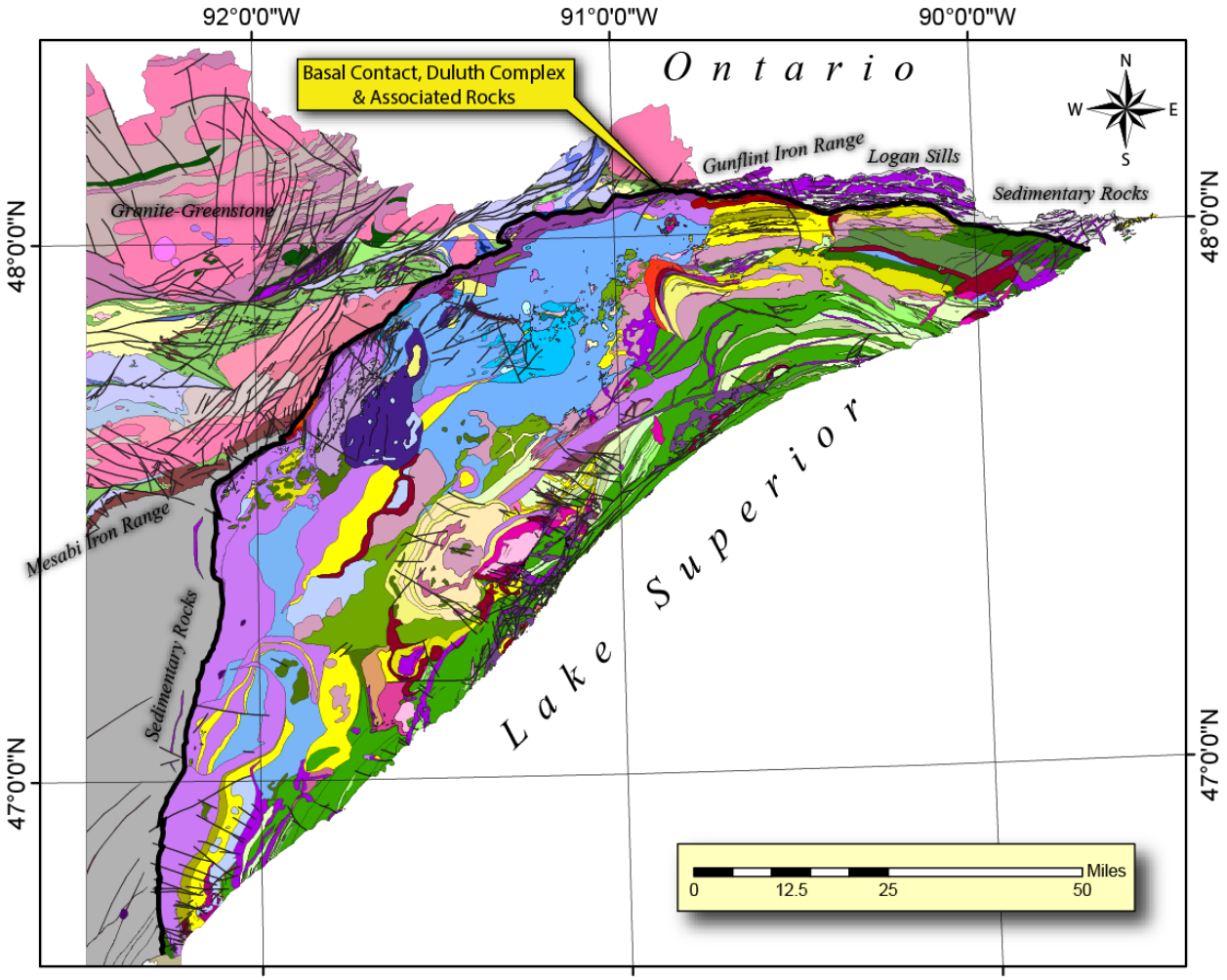


Figure 7-5. Geologic map of northeastern Minnesota.

Dahlberg et al., 1989, Kuhns et al., 1990, Severson, 1994, Zanko et al., 1994, Hauck et al., 1997, Peterson, 1997, Peterson, 2001c, Miller et al., 2002, Peterson, 2002d, Patelke, 2003, Severson and Hauck, 2003).

The SKI is shallow dipping (~20º to the east-southeast) sill-like intrusion dominantly composed of troctolitic cumulates that are exposed in an 8 x 32-km arcuate band along the northwestern margin of the Duluth Complex. Footwall rocks include the Paleoproterozoic Virginia Formation in the Serpentine and Dunka Pit deposits, the Paleoproterozoic Biwabik Iron Formation in the Dunka Pit and Birch Lake deposits, and the Archean Giants Range batholith from the northern Birch Lake deposit north to the Spruce Road deposit. The presence of shallow-dipping Biwabik Iron Formation inclusions as far north as the Spruce Road deposit indicates that the majority of Paleoproterozoic units were assimilated and removed from the footwall during emplacement of the SKI, leaving the Giants Range batholith as the dominant footwall rock type. Alternately, the Virginia and Biwabik Iron Formations may simply have been largely eroded prior to the development of the Mid-Continent Rift. Also present as inclusions in the SKI are mafic volcanic hornfels (North Shore Volcanic Group), quartz sandstone hornfels (either the Puckwunge or Nopeming sandstones), and anorthosite (of the Anorthosite series). Anorthositic series rocks about the SKI on the northeast – and enclose an interpreted SKI feeder dike (the NLM) that extends farther northeast – the PRI forms the southern sidewall of the SKI, and the BEI and Anorthositic series rocks overlie the SKI to the east. On the regional Duluth Complex map of Miller et al. (2001), the SKI is subdivided into five major map units. These are, from the base upward,

1. Heterogeneous sulfide-bearing troctolite, gabbro, and norite with localized hornfels inclusions,
2. A thick unit of subophitic to ophitic augite troctolite,
3. Discontinuous and localized layers of poikilitic leucotroctolite,
4. A thick homogeneous sequence of ophitic troctolite, and
5. A thick uppermost sequence of homogeneous troctolite that contains numerous anorthositic layers.

Severson (1994) and Zanko et al. (1994) further subdivided the SKI into 17 different lithostratigraphic units that are present in over 180 drill holes over a strike length of 31 kilometers. Sulfide mineralization is confined to the BH, BAN, UW, and U3 units near the base of the intrusion, and to a lesser extent the U1, U2, and PEG units. Major marker horizons that are correlated in drill holes include three horizons with abundant cyclic ultramafic layers (U1, U2, and U3 units) and a pegmatite-bearing unit (PEG unit) that was initially recognized by Foose (1984). The understanding of the significance of a large anorthositic inclusion, originally intersected in six deep drill holes east of the Maturi deposit, and its role in magma dynamics of the SKI has been a key feature in the development of an exploration model for Duluth Metals Limited's Maturi Extension deposit (Peterson, 2001c).

Terminology

It is important to note the terminology utilized in this field trip guide for: 1) volcaniclastic rocks; 2) bedding characteristics; and 3) description and unit coding of outcrops in the Duluth Complex. Use of consistent terminology is required in order to accurately describe these geological features.

Volcaniclastic rocks contain abundant volcanic material irrespective of their origin or depositional environment. Such rocks can be formed directly from volcanic eruptions (whether subaerial or subaqueous), result from resedimentation of non-lithified volcanic deposits (for example, resedimentation of pyroclasts prior to lithification), or result from weathering and resedimentation of pre-existing lithified volcanic rocks.

Primary (juvenile) volcaniclastic particles result directly from eruptive processes, and are of three types:

- *Pyroclasts*, which form by explosive fragmentation of magma into particles (including ash, highly vesiculated glass (pumice, scoria), crystals and crystal fragments, and lithic fragments);

- *Hydroclasts*, which form by explosive interaction with external water (via phreatic (steam only) and/or phreatomagmatic (steam and magma) explosions) or by non-explosive quenching and granulation of lava (for example, the formation of hyaloclastite fragments on the margins of submarine lava flows or intrusions into wet sediments); and
- *Autoclasts*, which form by frictional breakage of moving viscous lava flows (for example, to form carapace breccias on the margins of subaerial lava flows).

Based on these different types of fragmentation, four types of primary volcaniclastic deposits have been identified by White and Houghton (2006):

- *Pyroclastic deposits*, which are generated from volcanic plumes and jets or pyroclastic density currents as particles first come to rest. Deposition mechanisms associated with these processes include suspension settling, traction, or *en masse* freezing;
- *Autoclastic deposits*, which are generated during effusive volcanism when lava cools and fragments as a result of thermal processes, or recently cooled lava breaks during flow. Deposition for these types of rocks is under the influence of continued lava flowage;
- *Hyaloclastite deposits*, which are generated during effusive volcanism when magma or flowing lava is chilled and fragmented due to contact with water. Deposition of such deposits is is influenced by the continued emplacement of the lava in the presence of water, and the thicknesses of the hyaloclastite deposits can be dictated by the temperature of the magma, the effusion rate, and the distance from the volcanic vent (Cas and Wright, 1987; Gibson et al., 1999; Newkirk et al., 2001a, 2001b); and
- *Peperite deposits*, which are generated when magma intrudes into unconsolidated clastic material and mingles with (generally wet) debris to form a volcaniclastic deposit (McPhie et al., 1993). Deposition of peperite deposits takes place essentially *in-situ*.

Secondary volcaniclastic particles are known as epiclasts:

- *Epiclasts* are lithic clasts and/or crystals derived from physical weathering and erosion of pre-existing rocks. Epiclasts are volcaniclasts when the pre-existing rocks are volcanic.

The terminology for volcaniclastic rocks has historically been somewhat confusing because many different classification schemes have been developed (for example Fisher, 1961; Fisher 1966; Schmid, 1981; Cas and Wright, 1987; McPhie et al., 1993; White and Houghton, 2006), and different classification schemes are preferentially used in different parts of the world. As a result, the terminology relating to volcaniclastic rocks is commonly misused or misinterpreted. Four classification schemes that have been used most in the recent geological literature include:

- Fisher (1961, 1966) – Classification based on particle size, particle formation, or particle fragmentation mechanism;
- Schmid (1981) – Particle type within the deposit;
- Cas and Wright (1987) – Mode of fragmentation and deposition; and
- McPhie et al. (1993) – Transport and deposition mechanisms.

According to R. V. Fisher (1998), the difficulties with volcaniclastic rock classification can be understood because "volcaniclastic rocks are essentially igneous on the way up and sedimentary on the way down". In fact, Fisher's thesis advisor, when observing the volcaniclastic rocks that were the focus of his thesis studies, indicated that they were "the ugliest and most undistinguished rocks I've seen in my 30 years of petrology!" Also, classification is especially difficult in ancient volcaniclastic rocks because key aspects

of classification can be obscured by subsequent metamorphism and/or structural deformation (e.g. particle type, particle size) or because genetic processes cannot be ascertained unambiguously (e.g. transport and deposition mechanism, fragmentation mechanisms).

For this field trip guidebook, we will utilize Fisher's (1966) classification (Figure 7-6) for volcaniclastic rocks. This classification scheme is based on the relative proportions of ash-sized material (< 2mm), lapilli-sized material (2-64mm), and blocks/bomb sized material (>64mm) in the rock. Both Gibson et al. (1999) and Mueller and White (2004) suggest that this classification be used for field-based rock classification (mapping, diamond drill core logging, petrography) of ancient volcaniclastic deposits for the following reasons:

- The classification scheme is "field-user friendly" because it accommodates both the historically important pyroclastic rock names and enables comparison at both the hand sample and thin section scale (Mueller and White, 2004);
- It is a Wentworth-based scale, and thus enables comparison of volcaniclastic deposits to sedimentary deposits; and
- Rock classification does not require knowledge of the specific transport mechanism or depositional processes involved with the genesis of the deposit.

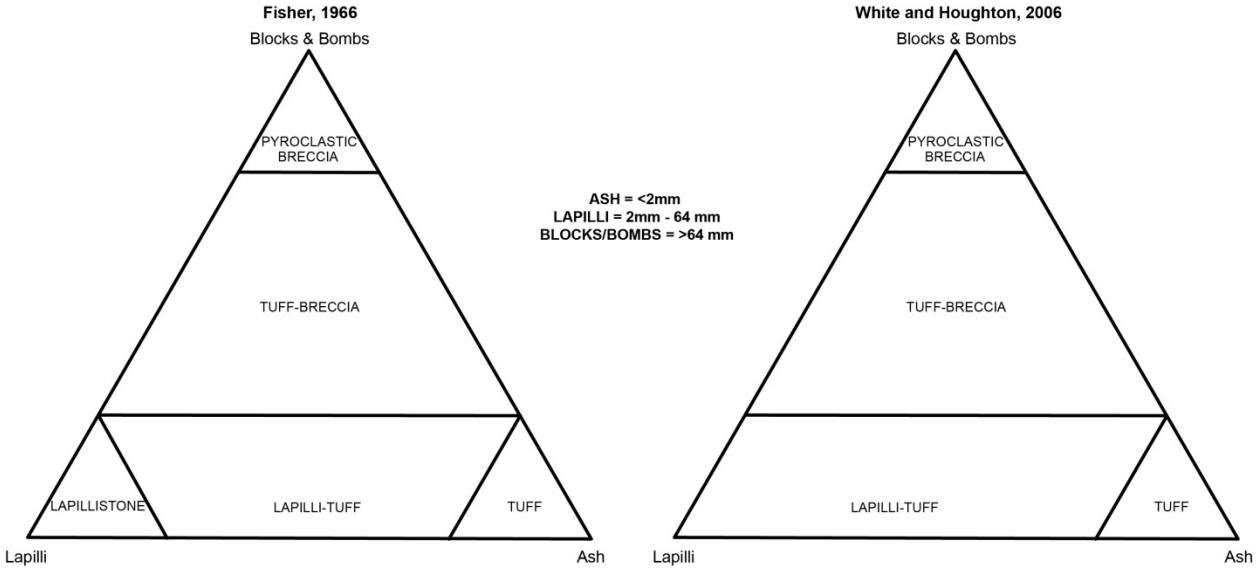


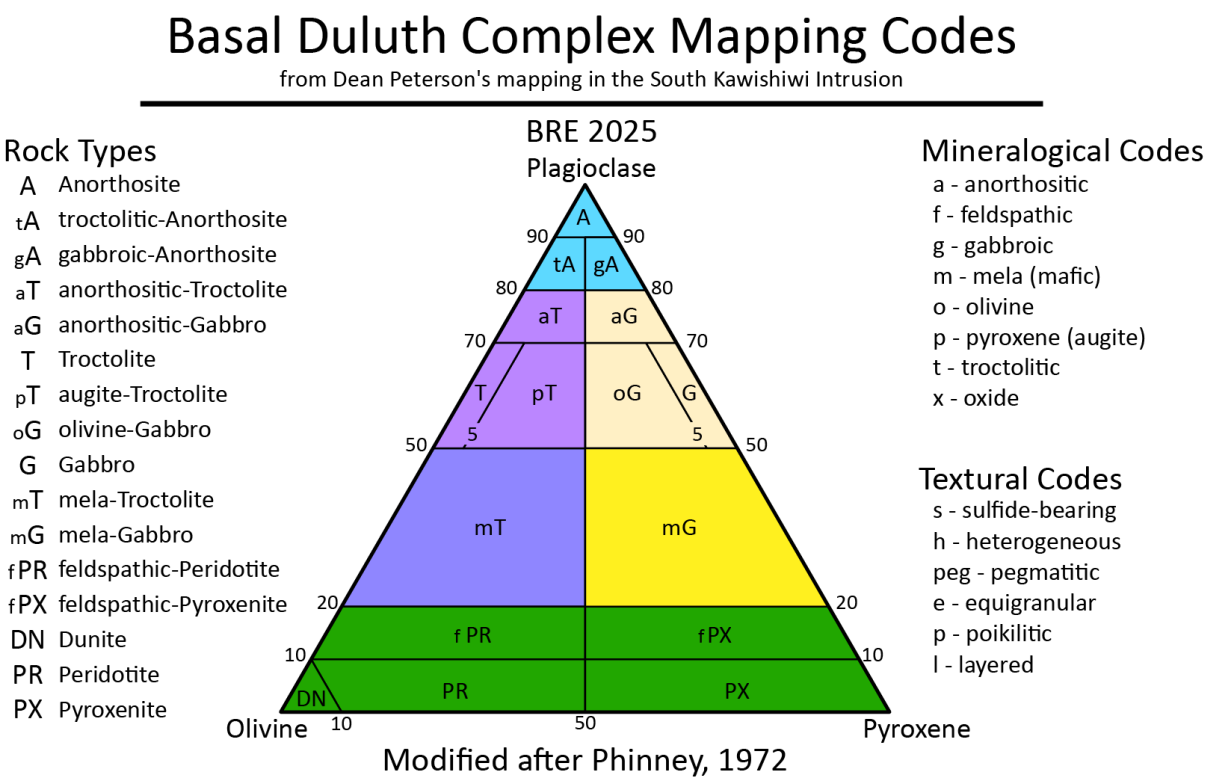
Figure 7-6. Volcaniclastic rock classification schemes of Fisher (1966) and White and Houghton (2006). This field trip guidebook will classify volcaniclastic rocks using Fisher's (1966) classification scheme.

More recently, White and Houghton (2006) have developed a modified version of Fisher's (1966) volcaniclastic classification scheme (Figure 7-6). The scheme is essentially equivalent to the Fisher (1966) scheme, with the exception that the lapill-tuff field in the White and Houghton (2006) classification comprises the lapilli-tuff and lapillistone fields of Fisher's (1966).

Specific terms for bedding thicknesses are also used in this guidebook. The terminology for bedding thickness has been adopted from McPhie et al. (1993) and includes:

- Laminated <1 centimeters thick
- Very thinly bedded 1-3 centimeters thick
- Thinly bedded 3-10 centimeters thick
- Medium bedded 10-30 centimeters thick

- Thickly bedded 30-100 centimeters thick
- Very thickly bedded >100 centimeters thick



Note: This sheet depicts letter codes and colors to be used in outcrop mapping in the South Kawishiwi Intrusion (SKI) of the Duluth Complex. A three-part system is used to name the rocks: prefix (mineralogic code) - rock type (capital letter(s)) - suffix (textural code). For example, pTp is a pyroxene (augite) Troctolite with poikilitic texture and an oxG is an olivine-oxide Gabbro. Other rock unit codes and colors are given below.

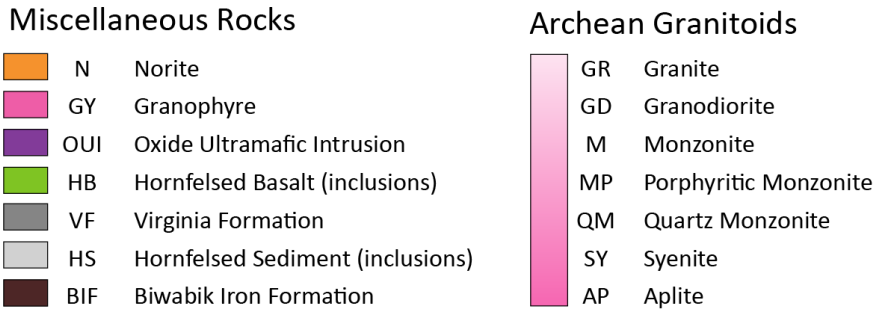


Figure 7-7. The classification scheme used to describe and code mafic intrusive rocks within the Duluth Complex, modified after Phinney, 1972.

Classification of outcrops and map units within the Duluth Complex have relied on the early work of William Phinney (Green et al., 1966; Phinney 1969, and Phinney, 1972) and is given in Figure 7-7.

FIELD TRIP STOPS

Table 7-2. Simplified description of the twenty-field trip stops presented in this guidebook. Also included are the coordinates (UTM, Nad83, Zone 15N and Lat-Long), mileage along the route to the stop, and the age of features that will be observed and discussed on the outcrops.

STOP	TERRANE	STOP DESCRIPTION	UTME	UTMN	LONGITUDE	LATITUDE	MILES
0		ILSG Venue, Mountain Iron	530889	5262874	-92.58972	47.51856	0.00
1		Confusion Hill: Marginal zone, Giants Range batholith (GRB), origin of local topography	534317	5269428	-92.54368	47.57736	5.93
2		Lake Vermilion Formation greywackes	547273	5293370	-92.36881	47.79196	18.63
3		Fragmental felsic volcanic rocks of the Gafvert Lake complex	553454	5294469	-92.28615	47.80136	4.47
4		Soudan Mine classic iron formation outcrop (No Hammering)	557144	5296585	-92.23659	47.82007	2.98
5		Northern margin of the wedge-shaped Murray shear Zone	559366	5296388	-92.20694	47.81810	1.66
6		Basalt sheet & pillowed lava flows of the Lower Ely Greenstone	561999	5297811	-92.17157	47.83066	1.98
7		Mud Creek Shear Zone: separates the Soudan & Newton Belts of the Wawa-Abitibi	564288	5302699	-92.14026	47.87441	7.59
8		Variolitic pillowed basalt flows, Newton Belt	585753	5309482	-91.85191	47.93291	20.20
9		Giants Range Batholith, footwall to the northern South Kawishiwi Intrusion (SKI)	590518	5296544	-91.79084	47.81588	11.51
10		Cu-Ni-PGE mineralized troctolites of the Maturi SW deposit	590592	5293118	-91.79056	47.78505	2.18
11		Basal SKI magmatic slurry igenous breccia, an important outcrop (No Hammering)	590437	5292619	-91.79273	47.78058	0.33
12		Main AGT (augite-troctolite) unit of the SKI	594727	5296295	-91.73468	47.81303	5.34
13		Spruce Road Cu-Ni-PGE deposit bulk sample site and saprolitic discovery burrow pit	598885	5298553	-91.67864	47.83272	3.39
14		Nickel Lake Macrodike: feeder dike to the SKI	601959	5298393	-91.63761	47.83080	2.81
15		Middle SKI: Remnant saprolitic corestones in layered troctolites	600176	5291703	-91.66297	47.77090	10.43
16		Anorthosite Series of the Duluth Complex exposed in a large roadcut	601381	5290418	-91.64720	47.75916	1.18
17		Bald Eagle Intrusion troctolite	601921	5288133	-91.64053	47.73852	1.64
18		Vermilion Moraine: boulder-rich end moraine composed almost entirely of SKI troctolite	589247	5282737	-91.81064	47.69185	10.62
19		Biwabik Iron Fm. - Basal Duluth Complex Contact, Dunka Pit area	585687	5282948	-91.85803	47.69423	2.99
20		GRB migmatite with a pyroxenite/lamprophyre dike	571144	5281936	-92.05199	47.68689	10.92
0		ILSG Venue, Mountain Iron	530889	5262874	-92.58972	47.51856	32.95

Age of geologic features observed at the field trip stop

- *Quaternary*
- *Mesoproterozoic Duluth Complex*
- *Paleoproterozoic Biwabik Iron Formation*
- *Neoarchean Vermilion granite-greenstone belt of the Wawa-Abitibi Subprovince*

Stop 1: Laurentian Divide at Confusion Hill

Longitude/Latitude: 47.51868699°N, -92.58996713E

UTM NAD 83 Zone 15N: 530870E, 5262888N

Exposed near this wayside and in road cuts on both sides of the highway is an array of variably layered intrusions having both tonalitic (white) and dioritic (black) compositions. A cursory look shows intrusive relationships that conclusively demonstrate that diorite was emplaced into tonalite at one locality, and at another, tonalite was emplaced into diorite. In detail, all compositions intermediate between the two end members are also present locally. Although the dioritic component is abundant here, the bulk of the mapped unit is tonalitic. Emplacement of this unit, now known as the Lookout Mountain tonalite, probably involved some degree of magma mingling. Dikes of tonalite that cut the adjacent high-grade supracrustal rocks of the Minntac sequence contain metamorphic fabrics, yet little evidence of metamorphic origin can be seen in the interior of the body, implying it is syntectonic with respect to D_2 deformation. U-Pb zircon dates (Boerboom and Zartman, 1993) of two components of the batholith exposed to the north bracket the age of D_2 deformation between about 2674 and 2682 Ma. Exposures at Confusion Hill are a small part of the Giants Range batholith, which forms the core bedrock of the Laurentian (drainage) divide. The batholith is a 40-mile wide belt of intrusions that can be traced on geophysical maps and outcrop east to the Mesoproterozoic Duluth Complex, and west beyond the western border of Minnesota. It separates Archean supracrustal sequences in the Virginia horn from those of the Tower-Soudan area - making stratigraphic correlation between the two districts speculative.

Return to bus.

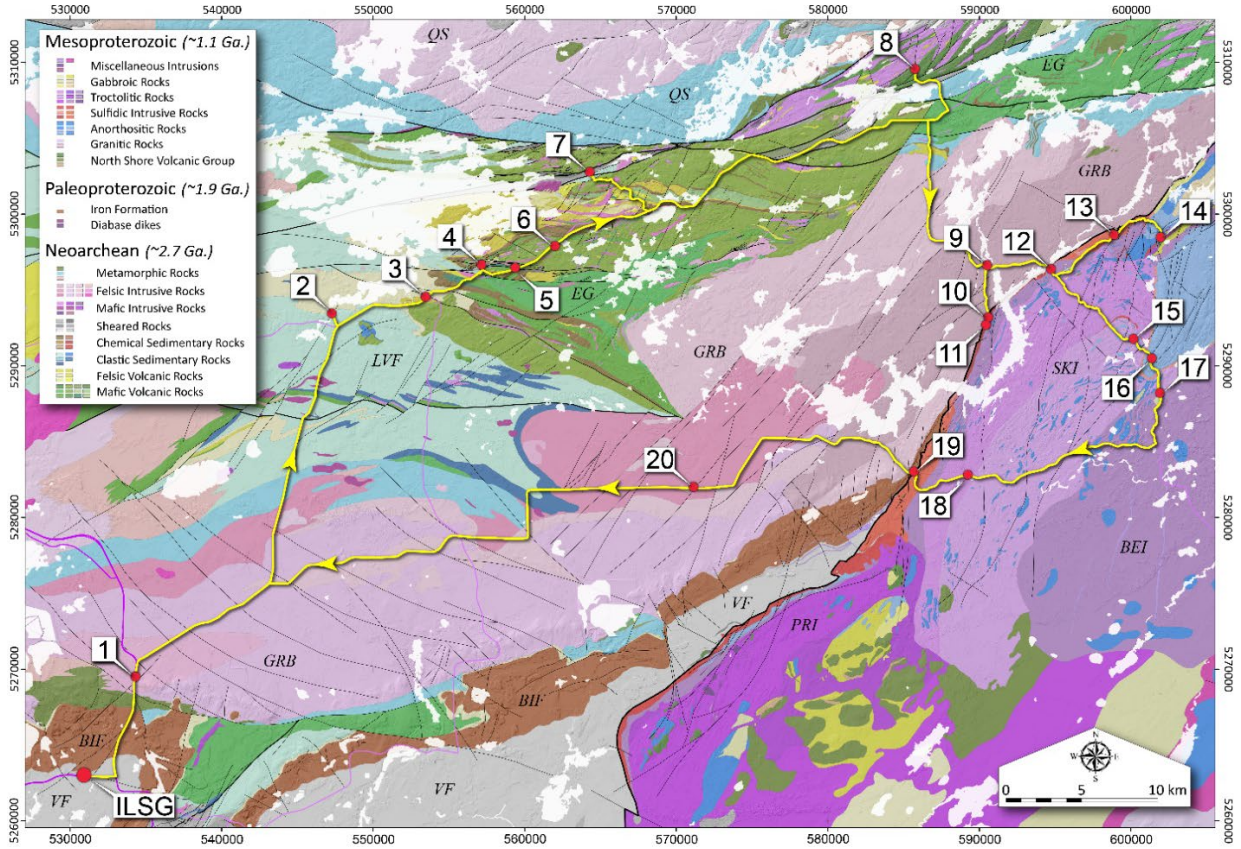


Figure 7-7. Simplified bedrock geology map overlain by the field trip stops and traveled route.

Stop 2: Pike River Dam Greywackes

Longitude/Latitude: 47.57736062°N, -92.54367719E

UTM NAD 83 Zone 15N: 534317E, 5269428N

This glacially scoured outcrop exposes a nearly perfect cross-section of straight-bedded, variably graded, feldspathic graywacke and black slate. The feldspar-rich, dacitic composition of sandy textured beds is presumed to represent derivation from the Gafvert Lake felsic volcanic sequence exposed to the east in the Soudan area. Regionally, a series of outcrops from Gafvert Lake westward shows an irregular transition from proximal, possibly subaerial deposition on the east, to distal submarine turbiditic fan deposition to the west. The beds contain numerous "soft-sediment" deformation features including load structures, flames, intrafolial slump folds, and possibly some of the cross-stratal faulting. Bedding is nearly vertical, and graded beds indicate stratigraphic younging to the south. This topping direction, and the presence of a weak D_2 cleavage that is left of bedding, indicate westward structural facing in the cleavage; consistent with a position on the south limb of a large, south-overturned, regional, D_1 fold structure—the western extension of the Tower–Soudan Anticline. Northeast-trending kink bands, fault zones, and raised quartz veins traversing the outcrop.

One of the truly classic outcrops of greywacke of the Lake Vermilion Formation is beautifully exposed at this stop. Prior to about the 1950s, no depositional mechanism could satisfactorily explain the coincidence in graywacke of; 1) coarse sand derived from a source many kilometers distant and having an altered clayey matrix; 2) interbedded black slate; and 3) the lack of evidence for reworking in shallow water (indicative of deposition below wave base). This was changed when the concept of turbidity currents was introduced to the geological profession by Kuenen and Migliorini (1950). Despite widespread publication on turbidites in more modern geologic settings through the 1950s and 1960s, the facies model was not

refined and applied to Archean and Proterozoic strata in the Lake Superior region until somewhat later (Morey, 1965; Ojakangas, 1966).

Return to bus.

Stop 3: Gafvert Lake Sequence Volcaniclastic Rocks

Longitude/Latitude: 47.80135914°N, -92.28615141E

UTM NAD 83 Zone 15N: 553454E, 5294469N

This relatively new roadcut (approximately 15 years old) exposes rhyodacitic to dacitic composition Gafvert Lake Sequence lapilli tuffs and tuff breccias. The deposits have tentatively been interpreted to represent mass flow units produced by slumping of volcanic and volcaniclastic material from the Gafvert Lake volcano into an adjacent, probably submarine basin.

Close inspection of the unit indicates the presence of a variety of lapilli and blocks including: 1) subrounded to subangular plagioclase ± quartz-phyric coherent dacite to rhyodacite; 2) subrounded to subangular pumice; 3) angular carbonate-rich fragments; 4) angular chert fragments; and 5) local subangular to angular massive sulfide fragments. Locally, abundant (up to 10%) <1mm euhedral pyrite cubes are disseminated in the matrix. The presence of both carbonate and massive sulfide fragments, as well as plagioclase- and quartz phyric coherent rhyodacite to dacite lapilli, may suggest the slumps are derived from a Gafvert Lake sequence subaqueous lava dome that was affected by local hydrothermal alteration and the deposition of chemical exhalates (e.g. carbonate, chert and massive sulfide fragments).

Structurally, this outcrop occurs on the southern margin of an east-southeast – west-northwest trending D_2-associated structure that extends from Pike Bay (northwest) to south of Putnam Lake (southeast). Here one can observe a strong, steeply dipping E-NE foliation and a well-developed lineation that plunges approximately 70° E.

Return to bus.

Stop 4: Soudan Member Banded Iron Formation

Longitude/Latitude: 47.820074°N, -92.2365908E

UTM NAD 83 Zone 15N: 557144E, 5296585N

(NOTE: Modified from Peterson et al., 2009 and Hudak and Peterson, 2014.)

This classic exposure of the Soudan iron-formation member of the Ely Greenstone Formation lies on the north limb of the Tower-Soudan anticline approximately 75 meters north of the stratigraphic top of the volcanic sequences known collectively as the Lower member of the Ely Greenstone. The outcrop displays two generations of tight folding in delicate laminae of chert (creamy white), chert-hematite jasper (red), and magnetite-chert (black to silver-colored). The second generation of folds (F_2) is tectonic in origin, having subvertical axial surfaces that trend east, and steeply plunging axes. Most display Z-asymmetry. The earlier folds ($F_{0\text{-}1}$) appear to have been sharply refolded to produce complex interference patterns. Lundy (1985) studied folding at this locality and concluded that some of the apparent interference structures are the product of early-formed sheath folds that did not involve refolding by D_2. The F_1 structures are predominantly intrafolial and exhibit a great variety of style and orientation; implying they formed by layer-parallel, soft-sediment slumping (Fig. 7-8). Lundy's mapping of this outcrop is an interesting demonstration of unraveling details at a single outcrop that led to recognition that D_1 deformation was not systematic here, but likely soft sediment. Furthermore, it is a microcosm of regional-scale deformation.

It is interesting to observe the rhythmic microlaminae (1 mm or so thick) in various cherty beds exposed here and speculate about the paleoenvironment—that is, whether these represent daily heating/cooling, tidal, climatic, annual, or some other repetitive influence (e.g waxing/waning of a hydrothermal system) in the depositional environment. What is known about units of iron-formation in the Ely Greenstone, of which there are many, is that deposition occurred in deep water (below wave base) during periods of relative volcanic and tectonic quiescence by the slow subaqueous "rain" of chemical precipitates.

The deep excavations in this area are the early workings of the Soudan iron mine, the first in Minnesota. The mine produced about 16 mt of high-grade hematite ore (60-63 percent iron converted to a park. Most of the production came from underground workings that began here in 1900, and which now can be visited on guided tours. The mine previously housed several underground physics research facilities. These include Soudan 1 (23rd level) which studied neutrino decay; 2) Soudan 2 (27th level), also to study neutrino decay; and 3) the MINOS (Main Injector Neutrino Oscillation Search) lab, which was built on the 27th level adjacent to Soudan 1 and studied the decay of neutrinos within the earth as they passed from Fermilab to Soudan (Peterson et al., 2009b).

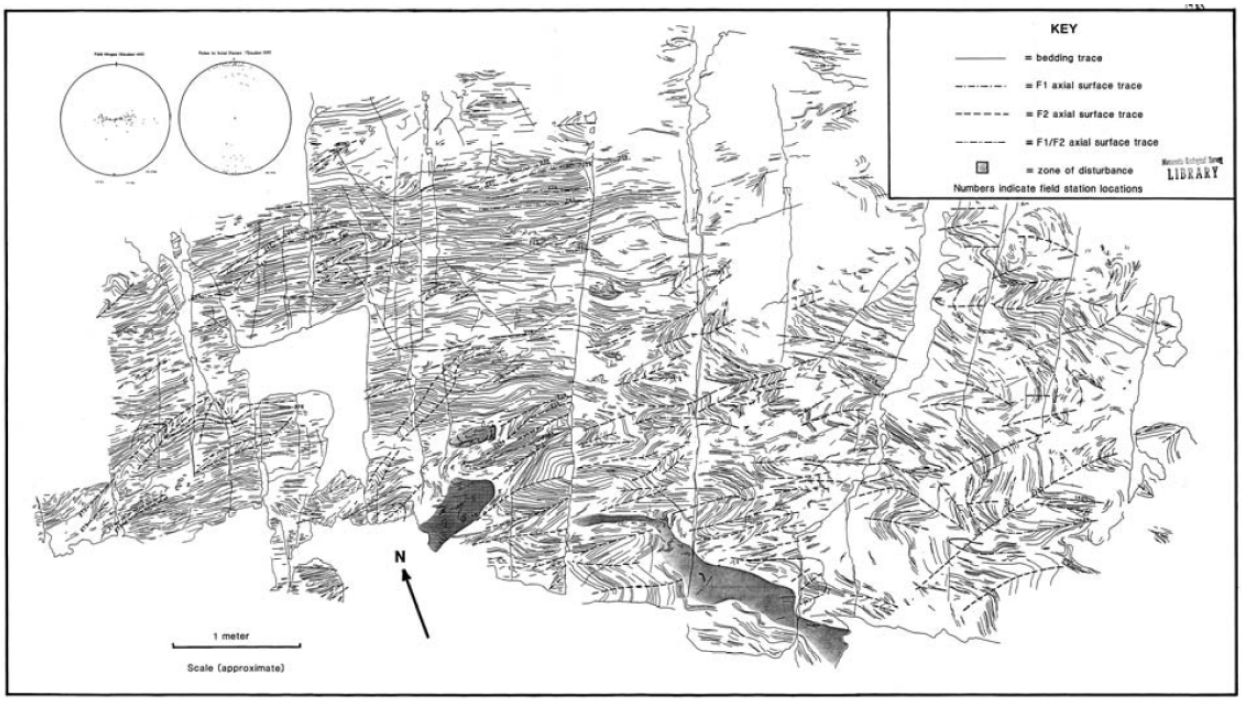


Figure 7-8. Outcrop map showing bedding trajectories and multiple generations of folds and faults (from Lundy, 1985). F1 folds are non-systematic and include both nappe- and sheath fold geometries.

Return to bus.

Stop 5: Murray Shear Zone Along Hwy 1/169

Longitude/Latitude: 47.81809993°N, -92.20694376E

UTM NAD 83 Zone 15N: 559366E, 5296388N

A series of roadcuts along Highway 169 expose a transect through the northern edge of the Murray Shear Zone, which is one of the most striking Neoarchean structural features in the Tower-Soudan area

(Peterson and Patelke, 2003). This series of outcrops perfectly display a classic feature of Neoarchean ductile (shear zone) structures - strain partitioning (Figure 7-9). A close look at these outcrops also gives one hints of broader economic geology implications via the presence of carbonate alteration of the chlorite schists. The carbonate (ankerite and/or ferro-dolomite) strain hardens the ductile deformed schistose rocks and allows for subsequent brittle deformation (and perhaps orogenic gold mineralization in cross-cutting quartz-ankerite-sulfide veins.

On the larger scale, the D_2 Murray shear zone transposes rocks 3-5 km eastwards in the zone bounded by its northern and southern strain partitioned boundaries. The overall geometry of this panel of

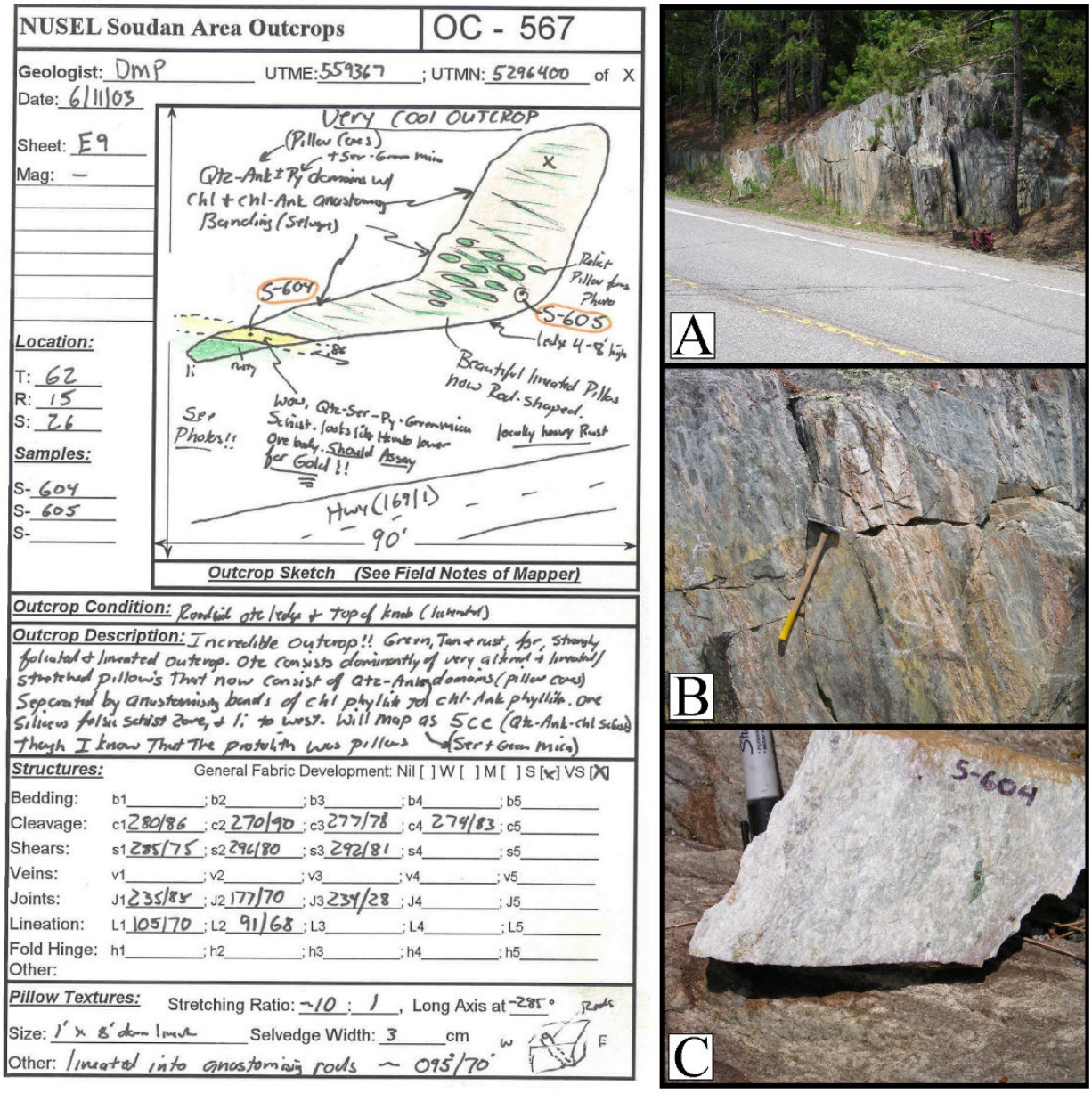


Figure 7-9. Scanned image of the field sheet used to map outcrop OC-567. On the right are digital photographs of outcrop OC-567: A) the overall outcrop view looking WNW; B) view to the north of steeply east plunging, lineated and rod-shaped pillowed andesite (rock hammer 68cm for scale); and C) close-up view of rock sample S-604, taken from the west side of the outcrop (bright zone on the left side of picture A). Data from Peterson & Patelke, 2003.

rocks is like the geometry of "wedge-shaped shear zones" described in detail by Ramsey and Huber (1987). Peterson's mapping and collection of structural data in the Murray shear zone panel is largely confined to a series of outcrops along the northern edge of the zone. Field observations of these outcrops indicate that the strain symmetry along this boundary is largely constrictional, with a dominant steeply east-dipping, elongate and rod-shaped structural fabric. A stereonet projection of planar and linear structural features within the Murray panel is shown in Figure 7-10. The mean value of the strike and dip of planar features is 282°/82°, and the trend and plunge of linear features has a mean orientation of 87°/71°. The overall map-scale internal geometry of the Murray panel clearly shows dextral asymmetry, with a strong sigmoidal wrapping of iron-formation (see field trip geologic maps) to the northeast.

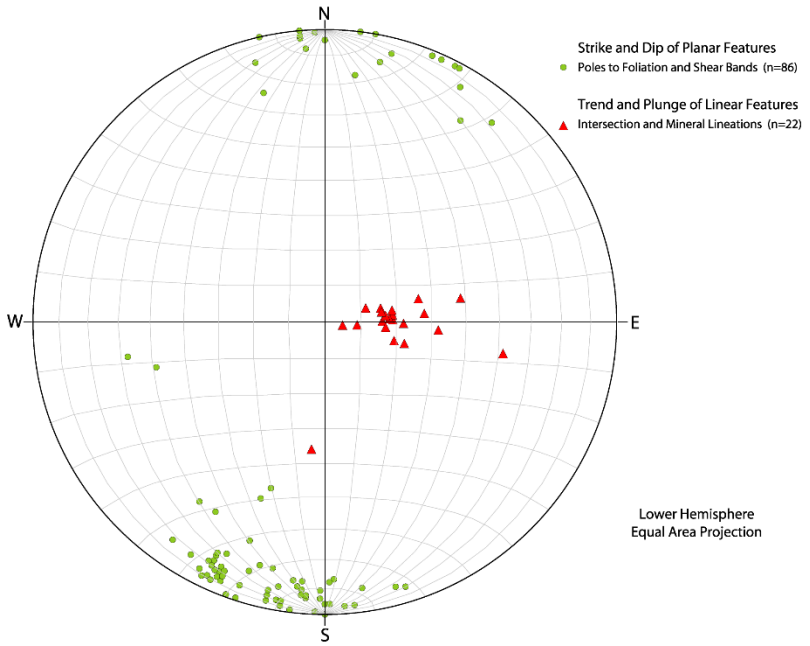


Figure 7-10. Stereonet projections of foliation, shear fabrics, and linear features from the Murray shear zone.

An estimate of the amount of displacement of the rocks within the panel of rocks bounded by the Murray shear zone is given in Table 7-3. These values were calculated geometrically by using the average plunge of measured lineations (71°) and two measured lines of possible correlative stratigraphy offset by the bounding shear zones. The calculated total displacement values (net slip) are quite large (up to 13.8 km, or 43,000 feet of net slip), but the displaced rocks would still fall within the range of depth generally associated with greenschist facies metamorphism.

Table 7-3. Calculated displacement along the Murray shear zone

Lineation Plunge	Strike Slip	Dip Slip	Net Slip
71°	4.5	13.1	13.8
71°	3.0	8.7	9.2

Return to bus.

Stop 6: Lower Ely Member (Central Basalt) Sheet and Pillowed Flows

Longitude/Latitude: 47.8306566°N, -92.17157352E

UTM NAD 83 Zone 15N: 561999E, 5297811N

(NOTE: Modified from Field Trips of Hudak et al., 2004, 2014; Peterson et al., 2005, 2009).

This classic outcrop has been visited during field trips associated with the 2004, 2009 and 2014 ILSG conferences (Hudak et al., 2004; Peterson et al., 2009; Hudak et al., 2014). ***This is a no-hammer outcrop, as the preservation of the delicate textures here rivals those observed in other classic Neoarchean camps in the Superior Province containing well-preserved volcanic textures such as Noranda, Quebec and Timmins, Ontario.*** The description and figure below have been modified from Peterson et al. (2009) and Hudak et al. (2014).

The Central Basalt sequence (Peterson and Patelke, 2003, Peterson, 2005) comprises a steeply north-dipping (75°- vertical), north-facing sequence of sparsely amygdaloidal pillowed and massive lava flows of basalt andesite to basalt composition that are believed to be correlative with the tholeiitic Armstrong Lake volcanic sequence mapped in the Eagles Nest quadrangle (Jirsa et al., 2001), approximately 11km to the east. Hudak et al. (2007), Jansen et al. (2009), and Hudak et al. (2012) have shown that the lowermost sections of the Central Basalt Sequence are composed of submarine basaltic andesite to basalt lava flows that have rare earth element lithogeochemical patterns similar to mafic rocks in oceanic volcanic arcs. However, locally, submarine basalt lava flows that occur within 50-200m stratigraphically below the contact between the Central Basalt Sequence and the overlying Soudan Member of the Ely Greenstone Formation illustrate MORB-like or back-arc basin-like lithogeochemical patterns. This change in rare earth element characteristics may be interpreted to indicate a change from an oceanic arc to back-arc environment immediately prior to the deposition of the Soudan Member. Relative to massive and pillowed basalt and andesite flows in the Fivemile Lake sequence, Central Basalt sequence lava flows are notably less amygdaloidal, and lack multiple pillow rind structures. In addition, the Central Basalt sequence lacks the thick sequences of scoria-rich basalt-andesite lapilli tuffs that are commonly interstratified with lava flows in the Fivemile Lake sequence. These characteristics of the Central Basalt sequence indicate eruption and deposition in a deeper submarine environment than the stratigraphically older Fivemile Lake sequence and suggest overall increasing water depth during the temporal development of the Lower Ely. Deepening of the water column could be accommodated by extensional tectonics and normal faulting associated with the development of the proposed back-arc environment.

At this stop, the outcrop comprises two east-southeast striking massive basalt flows, ranging from at least five to nine meters in thickness, that are separated by a ten-meter-thick flow unit comprising pillows and pillow lobes (Fig. 7-11). All three lava flows at this vicinity illustrate tholeiitic, MORB-like lithogeochemistries (Hudak et al., 2007).

Flow 1, at the southern part of the outcrop, is composed of a pale- to dark green, faintly feldspar-phyric (~10% 0.5-1 mm laths), sparsely amygdaloidal, basalt sheet flow that locally exhibits tortoise-shell jointing formed in response to contraction during cooling. The uppermost 10-40 cm of the coherent part of Flow 1 is generally silicified and epidotized. Petrographic observations indicate that this section of the flow also contains up to 70% <0.1 cm round spherulites. An irregular contact occurs between the coherent basalt flow and an overlying one- to two-meter-thick unit of dark green, exceptionally well-preserved perlitic in-situ hyaloclastite and associated self-peperite (c.f. Batiza and White, 2000).

The hyaloclastite formed from non-explosive fracturing of the basalt glass developed on the flow top due to quenching by water, whereas the perlite formed following deposition by hydration of volcanic glass. An irregular contact occurs between the hyaloclastite and Flow 2, which is composed of north-facing mattress- to bun- shaped pillow lavas and pillow lobes with numerous “neck and knob” structures. Individual Pillow structures have well developed perlitic hyaloclastite margins that range from 1-4 cm in

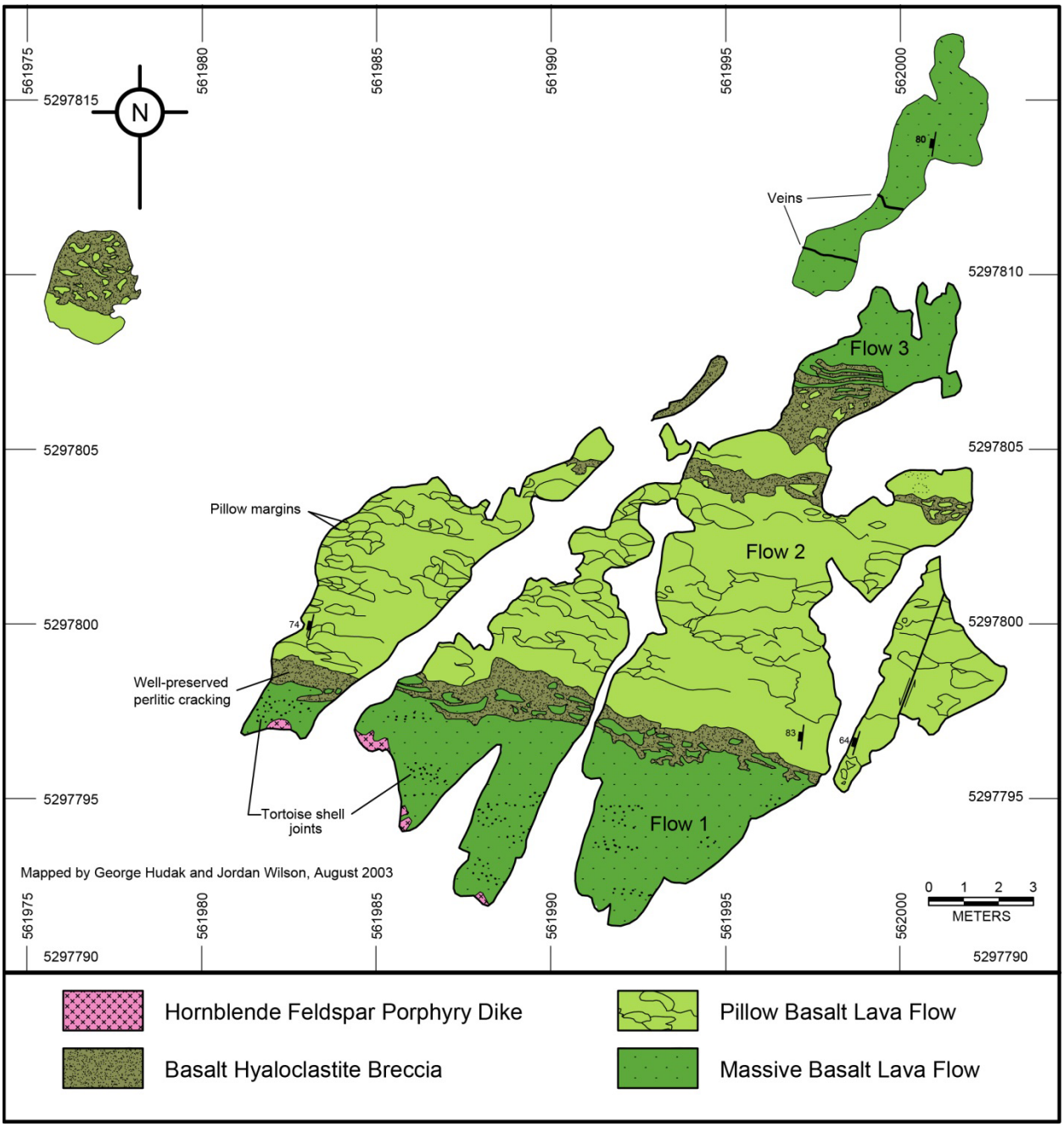


Figure 7-11. Detailed geological map of sheet flows, pillow lavas, and associated hyaloclastite deposits at Field Trip 3, Stop 1 (after Hudak et al., 2014; Hudak and Peterson, 2014).

width. Pillow buds indicate propagation from east to west, suggesting the volcanic vent was located east of this location. The coherent pillows and lobes are overlain by up to 2.5 meters of hyaloclastite breccia that contains 20-40% subrounded to subangular pale gray green basalt lapilli in a jigsaw puzzle-fit dark green perlitic hyaloclastite matrix. The upper contact of Flow 2 and the overlying basalt sheet flow (Flow 3) is irregular, and is marked by thin (1-8 cm thick), sheet- like basalt fragments that are up to 1.6 meters in length. These fragments locally appear to be isoclinally folded about an east-west-trending fold hinge. Although the genesis of this structure is currently not well understood, it may be due to syneruptive deformation of either thin slabs of hot, basal flow margin crust from the overlying flow, or thin injections of basalt magma into the hyaloclastite from either the underlying pillows or the overlying sheet flow. Flow

3 comprises an at least ten-meter-thick pale green-gray, slightly feldspar-phyric, sparsely amygdaloidal sheet flow. Steep, NNE-trending west dipping D_3 joints are well developed in this unit, as are lens-shaped psuedo-pillows that are up to 50 cm in diameter.

Return to the bus by walking back down the hill.

Stop 7: Mud Creek Shear Zone

Longitude/Latitude: 47.87440908°N, -92.14025702E

UTM NAD 83 Zone 15N: 585753E, 5309482N

This outcrop shows highly strained rocks in the Mud Creek shear zone. The rock type is a quartz-iron carbonate-sericite schist, having quartz and tourmaline knots, abundant pyrite, and trace amounts of gold. Its protolith is unknown, because of the intense deformation, but could be any of several rock types in the region, including quartzofeldspathic porphyry, basaltic metavolcanic rocks, or graywacke. The shear fabric trends east-northeast, and lineations plunge at shallow angles to the east. Development of this shear zone, which occupies most of the valley of Mud Creek, is a product of largely dextral transpressive deformation that has been partitioned into discrete zones, presumably late in D_2 deformation. It is generally believed that gold-bearing mineralization was introduced during these later deformation events, and the Mud Creek shear zone and environs have attracted considerable attention as a gold target (Peterson, 2001, Peterson and Patelke, 2004a, 2004b). The Mud Creek shear is a broad, anastomosing zone that forms the boundary between rocks of the Ely Greenstone and Lake Vermilion Formation on the south, and volcanic and iron formation-bearing rocks known informally as the Bass Lake sequence on the north. The Bass Lake rocks may be equivalent to parts of the Newton Lake Formation exposed north of Ely, but a complex series of faults in the intervening area makes this correlation speculative.

Return to bus.

Stop 8: Newton Lake Formation Variolitic Pillow Lavas and Hyaloclastite

Longitude/Latitude: 47.93291301°N, -91.85191152E

UTM NAD 83 Zone 15N: 585753E, 5309482N

(NOTE: Modified from Field Trip Stop 5-16 (Jirsa et al., 2004), and Field Trip Stop ET-1 (Peterson et al., 2009)).

The Neoarchean Newton Lake Formation is composed primarily of tholeiitic and komatiitic pillowed mafic lava, diabasic gabbro, differentiated mafic-ultramafic sills, intermediate-mafic pyroclastic rocks and siliceous marble with minor felsic-intermediate volcaniclastic rocks and lava flows. This formation is approximately 2,350 m thick. The unit overlies the Knife Lake Group in central part of the Vermilion district and the Lake Vermilion Formation in western part of Vermilion district (USGS National Geologic Map Database, https://ngmdb.usgs.gov/Geolex/UnitRefs/NewtonLakeRefs_9525.html).

The Newton Lake Formation differs from the Ely Greenstone Formation in that the former contains a high proportion of mafic-ultramafic sills and lava flows, abundant diabasic sills and rare iron-formation. Lava flows in the Newton Lake Formation typically have larger MgO and incompatible element contents than those of the Ely Greenstone Formation, and some are classified as komatiites and komatiitic basalt (Schulz, 1980; Jirsa et al., 2004; Grotte and Hudak, 2014). The Newton Lake Formation (and possibly equivalent Bass Lake sequence) appears to be younger than the Lower Ely Member (~2723 MA; Peterson et al., 2001) with an age date of ~2715 MA (Jirsa, 2016) and was previously interpreted to be the youngest Archean supracrustal sequence in the Vermilion district until the Gafvert Lake Sequence was dated at

approximately 2689 MA (Lodge et al., 2013). Rocks having nearly identical composition and stratigraphic/structural setting occur in Itasca County some 80 kilometers to the west (Jirsa, 1990; Jirsa et al., 2004).

A sequence of exceptionally well-preserved steeply-dipping, south-topping, lower greenschist facies metamorphosed Newton Lake Formation variolitic pillow lavas is exposed along a series of outcrops located on the west side of the road approximately one-half mile north of CR-88 on the Echo Trail. Variolites are defined as "a spherulite-like radiating aggregate composed of feathery, needle-like crystals of plagioclase and pyroxene that occur in mafic volcanic rocks (typically basalt). Variolites may result from devitrification but are commonly believed to be formed in subaqueous rocks by quench-induced crystallization (Cas and Wright, 1987, p. 420). According to Arndt and Fowler (2004), variolites result from either magma mingling or blotchy alteration, or they are a type of plagioclase spherulite.

A generalized cross-section through these pillows from a detailed field and petrographic study of this outcrop (Grotte and Hudak, 2014) is presented in Figure 7-12A. Pillows vary from "bun-" to "mattress-" shaped (Dimroth et al., 1978) and range from <1 to >2.5 meters in diameter.

Pillow shapes, as well as the local occurrence of quartz-filled vacuoles within individual pillows, indicate younging directions to the south. Pillow cores tend to be dark green to pale yellow-green in color depending upon the abundance of secondary epidote alteration. The pillow cores commonly contain massive, globular variolites with local <1cm diameter spherical variolites., and are locally variolitic (Figure 7-12B). Pillow selveges are well preserved and commonly contain concentric zones globular to spherical

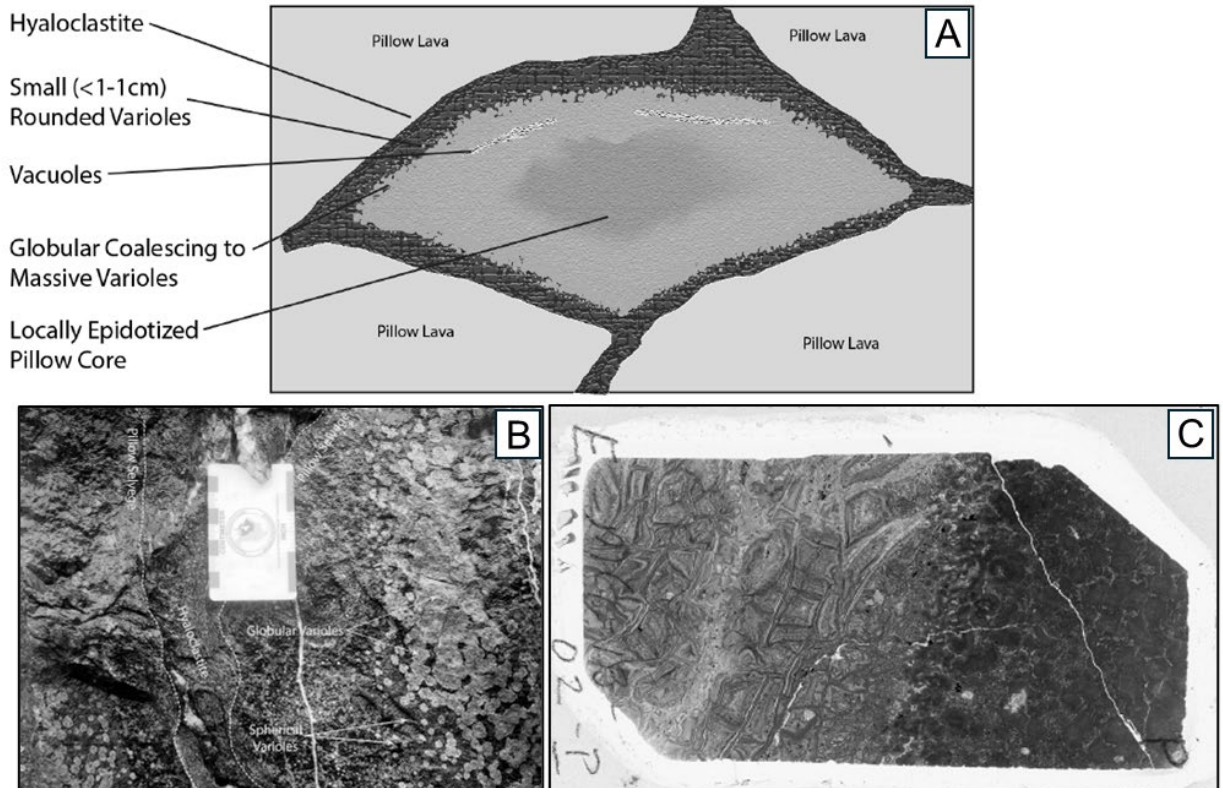


Figure 7-12. Summary of field and petrographic observations of Newton Lake Formation variolitic pillow lavas at this location (from Grotte and Hudak, 2014). A) Generalized cross-section through a Newton Lake Formation pillow lava at this location. B) Outcrop photo of the margin of a pillow lava at this location noting the transition from well-preserved interpillow hyaloclastite into a variolitic pillow selvege. C) Thin section scan illustrating the well preserved cuspate, angular shards comprising the interpillow hyaloclastite. Dark spherical shapes on the right half of the photo are variolites.

variolites that mimic individual pillow shapes. Interpillow hyaloclastite is extremely well preserved and is composed of jigsaw-puzzle-fit angular cuspate shards that were originally glass but are now composed of fine-grained alteration minerals (Figure 7-12C).

Petrographic observations (Grotte and Hudak, 2014) indicate that variolites in this exceptional exposure of Newton Lake Formation pillow lavas are dominantly composed of rounded to oval, radiating plagioclase spherulites with rare, axiolitic plagioclase spherulites locally present. The presence of needle-like to acicular skeletal plagioclase crystals and absence of phenocrysts suggest that the pillow lava flows at this location erupted at temperatures above the liquidus and experienced relatively large degrees of undercooling before undergoing rapid crystallization on the Neoarchean seafloor.

As indicated in Jirsa et al. (2004), the Newton Lake is separated from the Ely Greenstone to the south by a complex zone of faulting (Shagawa Lake and Sibley faults) developed within sedimentary rocks of the Knife Lake Group. Although relatively undeformed conglomerate and sedimentary rocks of the Knife Lake Group are exposed just a few miles to the east, they are typically so sheared and altered in this area as to obscure lithologic and sedimentary interpretations.

Return to bus

Stop 9: Giants Range Batholith

Longitude/Latitude: 47.81587746°N, -91.79083789E

UTM NAD 83 Zone 15N: 590518E, 5296544N

(NOTE: Modified from Hudak and Peterson, 2014).

Footwall rocks to the northern part of the South Kawishiwi Intrusion are part of the Neoarchean Giants Range batholith (GRB). At this exposure along Highway 1, the GRB consists of porphyritic hornblende quartz monzonite that contains distinctive 1-2cm diameter potassium feldspar phenocrysts. One may also observe a distinctive foliation represented by alignment of black to dark green amphiboles and locally dark brown biotite.

The massive nature of this unit creates an excellent footwall for Duluth Complex-associated intrusions and associated Cu-Ni-PGE deposits as the GRB lacks bedding and thus rare (if ever) gets incorporated into the mineralized zone as barren xenoliths. Additionally, melting of the GRB beneath long-lived magma channels (Peterson and Boerst, 2013) at the base of the Maturi deposit has contaminated the South Kawishiwi intrusion, inducing additional sulfide immiscibility and the genesis of Ni- and Co-rich massive sulfide bodies.

Return to bus

Stop 10: Maturi SW Roadcuts of BH and U3 Units

Longitude/Latitude: 47.78505228°N, -91.79056387E

UTM NAD 83 Zone 15N: 590592E, 5293118N

Classic roadside exposures of heterogeneous sulfide-bearing troctolite and layered melatroctolite of Severson's (1994) Basal Heterogeneous (BH) and Ultramafic 3 (U3) units of the SKI. A large core-stone is well exposed in the weakly saprolitic heterogeneous troctolite outcrop. Several small xenoliths of fine-grained troctolite can be observed on top of the outcrop and are interpreted as Stage 1 chilled margin autoliths (Peterson and Boerst, 2013). Within the exposure of the overlying U3 layered melatroctolite, olivine layers strike 17° and dip steeply 51° to the ESE. The steep dip is apparently associated with two

defined north-south trending faults east of these exposures. Recent drilling by Twin Metals Minnesota in this area has led to the definition of the Maturi SW deposit.

Return to bus

Stop 11: SKI Magmatic Slurry Igneous Breccia

Longitude/Latitude: 47.780584°N, -91.79273111E

UTM NAD 83 Zone 15N: 590437E, 5292619N

At this stop, we'll examine perhaps the best exposure of Severson's (1994) BH unit in the whole of the SKI. The heterogeneous troctolitic rocks at this stop are generally poorly mineralized and thus lack a gossanous saprolitic weathering profile which lets one see the true nature of the heterogeneity within the troctolite. We believe that all geologists who log drill core within the Cu-Ni-PGE deposits of the Duluth Complex (or who attempt to model such deposits for mine planning purposes) should be required to spend several days examining the rocks within the area around both Stops 10 and 11. All participants should imagine a drill core cutting this exposure and how they would interpret the geology of that core without first examining this outcrop. Such thoughts are why the Precambrian Research Center's field camp had for many years its students complete a 1:5,000-scale bedrock geology map of this area.

Return to bus

Stop 12: Main AGT

Longitude/Latitude: 47.81303067°N, -91.73468023E

UTM NAD 83 Zone 15N: 594727E, 5296295N

Recent road cut along the south side of Minnesota Highway #1 of massive, extremely homogeneous augite troctolite of the Main AGT unit of Severson (1994). Troctolite of the Main AGT unit differs from the Middle and Upper SKI troctolite in two distinctive ways: 1) ophitic augite crystals are black, distinctly associated with Fe-Ti oxides + apatite, and occur as high-density ophitic crystals from 1 to 3 inches in diameter. In the Middle and Upper SKI, ophitic augite crystals are brown, not associated with Fe-Ti oxides, and occur as large (up to 15 inches) low-density grains; and 2) The Main AGT is never layered. Geologists at Duluth Metals interpret the units' homogeneity and lack of layering as evidence that the Main AGT magma lacked phenocrysts of olivine and plagioclase and represents the end product of topdown and bottom-up solidification of a basaltic liquid. We currently interpret the Main AGT as the solidification of much of the "carrier liquid" of the underlying sulfide-bearing BMZ magmatic slurry.

Return to bus

Stop 13: Spruce Road Bulk Sample Site/Discovery Burrow Pit

Longitude/Latitude: 47.83271644°N, -91.67864227E

UTM NAD 83 Zone 15N: 598885E, 5298553N

Beginning in the late 1940s, the U.S. Forest Service utilized locally derived glacial tills and weathered bedrock gossans as road building materials during the construction of the Spruce Road. As we take a short hike into one of these borrow pits, we will walk by the 1973 INCO bulk sample site in the Spruce Road deposit and visit several outcrops with fresh Cu-Ni sulfide minerals. This short stop will examine the bottom of an old borrow pit where participants can walk on and sample sulfide-bearing

troctolite gossans. Please note the friable nature of the rocks in the weakly saprolitic exposure and look for rounded core-stones where weathering over the eons was less intense.

Return to bus

Stop 14: Nickel Lake Macrodike

Longitude/Latitude: 47.83079527°N, -91.63760896E

UTM NAD 83 Zone 15N: 601959E, 5298393N

The Nickel Lake Macrodike (NLM) is a northwest to southwest-trending, steeply dipping, asymmetric troctolitic and gabbroic intrusion interpreted to be a feeder dike for the northern portions of the SKI. The macrodike is interpreted to be located within a major rift-parallel normal fault (down to the southeast) now obscured by intrusion of NLM igneous rocks. Regional southward tilting (based on the deep level of erosion of the northern Bald Eagle Intrusion directly east of this area) leads to the interpretation that the southwest end of the NLM (near Omaday Lake) is structurally higher than the northeastern portion of the dike, and represents the location where magma flow changed from dike-like to sill-like, as it exited

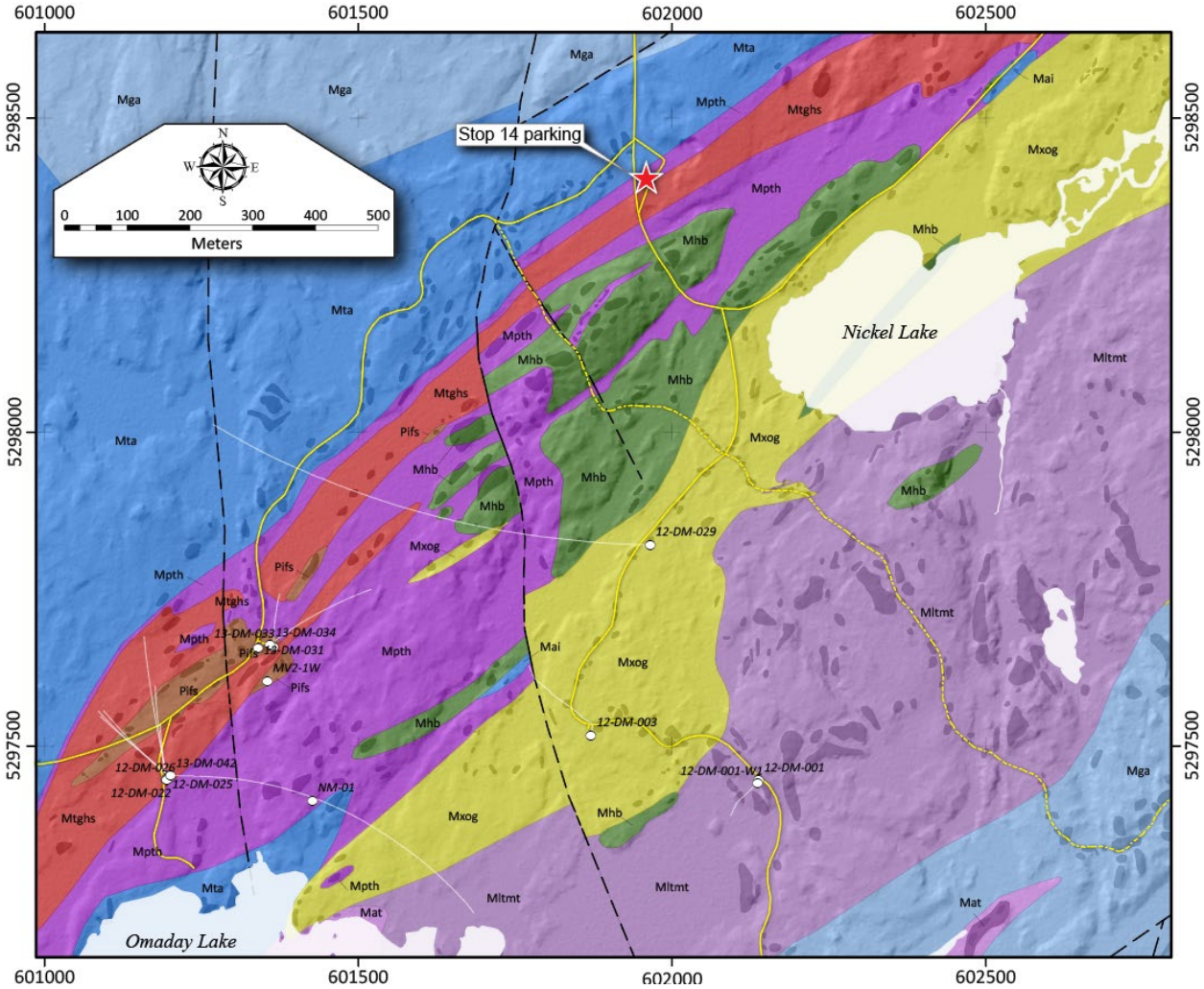


Figure 7-13. Bedrock geology map of the southwestern end of the Nickel Lake Macrodike.

the dike – thus the magma velocity slowed – and entered the growing SKI magma chamber. Excellent potential exists for Ni-Cu rich massive sulfide at the basal contact where the dike enters the SKI (Section 31, T62N, R10W).

The 6.5km long by 1.0 km wide macrodike is composed of three main units: 1) inclusion-rich, locally sulfide-bearing, heterogeneous troctolite (unit Mpth) along the northwestern margin; 2) layered troctolite, melatroctolite, and dunite (unit Mltmt) along the southeastern margin; and 3) a late, cross-cutting, coarse-grained to pegmatitic oxide-rich, olivine-gabbro to melagabbro (unit Mxog) traversing generally through the center. Small (< 1m) to large (hundreds of meters long) xenoliths include Mesoproterozoic Anorthositic Series wall rocks (unit Mai) and North Shore Volcanic Group basalts (unit Mhb), and Paleoproterozoic Biwabik Iron Formation (unit Pifs) and Virginia Formation (unit Pvf). For this field trip we are simply going to take some walks in the bush, mostly along logging roads and snowmobile trails as time allows and look at numerous outcrops of the NML and adjacent rocks and discuss geology as we see it. Numerous detailed bedrock geology maps, reports, and presentations of the NLM and adjacent areas have been published over the last couple of decades (Peterson, 2002a, 2002b, 2002c, 2006a, 2006b, 2006c, 2008, Peterson and Albers, 2007) and a compilation of detailed geologic mapping data for the southwestern NLM is given in Figure 7-13.

Return to bus

Stop 15: Remnant Saprolite, Middle SKI

Longitude/Latitude: 47.77089981°N, -91.66297244E

UTM NAD 83 Zone 15N: 600176E, 5291703N

A short field trip stop to examine locally layered troctolitic rocks of the Upper SKI of Peterson and Boerst (2013). This outcrops in this area epitomizes the "Sea of Troctolite" that occurs throughout the vast majority of the SKI (Middle and Upper SKI of Peterson and Boerst, 2013). Careful attention will be given to an outcrop next to the bus where spheroidal weathering of the troctolite is forming rounded core stones of troctolite, which we'll see once again at stop 18.

Return to bus

Stop 16: Anorthosite Series Roadcut

Longitude/Latitude:: 47.75915521°N, -91.64719916E

UTM NAD 83 Zone 15N: 601381E, 5290418N

Large, glacially polished roadside outcrop of the gabbroic and troctolitic anorthosites of the Anorthositic Series of the Duluth Complex. At this location these anorthositic rocks form the eastern sidewall of the SKI and are cut by a series of northeast-striking valleys. The valleys were interpreted by geologists of Duluth Metals Limited as steeply west-dipping reverse faults that were formed by emplacement of the SKI immediately to the west. Approximately 2.5 km to the southwest of this roadcut Cold Spring Granite Company quarries a large gabbroic anorthosite xenolith similar to this stop in their Mesabi Black quarry.

Return to bus

Stop 17: Bald Eagle Intrusion

Longitude/Latitude: 47.7385175°N, -91.6405279E

UTM NAD 83 Zone 15N: 601921E, 5288133N

A quick stop to observe a roadside outcrop of troctolite of the Bald Eagle Intrusion (BEI). The BEI is a large (4.5 to 16.5 km x 31 km) troctolitic to gabbroic body that was emplaced partially within Anorthositic series rocks, the SKI, and the Greenwood Lake Intrusion (see BEI on Figure 7-7). Weiblen (1965) mapped the well-exposed northern portion of the intrusion and showed that it is funnel-shaped and consists of an outer zone of troctolite and an inner zone of olivine gabbro. In the poorly exposed southwestern portions of the intrusion, field mapping by Green et al., (1966) and Foose and Cooper (1978) showed the BEI and SKI in direct conformable contact. Steep foliation and modal layering (Weiblen, 1965, Green et al., 1966) integrated with a distinct gravity anomaly over the northern BEI imply that the northern part of this intrusion is funnel shaped and necks down to a steep feeder dike. Weiblen and Morey (1980) interpreted the limited cryptic variation (Weiblen, 1965), the steep dip of lamination and layering, and adcumulate nature of the BEI as indicative of its being an open conduit to higher intrusions and perhaps volcanic flows.

Petrologic observations and geophysical interpretations (Chandler, 1990, Chandler and Ferderer, 1989) suggest that the BEI and SKI were emplaced by successive overplating of magmas from a common feeder centered on the northern BEI and extending along the trace of the NLM that links the BEI and SKI. In a related analogy, Cartwright and Møller-Hansen (2006) have shown that interconnected sill complexes transect the middle to upper crust over a vertical distance of 8-12 km offshore of Norway. The geometry of the gravity and magnetic anomalies of the BEI, as well as the overall Midcontinent Rift is very similar to the pattern of the seismic reflections profiles of active ridge systems (Vislova, 2003). In detail, the geophysical expressions of the BEI have the same shape and dimensions as the "bulls' eye" pattern of low velocity seismic reflection anomalies along the East Pacific Rise. These anomalies are interpreted to define regions of melt concentrations, i.e., active magma chambers. These data suggest that the BEI could be a "frozen" dynamic magma chamber (Weiblen et al., 2005, Peterson and Hauck, 2005).

Eight exploration holes drilled by Duluth Metals Limited in 2011 revealed several new distinct features of the BEI. All of these holes encountered chromitite layers within horizontally layered troctolites with many of the chromitite horizons occurring as "rip up" clasts within troctolites. Duluth Metals Limited's hole LOD-06, drilled 12km SSW of this field trip stop, encountered flowing gas at a depth of 1,778 feet. The gas was analyzed and found to contain >10% helium. This is the site where Pulsar is currently exploring with the aim of producing helium gas.

Return to bus

Stop 18: Vermilion Moraine

Longitude/Latitude: 47.6918526°N, -91.81063993E

UTM NAD 83 Zone 15N: 589247E,5282737N

In common with most of the high latitude regions of North America, northeastern Minnesota was repeatedly glaciated during the ice ages of the Pleistocene Epoch. Glaciogenic sediments and landforms in this 2025 ILSG field trip area are associated with the Rainy Lobe of the Laurentide ice sheet. While there are a number of possible definitions of what constitutes the Rainy Lobe – sedimentological, textural, compositional, and association with particular geomorphic features – a definition rooted in glacial dynamics perhaps works best. In this sense, the Rainy Lobe refers to that portion of the Laurentide ice sheet lying northwest of Lake Superior (occupied by the Superior Lobe), and east of the Winnipeg Basin and Red River Valley (occupied by the Red River Lobe). In common, Rainy Lobe landforms and glaciogenic sediments

reflect a general northeast to southwest ice flow direction, and a Labradoran (northeastern) sediment provenance.

In common with much the Canadian Shield, glacial erosion has nearly completely stripped preglacial regolith from bedrock north of the Laurentian Divide. However, preglacial saprolites are a common occurrence underlying glaciogenic sediments in central and western Minnesota; the nearest such occurrences are exposed in open pit mines of the Mesabi Range, on the south flank of the Giant's Range.

Approximately 12,400 years ago, the retreating Rainy Lobe made a last stand in northern Minnesota to form the West-Northwest to East-Southeast trending Vermilion Moraine. This stop includes a quick walk over the end of the Vermilion Moraine and a view to the south over a glacial lake plain (Fig. 7-14).

Return to bus

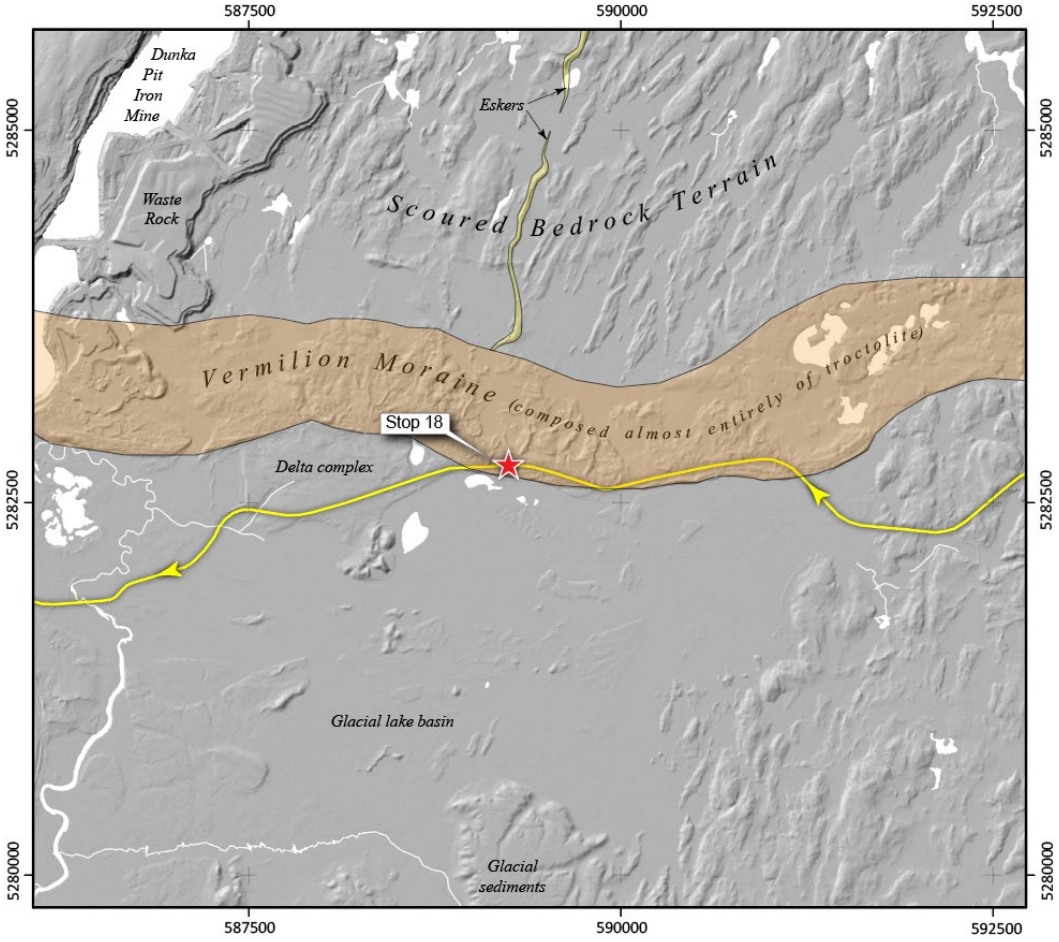


Figure 7-14. Annotated lidar digital elevation model showing glaciogenic landforms in the stop 18 area.

Stop 19: Contaminated Basal SKI, Dunka Pit Area

Longitude/Latitude: 47.69423099°N, -91.85803438E

UTM NAD 83 Zone 15N: 585687E, 5282948N

The recently permitted extension of Cliffs Natural Resources Northshore mine required the rerouting of St. Louis County Road 623 to the north. The building of the new road resulted in the exposure of rocks of the ~1.85 Ga. Biwabik Iron Formation and the 1.1 Ga. South Kawishiwi intrusion. This short stop will include the examination of three new roadside outcrop areas, including: 1) Metamorphosed Biwabik Iron Formation, 2) Sulfide-poor gabbroic rocks, and 3) Sulfide-rich (pyrrhotite-dominant)

contaminated noritic rocks. Geochemical analyses of rock samples from these three outcrop areas (completed by Duluth Metals in 2012) are given in Table 7-4.

Table 7-4. Geochemical analyses of rock samples taken from the roadside outcrops of Stop 19.

Sample ID	DMR0446	DMR0447	DMR0164	DMR0165	DMR0448	DMR0449	DMR0450	DMR0451
Rock Type	Iron Formation	Iron Formation	Olivine Gabbro	Biotitic Gabbro	Sulfidic Norite	Sulfidic Norite	Sulfidic Norite	Sulfidic Norite
Outcrop #	1	1	2	2	3	3	3	3
Cu (ppm)	4	0	357	218	3960	2630	4380	4270
Ni (ppm)	0	0	82	87	1230	761	1030	1120
Co (ppm)	2	13	44	53	191	117	168	183
Pt (ppb)	5	1	1	1	9	20	6	16
Pd (ppb)	1	3	1	2	53	40	58	60
Au (ppb)	1	1	1	1	18	15	23	23
S (%)	-0.01	-0.01	0.02	-0.01	2.61	1.62	1.58	1.79
SiO2 (%)	51.35	38.71	48.14	47.28	42.67	51.62	41.25	43.53
Al2O3 (%)	0.25	0.45	15.21	15.06	15.02	17.56	13.81	13.71
Fe2O3 (%)	40.11	55.01	15.64	16.35	21.04	11.98	22.12	21.34
CaO (%)	6.07	3.33	7.87	8.00	7.51	5.39	6.29	6.90
MgO (%)	1.93	1.52	4.93	5.47	7.15	5.13	6.01	6.97
Na2O (%)t	0.06	0.06	2.90	2.62	2.25	2.72	1.99	2.34
K2O (%)	0.01	0.01	1.12	1.10	0.68	2.54	0.56	0.63
Cr2O3 (%)	-0.01	-0.01	0.02	0.01	0.02	0.03	0.02	0.02
TiO2 (%)	-0.01	0.05	3.12	3.47	1.77	0.76	1.90	2.31
MnO (%)	0.97	0.51	0.19	0.20	0.16	0.08	0.14	0.18
P2O5 (%)	0.06	0.07	0.43	0.34	0.23	0.05	0.26	0.26
LOI (%)	-0.95	-1.37	0.05	-0.09	1.25	1.80	5.13	1.02

Photographs of the Biwabik Iron Formation (outcrop #1) and sulfidic norite of the South Kawishiwi intrusion (outcrop #3) are presented in Figure 7-15.



Figure 7-15. Field photographs of roadside outcrops of stop 5. (A) outcrop of the Biwabik Iron Formation, (B) closeup shot of bedding in granular iron formation (GIF), (C) rusty weathering and gossanous outcrop of the basal mineralized zone of the South Kawishiwi intrusion, and (D) pyrrhotite-rich norite.

Return to bus

Stop 20: Giants Range Batholith Migmatite/Pyroxenite-Lamprophyre Dike

Longitude/Latitude: 47.68689429°N, -92.05199159E

UTM NAD 83 Zone 15N: 571144E, 5281936N

This field trip ends where we began, within the Neoarchean Giants Range Batholith. This roadside outcrop of the Embarrass tonalite, an early phase of the GRB that was first mapped by Griffin and Morey (1969) and later remapped by Terry Boerboom in 2015. The outcrop, as mapped by Terry Boerboom, consists of intermixed migmatitic biotite-schist and tonalitic gneiss crosscut by a lamprophyre/pyroxenite dike. Approximately 4-miles to the west of this outcrop the Embarrass Tonalite was originally dated by U-Pb zircon at 2718 ± 67 Ma by Peterman in Southwick (1994). This data has been superseded by a second U-Pb zircon age of 2687 ± 0.6 Ma by Jirsa (2016).

RETURN TO MOUNTAIN IRON COMMUNITY CENTER

Acknowledgements

Characterizing and evaluating the detailed geology of northeastern Minnesota has been a team effort involving former NRRI geologists, former and current Minnesota Geological Survey geologists and geophysicists, personnel from the Minnesota Department of Natural Resources and students and faculty from the Precambrian Research Center Field Camp, the University of Minnesota Duluth, the University of Minnesota Twin Cities, and the University of Wisconsin Eau Claire. Their efforts are appreciated. As well, permission to map private properties that was granted by local landowners and mineral exploration/mining companies is much appreciated. The authors would like to thank Jim Essig (Manager, Lake Vermilion / Soudan Underground Mine State Park) and James Pointer (Interpretive Supervisor, Lake Vermilion / Soudan Underground Mine State Park) from the MDNR for their support, assistance, and guidance while planning and conducting detailed geological mapping by the NRRI geologists during the DUSEL project and PRC students and faculty in Lake Vermilion State Park in 2010 and 2011. Funding from the Minerals Coordinating Committee, the University of Minnesota Permanent University Trust Fund, the National Science Foundation, the University of Minnesota Duluth Undergraduate Research Opportunities Program, the University of Minnesota Duluth Graduate School, The University of Wisconsin Oshkosh Student-Faculty Research Program, and many mineral exploration companies also enabled geological research in northeastern Minnesota.

References

Allen, D.J., Hinze, W.J., Dickas, A.B., and Mudrey, M.G., Jr., 1997, Integrated geophysical modeling of the North American Midcontinent rift system: New interpretations for western Lake Superior, northwestern Wisconsin, and eastern Minnesota, in Ojakangas, R.W., Dickas, A.B., and Green, J.C., eds.: Middle Proterozoic to Cambrian rifting, central North America: Geological Society of America, Special Paper 312, p. 47-72.

Allerton, Z., Hudak, G., Teyssier, C., Fayon, A., Danisik, M., Courtney-Davies, L, and Larson, P., 2024a, Geochronology campaign in northeastern Minnesota: Institute on Lake Superior Geology, Proceedings Volume 70, Part 1 – Program and Abstracts, p. 2-3.

Allerton, Z., Hudak, G., Teyssier, C., Fayon, A., Danisik, M., Courtney-Davies, L, and Larson, P., 2024b, Geochronology and geochemistry of hematite ore in northeastern Minnesota: Institute on Lake Superior Geology, Proceedings Volume 70, Part 1 – Program and Abstracts, p. 4-5.

Arndt, N., and Fowler, A., 2004, Textures in komatiites and variolitic basalts: in Erikson et al., The Precambrian Earth – Tempos and Events, Elsevier, p. 298-311.

Ayer, J. A., Goutier, J., Thurston, P. C., Dube, B., and Kamber, B. S., 2010, Tectonic and Metallogenic Evolution of the Abitibi and Wawa subprovinces: Summary of Field Work and Other Activities, 2010, Ontario Geological Survey Open File Report 6260, p. 3-1 – 3.6.

Batiza, R., and White, J. D. L., 2000, Submarine lavas and hyaloclastite: *in* Sigurdsson, H., Encyclopedia of Volcanoes: Academic Press, San Diego, CA, p. 361-381.

Bauer, R. L., 1985, Correlation of early recumbent and younger upright folding across the boundary between an Archean gneiss belt and greenstone terrane, northeastern Minnesota: Geology, v. 13, p. 657-660.

Boerboom, T. J., 2020, D-07, Geochronology Database: Minnesota Geological Survey – Open Data Site, https://mngs-umn.opendata.arcgis.com/datasets/d7903b83244a4878bcfb31f362bf5787_0/explore?location=46.147285%2C-92.317888%2C7.04.

Boerboom, T. J., and Zartman, R. E., 1993, Geology, geochemistry, and geochronology of the central Giants Range Batholith, northeastern Minnesota: Canadian Journal of Earth Science, v. 30, p. 2510-2522.

Bonnichsen, B., 1974, Geology of the Ely–Hoyt Lakes district, northeastern Minnesota: Minnesota Geological Survey, Open-File Report, 29 p.

Bonnichsen, B., Fukui, L.M., and Chang, L.Y., 1980, Geologic setting, mineralogy, and geochemistry of magmatic sulfide deposits, Duluth Complex, U.S.A.: Proceedings, 5th quadrennial International Association on the Genesis of Ore Deposits Symposium, Stuttgart, Germany, p. 545-565.

Cartwright, J., and Møller Hansen, D., 2006, Magma transport through the crust via interconnected sill complexes: Geology, v. 34, no. 11, p. 929-932.

Cas, R. A. F., and Wright, J. V., 1987, Volcanic Successions – Modern and Ancient: George Allen and Unwin, London, 528 p.
Chandler, V.W., 1990, Geologic interpretation of gravity and magnetic data over the central part of the Duluth Complex, northeastern Minnesota: Economic Geology, v. 85, no. 4, p. 816-829.
Chandler, V.W., and Ferderer, R.J., 1989, Copper-nickel mineralization of the Duluth Complex, Minnesota-A gravity and magnetic perspective: Economic Geology, v. 84, no. 6, p. 1690-1696.
Corfu, F. and Stott, G. M., 1998, Shebandowan greenstone belt, western Superior Province: U-Pb ages, tectonic implications, and correlations: Geological Society of America Bulletin, v. 110, p. 1467-1484.
Dahlberg, E.H., 1987, Drill core evaluation for platinum group mineral potential of the basal zone of the Duluth Complex: Minnesota Department of Natural Resources, Division of Minerals, Report 255, 60 p.
Dahlberg, E.H., Peterson, D.M., and Frey, B.A., 1989, Drill core repository projects (1988-1989): Minnesota Department of Natural Resources, Division of Minerals, Reports 255-1, 265, and 266, 316 p.
Dimroth, E., Cousineau, P., Leduc, M., and Sanschagrin, Y., 1978, Structure and organization of Archean subaqueous basalt flows, Rouyn-Noranda area, Quebec: Canadian Journal of Earth Sciences, v. 15, p. 902-918.
Driese, S. G., Jirsa, M. A, Ren, M., Brantley, S. L., Sheldon, N. D., Parker, D., and Schmitz, M. D., 2011, Neoarchean paleoweathering of tonalite and metabasalt: Implications for reconstructions of 2.69 Ga early terrestrial ecosystems and paleoatmospheric chemistry: Precambrian Research, v. 189, p. 1-17.
Fisher, R. V., 1961, Proposed classification of volcaniclastic sediments and rocks: Geological Society of America Bulletin, v. 72, p. 1409-1414.
Fisher, R. V., 1966, Rocks composed of volcanic fragments and their classification: Earth Science Reviews, v. 1, p. 287-298.
Fisher, R. V., 1998, Out of the Crater: Princeton University Press, 180 p.
Foose, M.P., 1984, Logs and correlation of drill holes within the South Kawishiwi intrusion, Duluth Complex, northeastern Minnesota: U.S. Geological Survey, Open-File Report 84-14, variously paged, 1 pl.
Foose, M.P., and Cooper, R.W., 1978, Preliminary geologic report on the Harris Lake area, northeastern Minnesota: U.S. Geological Survey, Open-File Report 78-385, 24 p., 1 pl., scale 1:12,000.
Gal, B., 2008, The South Filson Creek deposit, a Masters of geology thesis: Eotvos Lorand University, Budapest, Hungary.
Gibson, H. L., Morton, R. L., and Hudak, G. J., 1999, Submarine volcanic processes, deposits, and environments favorable for the location of volcanic-associated massive sulfide deposits: Reviews in Economic Geology, v. 8, p. 13-51.
Green, J.C., Phinney, W.C., and Weiblen, P.W., 1966, Geologic map of Gabbro Lake quadrangle, Lake County, Minnesota: Minnesota Geological Survey, Miscellaneous Map Series, Map M-2, scale 1: 31,680.
Griffin, W.L., and Morey, G.B., 1969, The geology of the Isaac Lakes quadrangle, St. Louis County, Minnesota: Minnesota Geological Survey Special Publication SP-8, 57p.
Grotte, M., and Hudak, G., 2014, A field and petrographic study of Neoarchean variolitic pillow lavas, Newton Belt, Vermilion District, NE Minnesota [abstract/poster]: Institute on Lake Superior Geology, v. 60, Part 1, p. 53-54.
Gruner, J. W., 1926, Hydrothermal alteration of iron ores of the Lake Superior type – a modified theory: Economic Geology, v. 32, p. 121-130.
Hauck, S., Severson, M., Ripley, E., Goldberg, S., and Alapieti, T., 1997, Geology and Cr-PGE mineralization of the Birch Lake area, South Kawishiwi intrusion, Duluth Complex: University of Minnesota Duluth, Natural Resources Research Institute, Technical Report, NRRI/TR-97/13, 32 p.
Hauck, S.A., Severson, M.J., Zanko, L.M., Barnes, S.-J., Morton, P., Aliminas, H.V., Foord, E.E., and Dahlberg, E.H., 1997, An overview of the geology and oxide, sulfide, and platinum-group element mineralization along the western and northern contacts of the Duluth Complex, in Ojakangas, R.W., Dickas, A.B., and Green, J.C., eds., Middle Proterozoic to Cambrian rifting, central North America: Geological Society of America Special Paper 312, p. 137-185.
Hooper, P., and Ojakangas, R., 1971, Multiple deformation in the Vermilion District, Minnesota: Canadian Journal of Earth Sciences, v. 8, p. 423-434.
Hudak, G. J., Heine, J., Newkirk, T., Odette, J., and Hauck, S., 2002a, Comparative geology, stratigraphy, and lithogeochemistry of the Fivemile Lake, Quartz Hill, and Skeleton Lake VMS occurrences, Vermilion district, NE Minnesota: A report to the Minerals Coordinating Committee, DNR, Minerals Division, State of Minnesota: Natural Resources Research Institute Technical Report NRRI/TR-2002/03, 390 pages.
Hudak, G. J., and Peterson, D. M., 2014, Non-Ferrous Mineralization Associated with the Wawa-Abitibi Terrane and Duluth Complex Cu-Ni-PGM Deposits, Northeastern Minnesota: Society of Economic Geologists, Guidebook Series, v. 47, 150 p.

Hudak, G. J., Heine, J., Lodge, R. W. D., and Jansen, A., 2012, Recent developments understanding the volcanic, magmatic, tectonic, and metallogenic evolution of the Ely Greenstone Formation, Vermilion District, NE Minnesota: Geological Association of Canada – Mineralogical Association of Canada, Abstracts and Program, v. 35, p. 59.

Hudak, G. J., Hoffman, A. T., Peterson, D. M., and Heine, J., 2007, Recent developments understanding the volcanic, magmatic, tectonic, and metallogenic evolution of the Ely Greenstone Formation, Vermilion District, NE Minnesota: 53rd Annual Meeting, Institute on Lake Superior Geology, Proceedings Volume 53, Part 1 – Program and Abstracts, p. 42-43.

Hudak, G. J., Radakovich, A., Pignotta, G., and Schwierske, K., 2014, Field Trip 2 – A Walk in the Park – Neoarchean Geology of Lake Vermilion State Park: Institute on Lake Superior Geology, Proceedings Volume 60, Part 2 – Field Trip Guidebook, p. 37-75.

Hudak, G.J., Heine, J., Jirsa, M.A., and Peterson, D.M., 2004, Field Trip 1 - Volcanic stratigraphy, hydrothermal alteration, and VMS potential of the Lower Ely Greenstone, Fivemile Lake to Sixmile Lake area: 50th Annual Meeting, Institute on Lake Superior Geology, Proceedings Volume 50, Part 2 – Field Trip Guidebook, p. 1-45.

Hudleston, P. J., Schultz-Ela, D., and Southwick, D. L., 1988, Transpression in an Archean greenstone belt, northern Minnesota: Canadian Journal of Earth Sciences, v. 25, p. 1060-1068.

Hudleston, P.J., 1976, Early deformational history of Archean rocks in the Vermilion district, north-eastern Minnesota: Canadian Journal of Earth Sciences, v. 13, p. 579-592.

Jansen, A. C., Hudak, G. J., Heine, J. J., and Peterson, D. M., 2009, Lithogeochemical evaluation of Neoarchean mafic volcanic rocks comprising the footwall to the Soudan Member of the Ely Greenstone Formation, northeastern Minnesota: 55th Annual Meeting, Institute on Lake Superior Geology, Proceedings Volume 55, Part 1 – Program and Abstracts, p. 46-47.

Jirsa, M. A., 2000. The Midway sequence: a Timiskaming-type pull-apart basin deposit in the western Wawa Subprovince, Minnesota: Canadian Journal of Earth Sciences, v. 37, p. 1-15.

Jirsa, M. A., Boerboom, T. J., and Peterson, D. M., 2001, Bedrock geological map of the Eagles Nest Quadrangle, St. Louis County, Minnesota: Minnesota Geological Survey, Miscellaneous Map M-114, scale 1:24,000.

Jirsa, M. A., Boerboom, T. J., Green, J. C., Miller, J. D., Morey, G. B., Ojakangas, R. W., and Peterson, D. M., 2004, Field Trip 5 – Classic outcrops of northeastern Minnesota: 50th Annual Meeting, Institute on Lake Superior Geology, Proceedings Volume 50, Part 2 – Field Trip Guidebook, p. 129-169.

Jirsa, M.A., 1990, Bedrock geologic map of northeastern Itasca County, Minnesota: Minnesota Geological Survey, Miscellaneous Map M-68, scale 1:48 000.

Jirsa, M.A., 2016, Preliminary geologic maps of Lake and St. Louis counties, northeastern Minnesota: Minnesota Geological Survey Open File Report OFR 16-4, https://conservancy.umn.edu/items/a68ec090-cf02-463a-8fcb-e3c05926d80e.

Jirsa, M.A., and Boerboom, T.J., and Peterson, D.M., 2001, Bedrock Geologic Map of the Eagles Nest Quadrangle, St. Louis County, Minnesota: Minnesota Geological Survey Miscellaneous Map M-114, scale 1:24,000.

Jirsa, M.A., Southwick, D.L., and Boerboom, T.J., 1992, Structural evolution of Archean rocks in the western Wawa subprovince, Minnesota: refolding of precleavage nappes during D2 transpression: Canadian Journal of Earth Sciences **29**:2146-2155.

Klinger, F. L., 1960, Geology and ore deposits of the Soudan Mine, St. Louis County, Minnesota: unpublished Ph. D. dissertation, University of Wisconsin, Madison, 96 p.

Kuenen, P.H., and Migliorini, C., 1950, Turbidity currents as a cause of graded bedding: Journal of Geology, 58:91-127.

Kuhns, M.J., Hauck, S.A., and Barnes, R.J., 1990, Origin and occurrence of platinum group elements, gold and silver in the South Filson Creek copper-nickel mineral deposit, Lake County, Minnesota: University of Minnesota Duluth, Natural Resources Research Institute, Technical Report NRRI/GMIN-TR-89-15, 60 p., 3 pls.

Lee, I., and Ripley, E.M., 1996, Mineralogic and oxygen isotopic studies of open system magmatic processes in the South Kawishiwi intrusion, Spruce Road area, Duluth Complex, Minnesota: Journal of Petrology, v. 37, no. 6, p. 1437-1461.

Listerud, W.H., and Meineke, D.G., 1977, Mineral resources of a portion of the Duluth Complex and adjacent rocks in St. Louis and Lake Counties, northeastern Minnesota: Hibbing, Minnesota Department of Natural Resources, Division of Minerals, Report 93, 74 p.

Lodge, R. W. D., Gibson, H. L., Stott, G. M., Hudak, G. J., Jirsa, M. A., and Hamilton, M. A., 2013, New U-Pb geochronology from the Timiskaming-type assemblages in the Shebandowan and Vermilion greenstone belts, Wawa Subprovince, Superior Craton: Implications for the Neoarchean development of the southwestern Superior Province: Precambrian Research, v. 235, p. 264-277.

Lundy, J. R., 1985, Clues to structural history in the minor folds of the Soudan Iron Formation, northeastern Minnesota: Unpublished M. S. thesis, University of Minnesota, Minneapolis, 144 p.
Marma, J.C., 2003, Magmatic and hydrothermal PGE mineralization of the Birch Lake Cu-Ni-PGE deposit in the South Kawishiwi intrusion, Duluth Complex, northeastern Minnesota: Unpublished M.S. thesis, University of Wisconsin: condensed version, University of Minnesota Duluth, Natural Resources Research Institute, Technical Report, NRRI/TR-2003/39, 112 p.
Marsden, R.W., Emanuelson, J.W., Owens, J.S., Walker, N.E., and Werner, R.F., 1968, The Mesabi Iron Range, Minnesota, in Ridge, J.D. (ed.), Ore Deposits of the United States, 1933-1967: New York, American Institute of Mining, Metallurgical, and Petroleum Engineers, Inc., The Grafton-Sales Volume, v. 1, p. 518-537.
McPhie, J., Doyle, M., and Allen, R., 1993, Volcanic Textures: A Guide to the Interpretation of Textures in Volcanic Rocks: CODES Key Centre, University of Tasmania, Hobart, Tasmania, 198 p.
Miller, J.D., Green, J.C., Severson, M.J., Chandler, V.W., and Peterson, D.M., 2001, Geological map of the Duluth Complex and related rocks, Northeastern Minnesota, Minnesota Geological Survey, Miscellaneous Map M119, scale 1:200,000.
Miller, J.D., Jr., Green, J.C., Severson, M.J., Chandler, V.W., Hauck, S.A., Peterson, D.M., and Wahl, T.E., 2002, Geology and mineral potential of the Duluth Complex and related rocks of northeastern Minnesota: Minnesota Geological Survey Report of Investigations RI-58, 207 p.
Morey, G.B., 1965, The sedimentology of the Precambrian Rove Formation in northeastern Minnesota (abs.): Institute on Lake Superior Geology, 11th Annual Meeting, St. Paul, Minnesota, Proceedings p. 25-26.
Morey, G.B., 1992, Chemical composition of the eastern Biwabik Iron Formation (Early Proterozoic), Mesabi Iron Range, Minnesota: Economic Geology, v. 87, p. 1649-1658.
Morey, G.B., and Cooper, R.W., 1977, Bedrock geology of the Hoyt Lakes–Kawishiwi area, St. Louis and Lake Counties, northeastern Minnesota: Minnesota Geological Survey, Open-File Report, scale 1:48,000.
Mueller, W. U., and White, J. D. L., 2004, 4.2 – Terminology of Volcanic and Volcaniclastic Rocks: *in* Eriksson, P. G., Altermann, W., Nelson, D. R., Mueller, W. U., and Catuneanu, O., (eds.), The Precambrian Earth: Tempos and Events: Developments in Precambrian Geology, v. 12, Elsevier, Amsterdam, p. 273-277.
Naldrett, A.J., 1997, Key factors in the genesis of Noril'sk, Sudbury, Jinchuan, Voisey's Bay and other world-class Ni-Cu-PGE deposits: Implications for exploration: Australian Journal of Earth Sciences, v. 44, no. 3, p. 283-315.
Newkirk, T., Hudak, G. J., and Hauck, S. A., 2001a, Preliminary lava flow morphology studies at the Five Mile Lake VMS prospect, Vermilion District, NE Minnesota: Implications for volcanic processes, volcanic paleoenvironments, and VMS exploration: Institute on Lake Superior Geology, 47th Annual Meeting, Proceedings Volume 47, Part 1- Program and Abstracts, p. 69-70.
Newkirk, T., Hudak, G. J., and Hauck, S. A., 2001b, Preliminary lava flow morphology studies at the Five Mile Lake VMS prospect, Vermilion District, NE Minnesota: Implications for volcanic processes, volcanic paleoenvironments, and VMS exploration: Geological Society of America Abstracts and Programs Volume 33, No. 6, p. A-398.
Ojakangas, R.W., 1966, Precambrian stratigraphy and structure of the Tower, Minnesota quadrangle (abs): Institute on Lake Superior Geology Proceedings, 12th Annual Meeting, Sault Ste. Marie, Michigan, Proceedings p. 17.
Patelke, R.L., 2003, Exploration drill hole lithology, geologic unit, copper-nickel assay, and location database for the Keweenawan Duluth Complex, northeastern Minnesota: University of Minnesota Duluth, Natural Resources Research Institute, Technical Report, NRRI/TR-2003/21, 97 pages, 1 CD.
Peterson, D.M., 1997, Ore deposit modeling of the footwall mineralization of the Duluth Complex: Minnesota Department of Natural Resources, Division of Minerals, Project 317, 55 p., 46 pls.
Peterson, D.M., 2001, Development of Archean lode-gold and massive sulfide deposit exploration models using geographic information system applications: targeting mineral exploration in northeastern Minnesota from analysis of analog Canadian mining camps: unpublished Ph. D. dissertation, University of Minnesota, Duluth, Minnesota, 503 p.
Peterson, D.M., 2001b, Development of a conceptual model of Cu-Ni-PGE mineralization in a portion of the South Kawishiwi intrusion, Duluth Complex, Minnesota: Society of Economic Geologists, Second Annual PGE Workshop, Sudbury, Ontario, 3 p.
Peterson, D.M., 2001c, Copper-Nickel-PGE mineral potential of the eastward extension of the Maturi Cu-Ni deposit, Duluth Complex, Lake County, Minnesota: University of Minnesota Duluth, Natural Resources Research Institute, Confidential Report of Investigations NRRI/RI-2001-02, 29 pages, 15 plates, 1 CD.
Peterson, D.M., 2002a, 3-Dimensional view through a mineralized system: the South Kawishiwi intrusion, Duluth Complex: Institute on Lake Superior Geology, 48th Annual Meeting, Thunder Bay, Ontario, v. 48.

Peterson, D.M., 2002b, Cu-Ni-PGE mineralization in the South Kawishiwi intrusion, northeastern Minnesota, Variation due to magmatic processes: Institute on Lake Superior Geology, 48th Annual Meeting, Thunder Bay, Ontario, v. 48.

Peterson, D.M., 2002c, Variation in the Cu-Ni-PGE mineralization in the South Kawishiwi intrusion, Duluth Complex, northeastern Minnesota: 9th International Platinum Symposium, Billings, Montana, USA, July 21-25.

Peterson, D.M., 2002d, Copper-Nickel grade maps for the Spruce Road deposit, South Kawishiwi intrusion, Duluth Complex: University of Minnesota Duluth, Natural Resources Research Institute, Report of Investigations NRRI/RI-2002/03, 99 p.

Peterson, D.M., 2002e, Shaded relief map of the basal contact of the South Kawishiwi intrusion, Duluth Complex, northeastern, Minnesota: University of Minnesota Duluth, Natural Resources Research Institute, Map Series NRRI/MAP-2002-01, scale 1:75,000.

Peterson, D.M., 2002f, Bedrock geology, sample location, and property position maps of the west Birch Lake area, South Kawishiwi intrusion, Duluth Complex, northeastern, Minnesota: University of Minnesota Duluth, Natural Resources Research Institute, Map Series NRRI/MAP-2002-02, scale 1:10,000.

Peterson, D.M., 2005, Bedrock Geologic and Volcanogenic Massive Sulfide Deposit Mineral Potential Map of the Lower Ely Greenstone and Adjacent Areas: Soudan, Eagles Nest, and Bear Island 7.5° Quadrangles, St. Louis County, Northeastern Minnesota: Unpublished geological map, North-Central Section of the Geological Society of America Meetings, Minneapolis, 1:20,000 scale.

Peterson, D.M., 2006a, 3D Visualizations of mafic Intrusions in the Duluth Complex, northeastern Minnesota, Institute on Lake Superior Geology, 52nd Annual Meeting, Sault Ste Marie, Ontario, May 8-12, 2006, Minnesota, v. 52.

Peterson, D.M., 2006b, Digital base for geological mapping within the northern South Kawishiwi intrusion: Lake and St. Louis Counties, northeastern Minnesota: University of Minnesota Duluth, Natural Resources Research Institute, Map Series NRRI/MAP-2006-01, scale 1:20,000.

Peterson, D.M., 2006c, New ideas on mineralization in the Duluth Complex, Oral presentation and online pdf file to the Mesabi Range Geological Society, December 20, 66 pages.

Peterson, D.M., 2008, Bedrock geologic map of the Duluth Complex in the northern South Kawishiwi intrusion and surrounding area, Lake and St. Louis Counties, Minnesota: Natural Resources Research Institute, Map Series NRRI/MAP-2008-01, scale 1:20,000.

Peterson, D.M. and Albers, P.B., 2007, South Kawishiwi Intrusion Cu-Ni-PGE mineralization in association with the Nickel Lake Macrodike, Institute on Lake Superior Geology, 53rd Annual Meeting, Field Trip Guidebook, Lutsen, Minnesota, Volume 53.

Peterson, D.M., Albers, P.B., and White, C.R., 2006, Bedrock geology of the Nickel Lake macrodike and adjacent Areas, Lake County, northeastern Minnesota: University of Minnesota Duluth, Natural Resources Research Institute, Map Series NRRI/MAP-2006-04, scale 1:10,000.

Peterson, D.M. and Boerst, K., 2013, Twin Metals Minnesota's Maturi Deposit, in Severson, M.J., Peterson, D.M., Ware, A., and Boerst, K., 2013, Cu-Ni-PGE Deposits of the Duluth Complex, Geology and Development: Precambrian Research Center, Workshop on the Copper, Nickel, Platinum Group Element Deposits of the Lake Superior Region, October 6-13, 2013, Field Trip Guidebook, pp. 45- 57.

Peterson, D.M., Gallup, C., Jirsa, M.A., and Davis, D.W., 2001, Correlation of Archean assemblages across the U.S.-Canadian border: Phase I geochronology (abs): Institute on Lake Superior Geology, 47th Annual Meeting, Madison, Wisconsin, Proceedings v. 47, Part 1, p. 77-78.

Peterson, D.M., and Hauck, S.A., 2005, Visualization of "Frozen" dynamic magma chambers in the Duluth Complex, northeastern Minnesota: Eos Trans. AGU 86(52), Fall Meet. Suppl., Abstract V23A-0680.

Peterson, D.M., and Jirsa, M.A., compilers, 1999, Bedrock geologic map and mineral exploration data, western Vermilion district, St. Louis and Lake Counties, northeastern Minnesota: Minnesota Geological Survey Miscellaneous Map M-98, scale 1:48,000.

Peterson, D.M., Jirsa, M. A., and Hudak, G. J., 2005. Field Trip 9: Architecture of an Archean Greenstone Belt: Stratigraphy, Structure and Mineralization: in Robinson, L., ed., 2005, Field Trip Guidebook for Selected Geology in Minnesota and Wisconsin: Minnesota Geological Survey Guidebook 21, p. 154-180.

Peterson, D.M., Jirsa, M., and Hudak, G., 2009, Field Trip 7 – Architecture of an Archean Greenstone Belt: Stratigraphy, Structure, Mineralization: 55th Annual Meeting, Institute on Lake Superior Geology, Proceedings Volume 55, Part 2 – Field Trip Guidebook, p. 178-215.

Peterson, D.M., and Patelke, R. L., 2003, National Underground Science and Engineering Laboratory (NUSEL): Geological site investigation for the Soudan Mine, northeastern Minnesota: Natural Resources Research Institute Technical Report NRRI/TR-2003/29, 88 p.

Peterson, D.M., and Patelke, R. L., 2004a, Bedrock Geology and Lode Gold Prospect Data Map of the Mud Creek Road Area, Northern St. Louis County, Minnesota: Natural Resource Research Institute Geologic Map NRRI/MAP-2004/01, 1:12,00 scale, available for free download at http://www.nrri.umn.edu/egg/REPORTS/MAP200401/MAP200401.html.

Peterson, D.M., and Patelke, R. L., 2004b, Field Trip 7 – Economic geology of Archean gold occurrences in the Vermilion District, northeast of Soudan, Minnesota: 50th Annual Meeting, Institute on Lake Superior Geology, Proceedings Volume 50, Part 2 – Field Trip Guidebook, p. 200-226.

Peterson, D.M., Patelke, R.L., and Severson, M.J., 2004, Bedrock geology map and Cu-Ni mineralization data for the basal contact of the Duluth Complex west of Birch Lake, St. Louis and Lake Counties, northeastern Minnesota: University of Minnesota Duluth, Natural Resources Research Institute, Map Series NRRI/MAP-2004-02, scale 1:10,000.

Peterson, D.M., Pointer, J., and Marshak, M., 2009b, Field Trip 3 – Soudan Iron Mine and Physics Lab Tour: 55th Annual Meeting, Institute on Lake Superior Geology, Proceedings Volume 55, Part 2 – Field Trip Guidebook, p. 100-109.

Peterson, D.M. and Severson, M.J., 2002, Chapter 4, Archean and Paleoproterozoic rocks forming the footwall of the Duluth Complex, in Geology and mineral potential of the Duluth Complex and related intrusions of northeastern Minnesota, Minnesota Geological Survey, Report of Investigations 58, pp. 76-93.

Phinney, W.C., 1969, The Duluth Complex in the Gabbro Lake quadrangle, Minnesota: Minnesota Geological Survey, Report of Investigations 9, 20 p.

Phinney, W.C., 1972, Duluth Complex, history and nomenclature, in Sims, P. K., and Morey, G. B., eds., Geology of Minnesota: A Centennial Volume: Minn. Geol. Survey, pp. 333-334.

Phinney, W.C., 1972, Northwestern part of Duluth Complex, in Sims, P.K., and Morey, G.B., eds., Geology of Minnesota: A centennial volume: Minnesota Geological Survey, p. 335-345.

Ramsey, J.G., and Huber, M.I., 1987, The Techniques of Modern Structural Geology, Academic Press Inc. (London) Ltd.

Ripley, E.M., 1986, Origin and concentration mechanisms of copper and nickel in Duluth Complex sulfide zones – a dilemma: Economic Geology, v. 81, p. 974-978.

Schmid, R., 1981, Descriptive nomenclature and classification of pyroclastic deposits and fragments; recommendations of the IUGS subcommission on the systematics of igneous rocks: Geology, v. 9, p. 41-43.

Schulz, K.J., 1980, The magmatic evolution of the Vermilion greenstone belt, NE Minnesota: Precambrian Research **11**:215-245.

Severson, M.J., 1994, Igneous stratigraphy of the South Kawishiwi intrusion, Duluth Complex, northeastern Minnesota: University of Minnesota Duluth, Natural Resources Research Institute, Technical Report NRRI/TR-93/34, 210 p., 15 plates.

Severson, M.J., and Hauck, S.A., 2003, Platinum-group elements (PGEs) and platinum-group minerals (PGMs) in the Duluth Complex: University of Minnesota Duluth, Natural Resources Research Institute, Technical Report, NRRI/TR-2003/37, 296 p., 1 CD.

Severson, M.J., Heine, J.J., and Patelke, M.M., 2009, Geologic and Stratigraphic Controls of the Biwabik Iron Formation and the Aggregate Potential of the Mesabi Iron Range, Minnesota: University of Minnesota Duluth, Natural Resources Research Institute, Technical Report NRRI/TR- 2009/09, 173 p. + 37 plates.

Sims, P. K., and Southwick, D. L., 1985, Geologic map of Archean rocks, western Vermilion district, northern Minnesota: U. S. Geological Survey, Miscellaneous Investigations Map I-1527, scale 1:48,000.

Southwick, D. L., (compiler), 1993, Bedrock geologic map of the Soudan-Bigfork area, northern Minnesota: Minnesota Geological Survey, Miscellaneous Map M-79, scale 1:100,000.

Southwick, D. L., Boerboom, T. J., and Jirsa, M. A., 1998, Geologic setting and descriptive geochemistry of Archean supracrustal and hypabyssal rocks, Soudan-Bigfork area, northern Minnesota: implications for metallic mineral exploration: Minnesota Geological Survey, Report of Investigations 51, 69 p.

Stott, G., Corkery, T., Leclair, A., Boily, M., and Percival, J., 2007, A revised terrane map for the Superior Province as interpreted from Aeromagnetic Data: 53rd Annual Meeting, Institute on Lake Superior Geology, Proceedings Volume 53, Part 1 – Program and Abstracts, p. 74-76.

Thompson, A., 2015, A hydrothermal model for metasomatism of Neoarchean Algoma-type banded iron formation to massive hematite ore at the Soudan Mine, NE Minnesota: unpublished M. S., thesis, University of Minnesota Duluth, 59 p.

Vislova, T., 2003, Petrology of the Bald Eagle intrusion and associated rocks and its relevance to crystallization in dynamic magma chambers in the Midcontinent Rift: Unpublished Ph.D. Thesis, University of Minnesota.

Weiblen, P.W., 1965, A funnel-shaped, gabbro-troctolite intrusion in the Duluth Complex, Lake County Minnesota: Unpublished Ph.D. Thesis, University of Minnesota, 161 p.
Weiblen, P.W., Morey, G. B., 1980, A summary of the stratigraphy, petrology, and structure of the Duluth Complex: American Journal of Science, vol. 280A, Part I, p 88-133.
Weiblen, P.W., Peterson, D.M., and Vislova, T., 2005, Implications of Midcontinent Rift and oceanic ridges analogies and 3-D interpretations of the subsurface structure of the Bald Eagle intrusion in the Duluth Complex and the East Pacific Rise: Institute on Lake Superior Geology, 51st Annual Meeting, Sault Ste Marie, Ontario, v. 51, 3 p.
White, C., 2010, The Nokomis Deposit, a Masters of Geology thesis: University of Minnesota, Duluth.
White, J. D. L., and Houghton, B. F., 2006, Primary volcaniclastic rocks: Geology, v. 34, no. 8, p. 677-680.
Wolff, J.F., 1917, Recent geologic developments on the Mesabi range, Minnesota: American Institute of Mining and Metallurgical Engineers Transactions, v. 56, p. 142-169.
Zanko, L.M., Severson, M.J., and Ripley, E.M., 1994, Geology and mineralization of the Serpentine copper-nickel deposit: University of Minnesota Duluth, Natural Resources Research Institute, Technical Report NRRI/TR-93/52, 90 p., 3 pls.

FIELD TRIP 8

Glacial Lake Norwood and the Koochiching Lobe

Phil Larson[1], Andrew Breckinridge[2], and Howard Mooers[3]

[1]*Vesterheim Geoscience PLC*
[2]*Natural Sciences Department, University of Wisconsin Superior, 202 Barstow Hall, Superior, WI 54880*
[3]*Department of Earth and Environmental Sciences, University of Minnesota Duluth, 1114 Kirby Drive, Duluth, MN 55812*

Introduction

The region north of the Giants Range is draped by sediment deposited during the final retreat of the Laurentide ice sheet from northeastern Minnesota. These sediments record the retreat of the Rainy Lobe ice margin to the northeast, the formation of Glacial Lake Norwood (GLN), two successive advances of the Koochiching Lobe from the northwest, and the opening of a western outlet of GLN and its succession by Glacial Lake Agassiz, all over the span of a few thousand years.

Historically, the Quaternary geology of this region has received scant attention. However, recent work integrating varve chronology, high resolution LiDAR digital terrain models, till geochemistry, rotasonic drilling, and mapping has resulted in substantially improved and nuanced understanding of the sedimentary processes active, and the sequence of events, during deglaciation. A key finding is that GLN was of significantly longer duration than previously believed, and consequently a stronger control on sediment and landform distribution in the region.

Within the footprint of GLN, there is scant evidence for preservation of glacigenic sediments predating the Late Wisconsinan. Interbedded till and glaciolacustrine sediment thicknesses up to 70 m thick preserve evidence of extremely high sedimentation rates in a dynamic sediment system. High rates of sediment delivery by the Koochiching Lobe and analogues from the west served as the dominant sediment source, while intense reworking by wave action in GLN was a dominant control on sediment distribution.

Historical Background

The earliest formal studies of glacial deposits in northeastern Minnesota were conducted by Upham (1894) who identified a series of moraines across Minnesota. He identified the Vermillion moraine as the 12th moraine in the deglaciation sequence, although he did not define its entire length. Elftman (1898) suggested two lobes for the northeastern portion of Minnesota because of observed till differences and provenances; he named these the Superior and Rainy lobes; the Rainy lobe referring to the ice flowing from the Rainy River areaWinchell (1899) compiled Upham, Elftman, and his own observations into a map of large portions of northeastern Minnesota and description of the surficial deposits. Winchell (1900) described evidence for glacial lakes in Minnesota, including naming Glacial Lake Norwood. Notably, he did not recognize the full extent of Glacial Lake Norwood, assigning portions of the Norwood basin to other glacial lakes.

Leverett (1932), based mostly on the work of his predecessors, proposed that northeastern Minnesota was glaciated by three separate lobes of ice. He recognized that the earliest drift in the area was the result of ice flowing from the Patrician [Labradoran] ice center located in the Hudson Bay Lowlands between the Keewatin and Labradorean ice accumulation centers.

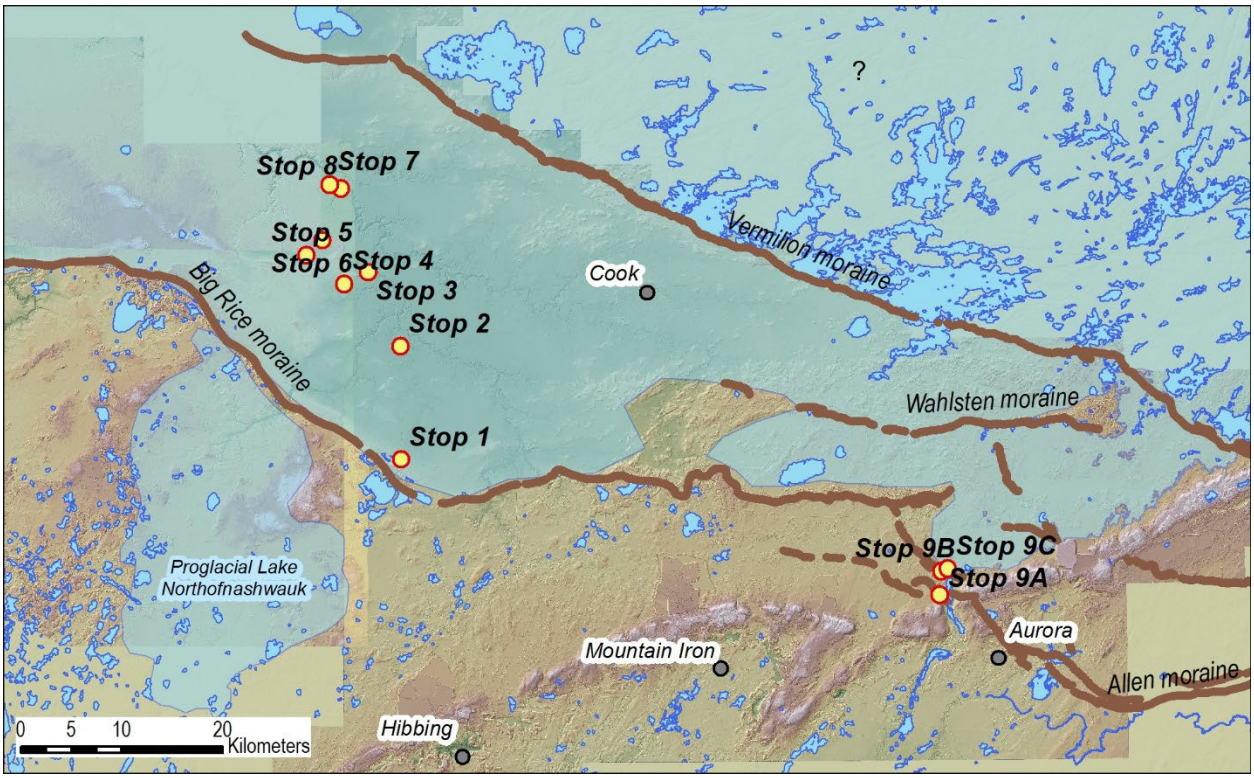


Figure 8-1. Extent of Glacial Lake Norwood (light green-blue). The lack of modern lakes (blue) in the GLN basin highlight area of significant glaciolacustrine sediment thickness. Major Rainy lobe recessional moraines (brown lines). Proglacial Lake Northofnashwauk is the high-level (elev. >1500') proglacial lake predating GLN dammed by the St. Louis sublobe.

Modern understanding of the surficial geology of northeastern Minnesota began with Wright Wright (1956), who was the first to conduct systematic fieldwork in the area between the border lakes and Lake Superior. Wright and Watts (1969) reconstructed the postglacial vegetational history of northeastern Minnesota, and established the first regional deglaciation chronology, including use of radiocarbon dates to establish absolute ages to deglaciation. These early efforts were summarized in the comprehensive general glacial geologic framework of Minnesota Wright (1972).

The United States Geological Survey conducted a comprehensive study of surficial geology and groundwater availability on the Mesabi Iron Range. An initial map (Cotter, Young, and Winter 1964) was later followed by additional publications on the glaciation sequence (Winter 1971) glacial sediment composition (Winter, Cotter, and Young 1973), and groundwater hydrology in glacial drift-hosted aquifers (Winter 1973).

Hobbs (1983) provided the first comprehensive account of Glacial Lake Norwood's extent and history. At that time, he rechristened GLN as Glacial Lake Koochiching, not recognizing the continuity with Winchell's (1900) definition of GLN. In this respect he was hampered by the paucity of well-defined strandlines for the upper levels of GLN in the rocky meltout till underlying much of the southern portion of the basin. He also posited a late, lower elevation outlet for Glacial Lake Koochiching southward along the Prairie River; recent (2012) LiDAR elevation data (MNDNR 2012) combined with a better defined isostatic rebound reconstruction (Breckenridge 2015) suggest the existence of a southern outlet to GLN untenable. Significantly, Hobbs recognized that Glacial Lake Norwood expanded westward, ultimately establishing an outlet via the McIntosh Channel into Glacial Lake Climax. Continued retreat of the Red River lobe ice margin resulted in coalescence of Glacial Lake Climax and GLN into Glacial Lake Agassiz at the Herman level at 13.9±0.3 cal kyr BP (Lepper et al. 2007).

Björck (1990) expanded Wright and Watts (1969) pioneering work by collecting radiocarbon dates north of the Giants Range. He obtained basal radiocarbon dates from Sabin Lake (located in the outflow to GLN) of 10,230±230 and 10,320±170 14C kyr BP. Bjorck's oldest date was 12,100±150 14C kyr BP from Heikkila Lake, located within the Big Rice moraine. Lowell et al. (2009) reported a radiocarbon date from north of the Vermilion moraine of 12,000±85 14C kyr BP, assigning a minimum age to the Vermilion phase and the moraines to the south of 13.9±0.2 cal kyr BP. These dates establish that Glacial Lake Norwood and drainage through the Embarrass Gap persisted long after the Laurentide ice sheet margin retreated from the Vermilion moraine.

Johnson et al. (2016) assigned the glacigenic deposits in northeastern Minnesota to a formal statewide lithostratigraphic framework.

Essentially all the aforementioned published work was opened to critical re-examination and revision upon release of 1m resolution LiDAR-derived digital terrain models in the spring of 2012 (MDNR 2012). This data provides resolution orders of magnitude greater than previous topographic models, allowing for vastly improved recognition of some classes of glacigenic landforms, and recognition for the first time of entire new classes of landforms. These advances allowed for significant refinement in mapping of glacial landforms, interpretation of sediment-landform relationships, and development of deglaciation process models.

Breckenridge (2015) mapped glacial lake strandlines and developed an isostatic rebound model for much of northern Minnesota, including much of the Glacial Lake Norwood basin, demonstrating the previously unrecognized widespread extent of both Glacial Lake Norwood and the early, high levels of Glacial Lake Agassiz. Bauer et al. (2022) published a surficial geologic map and Quaternary stratigraphic interpretation of much of the GLN basin, relying primarily on the lithostratigraphic mapping approach favored by the Minnesota Geological Survey, but also incorporating landform interpretation based on the 2012 LiDAR data.

Glacial History

Northeastern Minnesota was continuously covered by ice from the earliest Late Wisconsin ice advance approximately 28 kyr bp until about 11 kyr bp by the Rainy lobe of the Laurentide ice sheet (Clayton and Moran 1982); (Mooers and Lehr 1997)). Although the Glacial Lake Norwood basin was subjected to multiple glacial cycles, the vast majority of glacigenic sediment was deposited during the last retreat of the Laurentide ice sheet during the Late Wisconsinan (<15 kyr bp). The Pleistocene stratigraphic record therefore principally reflects retreat of the ice sheet, and is composed of glacigenic sediment deposited at or near the ice margin.

Bedrock Geology and Preglacial Regolith

The GLN basin underlain by greenstone (metavolcanic and metasedimentary rocks) and granitoids of the ~2.7 Ga Wawa-Shebandowan Subprovince. The craton was intruded by mafic intrusives of the 2076 Ma Kenora-Kabetogama dike swarm (Southwick and Halls 1987; Buchan, Halls, and Mortensen 1996), while contact relationships indicate the Archean craton was peneplained by the time arenites, iron-formation, greywacke, and argillite of ~1.85 Ga Animikie Basin were deposited to the south. Minor mafic dikes related to the 1.1 Ga Midcontinent Rift are known to intrude the Archean craton north of the Giants Range; it is probable that additional similar intrusives have yet to be recognized or mapped.

Subsequent to cessation of the Midcontinent Rift, Precambrian bedrock in the GLN basin was subject to a nearly 1 billion year period of chemical weathering and saprolite formation. Saprolite formation was preferentially, but not necessarily, focused along joints, faults, and less weathering-resistant lithologies, forming deep linear weathering pendants beneath a more widespread blanket of saprolite.

Commencement of glaciation at the beginning of the Pleistocene ~3 Ma subjected the Superior craton to significant physical erosion for the first time in nearly a billion years. Successive glacial cycles

preferentially eroded unconsolidated saprolite, removing first the extensive saprolite blanket, and then excavating saprolite from deep weathering pendants. To the southwest of the GLN basin (central Minnesota), the preglacial saprolite is largely intact beneath Pleistocene glacigenic sediment. To the northeast (northwestern Ontario), preglacial saprolite has been essentially completely removed. Here, the rugged 'glacially sculpted' shield terrain characteristic of this region is better explained as the unweathered bedrock surface forming the base of the preglacial saprolite; bedrock has undergone relatively little actual glacial weathering.

In the GLN basin proper, preglacial saprolite removal by glacial erosion is incomplete, leaving patchy remnants of unconsolidated preglacial saprolite on the bedrock surface. Saprolite is occasionally intercepted in boreholes. Saprolite and incipient pendant weathering have been encountered associated with joints and fractures as deep as 100 m.

Pre-Late Wisconsinan

The overlying preglacial saprolite was removed by repeated cycles of erosion and deposition during the Pleistocene. Saprolite eroded as the ice sheet grew (relative early in a glacial cycle) was transported to the margin. The remnant saprolite was blanketed by glacigenic sediment as the ice margin receded (late in the glacial cycle. Subsequent glacial cycles removed both the older glacigenic sediment and additional saprolite.

Winter (1971) and Winter, Cotter, and Young (1973) described a dark-colored, sandy-silty calcareous till in exposures in open pit mines on the Mesabi Iron Range. Since this till, where present, occurred immediately above bedrock, they referred to it as the "basal till". Stark (1977) and (Lehr and Hobbs 1992) described occurrences of Winter's basal till in exposures in the Dunka Mine. The matrix of Winter's basal till is calcareous, and the pebble fraction contains carbonate clasts in addition to the granitic and metamorphic lithologies typical of Rainy lobe tills. A northeast-southwest pebble fabric in Winter's basal till strongly supports a northeastern provenance for this till, indicating the carbonate in pebbles and till matrix is derived from Paleozoic carbonates in the Hudson Bay Lowlands (HBL). A distinctive greywacke lithology (Prest, Donaldson, and Mooers 2000) associated with carbonate-bearing tills has been recovered from glacigenic sediments north of the Giants Range (this author), indicating older carbonate-bearing glacigenic sediment was actively reworked during the last retreat of the Laurentide ice sheet. Additional occurrences of this calcareous basal till have been intercepted in boreholes elsewhere in the GLN basin, indicating patchy remnants of preglacial saprolite and older (carbonate-bearing) glacigenic sediment are present beneath the relatively continuous blanket of glacigenic sediment deposited between ca. 15 kyr bp and 10 kyr bp during the last retreat of the Laurentide ice sheet.

Post-Last Glacial Maximum – Rainy Lobe

Recession of the Laurentide ice sheet margin following its last glacial maximum extent at ca. 20 kyr bp was characterized by rapid melting of ice during summer months followed by stabilization and minor re-advance during the winter. This process formed a series of small, annual recessional moraines, spaced 25-75 m apart, reflecting the long-term retreat rate of the ice sheet.

To a significant degree, glacigenic sediment deposited by the Rainy lobe of the Laurentide ice sheet during retreat of its margin from the southwest to northeast is the oldest Pleistocene sediment preserved in the GLN basin. Post-LGM Rainy lobe sediments are typically comprised predominantly of sediment eroded locally from Archean greenstone and granitoid lithologies; this results in significant lithologic and geochemical compositional variability(Larson, 2004; Larson & Mooers, 2004). Lodgment tills are commonly ~2 m thick, while sand and gravel deposited in subaqueous recessional moraines commonly form sharp-crested ridges 5-40 m thick. Distal glaciolacustrine sand and silt commonly drapes older basal lodgment tills and recessional moraines.

This process of gradual ice margin retreat was punctuated by surges, episodes of major re-advance and stagnation. These surges resulted in deposition of moraines significantly broader and thicker than annual recessional moraines. The surges may not reflect re-advance of the ice sheet as a whole, but were likely restricted to sectors of the ice margin on the order of 100s of km. They may therefore not be a direct physical reflection of climate fluctuations, but rather reflect internal ice sheet dynamics.

Most of the area exposed by ice margin retreat from the Giants Range was inundated in proglacial lakes, successively by Glacial Lake Nashwauk, Glacial Lake Norwood, and finally by Glacial Lake Agassiz. The extended interval between ice margin retreat, lake drainage, and establishment of terrestrial vegetation over most of this area significantly hinders the ability to establish a precise deglaciation chronology (compare Björck (1990)).

Allen Phase

The oldest major surge-stagnation moraine recognized in the GLN basin is the Allen moraine, which forms a WNW-ESE trending belt of stagnation topography (ice-walled lake plains, meltout tills, etc.), passing through the Embarrass Gap. Ice flow during the Allen phase was generally toward the SSW (bearing 190°).

Ice margin retreat from the Allen moraine and opening of meltwater drainage through the Embarrass Gap was the event that by definition resulted in formation of Glacial Lake Norwood. Further ice margin recession and deposition of annual recessional moraines suggests about 150 years before the next major surge-stagnation event.

Big Rice and Wahlsten Phases

The second major surge-stagnation moraine recognized in the GLN basin is the Big Rice moraine, a W-E trending belt of thick meltout till and stagnation topography. Ice flow during the Big Rice phase was generally toward the SSW (bearing 190°).

The third major moraine recognized in the TMM AOI is the Wahlsten moraine, an E-W trending belt of thick meltout till and stagnant ice topography. Ice flow during the Wampus phase was generally toward the S (bearing 180-190°), reflecting a significant reorientation in ice flow of the Laurentide ice sheet.

Annual recessional moraines associated with the Wampus and Wahlsten phases consist of both subaqueous moraines composed of sand, gravel, and meltout tills deposited in Glacial Lake Norwood, and subaerial moraines predominantly composed of meltout tills.

Vermilion Phase

The fourth and final major moraine recognized in the GLN basin is the Vermilion moraine, a 40 m high, 1-2 km wide, WNW-ESE trending belt of thicker meltout till, stagnant ice topography, and subaqueous debris flow fans. Ice flow during the Vermilion phase was generally toward the SSW (bearing 195-205°). The Vermilion moraine truncates the eastern extent of the Wahlsten moraine, reflecting a further significant reorientation in ice flow of the Laurentide ice sheet. The next moraine formed by a major surge-stagnation event lies >100 km to the northeast, suggesting an interval of >1000 years of gradual ice margin retreat after the Vermilion phase.

Glacial Lake Norwood

Retreat of the Rainy lobe margin north of the continental height of land at the Giants Ridge dramatically changed the character of sedimentation associated with the Laurentide ice sheet. South of the divide, meltwater generally flowed downslope away from the margin, depositing outwash in channels and as outwash plains with intervening rolling plains of subglacial lodgment till or moraines composed of hummocky supraglacial meltout till. Immediately upon marginal retreat north of the divide, ponding of meltwater against the ice sheet formed the first of a nearly continuous succession of proglacial lakes. Glacial

meltwater and other precipitation ponded against the ice sheet overflowed to the south through a series of successively lower outlets over the height of land, a process that continued until final collapse of the ice sheet in Hudson Bay.

Initially, a series of ephemeral lakes formed in stagnant ice north of the divide. These lakes were dammed in part by the advance of the St. Louis Sublobe into the Glacial Lake Upham I basin (see Knaeble et al. (2005) and Larson et al. (2014)) Associated strandlines and meltwater channels are only poorly defined, and meltwater likely drained southward through stagnant Rainy lobe ice karst and St. Louis sublobe ice. Once the active Rainy lobe ice margin receded to the Allen moraine, a stable, relatively long-lived meltwater outlet was established through the Embarrass Gap.

By definition, the first proglacial lake located north of the Laurentian Divide that drained through the Embarrass Gap is referred to as Glacial Lake Norwood. Three well-developed outlets to Glacial Lake Norwood are recognized, corresponding to relatively stable, long-lived lake levels. These are herein referred to as Glacial Lakes Norwood I, II, and III, corresponding to successively older and lower lake levels.

The initial stable lake level (Glacial Lake Norwood I) was controlled by an outlet channel with a modern floor elevation of about 450 m amsl. This channel was bounded by the Giants Range ridge to the south, and the Allen moraine to the north. The Allen moraine at this location is a major recessional moraine, approximately 500 m wide with in excess of 15 m of vertical relief above the meltwater channel.

The ice-cored Allen moraine formed an effective barrier to meltwater drainage blocking most of the Embarrass Gap until after the ice sheet margin retreated from the Vermilion moraine, a time interval of 100s to 1000s of years. Incision of the Glacial Lake Norwood I outlet was inhibited during this time interval in part because the channel was graded to its downstream inlet into Glacial Lake Upham II; only after drainage of this lake was further significant erosion and channel incision in the Embarrass Gap initiated (Larson and Mooers 2009).

Gradual collapse of the Allen moraine due to ice melt led to resulted in an episode of collapse and downcutting of the moraine dam, and establishment of a second, lower stable outlet level for Glacial Lake Norwood II in the Embarrass Gap at a modern floor elevation of about 443 m amsl. Paleoislands of outwash and esker sediment located in Glacial Lake Norwood considerable distances north of the Vermilion moraine display well-developed shoreline features corresponding to this outlet, indicating that the downcutting episode occurred well after ice margin retreat from the Vermilion moraine, and that Glacial Lake Norwood II stood at this stable lake level for a relatively long time interval.

A second collapse and downcutting episode through the Big Rice moraine led to establishment of the third, and final, lower stable outlet level corresponding to Glacial Lake Norwood III in the Embarrass Gap. An outlet with a modern floor elevation of about 433 m amsl corresponds to a second, lower well-developed strandline on esker and outwash paleoislands to the north.

During its relatively long history, Glacial Lake Norwood expanded along the receding ice margin to form a lake that ultimately extended ~400 km E-W and in excess of 100 km N-S. The lake experienced two major ice re-advances into its western arm, evidenced by thick (>70 m) accumulations of glaciolacustrine sediment and till. The large fetch of the lake resulted in vigorous wave erosion along its shoreline and the considerable fraction of the lakebed situated above wave base. Final drainage of Glacial Lake Norwood III occurred when a western outlet (the McIntosh spillway) flowing into an early (Herman) level of Glacial Lake Agassiz formed in the vicinity of Trail, MN, 260 km to the west of the Embarrass Gap.

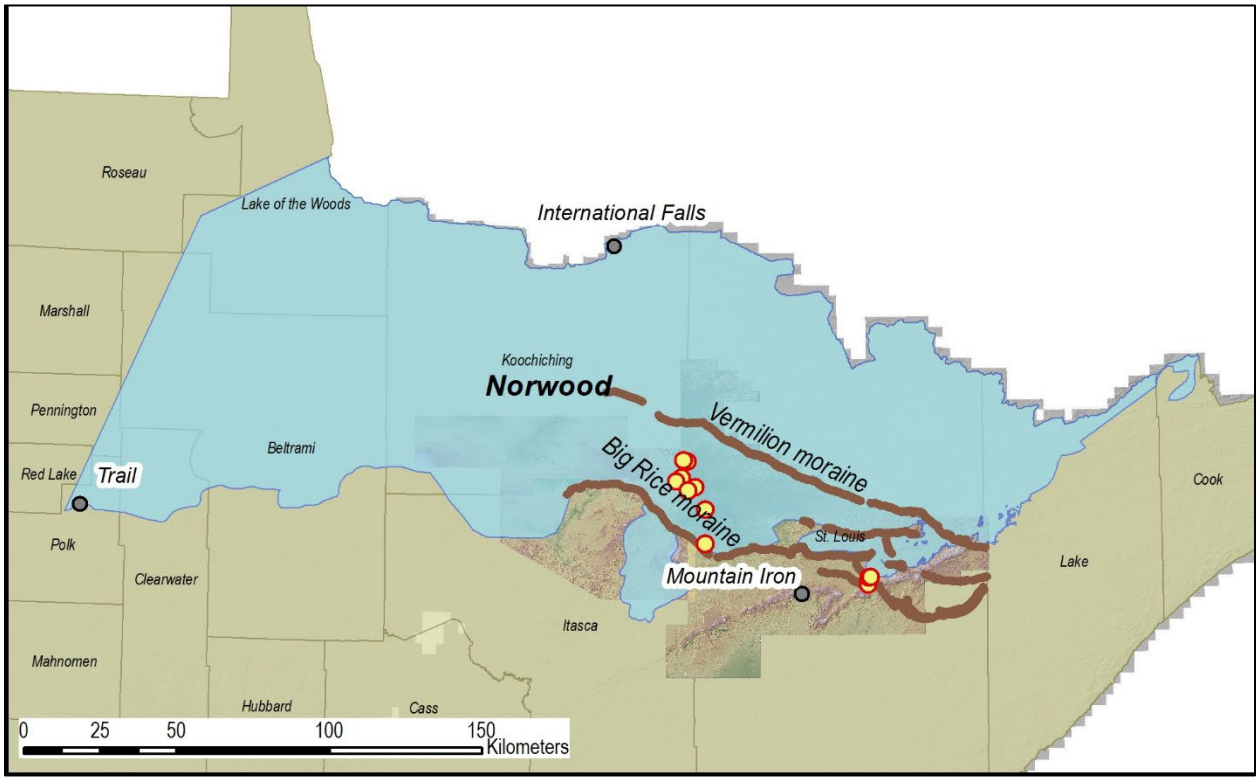


Figure 8-2. Outline of maximum extent of Glacial Lake Norwood in northern Minnesota. The lake extended over 350 km from east to west. The final outflow was westward into Glacial Lake Climax near Trail, MN.

Glacial Lake Norwood sediments generally consist of gravels and sands in littoral (shallow) environments, reflecting local reworking of till and outwash by wave action, and silt and clay in benthic environments, reflecting settling of suspended fine-grained sediment from the water column. In general, Glacial Lake Norwood sediment sequences fine upward, reflecting diminished wave erosion and the increasing distance of the primary sediment source (the receding ice margin).

Koochiching Lobe

Subsequent to retreat of the Rainy lobe from the Vermilion moraine, Koochiching lobe (KL) ice re-advanced into the Glacial Lake Norwood basin, this time from the west and the Red River lobe (Meyer, 1993). In marked contrast to the sandy-textured till and glaciofluvial sediment associated with the Rainy lobe, KL diamicton is calcareous, and distinctly finer grained than Rainy lobe till; these sediments are placed in the Blackduck Formation in the MGS lithostratigraphic framework (Johnson et al., 2016). Based on rotosonic drilling, diamictons associated with at least two distinct advances into the GLN basin are present in the field trip area, separated by fine-grained glaciolacustrine sediment. The genesis of these diamictons – till or subaqueous debris flow – are enigmatic; fine-grained lacustrine sediment may grade upward into normally consolidated diamicton, which may grade upward into overconsolidated diamicton of similar composition.

The Koochiching lobe advances overran older Rainy lobe landforms, including the Vermilion moraine. There is little evidence for erosion and entrainment of older glacigenic sediment by the KL, and no well-defined moraines or other landforms define the limits of the advances. Sediment was deposited from suspended sediment plumes or debris flows in the proglacial GLN, or as subglacial lodgment till. Although KL ice thickness is unknown, it was sufficiently thick relative to the depth of GLN to preclude development of a calving margin.

The majority of sediment shed by the advancing Koochiching lobe was deposited as glaciolacustrine sediment in GLN, and subject to a high degree of reworking in the lacustrine environment. Bedrock highs – shallow areas in GLN – are typically devoid of either older Rainy lobe or KL sediments. In places, a thin boulder lag containing limestone and dolomite clasts attests to the former presence of KL diamicton. In contrast, thicknesses of up to 70 m of till and glaciolacustrine sediment have been reported in intervening bedrock lows.

Two distinct till compositions attesting to two distinct source areas have been reported in KL sediments. The younger, overlapping KL till bears greater similarity to calcareous Red River and Des Moines lobe tills elsewhere in Minnesota. In contrast, an older KL till is characterized by a distinctly higher Na2O content, similar to tills exposed at surface in Hubbard and Wadena Counties.

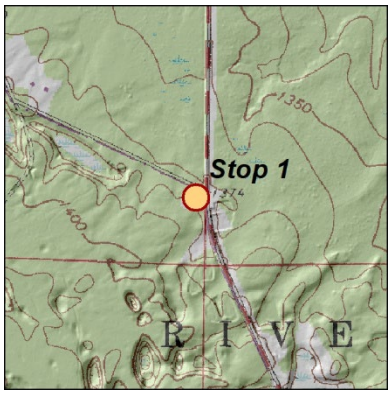
Even as the Laurentide ice sheet margin was broadly retreating from Minnesota, both from the Red River Valley and from the Arrowhead, the advances of the Koochiching lobe into the GLN served to block development of meltwater outlets to the north and west. Ultimately, stagnation and wasting of the KL led to westward propagation of GLN until development of the McIntosh spillway. The massive sediment accumulations associated with the KL – up to 70 m in places as previously noted – were deposited over a time interval on the order of 1000 years.

Description of Field Trip Stops

Stop 1: Glacial Lake Norwood strandline

498550E/5283740N (UTM Zone 15, NAD83)
(47.70704, -93.0193)

Side Lake 7.5’ USGS Quadrangle

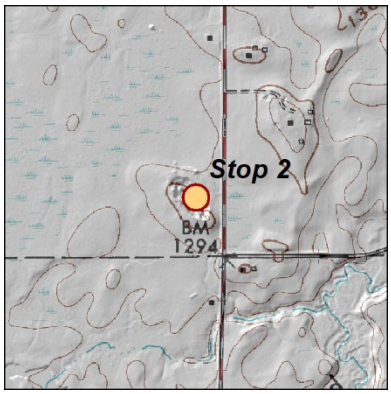


This site is located on the uppermost relatively well-developed beach associated with Glacial Lake Norwood. A well-developed boulder lag and wave-cut notch attest to a relatively long-lived stable lake at this level characterized by energetic wave action. To the south, ice collapse pits in the subaqueous deposited Big Rice moraine evidence long lived stagnant ice along this moraine trend. Locally, the Big Rice and other moraines served as ice-cored dams preventing southern outflow.

Stop 2: Gravel pit in minor Rainy lobe recessional moraine

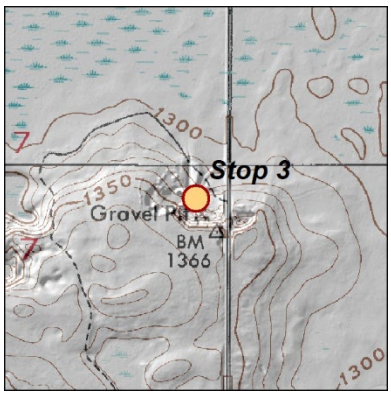
498480E/5294980N (UTM Zone 15, NAD83)
(47.80817, -93.0203014)

Bear River 7.5’ USGS Quadrangle



Here a small, sharp-crested subaqueous deposited recessional moraine has been developed into a gravel pit. The flanks of the moraine are draped by fine-grained glaciolacustrine sediment deposited in Glacial Lake Norwood.

Stop 3: Gravel pit in large Rainy lobe recessional moraine



495260E/5302290N (UTM Zone 15, NAD83)
(47.8739285, -93.0633884)

Bear River 7.5' USGS Quadrangle

This gravel pit is developed in a large subaqueous ice marginal fan(?) deposited at the margin of the retreating Rainy lobe. The fan was of sufficient height that its surface was above the GLN wave base, precluding deposition of finer-grained glaciolacustrine sediment. The presence of limestone and dolomite boulders on the fan surface indicate that this area was overrun by Koochiching lobe ice.

Stop 4: Wave-washed bedrock high

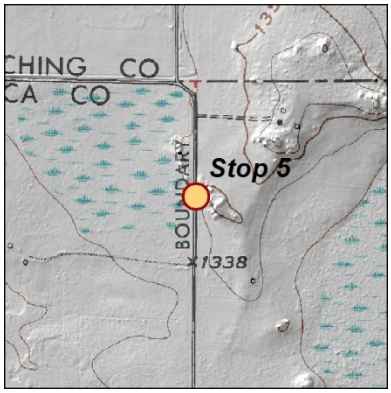


492880E/5301180N (UTM Zone 15, NAD83)
(47.8639194, -93.095198)

Bear River 7.5' USGS Quadrangle

This wave-scoured bedrock high evidences the intensity of wave action in Glacial Lake Norwood. Rainy lobe sediment has been almost completely washed away, no Koochiching lobe sediment is preserved, and no glaciolacustrine sediment has been deposited. The very large boulder – a Rainy lobe erratic - attests to the 'minimum' particle size of this 'boulder lag'.

Stop 5: Glacial striae and grooves



489180E/5304010N (UTM Zone 15, NAD83)
(47.8893303, -93.1447397)

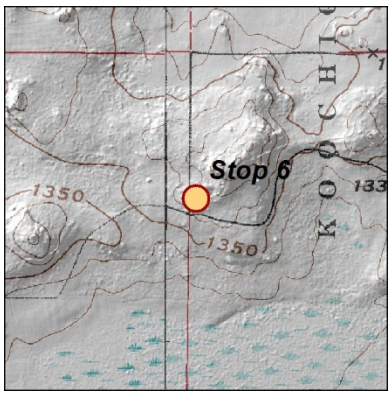
Rauch 7.5' USGS Quadrangle

Glacial striae and grooves on outcrop on either side of the road at this stop preserve evidence of ice flow directions for both the Rainy lobe (bearing 190° and 205°) and the later Koochiching lobe (bearing 140°). This indicates that Rainy lobe sediment was largely stripped from bedrock highs by wave action in Glacial Lake Norwood prior to advance of the Koochiching lobe from the west.

Stop 6: Borrow pit in reworked calcareous Koochiching lobe drift

490750E/5305460N (UTM Zone 15, NAD83)
(47.9024009, -93.1237689)

Silverdale 7.5’ USGS Quadrangle



This small borrow pit on the margin of a wave-scoured bedrock high contains abundant carbonate pebbles and cobbles. These originated from calcareous Koochiching lobe till deposited on the bedrock high and later eroded by wave action.

Stop 7: Slumping Koochiching lobe till and Glacial Lake Norwood

491460E/5311020N (UTM Zone 15, NAD83)
(47.9524357, -93.114379)

Silverdale 7.5’ USGS Quadrangle



This site exposes a sequence of interbedded Koochiching lobe diamicton (till and debris flows(?)) and fine-grained glaciolacustrine sediment adjacent to the Littlefork River. The slope, already prone to slumping by stream erosion at the toe, was further destabilized by construction of the road. In the near vicinity to the southwest, an exploration rotosonic borehole intercepted around 70 m of such sediment.

Stop 8: Samuelson Park

492580E/5310600N (UTM Zone 15, NAD83)
(47.9459716, -93.0993661)

Silverdale 7.5’ USGS Quadrangle



Bedrock underlying the small waterfall in the Littlefork River has been striated by the Rainy lobe (bearing 196°). In the upstream direction, boulders eroded from the basal Rainy lobe lodgment till are visible in the stream bed and banks. Such bedrock and boulder lags serve as knickpoints defining the bed of the Littlefork River; steep and commonly slumping slopes adjacent to the river attest to the significant erosion of Koochiching lobe and Glacial Lake Norwood sediment during the Holocene.

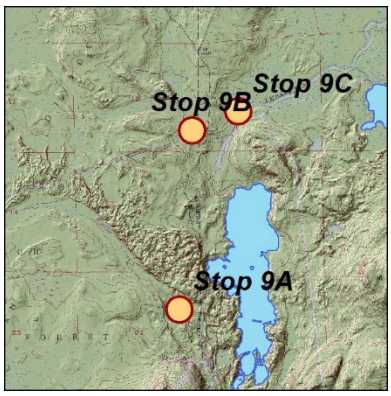
Stop 9: Embarrass Gap

9A: 551980/5270340N (UTM Zone 15, NAD83)
(47.583892, -92.3087077)

9B: 552150/5272700N (UTM Zone 15, NAD83)
(47.6056089, -92.3061663)

9C: 552760/5272950N (UTM Zone 15, NAD83)
(47.6078088, -92.2980211)

Biwabik 7.5’ USGS Quadrangle



These three stops are in the three successive major outlet channels for Glacial Lake Norwood. Stop 9A (elevation 450 m) is in a meltwater channel developed at the margin of the Rainy lobe, perhaps against an active ice margin. Stops 9B (elevation 443 m) and 9C (elevation 433 m) are two successively lower major outlets formed as the ice-cored Allen moraine collapsed over a time interval on the order of 1000 years. The outlet at 9C served as the stable outlet to Glacial Lake Norwood until opening of its final lower outlet to the west, through the McIntosh spillway in the vicinity of Trail, Minnesota.

REFERENCES

Bauer, Emily J., Mark A. Jirsa, Amy Radakovich Block, Terrence J. Boerboom, Val W. Chandler, Dean M Peterson, Kaleb G. Wagner, Elizabeth L. McDonald, Jennifer M. Dengler, Gary N. Meyer, and Jacqueline D. Hamilton. 2022. "Geologic Atlas of St. Louis County, Minnesota." Minnesota Geological Survey County Atlas Series C–51.

Björck, Svante. 1990. "Late Wisconsin History North of the Giants Range, Northern Minnesota, Inferred from Complex Stratigraphy." Quaternary Research 33:18–36.

Breckenridge, Andrew J. 2015. "The Tintah-Campbell Gap and Implications for Glacial Lake Agassiz Drainage during the Younger Dryas Cold Interval." Quaternary Science Reviews 117:124–34. https://doi.org/10.1016/j.quascirev.2015.04.009.

Buchan, Kenneth L., Henry C. Halls, and James K. Mortensen. 1996. "Paleomagnetism, U-Pb Geochronology, and Geochemistry of Marathon Dykes, Superior Province, and Comparison with the Fort Frances Swarm." Canadian Journal of Earth Sciences 33:1583–95.

Clayton, Lee, and Stephen R. Moran. 1982. "Chronology of Late Wisconsinan Glaciation in Middle North America." Quaternary Science Reviews 1:55–82.

Cotter, Ralph D., H.L. Young, and Thomas C. Winter. 1964. "Preliminary Surficial Geologic Map of the Mesabi-Vermilion Iron Range Area, Minnesota." USGS Miscellaneous Geologic Investigations Map I-403.

Elftman, A.H. 1898. "The Geology of the Keweenawan Area in Northeastern Minnesota, Part I." The American Geologist 21:90–109.

Hobbs, Howard C. 1983. "Drainage Relationships of Glacial Lakes Aitkin and Upham and Early Lake Agassiz in Northeastern Minnesota." Edited by James T. Teller and Lee Clayton. Geological Association of Canada Special Paper 26:245–59.

Johnson, Mark D., Roberta S. Adams, Angela S. Gowan, Kenneth L. Harris, Howard C. Hobbs, Carrie E. Jennings, Alan R. Knaeble, Barbara A. Lusardi, and Gary N. Meyer. 2016. "Quaternary Lithostratigraphic Units of Minnesota." Minnesota Geological Survey Report of Investigations 68:262.

Knaeble, Alan R., Gary N. Meyer, Lisa M. Marlow, Phillip C. Larson, and Howard D. Mooers. 2005. "Deposits and Landforms in the Region Glaciated by the St. Louis Sublobe." In Field Trip Guidebook for Selected Geology in Minnesota and Wisconsin, edited by Lori Robinson, Guidebook, 40–79. Minneapolis: Minnesota Geological Survey.

Larson, Phillip C., Alan R. Knaeble, Howard D. Mooers, and Lisa M. Marlow. 2014. "The St. Louis Sublobe and Glacial Lake Upham." Institute on Lake Superior Geology Field Trip Guidebook 60:102–18.

Larson, Phillip C., and Howard D. Mooers. 2009. "Glacial Geology of the Vermilion Moraine." Institute on Lake Superior Geology Field Trip Guidebook 55 (2): 81–99.

Lehr, James D., and Howard C. Hobbs. 1992. "Glacial Geology of the Laurentian Divide Area, St. Louis and Lake Counties, Minnesota." Minnesota Geological Survey Guidebook 18:82.

Lepper, Kenneth, Timothy G. Fisher, Irka Hajdas, and Thomas V. Lowell. 2007. "Ages for the Big Stone Moraine and the Oldest Beaches of Glacial Lake Agassiz : Implications for Deglaciation Chronology." Geology 35 (7): 667–70. https://doi.org/10.1130/G23665A.1.

Leverett, Frank. 1932. "Quaternary Geology of Minnesota and Parts of Adjacent States." USGS Professional Paper 161:149.

Lowell, Thomas V., Timothy G. Fisher, Irka Hajdas, K. Glover, Henry M. Loope, and T. Henry. 2009. "Radiocarbon Deglaciation Chronology of the Thunder Bay, Ontario Area and Implications for Ice Sheet Retreat Patterns." Quaternary Science Reviews 28 (17–18): 1597–1607. https://doi.org/10.1016/j.quascirev.2009.02.025.

MNDNR. 2012. "LiDAR Elevation, Arrowhead Region, NE Minnesota, 2011." Minnesota Department of Natural Resources. ftp://ftp.gisdata.mn.gov/pub/gdrs/data/pub/us_mn_state_mngeo/elev_lidar_arrowhead2011/metadata/metadata.html.

Mooers, Howard D., and James D. Lehr. 1997. "Terrestrial Record of Laurentide Ice Sheet Reorganization during Heinrich Events." Geology, no. 11, 987–90.

Prest, Victor K., J. Allan Donaldson, and Howard D. Mooers. 2000. "The Omar Story: The Role of Omars in Assessing Glacial History of West-Central North America." Géographie Physique et Quaternaire 54:257–70.

Southwick, David L., and Henry C. Halls. 1987. "Compositional Characteristics of the Kenora-Kabetogama Dyke Swarm (Early Proterozoic), Minnesota and Ontario." Canadian Journal of Earth Sciences 24:2197–2205.

Stark, James R. 1977. "Surficial Geology and Ground-Water Geology of the Babbitt-Kawishiwi Area, Northeastern Minnesota with Planning Implications." M.S. Thesis. M.S. Thesis, University of Wisconsin.

Upham, Warren. 1894. "Preliminary Report of the Field Work during 1893 in Northeastern Minnesota, Chiefly Relating to the Glacial Drift." Geological and Natural History Survey of Minnesota Annual Report 22:18–86.

Winchell, Newton H. 1899. "The Geology of the North Part of St. Louis County." Geological and Natural History Survey of Minnesota 4:222–65.

———. 1900. "Glacial Lakes of Minnesota." Geological Society of America Bulletin 12:109–28.

Winter, Thomas C. 1971. "Sequence of Glaciation in the Mesabi-Vermilion Iron Range Area, Northeastern Minnesota." USGS Professional Paper 750–C:C82–88.

———. 1973. "Hydrogeology of Glacial Drift, Mesabi Iron Range, Northeastern Minnesota." USGS Water Supply Paper 2029-A:31.

Winter, Thomas C., Ralph D. Cotter, and H.L. Young. 1973. "Petrography and Stratigraphy of Glacial Drift, Iron Range Area, Northeastern Minnesota." USGS Bulletin 1331–C:50.

Wright, Herbert E. 1956. "Sequence of Glaciation in Eastern Minnesota." Geological Society of America Guidebook 3:1–24.

———. 1972. "Quaternary History of Minnesota." In Geology of Minnesota: A Centennial Volume, edited by Paul K. Sims and G.B. Morey, 515–47. St. Paul, Minnesota.

Wright, Herbert E., and William A. Watts. 1969. "Glacial and Vegetational History of Northeastern Minnesota." Minnesota Geological Survey Special Publication 11.